

NONPLANAR PORPHYRINS AND THEIR BIOLOGICAL RELEVANCE: GROUND AND EXCITED STATE DYNAMICS

*A Thesis Submitted
in Partial Fulfilment of the Requirements
for the Degree of
DOCTOR OF PHILOSOPHY*

by

MANGALAMPALLI RAVIKANTH

to the

DEPARTMENT OF CHEMISTRY

INDIAN INSTITUTE OF TECHNOLOGY KANPUR

November, 1993

CHM-1993-D-RAV-N

2 4 JUN 1994 /chem

CENTRAL LIBRARY
I I T, KANPUR

Acc. No. A. 117954

TH
30 JUN 1994
S 1211

TO
AMMA
AND
NANNA

*for sacrificing your dreams
so that mine could come true!*

STATEMENT

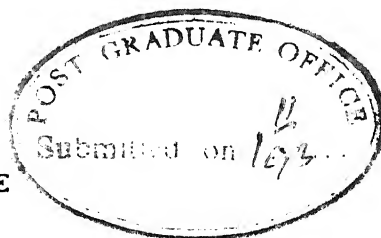
I hereby declare that the matter embodied in this thesis, **NONPLANAR PORPHYRINS AND THEIR BIOLOGICAL RELEVANCE; GROUND AND EXCITED STATE DYNAMICS**, is the result of investigations carried out by me in the Department of Chemistry, Indian Institute of Technology, Kanpur, India under the supervision of Dr. T.K. Chandrashekar.

In keeping with the general practice of reporting scientific observations, due acknowledgement has been made wherever the work described is based on the findings of other investigators.


M. RAVIKANTH

Kanpur
November, 1993

CERTIFICATE



IV

It is certified that the work contained in the thesis entitled, "NONPLANAR PORPHYRINS AND THEIR BIOLOGICAL RELEVANCE; GROUND AND EXCITED STATE DYNAMICS", by M RAVIKANTH, has been carried out under my supervision and same has not been submitted elsewhere for a degree.

A handwritten signature in cursive script, reading "T.K. Chandrashekar".

(T.K. Chandrashekar)
Thesis Supervisor
Department of Chemistry
Indian Institute of Technology
Kanpur 208 016, India

Kanpur
November, 1993


DEPARTMENT OF CHEMISTRY
INDIAN INSTITUTE OF TECHNOLOGY KANPUR, INDIA

CERTIFICATE OF COURSE WORK

This is to certify that **M. RAVIKANTH** has satisfactorily completed all the courses required for the Ph.D. degree. The courses include :

- CHM 605 Principles of Organic Chemistry
- CHM 624 Modern Physical Methods in Chemistry
- CHM 625 Principles of Physical Chemistry
- CHM 645 Principles of Inorganic Chemistry
- CHM 646 Bio-Inorganic Chemistry
- CHM 668 Advanced Inorganic Chemistry II
- CHM 800 General Seminar
- CHM 801 Special Seminar
- CHM 900 Post-graduate Research

M. Ravikanth was admitted to the candidacy of the Ph.D. degree in September, 1990 after he successfully completed the written and oral qualifying examinations.



(P K Ghosh)
Head
Department of Chemistry
IIT Kanpur



(Javed Iqbal)
Convener
Departmental Post Graduate Committee
Department of Chemistry
IIT Kanpur

NOTE OF THANKS

With profound sense of gratitude and sincerity, I express my indebtedness to my thesis supervisor Dr. T.K. Chandrashekar for the inspiration he lent to me both by excellent guidance as well as by his remarks, criticism, help, advice and comments throughout this research. He was kind, gentle and patient in guiding me. The amount of freedom and independence that he allowed me in my thesis work was almost unbelievable and enabled me to "discover" the field of vision for myself to get a broad background of this subject. I am very thankful to him particularly for his encouragement to develop my independent thinking and logical reasoning. The environment he provided made possible a great amount of productive and innovative work that otherwise could not have easily been done. He was always available for discussions and I consider my association with him a rewarding experience. Although, it is difficult to express my gratitude in words, I can only hope that some measure of gratefulness is expressed in this way.

This work has been completed under the soothing support of my parents. Although far away they have always been a source of inspiration and happiness to me. To them, this thesis is dedicated as a token of love and regard. I take this opportunity to convey my deeply felt love and regards to my sister, brothers and sister-in-laws for their love, encouragement and support.

I am greatly indebted to Dr. Damodar Reddy, without whose help the thesis could not have been completed. Frequent discussions with him and his constructive criticism helped immensely in the completion of this thesis. I am also debt to Mr. Ashutosh Misra for his help in the molecular mechanics calculations.

With a sense of special regard I would like to express my gratitude to Dr. V. Chandrasekhar for his keen interest in my work and timely suggestions.

I am extremely thankful to my labmates Damu, Pandian, Ravi

Kumar, Murali, Immi and Justin for providing cheerful atmosphere and help during the course of my investigations.

I am greatly indebted to Prof. S. Sarkar of this department for cyclic voltammetric measurements, Prof. H.D. Bist, Department of Physics for Raman measurements, Prof. S. Mitra, Chemical Physics group, TIFR Bombay for variable temperature magnetic susceptibility measurements and Prof. H.van Willigen, Department of Chemistry, University of Massachusetts, Harbor Campus, Boston, U.S.A. for triplet ESR measurements.

I would like to thank all faculty members for rendering me valuable suggestions and teaching me various courses.

I am very fortunate to be in the company of lively pals Dr. P.S.R. Prasad, Shankar, Diwakar and Arvind Galagali who provided elderly care and attention as and when I needed. Galag deserves a special mention. He was always ready to lend me a helping ear and a helping hand.

Words cannot convey the depths of my emotions towards my lovely special friends, Dr. Zahida Shirin, Dr. Beena Bhatia, Sangeeta, Damu, Madhav, Venkat, Murali and Pragati who have helped by reading the manuscript and offering constructive suggestions, in some cases saving me from serious blunders. I would not know how to express my thanks to them for providing many cheerful moments, pleasant tea sessions and for bearing with me in difficult times. Special mention should be made of Zahida for her constant encouragement and moral support under all circumstances.

It is unvarnished truth that this treatise would not have been materialised in the absence of friends and colleagues who have made my stay at I.I.T. Kanpur a memorable experience in my life. In naming them, I am likely to miss many of those who contributed in different ways. Nevertheless, the cooperation and help of Kamal, Prabhu, Dr. S. Sathiah, Sudhakar, Dr K. Ramesh, Pramod, Kalyan, Shaji, Kashi, Tamil, Samiran, Bhisma, Mondal, Raghunathan, Manabendra Ray, Samar, Saifuddin, Ram Sharan, Rashi, Sabhahit, Harish, Manjunath, Kuljeet, Ravindra, Dr. Leela Iyengar, Mrs. Dulali Biswas, Vandana, Indrani, Shalini, Nisha, Putti, Archana and Sonal is gratefully acknowledged. I am also thankful

to my cousins Padma, Indira and Rama Krishna for their encouragement.

I would also like to express my heartfelt thanks to Mrs. Asha Chandrashekar, Mrs. Sudha Chandrasekhar, Mrs. Uma Damodar, Mrs. Andal Ramesh, Prof. K. Subramanya and family. Prof. Raghavendra and family and Sri V.B. Parvathikar and family for their affection, love and hospitality.

Special thanks to Damu and Sangeeta for their understanding, encouragement and kind help in the final setting of this thesis.

I am grateful to messers Ahmed, Kanaujia, Bhauser and Dr. Raja Roy for their valuable help in the successful completion of my thesis.

The office help rendered by Sri Agnihotri, L.P. Tripathi and staff of Department of Chemistry is appreciated.

Finally, I wish to express my thanks to Mr. Gauri Singh, Jain and V.P. Gupta for neat tracings and Mr. Ghanshyam Rao Hoshing for his excellent and flawless typing.

Ravikanth

TABLE OF CONTENTS

	Page
SYNOPSIS	
CHAPTER 1 : GENERAL INTRODUCTION.....	1
CHAPTER 2 : GENERAL EXPERIMENTAL METHODS AND TECHNIQUES.....	41
CHAPTER 3 : SHORT CHAIN BASKET HANDLE PORPHYRINS; SYNTHESIS, STRUCTURE, OPTICAL AND ELECTROCHEMICAL PROPERTIES.	
3.1 Introduction.....	53
3.2 Work done in the Present Study.....	54
3.3 Experimental.....	55
3.4 Results.....	63
3.5 Discussion.....	82
3.6 Conclusions.....	95
CHAPTER 4 : EFFECT OF METAL IONS (Cu(II), Fe(III)) ON OPTICAL AND ELECTRONIC PROPERTIES OF SHORT CHAIN BASKET PORPHYRINS	
4.1 Introduction.....	98
4.2 Work done in the Present Study.....	100

SECTION A

SPECTRAL AND ELECTROCHEMICAL STUDIES ON
COPPER(II) DERIVATIVES OF BASKET HANDLE
PORPHYRINS

4.3 Experimental.....	101
4.4 Results.....	102
4.5 Discussion.....	113

SECTION B

SPECTRAL AND ELECTROCHEMICAL PROPERTIES
OF IRON(III) DERIVATIVES OF BASKET HANDLE
PORPHYRINS

4.6	Experimental	120
4.7	Results	123
4.8	Discussion	134
4.9	Conclusions	138

CHAPTER 5 : EFFECT OF PORPHYRIN RING DISTORTION ON
THE SINGLET AND TRIPLET EXCITED STATE
PROPERTIES.

5.1	Introduction	139
5.2	Work done in the Present Study	140

SECTION A

SINGLET EXCITED STATE PROPERTIES OF
BASKET HANDLE PORPHYRINS

5.3	Results	142
5.4	Discussion	156

SECTION B

PHOTOEXCITED TRIPLET ESR STUDIES ON
BASKET HANDLE PORPHYRINS

5.5	Introduction	164
5.6	Results	167
5.7	Discussion	174
5.8	Conclusions	180

CHAPTER 6 : MAGNETIC INTERACTION IN π -CATION RADICALS
OF COPPER(II) AND HIGH SPIN IRON(III)
DERIVATIVES OF SHORT CHAIN BASKET HANDLE
PORPHYRINS

6.1	Introduction.....	181
6.2	Work done in the Present Study.....	182

SECTION A

π -CATION RADICALS OF COPPER(II)
DERIVATIVES OF BASKET HANDLE PORPHYRINS

6.3	Experimental.....	183
6.4	Results.....	184
6.5	Disucssion.....	194

SECTION B

π -CATION RADICALS OF HIGH SPIN IRON(III)
DERIVATIVES OF BASKET HANDLE PORPHYRINS

6.6	Experimental.....	205
6.7	Results.....	206
6.8	Discussion.....	213
6.9	Conclusions.....	220

CHAPTER 7 : DIMERIZATION EFFECTS ON SPECTROSCOPIC
PROPERTIES OF WATER-SOLUBLE PORPHYRINS IN
AQUEOUS AND MICELLAR MEDIA

7.1	Introduction.....	222
7.2	Work done in the Present Study.....	223
7.3	Results.....	224
7.4	Discussion.....	234
7.5	Conclusions.....	249

CHAPTER 8 : SUMMARY.....251

APPENDIX	264
REFERENCES	286
LIST OF PUBLICATIONS	303

SYNOPSIS

The recent realisation of role of nonplanar macrocyclic conformations in biochemical function of tetrapyrrole pigments has resulted an intense research activity on characterisation and study of nonplanar porphyrin systems. This thesis is aimed at such a study. The thesis has been divided into eight chapters.

CHAPTER I : GENERAL INTRODUCTION

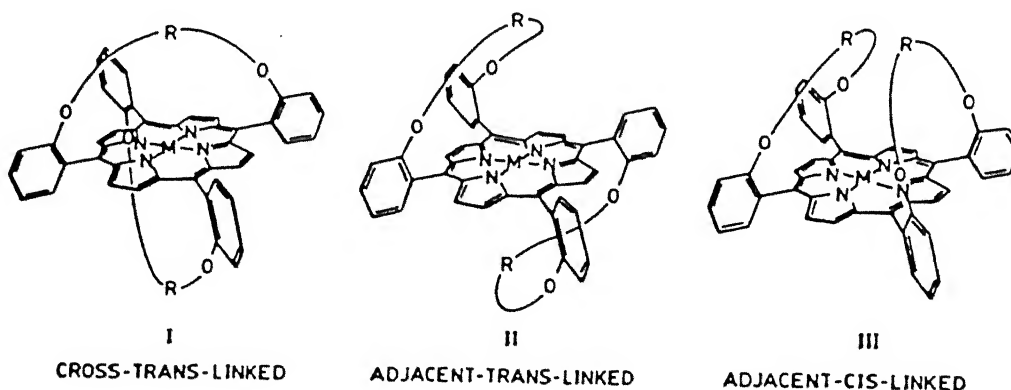
In this chapter a brief account of biochemical significance of ; (a) nonplanar conformations of porphyrin skeleton, (b) role of metalloporphyrin π -cation radicals and (c) importance of chlorophyll dimers in photosynthesis are presented. Furthermore, an overview of literature results on above aspects are also highlighted.

CHAPTER II : GENERAL EXPERIMENTAL METHODS AND TECHNIQUES

General experimental methods and techniques employed for the evaluation of various physical parameters reported in this thesis are described. In addition, a brief account of purification of various solvents, chemicals and methods of preparation of the starting materials and the precursor compounds are given.

CHAPTER III : SHORT CHAIN BASKET HANDLE PORPHYRINS; SYNTHESIS, STRUCTURE, OPTICAL AND ELECTROCHEMICAL PROPERTIES.

This chapter describes the effect of porphyrin ring distortion on spectral and electrochemical properties of the title compounds besides their synthesis and characterisation. Distortion in the porphyrin skeleton has been introduced by linking the meso phenyl rings of tetraphenylporphyrin (H_2TPP) at the ortho position. Three isomers have been isolated depending on the nature of the linkage (fig.). The degree of distortion has



been controlled by varying the length of the chain and the position of the link. The linking groups used are ; (a) simple alkyl chains of varying length, (b) alkyl chains containing an aromatic ring and (c) aromatic ring in (b) are substituted with electron withdrawing (Br^- or Cl^-) groups. Also pyrrole brominated porphyrins of one of the cross-trans-linked porphyrin derivative of type (c) are prepared. Characterisation of various porphyrin derivatives have been done using 1H -NMR, FAB mass and electronic spectra.

The spectral and electrochemical studies reveal the following:

(a) decrease in the energy gap between HOMO's and LUMO's upon increasing distortion. The magnitude of decrease depends on nature of the isomer and the chain length, (b) easier oxidations (80-260 mV less positive) and harder reductions (160-340 mV more negative) relative to planar H_2TPP , (c) substitution of bromines at the β -pyrrole positions further increases the degree of distortion.

To probe the existence of distortion, the structures of various isomers have been calculated using MOBY's energy optimization programme. The calculated structures clearly reveal the expected distortion in the porphyrin skeleton.

CHAPTER IV : EFFECT OF METAL IONS [COPPER(II), IRON(III)] ON OPTICAL AND ELECTRONIC PROPERTIES OF SHORT CHAIN BASKET HANDLE PORPHYRINS.

This chapter describes the effect of metallation on the optical and electrochemical properties of a few distorted porphyrins. It has been shown that the introduction of the metal does not alter the degree of distortion. The optical absorption red shifts and the redox potential shifts observed upon distortion and β -substitution have been analysed using a literature method. The analysis indicate ; (a) different stabilisation/destabilisation mechanisms for the optical absorption red shifts and (b) distortion results in perturbations of a_{1u}/a_{2u} separation while for β -substitution this separation is much larger. ESR studies indicate only small changes in the electronic structure of Cu(II)

CHAPTER V : EFFECT OF PORPHYRIN RING DISTORTION ON THE SINGLET AND TRIPLET EXCITED STATE PROPERTIES

The singlet and triplet excited state dynamics of short chain basket handle porphyrins, their dications and Zn(II) derivatives determined by fluorescence and photoexcited triplet ESR methods are described in this chapter. The effects of distortion are apparent in quenching, broadening and red shifts of the emission bands relative to the corresponding planar derivative and the maximum effects are observed for the most distorted isomer. Excited state potential data suggests easier oxidations and harder reductions relative to H_2TPP even in the first singlet excited state. Upon protonation, the emission bands experience a blue shift due to lack of expected resonance interaction. This is ascribed to the restricted rotation of porphyrin-phenyl bond imposed by the ortho substituent. The Zn(II) porphyrins show emission from S_1 and S_2 excited states with quenching of fluorescence. The decreased energy gap between S_1 and S_2 excited states in the distorted Zn^{2+} porphyrins promotes the $S_2 \rightarrow S_1$ internal conversion thereby decreasing $S_2 \rightarrow S_0$ fluorescence yield.

Zero field splitting parameters D and E of the various basket handle porphyrins calculated from photoexcited triplet ESR spectra show small but significant differences and this has been ascribed to the distortion of the porphyrin plane. The electron spin polarization (ESP) pattern (eaeaea) remain same as in H_2TPP indicating the usual spin-orbit coupling mechanism for intersystem crossing.

CHAPTER VI : MAGNETIC INTERACTIONS IN π -CATION RADICALS OF COPPER(II) AND HIGH SPIN IRON(III) DERIVATIVES OF SHORT CHAIN BASKET HANDLE PORPHYRINS.

This chapter gives the details of the studies on π -cation radicals of Copper(II) and high spin Iron(III) derivatives of short chain basket handle porphyrins and their magnetic properties. The direction and magnitude of few structurally sensitive skeletal modes shift upon radical formation in the Raman spectra of π -cation radicals of copper derivatives and the nature of the absorption spectra suggests an a_{2u} ground state for radical cations. The π -cation radicals of copper derivatives are diamagnetic both in solid and in SOLUTION due to antiferromagnetic exchange between the unpaired electron in the metal and porphyrin ring facilitated through the deformation of the porphyrin core. The diamagnetism in solution is in contrast to those observed for other copper meso aryl porphyrin radical cations. The antiferromagnetic exchange in both solution and solid is further confirmed in high spin Iron(III) derivatives. This study substantiates the emerging structure - magnetic property correlations that planar core leads to ferromagnetic coupling and ruffled core leads to antiferromagnetic coupling.

CHAPTER VII : DIMERISATION EFFECTS ON SPECTROSCOPIC PROPERTIES OF WATER-SOLUBLE PORPHYRINS IN AQUEOUS AND MICELLAR MEDIA.

The effects of cation-crown ether induced dimerisation on the optical and fluorescence spectra of free base 5,10,15,20-tetrakis

(4-carboxyphenyl)porphyrin (H_2tcp^{4-}) and 5,10,15,20-tetrakis (4-sulphonatophenyl)porphyrin (H_2tppc^{4-}) and their metal derivatives (Cu^{2+} , Ni^{2+} and Zn^{2+}) have been studied in aqueous and micellar media. Dimerisation induces a red shift of Q-bands in both optical and fluorescence spectra with quenching of fluorescence intensity. However, the Soret band experiences a blue shift in Cu^{2+} and Ni^{2+} derivatives, a red shift in Zn^{2+} derivatives and no shift in the free bases. The magnitude of these shifts depends on the structure of the metalloporphyrin as well as on the nature of the crown ether and cation present in solution. The formation constants for the dimer follow the order $Cu^{2+} \approx Ni^{2+} > H_2tppc^{4-} > Zn^{2+}$. In micellar media the dimerisation effect is observed only in anionic sodium dodecyl sulphate. In hexadecyltrimethylammonium bromide and Triton X-100, the porphyrins remain monomeric. An analysis of the data suggests that four cation-crown ether complexes are involved per dimer unit. The exciton formalism coupled with π - π interaction accounts for the observed shifts in Cu^{2+} , Ni^{2+} and free base porphyrins while a satisfactory interpretation has to take charge-transfer contributions into account for Zn^{2+} derivatives.

CHAPTER VIII : SUMMARY

The summary of the investigations carried out in this thesis is described.

CHAPTER 1

GENERAL INTRODUCTION

The occurrence of porphyrin rings in nature as ligands in such crucial and multiple roles as those spanned by the heme proteins¹, chlorophyll², vitamin B₁₂³ etc. suggests that some advantages might be associated with this macrocyclic structure. The biological function of metalloporphyrins can be broadly classified⁴ into following types : (1) Electron transport, e.g. cytochromes which are basically hemes are responsible for various biological redox reactions. (2) The chlorophylls contain redox inert magnesium as the central ion and form "organic" π -cation radicals on absorption of photons and such radicals play a prominent role in photosynthesis and biosynthesis of protochlorophyll. (3) Some heme proteins, e.g., hemoglobin, myoglobin, catalases and peroxidases, function in the transport and activation of molecular oxygen as well as on the decomposition of hydrogen peroxide. (4) The metabolism of naturally occurring tetrapyrrole metal complexes includes irreversible oxygenation and hydrogenation reactions e.g. cytochrome P₄₅₀, bile pigment formation and protochlorophyll hydrogenation.

One of the main reasons for nature to choose porphyrin ligand for doing such diverse functions in biology is that porphyrin macrocycle is conformationally flexible and can adopt nonplanar conformations in a wide variety of biological systems. The X-ray structures solved for several biomolecules supports this observation. For example, the domed porphyrins present in several heme proteins¹ involved in oxygen transport, peroxide reduction and disproportionating the mitochondrial electron transport chain and drug metabolism. The nickel tetrapyrrole cofactor F_{430} present in methyl reductase⁵ enzyme which catalyses the production of methane is also in domed conformation. Nonplanar conformational distortion of tetrapyrrole pigments of photosynthetic reaction centres² have been suggested to control the photophysical properties. The highly puckered and distorted corrin ring of vitamin B_{12} helps in weakening of the cobalt-carbon bond to generate a 5'-deoxyadenosyl radical³.

Another unique property identified in this macrocyclic chemistry is the involvement of their cation radicals as intermediates in many catalytic cycles such as catalases, peroxidases⁶, chloroperoxidases, cytochrome P_{450} ⁷, photosynthesis² etc. Aggregation of tetrapyrrole pigments is also one of the properties of significance in biological systems. It is generally accepted that dimers and higher aggregates of chlorophyll molecules play an important role in photosynthesis.

Before a detailed discussion on the contents of this thesis is described, a brief survey on the biochemical significance of nonplanarity in the porphyrin ring, involvement of porphyrin

π -cation radicals as intermediates in many catalytic cycles and importance of special pair at the reaction center of photosynthesis are described. Furthermore, a brief survey of literature on these aspects is also presented.

1.1 (a) BIOCHEMICAL SIGNIFICANCE OF NONPLANAR PORPHYRINS

Nonplanar porphyrin cores are found in several biomolecules and brief description of these is outlined below.

1.1.1 HEME PROTEINS

Heme proteins are a class of biologically important macromolecules which have three distinct functions : Myoglobin (Mb) and Hemoglobin (Hb) serve as reversible oxygen transfer proteins, the cytochrome b's and c's function as reversible one electron transfer agents and cytochrome P₄₅₀⁷ and peroxidases⁶ are involved in irreversible covalent transformations of substrates. In spite of these diverse functions, all heme proteins have the unifying feature of a common active site or prosthetic group composed of an iron-porphyrin complex. Nonplanar distortions such as doming of the macrocycle have been observed in the X-ray crystal structures of some heme proteins such as Myoglobin and Hemoglobin.

Hemoglobin contains a iron(II) protoporphyrin-IX complex. The ferrous(II) protoporphyrin-IX is held within a cleft in the protein principally by noncovalent, largely apolar interactions. In addition to binding to the porphyrin ring, the iron is covalently linked by axial binding to atleast one endogenous ligand. In the ferrous resting state of Myoglobin and Hemoglobin,

it is an imidazole group of a nearby histidine residue while the second axial position is the one which reversibly binds an oxygen molecule as well as a number of other small ligands such as CO and NO.

An explanation of the cooperative effect is central to the understanding of the role of Hemoglobin. The distance between heme groups in the tetramer is considerable and so the effect must be transmitted through the protein structure. Uptake of O₂ is associated with substantial conformational changes. These conformational changes are associated with the reversible interconversion of a tensed (T), low affinity form of Mb into a relaxed (R), high affinity form. It is usually this process that is triggered by the movement of the iron atom towards the plane of the heme group in response to the binding of dioxygen. This mechanism put forward by Perutz and Hoard was mainly based on the structures of iron(II) porphyrins. The deoxy form of Hemoglobin is high spin due to its larger size which prevents it moving into the hole in the porphyrin cavity. Binding of dioxygen results in the formation of low spin iron(II) which is smaller and able to move into the plane of the porphyrin group. The resulting change in Fe-N (imidazole) bond length is magnified through the interactions in Hemoglobin so that substantial conformational changes occur.

The X-ray structure of heme proteins by Perutz⁸ and Deathearage group^{1b} confirms the presence of porphyrin macrocycle in a domed conformation. The most striking feature of the results is the extensive perturbation of the β -heme, contrasted with the almost complete lack of perturbation of the α -heme. Model studies

provided two possible explanations for the array of positive and negative features on the β -heme. The first is that in Mn(III) Hb, the β -hemes are six coordinate but undergo a very marked ruffling with a slight shift of the Mn towards the proximal histidine. The second is that difference Fourier electron density maps showed negative peak (HM1B : displacement of water or ruffling of heme in pyrrole II and IV) arising partly from the loss of the water molecule which occupies the sixth coordination position of the Fe(III)Hb and partly from a resultant ruffling of the porphyrin, which also produces positive peaks (HM2B, HM3B and HM5B : Motion of heme towards proximal side by pyrroles II and III; Motion of heme towards proximal side by methyl of pyrrole III and shift of pyrrole IV respectively) on the proximal side. Thus, β -heme is only five coordinate in crystals of Mn(III)Hb but the α -heme remains six coordinate.

This interpretation is supported by a number of lines of evidence⁹, consistent both with the perturbation in the surrounding globin and more importantly, with the structures of related Mn and Fe porphyrins. The location of the center of the negative peak HM1B coincides with the position of the water molecule in Fe(III)Hb. Loss of ligand from the β -heme might be expected to produce a narrowing of the heme pocket. This is observed, most notably by the side chain of valine E11 but also in other sections of the E-helix. The disposition of the positive and negative features on the β -heme itself is consistent with the conversion of an almost planar heme to a quasi- S_4 ruffled heme. This is exactly conversion noted by Day et.al.¹⁰ by comparing the crystal structures of high spin six coordinate Mn(III)(TPP)(N₃)

$(\text{CH}_3\text{OH})\cdot\text{CH}_3\text{OH}$ and high spin five coordinate $\text{Mn(III)(TPP)(N}_3\text{)}$. The former structure is almost planar, with no porphyrin atom more than 0.06 \AA out of the mean plane; the latter is extensively ruffled in accordance with quasi- S_4 symmetry. Similar quasi- S_4 ruffling of a high spin five coordinate Mn(III) porphyrin was noted by Chen^{10c}. In this case the maximum deviations of porphyrin core atoms from the mean plane were $+0.47 \text{ \AA}$ and -0.49 \AA . Two pyrroles lay exclusively above the mean plane and two exclusively below; the four methine carbons were nearly in the mean plane, deviating from it by less than 0.15 \AA . Hoard has emphasized that such ruffling of the porphyrin core, although leading to a less favourable delocalisation of π -bonding, favours stronger complexing and shorter metal-pyrrole nitrogen bonds than in a planar core.

Energy minimization calculations by Gelin and Karplus¹¹ also suggested a domed conformation for the heme group and is unstrained inside the globin. Furthermore, the nonbonding protein-heme interactions in the T-state constrain the porphyrin to a domed configuration. The additional energy required to undome the porphyrin ring upon oxygenation is reflected in the lower T-state dioxygen affinity.

1.1.2 PHOTOSYNTHESIS

Photosynthesis is a process by which light energy is converted via a separation of charge into a chemical potential. The potential thus created is used in green plants to reduce CO_2 to sugars. This process is mediated by two photosystems located in the thylakoid membranes of chloroplasts. Illumination leads

to; (1) The generation of transmembrane proton gradient for the formation of ATP and (2) The creation of the reducing power for the production of NADPH. Light absorbed by chlorophylls in the light harvesting complex of photosystem II funnels into the reaction center P680. An electron is transferred from the excited P680^{*} to pheophytin and then to plastoquinones attached to Q_A and Q_B to form reduced plastoquinone (QH₂). The reaction centre regains electrons from water by the action of a manganese-containing protein, which causes the evolution of O₂. Thus, the net reaction catalysed by photosystem II is the light-induced transfer of electrons from water to plastoquinone. The critical event at all photosynthetic reaction centres is the light induced transfer of an electron to an acceptor against an electrochemical potential gradient.

Electrons from photosystem II flow to photosystem I through the cytochrome bf complex. This transmembrane complex pumps protons into the thylakoid space as electrons are transferred from H₂ to plastocyanin, a water-soluble protein. Photosystem I mediates the light activated transfer of electrons from plastocyanin to P700 and then to ferridoxin, a powerful reductant. Ferridoxin - NADP reductase, a flavoprotein located on the stromal side of the membrane, then catalyzes the formation of NADPH. Thus, the interplay of photosystems I and II leads to the transfer of electrons from H₂O to NADPH and the concomitant generation of a proton gradient for ATP synthesis. ATP and NADPH formed in the light reactions of photosynthesis are used to convert CO₂ to hexoses and other organic compounds during dark phase of the photosynthesis.

The crystallographic data for the reaction centre (RC) of the photosynthetic bacterium *R. viridis*^{2,12} resulted in extensive information concerning the spatial arrangement of the prosthetic groups involved in the primary charge separation events (Fig. 1.1). These prosthetic groups include four bacteriochlorophyll-b (Bchl-b), two bacteriopheophytin-b (Bph-b) and two quinone molecules which are located in two protein subunits M (medium weight) and L (light weight), forming the M and L branches of the RC. The two molecules of Bchl-b, commonly referred as special pair, is the primary donor, transfers an electron to neighbouring pheophytin molecule upon absorption of a photon. It is observed that the two molecules in a special pair overlap with their pyrrole rings I in such a way that when viewed in a direction perpendicular to the ring planes, the atoms of these rings eclipse each other. The orientation of the rings leads to a close proximity between the ring I acetyl groups and the Mg^{2+} ions. However, the acetyl groups do not act as ligands to the Mg^{2+} ions. The pyrrole rings I of both Bchl-b molecules are nearly parallel and Ca. 3.2 \AA° apart. Both tetrapyrrole rings, however, are nonplanar; planes through the pyrrole nitrogens of each Bchl-b form an angle of 11.3 \AA° .

The Bchl-b molecules of the special pair^{12a} are arranged with a nearly perfect two fold symmetry. The Bchl-b rings of the special pair are nearly parallel to this symmetry axis. A more subtle deviation from symmetry is the different degree of nonplanarity of the two Bchl-b ring systems of the special pair. The tetrapyrrole ring of BC_{MP} is considerably more deformed than that of BC_{LP} . This can cause an unequal charge distribution

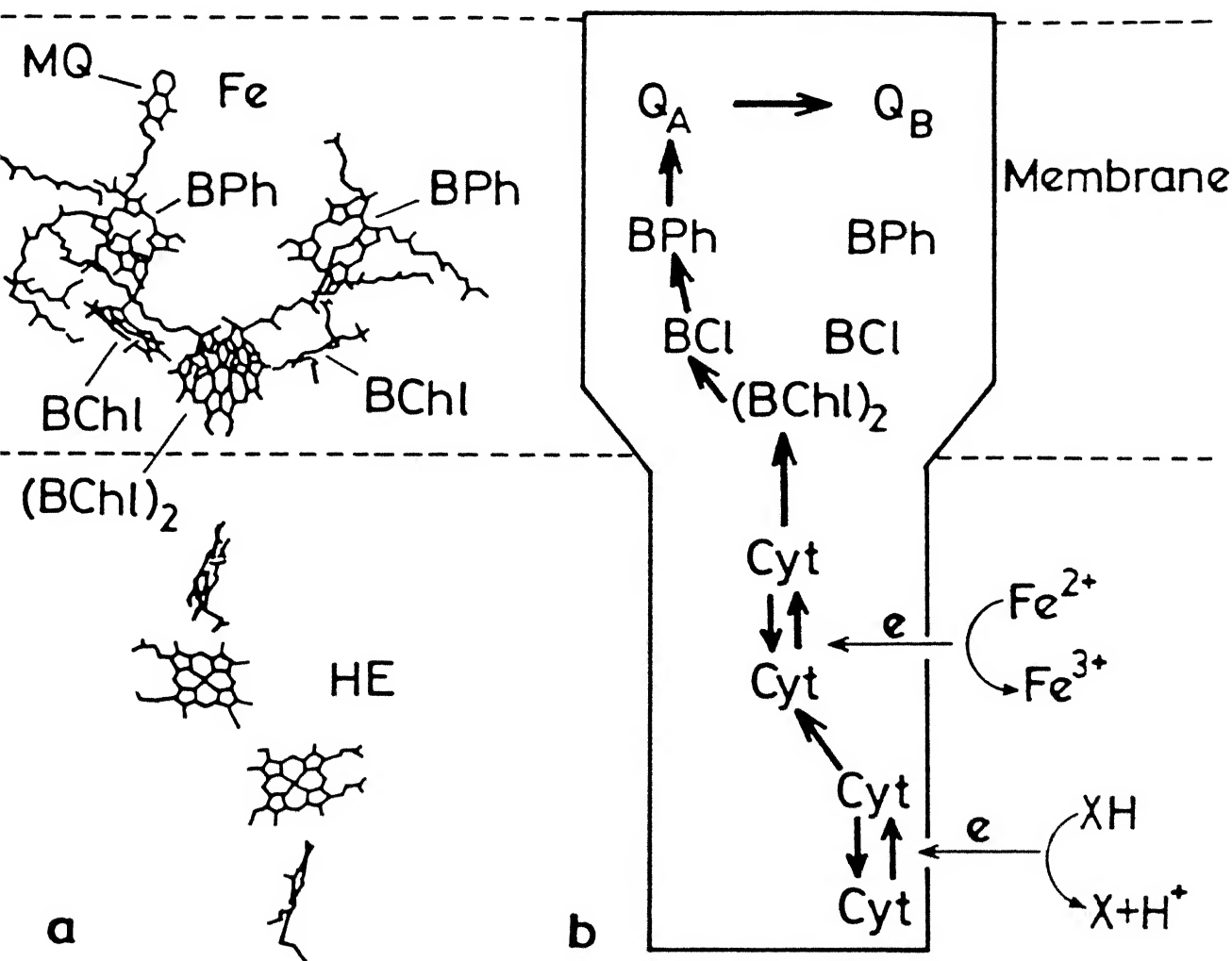


Fig. 1.1 : Schematic representation of the molecular structure of the reaction-centre complex in the photosynthetic bacteria *R. viridis* (taken from Ref. 2(d)).

between the two Bchl-b systems of the special pair, which in turn can be part of the reason for unidirectional electron transfer¹³, essential for the photosynthesis process.

1.1.3 VITAMIN B₁₂

Vitamin B₁₂ and its derivatives³ are transition metal complexes containing a cobalt atom at the center of the molecule. The general structural features of the molecule as shown in fig. 1.2 are: The central cobalt(III) ion bound by four nitrogen atoms from the pyrrole groups of a macrocyclic corrin ring. The corrin ring resembles porphyrin ring apart from having one methine group less. The corrin ring is usually nonplanar, however, the various X-ray analyses have shown that the actual conformation of the ring depends markedly on the nature of the functional groups attached to its periphery. Because of the lack of conjugation, the corrin ring is quite flexible and conformational changes may therefore occur very easily. Besides the four equatorial pyrrole ligands, in most B₁₂ derivatives, two more axial ligands are present. The lower, fifth ligand is an α -5,6-dimethylbenzimidazole nucleotide. The sixth ligand varies from CN⁻, OH⁻, H₂O, CH₃ and 5'-deoxyadenosylcobalamin. The common reactions that vitamin B₁₂ catalyses include methyl group transfer reactions, reduction reactions and rearrangement reactions.

The structure of coenzyme B₁₂, as revealed by X-ray diffraction studies¹⁴ shows evidence for the importance of steric influences of Co-C bond stability (Fig. 1.2). The Co-C bond is quite long (2.05 Å) and the Co-C-C bond angle of 125° is much larger than the tetrahedral value of 109.5° apparently reflecting

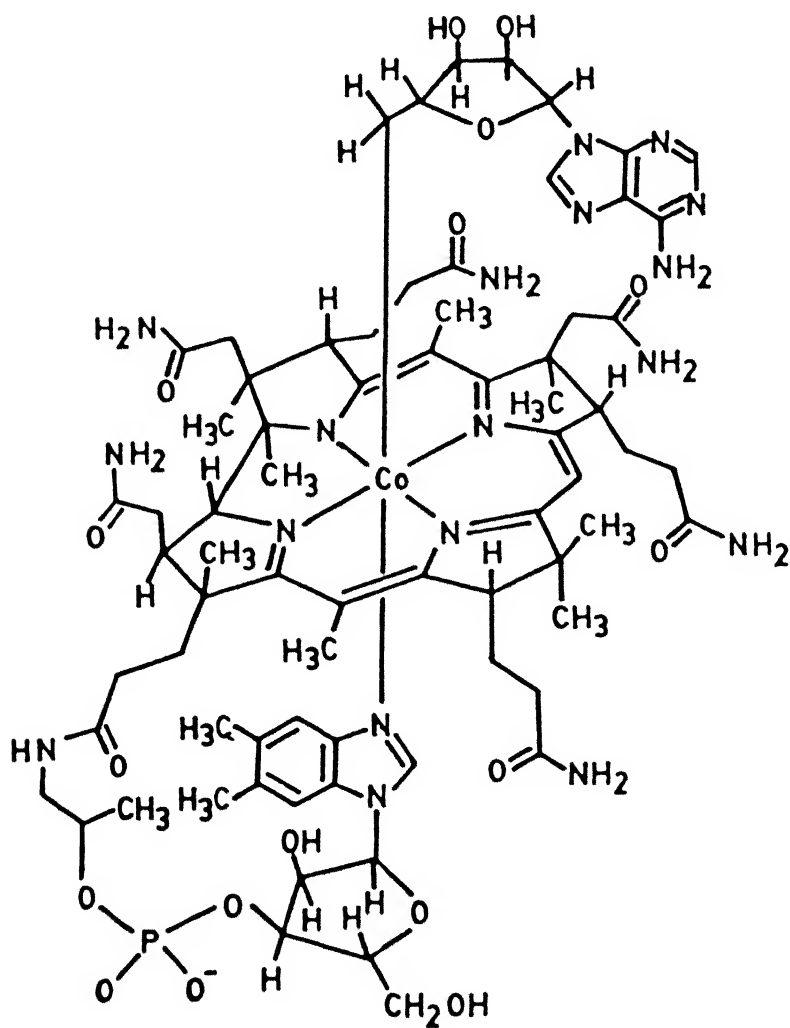
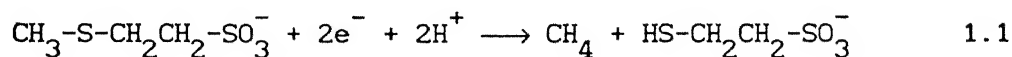


Fig. 1.2 : Structure of Vitamin B₁₂.

repulsions between the 5'-deoxyadenosyl group and substituents on the corrin ring. Consistent with this is the identification of **several** close contacts ($\sim 3 \text{ \AA}$) between atoms of the 5'-deoxyadenosyl group and atoms of the corrin ring and its substituents. In light of these considerations it seems highly likely that the enzyme-induced Co-C bond weakening is due to steric influences namely, an upward conformational distortion of the corrin ring that increases the steric repulsion of the 5'-deoxyadenosyl substituent and induces dissociation of the Co-C bond. The results of the cited structural and bond dissociation studies on coenzyme B_{12} model compounds support the plausibility of this view and suggest that only a modest distortion of the already crowded coenzyme molecule is sufficient to effect the necessary Co-C bond weakening.

1.1.4 METHYL REDUCTASE

Coenzyme F_{430} , the hydrocorphinoid nickel(II) complex⁵ (Fig. 1.3) belongs to the unique group of coenzymes mediating the reduction of CO_2 to methane in methanogenic bacteria. As a cofactor of methylcoenzyme M reductase it is involved in the reductive cleavage of S-methyl coenzyme M to coenzyme M and methane, an exergonic step coupled to the synthesis of ATP.



Ni(I) has been implicated as a catalytic transient in the enzymic methanogenesis. However, the conformations of F_{430} that control the reactions are unknown, as are the consequences of metal reduction. The involvement of Ni(I) is confirmed with the detection of an EPR signal in whole cells of Methanobacterium

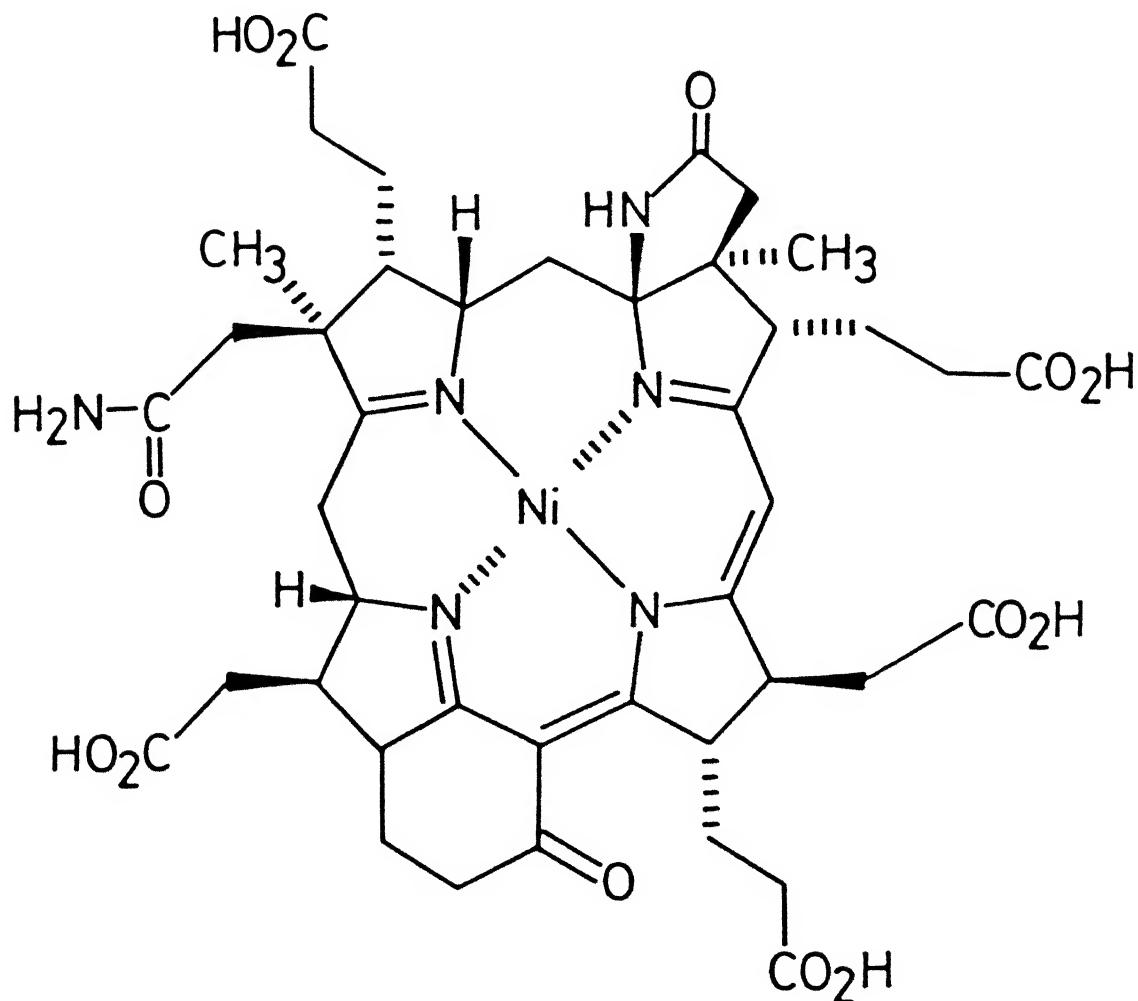


Fig. 1.3 : Structure of Co-factor F₄₃₀.

thermoautotrophicum. The g values and hyperfine coupling associated with this signal are consistent with a d^9 -Ni(I) ion coordinated by four nitrogen atoms. EXAFS studies indicated that the F₄₃₀ skeleton is flexible enough to accommodate changes of 0.2 \AA around Ni(II). Therefore it can equally accommodate the distortion concomitant with reduction to Ni(I).

1.2 BIOCHEMICAL SIGNIFICANCE OF PORPHYRIN π -CATION RADICALS

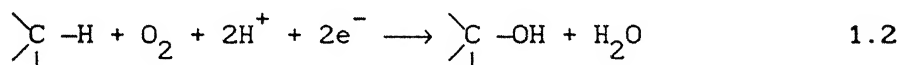
Porphyrin π -cation radicals are involved as intermediates in various biological processes mediated by catalases, peroxidases⁶,

cytochrome P_{450} , chloroperoxidase⁷ and chlorophylls². Basically, electron transfer reactions of biological systems can be broadly classified into three categories : (i) Electron transfer involving only the metal centre, eg., cytochromes (ii) Electron transfer involving only porphyrin π -system eg., chlorophyll and pheophytin. (iii) Electron transfer involving both metal center and porphyrin π -system ex. cytochrome P_{450} , catalases, peroxidases and chloroperoxidases.

Because of the large body of literature data on porphyrin π -cation radical systems only specific examples relevant to present study are described.

1.2.1 CYTOCHROME P_{450}

The P_{450} enzymes⁷ catalyze the incorporation of one atom of dioxygen into hydrocarbon substrates with concomitant reduction of the other oxygen atom as shown in equation 1.2.



Several other types of oxygen transfer reactions are catalysed by P_{450} , including epoxidation, N-dealkylation, O-dealkylation and sulfoxidation. The catalytic cycle is depicted in Fig. 1.4. The first step involves the conversion of low spin six coordinate ferric resting form 1 to a high spin five coordinate state 2 upon substrate binding. Reduction leads to a high spin five coordinate derivative 3 capable of binding dioxygen 4 or carbon monoxide 5. One electron reduction of the oxygen adduct, the least stable intermediate in the reduction cycle leads to release of water and the hydroxylated product, likely after transient formation of

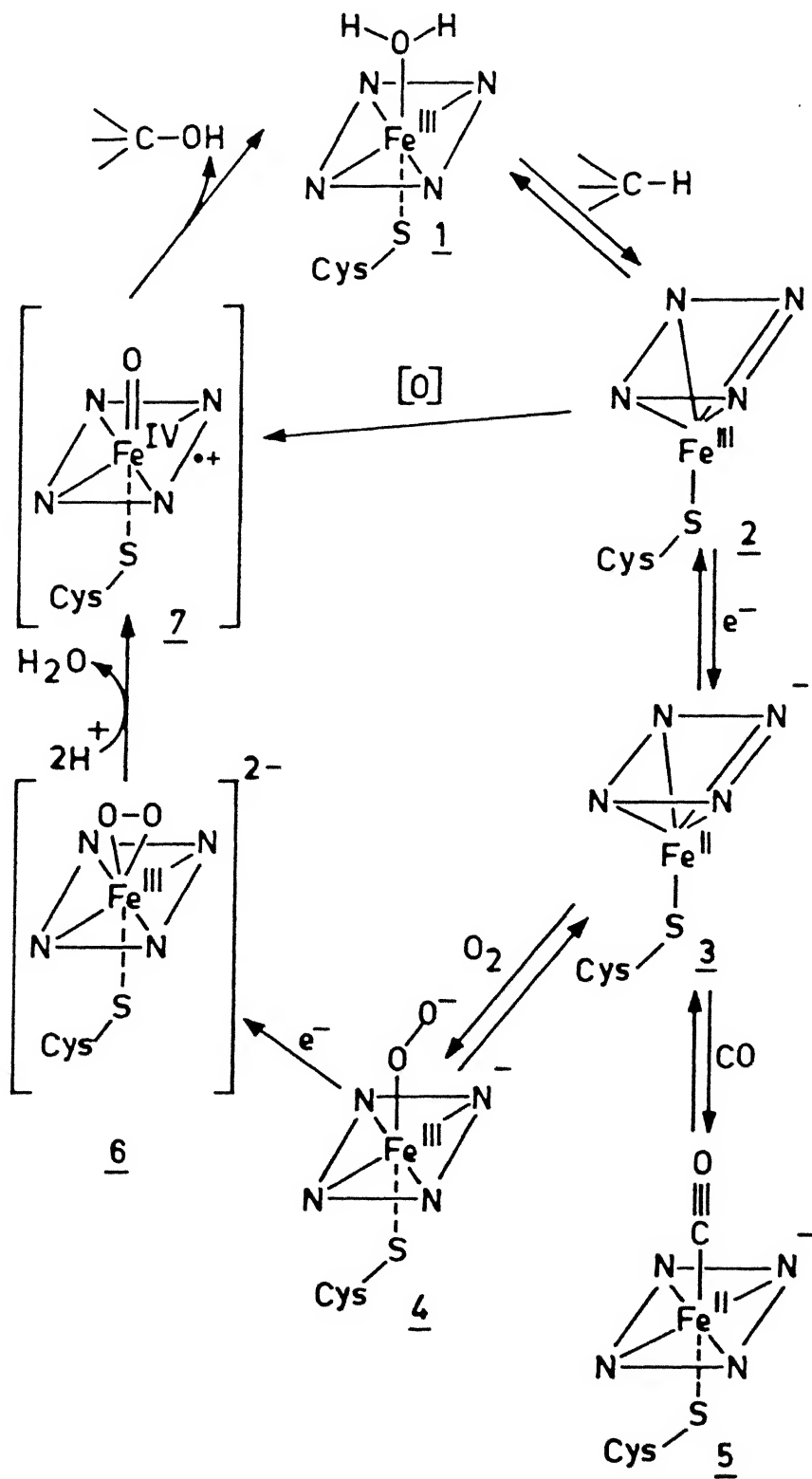


Fig. 1.4 : Catalytic cycle of cytochrome P-450 and the postulated

species such as 6 and 7 in which both metal and porphyrin ring are oxidised. During this cycle, iron exists in various oxidation states, both high and low spin as shown in Fig. 1.5.

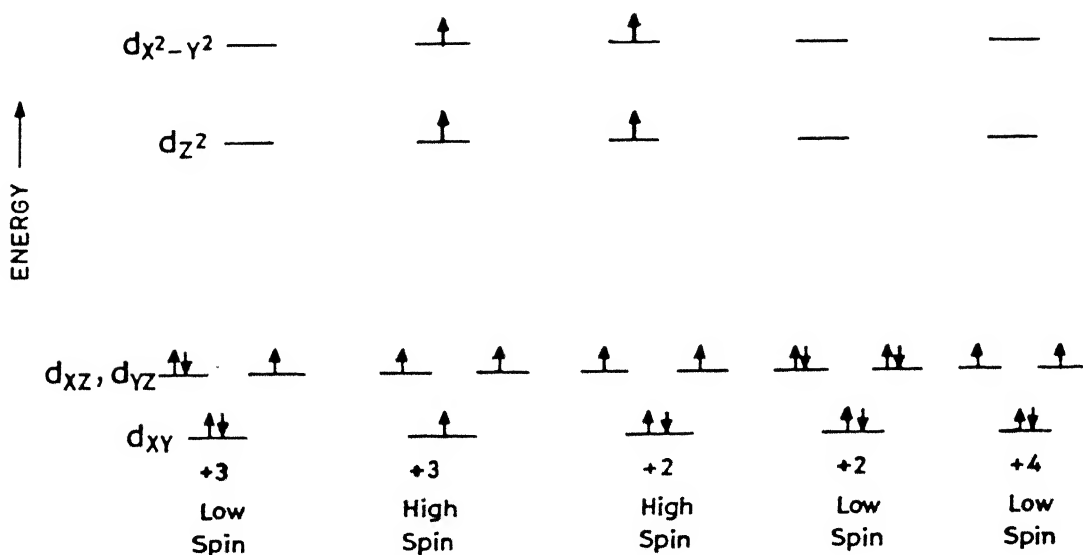


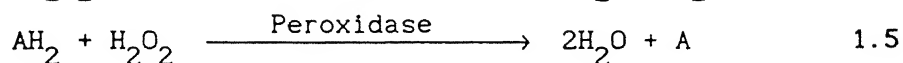
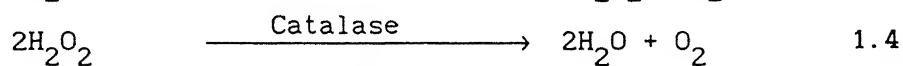
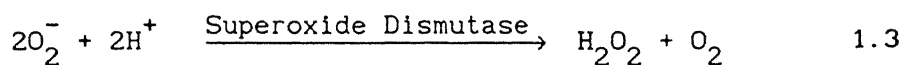
Fig. 1.5 : Electronic structures of iron porphyrin intermediates thought to exist in the cytochrome P-450 catalytic cycle.

Thus the complex cytochrome P_{450} hydroxylation cycle is possible as a consequence of the rich coordination and redox chemistry apparent for iron porphyrins.

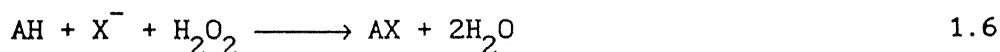
1.2.2 CATALASE, PEROXIDASE AND CHLOROPEROXIDASE

The utilization of oxygen in several biosystems inevitably involves the production of toxic oxygen products, particularly O_2^- and H_2O_2 . Thus, to survive, all aerobic cells must have a

complement of intracellular enzymes whose major activity is to convert O_2^- and H_2O_2 into nontoxic forms of oxygen, O_2 or H_2O as depicted below.



Catalases and peroxidases⁶ protect against the build up of dangerous concentrations of H_2O_2 in living systems as a consequence of only partial reduction of dioxygen. Peroxidases catalyze the oxidation of H_2O_2 in the presence of any organic substrate that undergoes oxidation. Catalases catalyze the disproportionation of H_2O_2 and so may be regarded as a special example of peroxidase activity in which the substrate oxidised by H_2O_2 is another molecule of H_2O_2 . The chloroperoxidase⁷ is unique in its ability to catalyze the hydrogen peroxide dependent oxidation of I^- , Br^- or Cl^- and resultant formation of carbon-hydrogen bonds with halogen acceptors such as β -diketones.



As shown in equation 1.6, the chloroperoxidase catalysed halogenation process occurs with concomitant reduction of H_2O_2 to H_2O .

All these three contain the ferriprotoporphyrin -IX and the catalytic cycle of these are shown in Fig. 1.6. In contrast, ferric and higher oxidation states of iron, the first step of the catalytic cycle involves the resting enzyme in the high spin five coordinate ferric state 1, reacts with hydrogen peroxide to form a

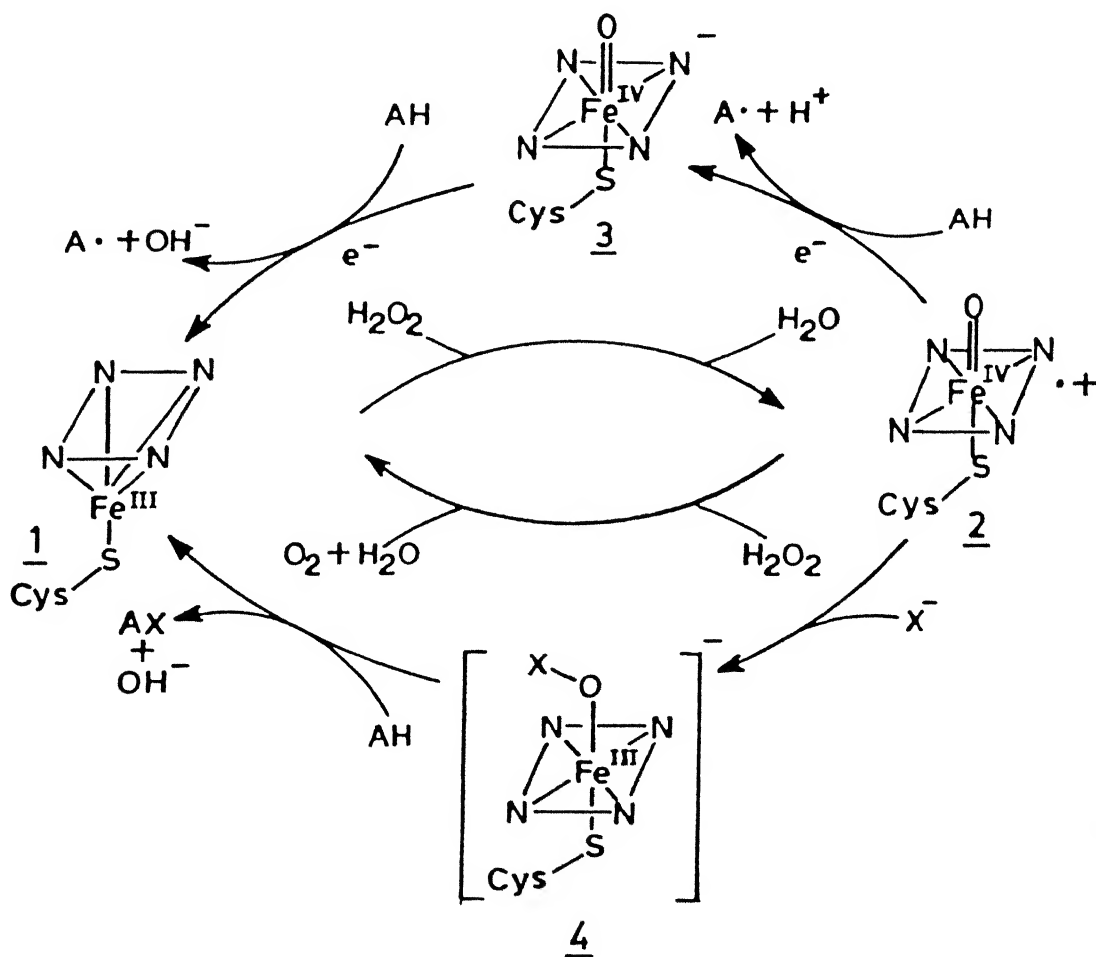


Fig. 1.6 : Catalytic cycles of chloroperoxidase and the postulated structures of the intermediates. The structures of the intermediates in the peroxidase (1 → 2 → 3 → 1) and catalase (1 → 2 → 1) modes have been partially characterized (taken from Ref.7).

high valent iron - oxo derivative known as compound I, which is formally two oxidation equivalents above the ferric resting state. On the basis of extensive spectroscopic and magnetic data the compound I (2) is identified as $\text{Fe}^{\text{IV}} = \text{O}$ (porphyrin radical cation) structure. In the catalase mode, compound I interacts with a second molecule of H_2O_2 , oxidising it to dioxygen and returning the heme iron to the ferric resting state, (1). In the peroxidase mode, compound I (2) serves as a one electron oxidant, converting organic substrates (AH) into radical products (A') with concomitant reduction of compound I to compound II (3), which likely has a $\text{Fe}^{\text{IV}} = \text{O}$ structure. Oxidation of a second substrate molecule regenerates the ferric resting state 1, ready for another round of catalysis. In the chlorination mode, it has been proposed that compound I reacts with chloride to produce a hypochlorite (OCl^-) adduct (4), (also known as X) which serves as the active chlorinating agent.

Thus, the ubiquity of metallo porphyrins in nature and the varied functions they perform suggest that besides modifying metal redox potentials or binding the metal at an appropriate site in the protein, the porphyrin ring itself possess properties necessary for proper biological functions.

1.3 BIOCHEMICAL SIGNIFICANCE OF CHLOROPHYLL DIMERS IN PHOTOSYNTHESIS

The X-ray structure of the reaction centre solved for the *R. viridis* by Deisenhofer and coworkers² suggests that primary electron donor unit at the reaction centre consists of a "special

pair" of Chl a (P700) molecules bridged by two water ligands. Most of the available information related to the function and organization of chlorophyll in photosynthetic organisms has been based on studies of the visible absorption, fluorescence and circular dichroism spectra of intact chlorophyll and various fractionated chloroplast preparations. From the observation that in all condensed forms of chlorophyll (e.g., monolayers, crystals and colloidal solutions) the absorption maximum occurs at lower energy than that of monomeric chlorophyll in solution, and from the fact that chlorophyll *in vivo* exhibits a red shift, it has been suggested that the chlorophyll in green plants occurs in an aggregated state. Although other interactions (chlorophyll-protein interactions) could give rise to the observed red shift, the existence of aggregated chlorophyll *in vivo* seems to have been widely accepted because of several crystal structures solved for chlorophyll and its derivatives. The observed red shifts in the absorption maxima are due to excitonic interactions between two chlorophyll units of the special pair.

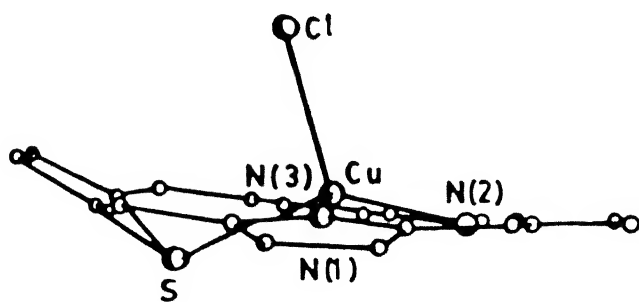
1.4 REVIEW OF LITERATURE

1.4.1 NONPLANAR PORPHYRINS

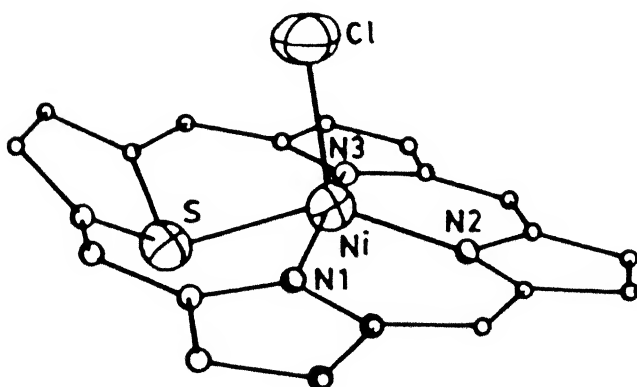
It is now well understood that porphyrin molecule is highly flexible and it is possible to alter the planar structure of porphyrin with slight modification in the porphyrin core or steric crowding at the peripheral substituents attached to the methine (C_m) and β -carbons (C_β). Recently several reports have appeared on nonplanar porphyrins in view of their biological relevance.

Core modified porphyrin derivatives¹⁵ are prepared by substituting nitrogen with heteroatoms such as S, O, Se, Te etc. The general effect of heteroatom substitution alters the interior of the porphyrin skeleton while the external shape relatively remains unaffected as long as the respective heteroatom substituted ring remain near the porphyrin plane. The structures of STPPH and S₂TPP indicates that porphyrin plane is almost planar with a small distortion. Interestingly, metalloderivatives^{15e,1} of heteroatom substituted porphyrins showed severe nonplanarity in the porphyrin ring. The structures solved for various metalloderivatives of monothiaporphyrin (Fig. 1.7) suggests that the thiophene ring is sharply bent out of the N₃ pyrrole core while the pyrrole rings are slightly tipped away from the ring. The thiophene ring had to distort from its intrinsic planar geometry to accomodate the coordination of these metal ions. The bending of the thiophene ring allows this group to coordinate the metal ion in η^1 fashion through sulfur atoms, which acquires a pyrimidal geometry. The limited core size of the macrocycle needs to accomodate the metal ion in folding environment.

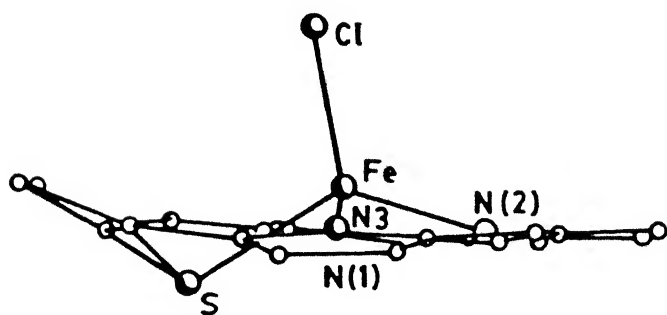
N-substituted porphyrins and metalloporphyrins¹⁶ (Fig. 1.8) showed severe distortion in the porphyrin skeleton. Levallee et.al. have determined the crystal structures of chlorozinc(II) complexes of N-substituted porphyrins such as [Zn(PhTPP)Cl]¹⁷, [Zn(MeTPP)Cl]^{18,19} [Zn(BzTPP)Cl]¹⁹ and also [Fe(MeTPP)Cl]¹⁹ have showed that the three non-N-substituted pyrrole rings are tilted in the direction opposite to that of the N-substituted pyrrole ring to bind a metal ion with similar bond distances. The slants of the three non-N-substituted pyrrole rings are correlated with



(a)



(b)



(c)

Fig. 1.7 : (a) X-ray structure of Cu(II) derivative of tetraphenyl-21-thiaporphyrin (view of the inner core), (b) X-ray structure of Ni(II) derivative of tetraphenyl-21-thiaporphyrin (view of the inner core) and (c) X-ray structure of Fe(II) derivative of tetraphenyl-21-thiaporphyrin (view of the inner core).

the slant of the N-substituted pyrrole ring in the opposite direction. A similar tendency in distortion is observed in the free base porphyrins though the N3 pyrrole ring can be hardly

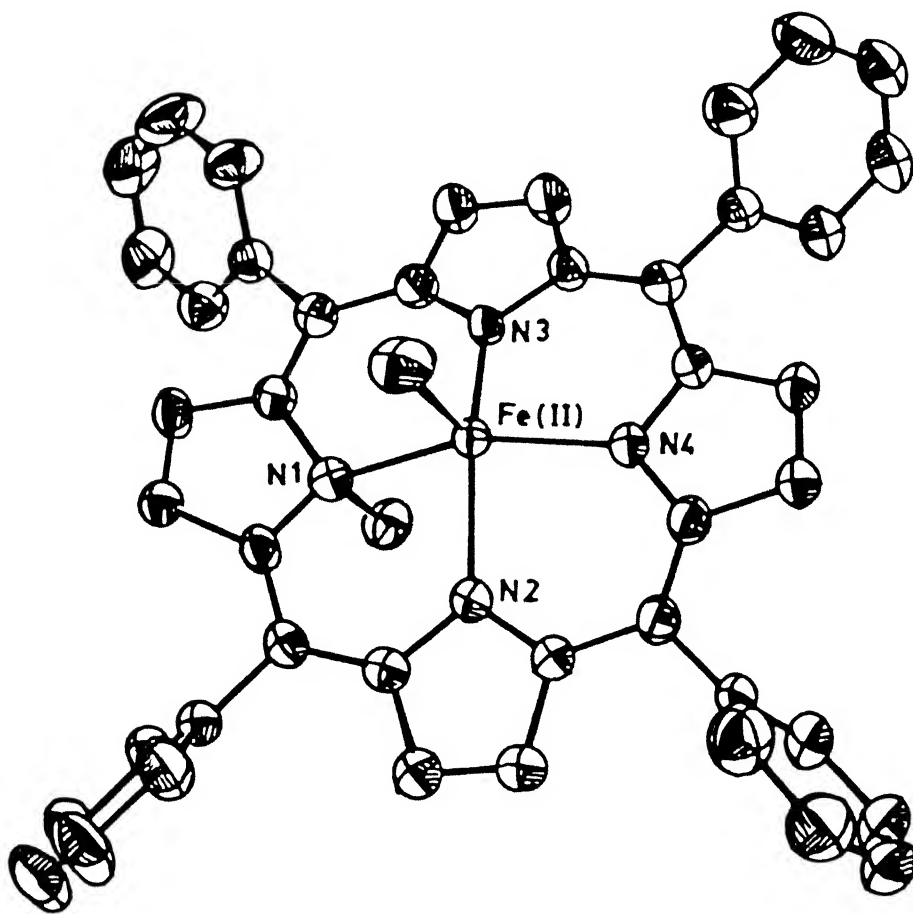


Fig. 1.8 : X-ray structure of Fe(II) derivative of N-methyl-tetraphenylporphyrin.

tilted in the direction opposite to the N1 pyrrole ring without a metal ion being bound. The magnitude of distortion depends on the nature of the substituent. The porphyrin ring system of N-o-tolyl-5,10,15,20-tetraphenyl porphyrin ((H(o-tolTPP)) is

highly distorted from planarity in comparison with that of the N-methylated porphyrin²⁰. The kinetics for metallation of H(o-tolTPP) with Zinc(II) ion has revealed that the distortion of the porphyrin core is favourable to the complexation rate.

The N-substituted pyrrole ring of H(o-tolTPP) (N1 Pyrrole ring) forms the most highly canted plane from the N1-N2-N4 reference plane with a dihedral angle of $57.3(2)^{\circ}$. The two adjacent pyrrole rings (N2- and N4-pyrrole rings) are tilted in the direction opposite to that of the N1-pyrrole ring. The dihedral angles are $19.3(2)^{\circ}$ and $16.4(2)^{\circ}$ for the N2- and N4-pyrrole rings, respectively. The protonated N3-pyrrole ring opposite to the N1-pyrrole ring forms an almost coplanar plane with respect to the reference plane. The dihedral angles of the N1-pyrrole ring and the N2- and N4-pyrrole rings for H(o-tolTPP) are much larger than those of the corresponding rings for H(MeTPPBr₄) (27.7° for the N1 pyrrole ring and 10.2 and 11.3° for the N2- and N4-pyrrole rings, respectively), though the N3-pyrrole ring for H(o-tolTPP) is less canted than that for H(MeTPPBr₄) (8.1°) in the same direction as the N1 pyrrole ring. Consequently, the bulkier N-o-tolyl group compels the porphyrin ring system to be more distorted than the N-methyl group.

Introduction of bulky groups, either electron donating or electron withdrawing groups,²¹ results in distortion in the porphyrin plane. Hursthouse et.al. first reported structure determination of a metal free porphyrin with a single meso substituent. The structure solved for 5-benzoyloxyoctaethyl porphyrin²² clearly exhibited significant ruffling with an alternation in geometry of the central hole, compared to that in

planar porphyrin. This ruffling is most marked for pyrrole rings A and B. These rings are inclined at angles of 6.4° and 3.9° to the mean plane of the four nitrogen atoms, and are at an angle of 9.9° to each other.

Guo-Zhang Wu et.al.²³ synthesized a series of meso substituted octaethylporphyrins and studied their optical and electrochemical properties. The X-ray structure solved for $\text{OEP}(\text{NO}_2)_4$ (Fig. 1.9) and its zinc derivative revealed a severe

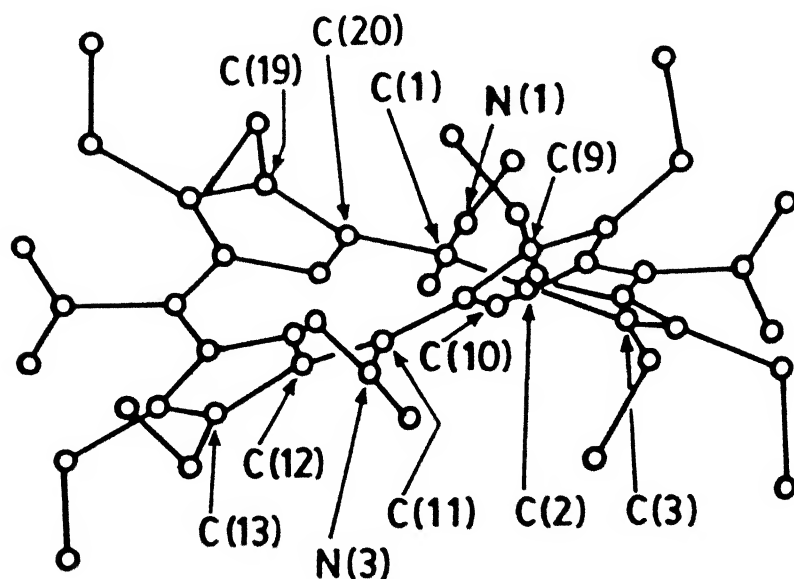


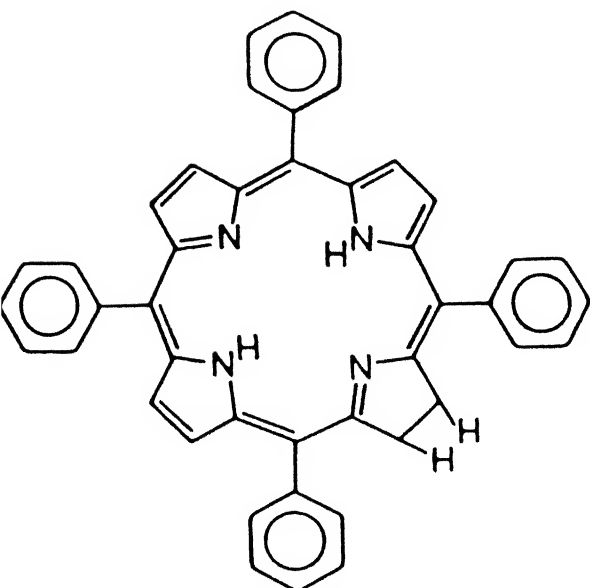
Fig. 1.9 : X-ray structure of $\text{OEP}(\text{NO}_2)_4$.

distortion in the porphyrin ring. The dihedral angle of the two mean planes, C(9), C(10), C(11), C(12), C(13), N(3) and C(2), C(3), C(1), C(19), C(20), N(1) is 45.4° and the nitro group is orthogonal to the plane of the porphyrin nucleus. Corresponding

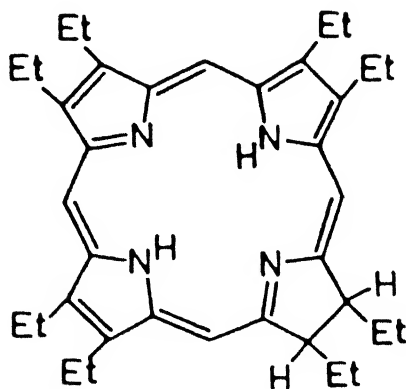
to the great deviation from planarity of the porphyrin nucleus, the absorption bands appear at the longest wavelength of the porphyrins studied here. Cyclic voltammetric studies are also in line with this.

The reduction of the porphyrin ring also leads to deformation as found in chlorins²⁴, bacteriochlorins²⁵ and isobacteriochlorins²⁶ (Fig. 1.10). These reduced rings are highly flexible and can assume a wide range of conformations, influenced in part by the occupancy of the porphyrin pocket. For example, the porphyrin macrocycle of Fe(OEP) is essentially planar while the chlorin macrocycle of Fe(OEC) is significantly S_4 ruffled²⁷. In (5,10,15,20-tetramethyl isobacteriochlorin) nickel(II), (NITMIBC), the isobacteriochlorin macrocycle exhibits an S_4 ruffled conformation and a bond length pattern indicative of reduction in aromaticity, both of which are more pronounced than those found in the corresponding porphyrin ((5,10,15,20-tetramethylporphinato) nickel(II), Ni(TMP) and chlorin (5,10,15,20-tetramethylchlorinato) nickel(II), Ni(TMC) structures²⁸. This reduction in aromaticity is consistent with the ^1H NMR spectra, which point to ring currents in the order Ni(TMIBC) < Ni(TMC) < Ni(TMP). Stolzenberg and coworkers²⁹ in a recent series of papers have related the distorted conformation of nickel hydroporphyrins with stability of the macrocycle. X-ray structural studies show that the macrocycle in nickel hydroporphyrin complexes invariably experiences a marked S_4 ruffling and is saddle shaped.

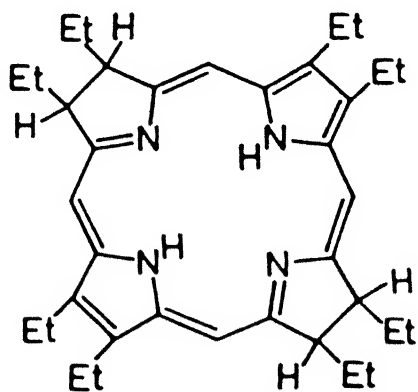
Barkigia et.al.³⁰ and Fajer et.al.³¹ independently considered theoretically the possibility that conformational variations can affect the highest occupied (HOMOs) and lowest unoccupied (LUMOs)



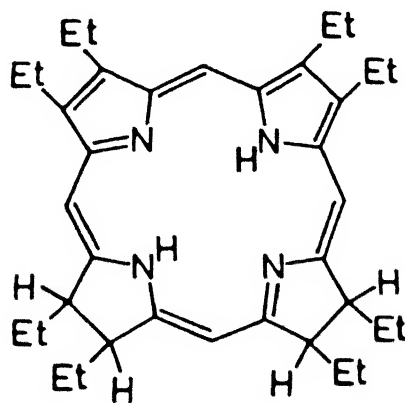
TETRAPHENYLCHLORIN



OCTAETHYL CHLORIN



OCTAETHYL BACTERIOCHLORIN



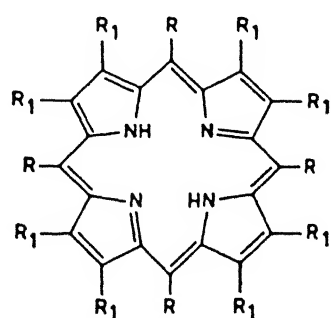
OCTAETHYL ISOBACTERIOCHLORIN

Fig. 1.10 : Structures of various reduced porphyrins.

molecular orbitals of the chromophores and thereby modulate their redox potentials and light absorption properties. This concept was tested by taking a sterically distorted porphyrin of known structure which exhibits experimental optical and redox properties in solution consonant with theory and extend the calculations, using crystallographic data for the *R. viridis* primary donor, to show that a redox assymetry is possible in the Bacteriochlorophyll subunits that comprise the special pair of that bacterium.

Recently several papers appeared on sterically crowded nonplanar porphyrin systems³²⁻³⁴ (Fig. 1.11). The X-ray structures³² of the peripherally crowded porphyrins (2,3,7,8,12,13,17,18-octaethyl-5,10,15,20-tetraphenylporphinato) Zn(II)-3 MeOH solvate (ZnOETPP.3MeOH) and 2,3,7,8,12,13,17,18-octamethyl-5,10,15,20-tetraphenylporphinato) Zn(II)-Pyridine-2 CHCl₃ (ZnOMTPP.Py-2-CHCl₃) are severely nonplanar and assume saddle shapes. ¹H NMR data reveals that the conformational distortions are maintained in solution. The consequences of distorting the macrocycles are significant : optical, redox, basicity and excited state properties are altered in agreement with previous theoretical calculations^{30,31}. These results form part of an expanding body of structural information that clearly demonstrates that porphinoic skeletons are flexible and that distortions of the macrocycles can be imposed by steric interactions *invitro* and *invivo*.

Shelnutt et.al.³³ used molecular mechanics calculations to evaluate the varying degree of nonplanarity present in the porphyrin macrocycle of several recently synthesized nickel porphyrins which bear alkyl or phenyl groups at all twelve

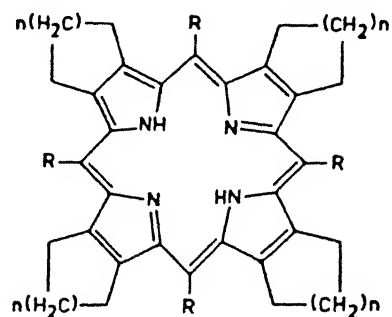


$R = C_6H_5$; $R_1 = CH_3$

$R = C_6H_5$; $R_1 = CH_2CH_3$

$R = C_6H_5$; $R_1 = CH_2CH_2CH_3$

$R = R_1 = C_6H_5$



$n = 1$ $R = C_6H_2(3,4,5-OCH_3)$

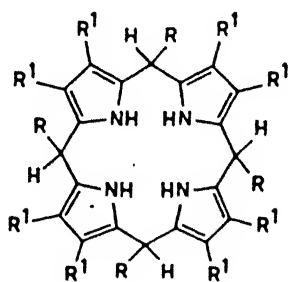
$n = 1$ $R = (CH_2)_4CH_3$

$n = 1$ $R = CH_2CH_3$

$n = 1$ $R = C_6H_5$

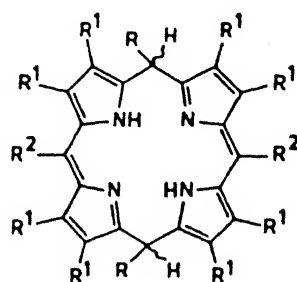
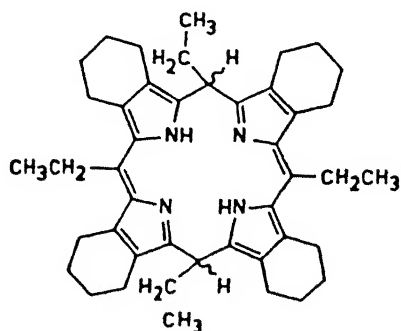
$n = 2$ $R = C_6H_5$

$n = 3$ $R = C_6H_5$



$R = C_6H_5$; $R^1 = CH_3$

$R = C_6H_5$; $R^1 = CH_2CH_3$



$R = CH_3$; $R^1 = CH_2CH_3$; $R^2 = H$

$R = R^2 = C_6H_5$; $R^1 = CH_3$

Fig. 1.11 : Molecular structures of some highly substituted porphyrins.

peripheral positions such as NiOETPP, NiOPTPP, NiDPP, NiTC₆TPP and NiC₇TPP. The structural parameters obtained from these calculations were then used to investigate the relationship between core size and the frequency of the structure - sensitive Raman lines (ν_4 , ν_3 , ν_2 and ν_{19}). All Raman line in NiOATPP normally referred as core-size markers are found to be significantly shifted to lower frequencies with respect to their positions in NiOEP, suggesting that the molecule is in a highly nonplanar conformation.

Very recently, Sparks et.al.³⁴ investigated two more aspects of nonplanarity in the highly nonplanar octaalkyl tetraphenylporphyrins (OATPP). In the first part, the effect of central metal ion on the coformation of the OATPP macrocycle has been determined. Crystallographic studies reveal that the sterically encumbered, nonplanar octaethyl tetraphenyl porphyrin (OETPP), remains sufficiently flexible to show a small decrease in nonplanarity for large metal ions. As the metal size increases, both OEPs and OETPPs exhibit expansion of the meso bridges (increase in the C _{α} -C_m bond length and C _{α} -C_m-C _{α} bond angle) and a movement of the coordinating nitrogen atoms away from the metal atom (increase in the M-N bond length and C _{α} -N-C _{α} bond angle and a decrease in the N-C _{α} bond length). In the second part, a combination of molecular mechanics and INDO/CI molecular orbital calculations predict the optical spectra of a series of highly substituted OATPPs with increasing nonplanar distortion.

Interestingly, structural investigations of copper and nickel complexes of dodecasubstituted porphyrins³⁵ bearing aryl groups at the meso positions (Fig. 1.12) and propeno rings at the

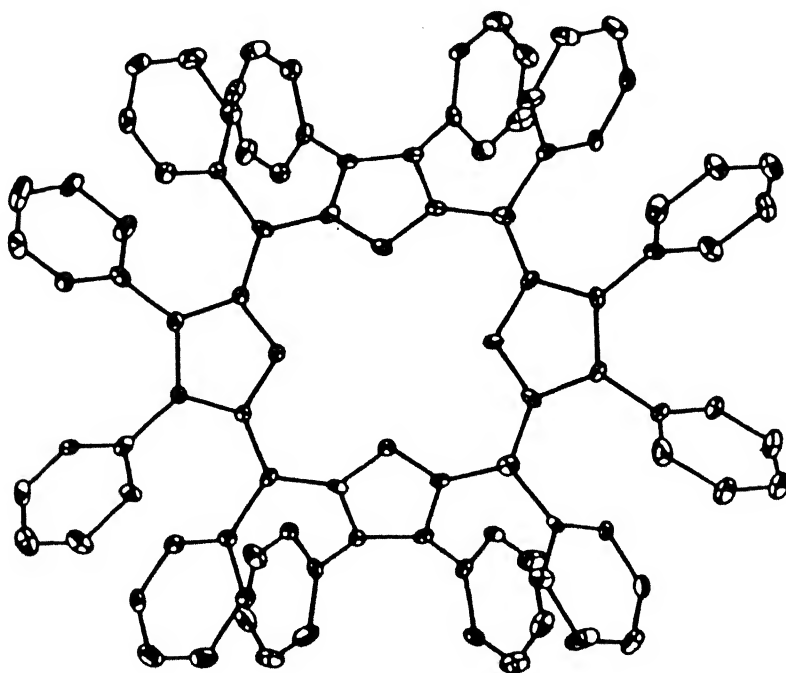


Fig. 1.12 : Molecular structure of Dodecaphenylporphyrin.

β -positions reveal considerable differences in their macrocycle conformations. While the nickel complex $\text{NiTCST}(3,4,5\text{-OMeP})\text{P}$ was found to exhibit a nonplanar conformation which is considerably more planar than that of other dodecasubstituted porphyrins, the corresponding copper complex $\text{CuTCST}(3,4,5\text{-OMeP})\text{P}$ was planar. $\text{CuTCST}(3,4,5\text{-OMeP})\text{P}$ thus represents the first example of a completely planar dodecasubstituted porphyrin. This change which moves the methylene and aryl substituents further apart, effectively removes the steric repulsion responsible for the very nonplanar conformations observed for other dodecasubstituted porphyrins. The identification of a planar dodecasubstituted

porphyrin further indicates the flexibility of the tetrapyrrole macrocycle and has implications for the study of nonplanarity in synthetic porphyrins and metallotetrapyrrole containing biomolecules.

1.4.2 PORPHYRIN π -CATION RADICALS

a) Nature of the Radical

From biochemical importance of cation radicals given in the Section 1.2, it is noted that transfer of an electron to or from the metal as well as porphyrin ring play crucial role in the catalytic cycles of heme proteins^{6,7}.

Early research on porphyrin π -cation radicals was confined to generating various oxidised metalloporphyrins polarographically and electrochemically and characterising them with different spectroscopic techniques³⁶. Optical and ESR spectral studies indicated the possibility of formation of two types of π -cation radicals, A_{1u} and A_{2u} , upon one electron oxidation of porphyrin, depending on the ground state which is lower in energy. Spiro and coworkers³⁷ used resonance Raman spectroscopy extensively for studying molecular and electronic structure in porphyrin radicals. The frequencies of resonance Raman bands are sensitive to the nature of the resonant electronic states. Several studies on resonance Raman spectra have appeared in recent years³⁸. The direction of structurally sensitive Raman bands gives the nature of the porphyrin radical (A_{1u} and A_{2u}) formed. A combined analysis of optical, ESR and Raman spectral studies suggested that generally all MOEP $^{\cdot+}$ are of A_{1u} type and MTPP $^{\cdot+}$ are of A_{2u} type.

b) Development of Synthetic Methods

The chemistry of metalloporphyrin cation radicals gains more momentum when both metal as well as porphyrin ring are redox active. In this type of paramagnetic metalloporphyrin radicals, the correct formulation of the oxidised species is a major concern. Because of biological relevance, more work has been done on iron(III) porphyrins. Wolberg and Manassen^{36c} were first to report the five coordinate FeX(TPP) in which X is a univalent monodentate anionic ligand, and can be oxidised electrochemically to one electron oxidation product $[\text{FeX(TPP)}]^{+\bullet}$. A low spin iron(III) porphyrin π -radical formulation was given to the species. Independent work by Felton, Dolphin, Fajer and coworkers³⁹ confirmed the electrochemical synthesis but proposed high spin Fe(IV) electronic ground state for $[\text{FeCl(TPP)}]^{+\bullet}$, on the basis of UV-vis and ^1H NMR spectroscopy. Later Phillippi and Goff⁴⁰ challenged these conclusions based on electrochemical and chemical methods and suggested a reinterpretation of the earlier work⁴¹. It turns out that the singly oxidised species derived from FeCl(TPP) and FeCl(OEP) are better formulated as high spin iron(III) porphyrin π -cation radicals rather than iron(IV) complex. To confirm this, they looked for the development of better synthetic procedure to prepare iron(III) porphyrin π -cation radicals and characterized them completely. Gans et.al.⁴² for the first time synthesized, isolated and characterized $\text{FeCl(TPP)}(\text{SbCl}_6)$ by stirring a solution of FeCl(TPP) with a stoichiometric amount of phenoxathiin hexachloroantimonate in dry CH_2Cl_2 followed by filtration, precipitation with hexane and recrystallisation in 1,1,2,2-tetrachloroethane-hexane. Magnetic

susceptibility, ^1H NMR and Mössbauer studies indicated a spin coupled Fe(III) porphyrin radical cation state.

Shimomura and coworkers⁴³ came out with much easier way for identification of metal vs porphyrin ring centered oxidation using infrared spectroscopy. By systematically studying on various oxidised metalloporphyrins using IR, they concluded that a diagnostic porphyrin ring centred IR active mode is present at $\sim 1280\text{ cm}^{-1}$ in all $\text{TPP}^{\cdot+}$ complexes and at $\sim 1550\text{ cm}^{-1}$ in $\text{OEP}^{\cdot+}$ complexes which offers an apparently simple unique criterion for formulating the electronic structures of oxidised metalloporphyrins.

(c) Structures

The structures of a number of π -cation radicals⁴⁴⁻⁴⁸ have been solved to understand the type of structural change occurring in the porphyrin ring by abstraction of an electron from π -electron cloud. Surprisingly, an unusual D_{2d} ruffled core is found in several of these π -cation radicals as shown in Fig. 1.13. The D_{2d} ruffled core in these so called saddle shaped species has the pyrrole rings displaced alternatively, above and below the mean plane of the core. The meso carbon atoms are found to be in or nearly in the plane of the core. This conformation differs from the more usual D_{2d} ruffled core by a 45° rotation of the point group symmetry operators around the major two fold axis (perpendicular to the mean plane).

A summary of the structural parameters of the metal complexes of known structures are given in table 1.1. From this data, it is clear that all these species are dimers in the solid state with strong π - π interactions in such a way that the two porphyrin rings

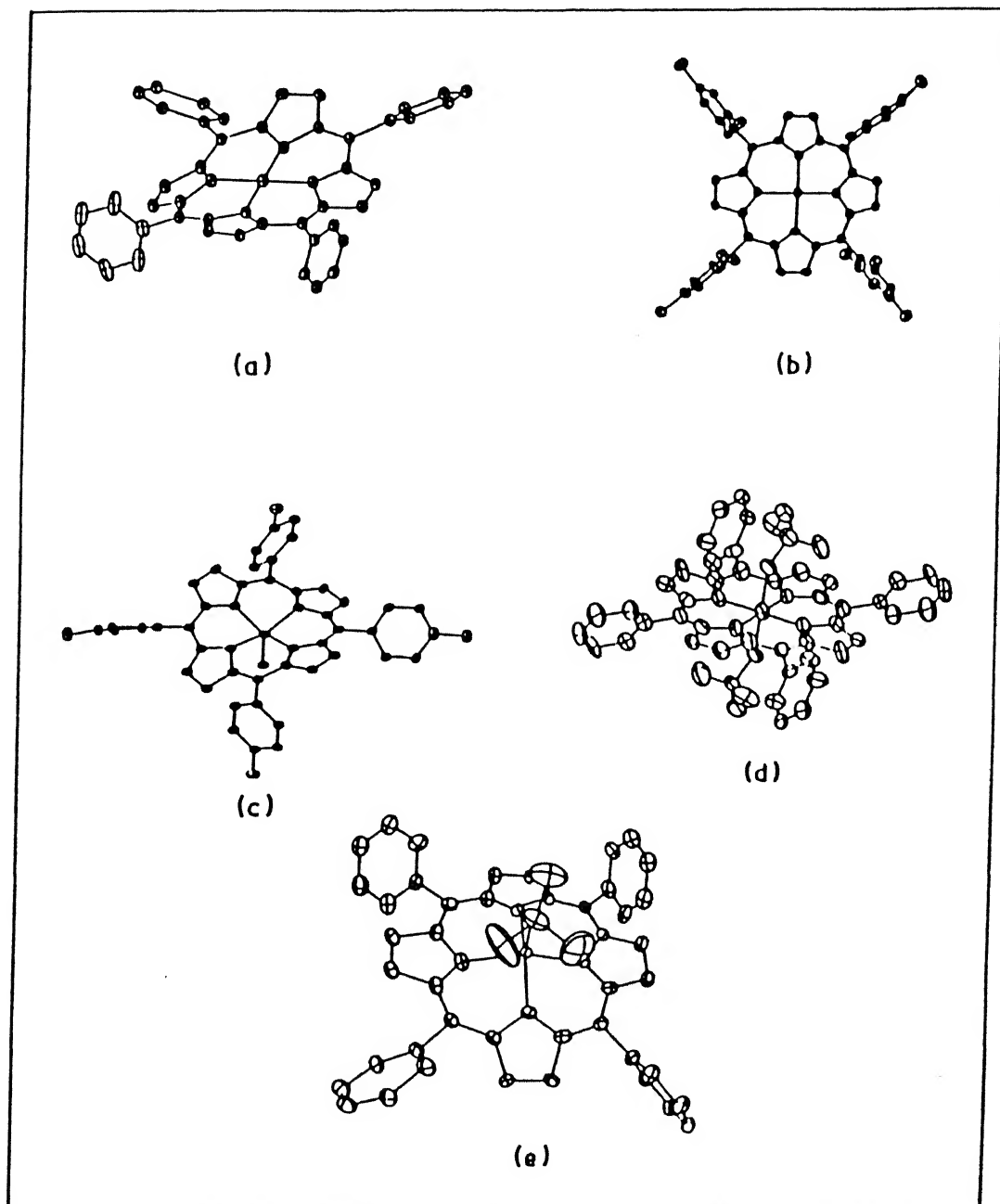


Fig. 1.13 : X-ray structures of (a) $[\text{CuTPP}'][\text{SbCl}_6]$,
 (b) $[\text{CuTMP}'][\text{SbCl}_6]$, (c) $[\text{FeTPPCl}'][\text{SbCl}_6]$,
 (d) $[\text{FeTPP}(\text{OCIO}_3)_2]$ and (e) $[\text{MgTPP}(\text{OCIO}_3)]$.

have individual pyrrole rings nesting into each other. The dihedral angles (average value 41.5°) between meso aryl groups and porphyrin core are exceptionally small to help the dimer formation in these species. Reed and coworkers expressed the view that unusual saddle shaped S_4 ruffled porphinato core observed in the π -cation radical species is a necessary molecular distortion required to allow dimerisation and not an intrinsic property resulting from some distinctive electronic state of the π -cation.

Table 1.1 : Stereochemical parameters of π -cation complexes (\AA°)

Complex	Type	M-N _p	Ax, M-Ax	M-C _t	M-M	Ref
ZnTPP(OCIO ₃)	Dimer	2.076	0, 2.079	0.34	6.932	46
MgTPP(OCIO ₃)	Dimer	2.096	0, 2.012	0.52	7.193	46
[CuTPP] ^{•+}	Dimer	1.988	-	0.06	5.433	44
[FeTPPCl] ^{•+}	Dimer	2.070	Cl, 2.168	0.37	5.393	45
FeTPP(OCIO ₃) ₂	Monomer	2.045	0, 2.130	0	-	45

This argument is supported by the observation that the same type of conformation exists in a number of neutral TPP derivatives. Another important feature should be noted that all cation radical species with saddle conformation and substantial C_b displacements are binuclear or four or five coordinate species. This fact clearly allows for strong interporphyrin interactions in the solid state leading to saddle conformation and this feature is not likely to be present in species with axial ligands on both sides of the species as observed in Fe(TPP)(OCIO₃)₂⁴⁵ which is planar. Saddle conformation will not be possible for meso aryl species

with sufficiently bulky ortho substituents that do not allow near coplanarity of the peripheral aryl groups as observed in planar $[\text{CuTMP}][\text{SbCl}_6]^{49}$, in which the ortho methyl substituents on the TMP (Tetramesityl porphyrin) ligand are expected to provide steric hindrance to prevent the type of π - π solid state aggregation in the TPP derivatives.

Magnetic Properties

In recent years much attention has been paid to the magnetic properties of π -cation radicals of paramagnetic metalloporphyrins. The core conformations of π -cation radicals may have profound influences on the observed magnetic properties^{45,47,50,51}. When a paramagnetic metalloporphyrin complex is oxidised to a π -cation radical, the opportunity exists for magnetic interactions between the unpaired electrons of the metal and the ligand. If the unpaired electrons are far off, they remain as noninteracting spins but if they are in proximity, they interact either antiferromagnetically or ferromagnetically. Extensive studies on paramagnetic metalloporphyrin π -cation radicals revealed the importance of porphyrin core conformation on magnetic properties. The common observation is that, all planar porphyrin cores lead to ferromagnetic coupling and nonplanar prophyrin cores show antiferromagnetic coupling. The ferromagnetic interaction between the metal and ligand spins is conceptually the same as Hund's rule of maximum multiplicity. It differs only in that the orbitals are not exactly degenerate. The exchange interaction between the unpaired electrons, which because of their mutual proximity must feel of each others presence but are forbidden by symmetry to overlap, gives rise to the higher multiplicity.

When the metal and ligand orbitals can undergo a symmetry allowed overlap, as observed in ruffled core metalloporphyrin π -cation radicals, an antiferromagnetic coupling is observed. This is conceptually indistinguishable from bond formation whereby a metal electron and a ligand electron are spin paired in a bonding molecular orbital. The spin state of lower multiplicity is lower in energy. Since, energetically, overlap terms quickly dominate over exchange terms, it is likely that rather little departure from strict orthogonality producing symmetry is required for antiferromagnetic coupling to dominate over ferromagnetic coupling. It may be possible eventually to manipulate this trade-off of opposing effects to identify and control the type of interaction desired. The variable of particular d orbital occupation, A_{1u} or A_{2u} type of radical, porphyrin symmetry and lattice symmetry suggest a rational way of approaching this problem.

Goff and coworkers^{40,42,52} extensively used paramagnetic NMR in identifying the nature of coupling present between the unpaired electron present on the metal and porphyrin ring, in metalloporphyrin π -cation radicals. NMR spectroscopy does probe the environment of protons at the extreme periphery of the ligand; the chemical shifts of these protons are strongly influenced by the spin state of the metal ions. The downfield ortho, para protons and upfield meta protons is a characteristic feature observed in antiferromagnetically coupled metalloporphyrin π -cation radicals in contrast to upfield ortho, para protons and downfield meta protons in ferromagnetically coupled systems. The difference in these phenyl proton shifts are due to different spin

density at the methine and pyrrolic carbon atoms based on A_{1u}/A_{2u} type of radical.

d) Cation Radicals of Porphyrin Dimers

Recently two papers^{53,54} appeared on the preparation and characterization of singly oxidised metalloporphyrin dimers. These dimers possess a single electron hole per pair of porphyrin rings with a hole delocalised over two porphyrin rings. The crystal structure solved for Ni and Cu dimers of $[\text{MOEP}^{\cdot/2}]_2^+$ shows that the deviations from exact planarity in the unique porphyrin core of $[\text{Cu}(\text{OEP}^{\cdot/2})_2]^+$ are small but nonzero whereas the porphyrin core in the $[\text{Ni}(\text{OEP}^{\cdot/2})_2]^+$ cation radical displays S_4 ruffling.

In a very recent paper⁴², Tokita and coworkers prepared a novel dioxoruthenium(VI) porphyrin cation radical and carried out oxidation reactions of diphenyl sulfide and some olefins. The results show that the π -cation radicals exhibit greater reactivity than neutral derivatives and reactivities for A_{2u} type of radicals are greater than A_{1u} type radicals.

1.5 AIM OF THE PRESENT STUDY

The previous sections clearly indicated the preference for the nonplanar conformations of the porphyrin ring in many biomolecules, the importance of magnetic interactions in paramagnetic metalloporphyrin π -cation radicals and the presence of excitonic interactions between two chlorophyll units of special pair at the reaction center of photosynthesis and its effect on spectral properties. This thesis aims at a better understanding of all these aspects by synthesising and studying simple model

porphyrin compounds. The thesis is divided into three parts: Part I describes the effect of nonplanarity in the porphyrin skeleton on the ground and excited state properties. The nonplanarity of the porphyrin skeleton is due to the introduction of a short bridging group across the porphyrin periphery. Part II describes magnetic interactions between unpaired electron in the metal and unpaired electron in the porphyrin ligand in Cu(II) and high spin Fe(III) deformed porphyrins. Part III describes the electronic interactions between the porphyrins which are oriented in a face to face geometry. The face to face orientation in this species are induced by addition of crown ethers and alkali metal cations. The spectroscopic changes observed upon dimer formation in these systems has been explained on the basis of exciton formalism.

CHAPTER 2

GENERAL EXPERIMENTAL METHODS AND TECHNIQUES

In this chapter the general materials employed at different stages of the investigation are presented. A description of the synthetic methodology of the various precursor compounds used for the synthesis of porphyrins described in this thesis and purification procedure of all the chemicals and solvents are also given. This chapter is concluded with the brief description of various instruments used and methods for the calculation of various parameters studied in this thesis.

2.1 MATERIALS EMPLOYED

Pyrrole, Benzaldehyde, Salicylaldehyde, 1,5-dibromopentane and 1,6-dibromohexane were procured from Aldrich Chemical Company, USA and all were distilled prior to use.

Deuterated solvents CDCl_3 , CD_2Cl_2 and Crown ethers 18-Crown-6, 15-Crown-5 and 12-Crown-4 were also obtained from Aldrich Chemical Company, USA and all were used as received.

m-Xylene, p-xylene, trifluoroacetic acid, Tetrabutylammonium

bromide and Tris(4-bromophenyl)ammonium hexachloroantimonate were procured from Merck Chemical Company, W. Germany, and were used as received.

Buffer tablets, anhydrous potassium carbonate, sodium dithionate, potassium chloride, sodium chloride, lithium chloride and sodium hydroxide were obtained from Qualigens Fine Chemicals, Bombay, India and were used as received.

Imidazole, 1-methylimidazole, 2-methylimidazole and 4-methylimidazole were obtained from Sigma Chemical Company, USA and were used without further purification.

Aluminium oxide (basic and neutral), silica gel (60-120 mesh), iron powder and ammonium acetate were purchased from Acme Laboratory Chemicals, Bombay, India and were used as received.

N-bromosuccinamide, bromine, propionic acid, anhydrous sodium sulfate, anhydrous calcium chloride, conc. H_2SO_4 , conc. HCl were procured from S.D. Fine Chemicals, India.

The surfactants, sodium dodecyl sulfate, cetyltrimethylammonium bromide and Triton X-100 were purchased from B.D.H. Chemical Company, India.

Water-soluble porphyrins ($\text{H}_2\text{tcp}^{4-}$ and $\text{H}_2\text{tpps}^{4-}$) and their metallo derivatives (Ni^{2+} , Cu^{2+} and Zn^{2+}) were procured from Strem Chemicals, USA.

2.2 METAL SALTS EMPLOYED

Nickel(II)acetate tetrahydrate, Copper(II)acetate monohydrate and Zinc(II)acetate dihydrate were of A.R. grade obtained from

S.D. Fine Chemicals, India and were used as received.

2.3 SOLVENTS EMPLOYED FOR SPECTROSCOPIC MEASUREMENTS

- (a) Dichloromethane⁵⁵ (L.R. grade) from S.D. Fine Chemicals, India, was washed twice with 10% aqueous Na_2CO_3 solution, twice with water, dried over anhydrous calcium chloride overnight, distilled over P_2O_5 and stored over molecular sieves (4 Å).
- (b) Chloroform⁵⁵ (A.R. grade) from S.D. Fine Chemicals, (India) was distilled over P_2O_5 .
- (c) Benzene⁵⁵ (L.R. grade) from S.D. Fine Chemicals, India was stirred with conc. H_2SO_4 for 4 h. It was then washed with sodium bicarbonate solution followed by water. It was dried over anhydrous CaCl_2 overnight, distilled and stored over sodium wire.
- (d) Dimethylformamide from S.D. Fine Chemicals, India was distilled under reduced pressure and stored over molecular sieves.
- (e) Double distilled water was used for all studies in aqueous medium.

Methanol, Diethyl ether, Petroleum ether (60–80°C), Toluene and Tetrahydrofuran used at various stages of this work were procured from Qualigens fine chemicals, India.

2.4 SYNTHESIS OF PRECURSOR COMPOUNDS

2.4.1 SYNTHESIS OF 1,4-DIBROMOBUTANE⁵⁵

250g (170 ml) of 48% hydrobromic acid and 75g (41 ml) of concentrated sulphuric acid were taken in a 500 ml round-bottomed flask and 18.1g (20.5 ml, 0.25 mol) of redistilled tetrahydrofuran

(b.p. 65-66°C) was added. The reaction mixture was refluxed gently for 3h. The lower dibromide layer was separated and washed successively with water, 10% sodium carbonate solution, water and dried over anhydrous magnesium sulfate. The 1,4-dibromobutane was distilled and collected at 83-84°C/ 12mm Hg.

Yield : 60%

^1H NMR (CDCl_3) : 2.1 ppm (4H, $\beta\text{-CH}_2$), 3.4 ppm (4H, $-\text{CH}_2\text{Br}$).

2.4.2 $\alpha,\alpha',2,3,5,6$ -Hexabromo-p-xylene⁵⁶

2,3,5,6-Tetrabromo-p-xylene (1.0g, 2.37 mmol) was dissolved in carbon tetrachloride (100 cm^3) in a three-necked flask (500 cm^3) fitted with a dropping funnel (the tip of which extended to almost the bottom of the flask) and an efficient condenser leading to a gas absorption trap. The flask was heated with vigorous stirring and was illuminated with lamps (3x200 W) placed 50 cm from its upper portion. When the temperature of the oil bath reached 125°C, bromine (0.27 cm^3 , 5.22 mmol) was added dropwise over a period of 1 h. Stirring was continued at 125°C under illumination for additional 30 min. The mixture was then cooled to 60°C and poured into a beaker containing boiling light petroleum ether (100 cm^3). The solution was cooled slowly to room temperature with occasional stirring to prevent caking of the brown crystalline product which separated. The product was filtered off and washed thoroughly with light petroleum (60-80°C). It was recrystallised from chloroform-ethanol (3:1 v/v).

Yield : 62%

^1H NMR (CDCl_3) : 4.99 ppm (s, 4H, CH_2).

2.4.3 α,α' ,Dibromo-2,4,5,6-Tetrachloro-m-xylene⁵⁶

This was prepared from 2,3,5,6-Tetrachloro-m-xylene (1g, 4.09 mmol) and bromine (0.5 cm³, 9.01 mmol) following the above procedure.

Yield : 78%

¹H NMR (CDCl₃) : 4.8 ppm (s, 4H, CH₂).

2.4.4 α,α' ,Dibromo-m-xylene⁵⁶

m-Xylene (53g, 0.5 mmol) was placed in a 250 ml three necked round bottomed flask. Same procedure described above was followed with the addition of bromine (176g, 1.1 mmol) being completed over a period of 1 hour.

m.p. : 75-77°C

Yield : 48%

¹H NMR (CDCl₃) : 4.43 ppm (s, 4H, CH₂), 7.23 ppm (m, 4H, Ph).

2.4.5 $\alpha-\alpha'$, Dibromo-p-xylene⁵⁶

m.p. : 145-147°C

Yield : 60%

¹H NMR (CDCl₃) : 4.4 ppm (s, 4H, CH₂), 7.3 ppm (m, 4H, Ph).

2.4.6 Preparation of Tetrabutylammonium perchlorate (TBAP)

50g (0.16 mole) of tetrabutylammonium bromide was dissolved in 500 ml of distilled water and a white precipitate was obtained on addition of 31.2g (0.31 mole) of perchloric acid. The precipitate was filtered and the crude product was washed with large excess of water to remove excess perchloric acid. The crude product was recrystallised from ethanol and pure white crystalline

tetrabutylammonium perchlorate was obtained.

2.5 PHYSICO-CHEMICAL TECHNIQUES

The details of the instruments used for characterization and evaluation of spectroscopic data are presented below.

Electronic spectra were recorded on a SHIMADZU UV-160 spectrometer or Perkin-Elmer Lambda-2 spectrophotometer with an adjustable temperature unit.

Infrared spectra were recorded on a Perkin-Elmer model 580 spectrometer.

FAB mass spectra were recorded using a Jeol SX-120/DA-6000 mass spectrometer using Argon (6 KV, 10 mA) as the FAB gas. The accelerating voltage was 10 KV and the spectra were recorded at room temperature with m-nitrobenzyl alcohol as the matrix unless otherwise specified.

Electron paramagnetic measurements were made on a Varian E-109 X-band spectrometer at room temperature and at liquid nitrogen temperature.

Proton NMR spectra were recorded on Bruker WP-80 FT NMR spectrometer (80 MHz) and Bruker WM-400 FT NMR spectrometer (400 MHz).

Fluorescence spectra were recorded on a Perkin-Elmer LS 50 B luminescence spectrofluorimeter interfaced to a computer or on a Spex Ramalog System with Spex Photon counting and Spectra Physics model 165 Argon ion laser ($\lambda_{exc} = 528 \text{ nm}$) as the excitation source. The data analysis was done using the fluorescence data

manager programme.

Cyclic voltammetric studies were made with a BAS model CV-27 polarographic analyser utilising the three electrode configuration consisting of a Glassy carbon (working electrode), platinum wire (auxillary electrode) and Ag/AgCl (reference electrode) electrodes. An omnigraphic model 100 X-Y recorder was used to record the current-voltage output and/or Coulometric experiments were conducted on a PAR model 370 polarographic analyser utilizing the three electrode configuration of a platinum (BAS) as the working electrode. A RE 0074 X-Y recorder was used to record the current-voltage output. Half-wave potentials were measured as the average of the cathodic and anodic peak potentials.

The triplet ESR measurements were made on VARIAN E-9 X-band spectrometer. The spectra were recorded with and without field modulation at -150°C . The pulsed laser (wavelength 560 nm) source was used for photoexcitation. In method (A) the field modulation used was 100 KHz and light intensity modulation of 80 Hz with detection employing a pair of lock-in-amplifier tuned to the modulation frequencies. The field modulation amplitude employed was 40 G and the microwave power about 5 mW. The ESR signals were measured 0.5 μs after laser excitation. The spectra were recorded in the derivative form, and by using light modulation a doublet radical signal in the center of the spectrum is removed. Also, this detection method takes advantage of the signal enhancement provided by spin polarization. In the method B, no field modulation was used and the signal was detected after 1 μs of the laser excitation; with this technique the signal to noise ratio is

improved because of the large spin polarisation in the triplets shortly after their formation. The spectra were obtained in this method using absorption mode (not derivative mode).

The Raman spectra were excited by 457.9 nm radiation from a Spectra-Physics Model 2030-15 argon ion laser. A spex model 1415 excitation filter was used to filter out the plasma lines from the exciting line. The light, steered through a long optical path with the help of a series of mirrors and lens, enters the periscope assembly. The light leaves the periscope assembly to fall on the input lens (10X or 40X) of the Spex Model 1482 D Micromate on to the sample. The back-scattered radiation excited by ca. 8 mW incident radiation on a 0.5 μm diameter spot of the sample is viewed by the television camera through a filter on the visual display unit. Alternatively, the back-scattered radiation is collected and made to fall on the entrance slit of a Spex Model 1877D Triplemate fitted both with a liquid nitrogen-cooled charge-coupled multi-channel detector (CCD) and a photomultiplier tube (RCA C31034) for single-channel detection placed at the side exit slit of the scattering spectrophotometer assisted by a DM-3000 computer. The Triplemate consists of a filter and spectrograph stage. The filter stage has two modified Czerny-Turner spectrometers coupled in a subtractive mode, each using a 50 x 50 mm plane grating having 600 lines mm^{-1} and giving a bandpass of about 1100 cm^{-1} on 5 mm intermediate slit readings. In the spectrograph stage an asymmetric Czerny-Turner mount with a 64 x 64 mm^2 plane grating with 1200 lines mm^{-1} is used to produce a dispersion of 1.4 nm mm^{-1} , limiting the CCD spectral coverage to ca. 600 cm^{-1} owing to CCD length of 12.5 mm, although a focal

plane of 25 x 10 mm (high) could be obtained in this system. The spectra are reproducible to within $\pm 2 \text{ cm}^{-1}$ with a resolution of 2 cm^{-1} for one particular scan setting of the spectrometer.

The solution magnetic susceptibility measurements were made by the NMR method with a JEOL PMX-60 (60 MHz) spectrometer.

Variable temperature magnetic susceptibilities on powder were measured between 80-300 K on a computer controlled Faraday Magnetometer of models 300 and 321, George Associates, Berkeley, California, USA. A data translation A/D board and AT computer were used to monitor the microbalance output and temperature readings. The instrument was calibrated with a $\text{Hg}[\text{Co}(\text{NCS})_4]$ and had absolute accuracy of 0.5%. The raw data was corrected for the susceptibility of the holder and diamagnetism of the ligands (8.72×10^{-6} cgs units).

Molecular mechanics calculations were carried out using MOBY's geometry optimization programme. The computation of energies according to the classical force field is based on the AMBER forcefield. The parametrization has been derived for the treatment of protein and nucleic acid structures. In the original parametrization and in the form in which it is implemented in MOBY version 1.40 hydrogen atoms which are bound directly to carbon atoms are not explicitly considered but instead are incorporated into the parameter for each carbon atom (united atom approximation).

The force field calculations are performed only on the fragment (ant not root) centres, and are limited to a maximum of 150 centres. However, for each of these centres the complete

interactions in all existing centres (fragment and root) are computed exactly, so that the calculated energy value gives the current energy of the fragment center in the field of all centres.

MOBY's geometry optimization provides the ability to relax a structure and fit it into the MOBY forcefield. In addition, the effects of changes to an already optimized structure e.g., by exchange of groups within an existing system can be studied by means of geometry optimization.

MOBY offers two techniques for geometry optimization : steepest descent and Fletcher-Powell. Both techniques utilise energy gradients based on the cartesian coordinates of the center in order to minimise the potential energy of the system. The optimisation is divided into two operations : first the gradient is calculated at the current geometry in order to fix a direction in $3N$ dimensional space (N = no. of centres), in which the potential energy minimum is determined (Line Search). Second, the resulting geometry is used as the starting geometry for the next minimization step. These two steps (optimization cycle) are repeated until one of the completion conditions is satisfied.

The identification code of each center which serves to select the forcefield parameter is based on the atomic number of the center and the current number of neighbours is given as supplementary material at the end of the thesis.

2.6 METHODS OF ANALYSIS

2.6.1 Fluorescence yield

The fluorescence quantum yield, ϕ_f , of the various basket

handle porphyrins studied in this thesis were estimated from the emission and the absorption spectra by a comparative method following the equation,⁵⁷

$$\phi_f = \left\{ \frac{[F(\text{BHP})][A(\text{standard})]}{[F(\text{standard})][A(\text{BHP})]} \right\} \phi_f(\text{standard}) \quad 2.1$$

where $[F(\text{BHP})]$ and $[F(\text{standard})]$ are the integrated fluorescence intensity of the corresponding basket handle porphyrin and standard respectively and $[A(\text{BHP})]$ and $[A(\text{standard})]$ are the absorbance of basket handle porphyrin and standard respectively at the excitation wavelengths and $\phi_f(\text{standard})$ represents the quantum yield of the standard sample.

Free base tetraphenyl porphyrin⁵⁸ (H_2TPP , $\phi_f = 0.11$) was used as the standard for free base derivatives and their dications while ZnTPP ⁵⁹ was used as standard ($\phi_f^{S_1} = 0.033$ and $\phi_f^{S_2} = 0.00039$) for the Zn^{2+} derivatives of basket handle porphyrins.

2.6.2 Excited State Potentials

lib. No. A. 117954

The excited state redox potentials were estimated from the emission spectra and the ground state redox potentials following the relation⁶⁰

$${}^*E^\circ(\text{P}^+/\text{P}) = E^\circ(\text{P}^+/\text{P}) - E_{0-0}(\text{P}^-\text{P}^*) \quad 2.2$$

$${}^*E^\circ(\text{P}^-\text{P}^*) = E^\circ(\text{P}/\text{P}^-) + E_{0-0}(\text{P}-\text{P}^*) \quad 2.3$$

where $E_{0-0}(\text{P}-\text{P}^*)$ is the energy of the $Q(0,0)$ transition of the emitting excited state of the porphyrin, ${}^*E^\circ(\text{P}^-\text{P}^*)$ and ${}^*E^\circ(\text{P}^+/\text{P})$ are the excited state reduction and oxidation potentials respectively and $E^\circ(\text{P}^+/\text{P})$ and $E^\circ(\text{P}/\text{P}^-)$ refer to ground state

oxidation and reduction potentials respectively.

2.6.3 Magnetic Susceptibility

The solution magnetic susceptibility were measured using the method described by Evans⁶¹, by which one observes the paramagnetic relative shifts of the solvent signal (CD_2Cl_2) in complex solution and pure solvent using the equation

$$\text{Mass susceptibility } \chi_M = \frac{3\Delta f}{2\pi f m} + \chi_o + \frac{\chi_o (d_o - d_s)}{m} \quad 2.4$$

where Δf is the frequency separation between two dichloromethane peaks in Hz, f is the frequency at which the proton resonances are being studied in Hz, m is the mass of the substance contained in 1 ml of solution, χ_o is the mass susceptibility of the solvent, d_o is the density of the solvent and d_s is the density of solution. The last term in equation 2.4 is negligible for highly paramagnetic substances and hence can be ignored.

The magnetic moment was calculated using the equation

$$\mu = 2.84 \sqrt{\chi_M T} \quad 2.5$$

where χ_M is the molar magnetic susceptibility and T is the temperature of the NMR probe used. The solvent susceptibilities were taken from literature.

2.7 SUMMARY

A brief account of various solvents, chemicals and methods of preparation of the different starting materials used in the synthesis and studies is presented here. This chapter also describes the different spectrometers and other physical methods used in the present study.

CHAPTER 3

SHORT CHAIN BASKET HANDLE PORPHYRINS: SYNTHESIS, STRUCTURE, OPTICAL AND ELECTROCHEMICAL PROPERTIES

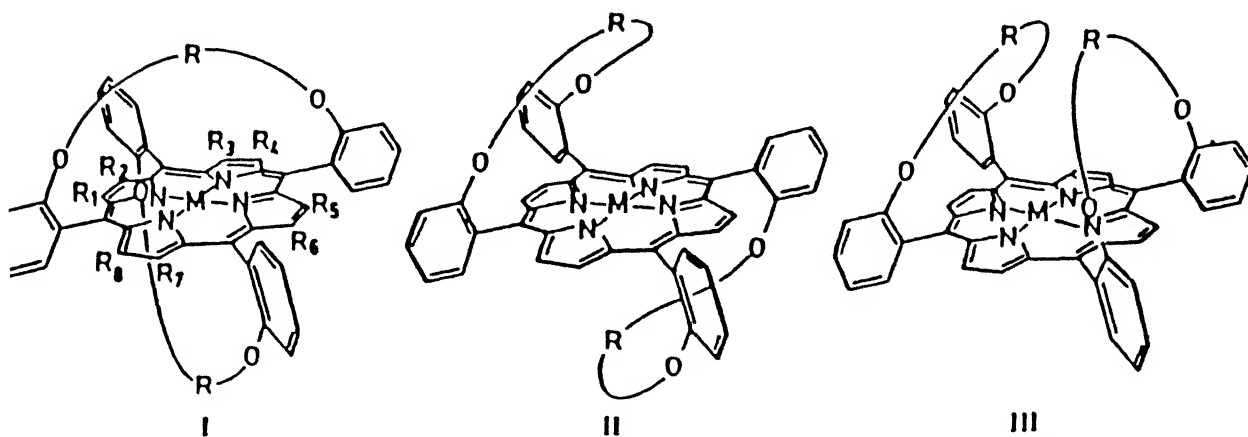
3.1 INTRODUCTION

The importance of nonplanar conformations of porphyrin ring in biology is highlighted in Chapter 1. The large body of structural data in literature clearly indicates the porphyrin rings ability to adopt a variety of nonplanar conformations. Recent attempts to correlate the structure of porphyrin with the biological function has led into intense research activity on synthesis and studies on porphyrins in a variety of nonplanar conformations. This has resulted in synthesis of several unusual porphyrins such as crowned⁶², picketfence⁶³, strapped⁶⁴, capped⁶⁵, sterically heavily substituted³⁵ and basket handle porphyrins⁶⁶. These investigations have reflected some of the nonplanarity effects on redox potentials, optical absorption spectra and spin delocalisation which can be correlated with those observed in biological systems. For e.g., INDO/S calculations³¹ indicate that the series of absorption maxima seen for the bacterio-

chlorophylls in the antenna complex of Prosthecochloris aestuarii in a low temperature glass can be partially explained by differences in the conformations of the individual chlorophylls.

3.2 WORK DONE IN THE PRESENT STUDY

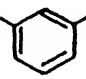
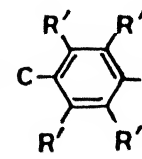
A series of short chain basket handle porphyrins with different chain lengths, substituents and the bridging groups (Fig. 3.1) have been synthesized and characterised. The covalent linkage of short chains across the porphyrin periphery induces deformation in the porphyrin skeleton and the effect of this deformation on the spectral and electrochemical properties have been investigated with the aim of relating these properties to the subtle structural changes of the porphyrin ring. The deformation into the porphyrin ring is introduced in a stepwise manner to observe the gradual increasing conformational dependence on the spectroscopic and redox properties. In the first step, a series of basket handle porphyrins containing short para or meta phenylenedimethylenedioxy chain, covalently linked at the ortho position of phenyl groups of 5,10,15, 20-tetraphenylporphyrin are synthesized. In the second step, electron withdrawing groups (Cl^- or Br^-) on meta or para phenylene group of the bridging chain are substituted to make the chain more rigid. In the final step, 1, 4 and 8 bulky electron withdrawing bromine groups are successively introduced at the β -pyrrole carbons. For comparison, the spectroscopic and redox properties of simple short chain alkyl bridged basket handle porphyrins reported by Simonis et.al. have been studied. These variations induce different degrees of distortions in the porphyrin skeleton and project a complete



CROSS-TRANS-LINKED

ADJACENT-TRANS-LINKED

ADJACENT-CIS-LINKED

- | | | |
|---|-------------------|---|
| (1) $R = -(CH_2)_4-$ | $R_1-R_8 = H$; | $M = 2H$: Butyl II and Butyl III |
| (2) $R = -(CH_2)_5-$ | $R_1-R_8 = H$; | $M = 2H$: Pentyl I, Pentyl II and Pentyl III |
| (3) $R = -(CH_2)_6-$ | $R_1-R_8 = H$; | $M = 2H$: Hexyl I, Hexyl II and Hexyl III |
| (4) $R = -H_2C$  CH_2- ; | $R_1-R_8 = H$; | $R' = H$; $M = 2H$: MSII and MSII |
| | | $R' = Br$; $M = 2H$: MSICl ₈ , MSII Cl ₈ and MS III Cl ₈ |
| (5) $R = -H$  CH_2- ; | $R_1 = R_8 = H$; | $R' = H$; $M = 2H$: PSI |
| | | $R' = Br$; $M = 2H$: PSIBr ₈ |

$R_1 = Br, R_2-R_8 = H$; $R' = Br$; $M = 2H$: PSIBr₉

$R_1 = R_3 = R_5 = R_7 = Br$ } $R' = Br$; $M = 2H$: PSIBr₁₂
 $R_2 = R_4 = R_6 = R_8 = Br$

$R_1-R_8 = Br$; $R' = Br$; $M = 2H$: PSIBr₁₆

Fig. 3.1 : Structures of free base short chain basket handle porphyrins.

picture of the magnitude of deformation induced. Various spectroscopic and electrochemical data presented in this chapter reflects the effects of such deformation in the porphyrin ring.

3.3 EXPERIMENTAL

3.3.1 2,2' (2,3,5,6-Tetrabromo-p- phenylenedimethylenedioxy) dibenzaldehyde a

$\alpha, \alpha', 2, 3, 5, 6$ -hexabromo-p-xylene (19g, 32.7 mmol) and anhydrous K_2CO_3 (13.5g, 98.3 mmol) were dissolved in dry DMF and stirred for 5 min. Freshly distilled salicylaldehyde (12g, 99.1 mmol) was added and stirring was continued for 7 h at room temperature. The completion of the reaction was monitored by tlc. Water (300 cm^3) was added, and the reaction mixture was extracted with chloroform ($3 \times 100\text{ cm}^3$). The chloroform layer was washed several times with water and sodium hydrogen carbonate solution and dried over anhydrous sodium sulfate. Diethyl ether was added to the concentrated chloroform layer to obtain a white crystalline product.

Yield : 90%

^1H NMR (CDCl_3) : 5.46 ppm (s, 4H, OCH_2), 6.9-7.9 ppm (m, 8H, Ph) and 10.4 ppm (s, 2H, CHO).

All other aldehydes were prepared as mentioned above and the details of characterization are given below.

3.3.2 2,2' (2,4,5,6-Tetrachloro-m-phenylenedimethylenedioxy) dibenzaldehyde b

Yield : 84%

^1H NMR (CDCl_3) : 5.72 ppm (s, 4H, OCH_2), 6.9-8.9 ppm (m, 8H, Ph) and 10.5 ppm (s, 2H, CHO).

3.3.3 2,2'-(m-Phenylenedimethylenedioxy)dibenzaldehyde c

Yield : 80%

^1H NMR (CDCl_3) : 5.17 ppm (s, 4H, OCH_2), 7.33 ppm (m, 4H, m-xylyl) 6.93 and 7.73 ppm (m, 8H, Phenyl), 10.37 ppm (s, 2H, CHO).

3.3.4 2,2'-(p-Phenylenedimethylenedioxy)dibenzaldehyde d

Yield : 75%

m.p. : 180-182°C

^1H NMR (CDCl_3) : 5.03 ppm (s, 2H, OCH_2), 7.42 ppm (s, 4H, p-xylyl), 7.0 and 7.72 ppm (m, 8H, Phenyl), 10.47 ppm (s, 2H, CHO).

3.3.5 2,2'-(1,4-Butyldioxy)dibenzaldehyde e

Yield : 69%

m.p. : 84°C

^1H NMR (CDCl_3) : 10.49 ppm (s, 2H, CHO), 7.82ppm (dd, 2H, o-Phenyl H), 7.49 ppm (t, 2H, p-Phenyl H), 7.02ppm (m, 4H, m-m'-Phenyl H), 4.18ppm (t, 4H, OCH_2), 2.10ppm (m, 4H, p- CH_2).

3.3.6 2,2'-(1,5-Pentyldioxy)dibenzaldehyde f

Yield : 79%

m.p. : 69-70°C

^1H NMR (CDCl_3) : 10.51ppm (s, 2H, CHO), 7.83ppm (dd, 2H, o-Phenyl H), 7.49ppm (t, 2H, p-Phenyl H), 7.01ppm (m, 4H, m-m'-Phenyl H), 4.09ppm (t, 4H, OCH_2), 1.91ppm (m, 6H, β and γ - CH_2).

3.3.7 2,2'(1-6-Hexyldioxy)dibenzaldehyde g

Yield : 85%

m.p. : 123-124°C

^1H NMR (CDCl_3) : 10.51 ppm (s, 2H, CHO), 7.82ppm (dd, 2H, o-Phenyl H), 7.53 ppm (t, 2H, p-Phenyl H), 7.00ppm (m, 4H, m-m'-Phenyl H), 4.13ppm (t, 4H, OCH_2), 1.91ppm (m, 4H, $\beta\text{-CH}_2$), 1.63ppm (m, 4H, $\gamma\text{-CH}_2$).

3.3.8 Preparation of meta-xylyl strapped porphyrin

The desired dialdehyde b and c (6.8 mmol) and pyrrole (13.6 mmol) in propionic acid (500 cm^3) were heated under reflux for 2 h. The reaction mixture was set aside overnight and was filtered to remove the foam type material. The solvent was evaporated under reduced pressure. The resultant crude compound was chromatographed over silica gel (60-120 mesh) using benzene and benzene-diethyl ether (9:1 v/v) as eluants.

For the simple unsubstituted meta-xylyl strapped porphyrin, only two isomers were obtained. A pink fraction which was eluted with only benzene was identified as MS III (adjacent-cis-linked). This was rechromatographed using silica gel (60-120 mesh) and the pure fraction was eluted with benzene (FAB Mass : calculated for $\text{C}_{60}\text{H}_{42}\text{N}_4\text{O}_4 = 883.01$; observed $m/z = 883$). Another red fraction eluted with benzene-diethyl ether (9:1 v/v) was identified as MS II (adjacent-trans-linked isomer). This was rechromatographed using silica gel (60-120 mesh) and the pure fraction eluted with benzene-diethyl ether (9:1 v/v) gave crystalline solid (2.4%) (FAB Mass : calculated for $\text{C}_{60}\text{H}_{42}\text{N}_4\text{O}_4 = 883.01$; observed $m/z = 883$).

All three isomers were obtained for the electron withdrawing substituted meta-xylyl strapped porphyrin. The least polar cross-trans-linked isomer obtained in benzene was rechromatographed using silica gel (60-120 mesh) and the fraction eluted with benzene gave a pure crystalline solid (2.5%) (FAB Mass : calculated for $C_{60}H_{34}N_4O_4Cl_8$, = 1158; observed m/z = 1156). The two remaining isomers, adjacent-trans-linked and adjacent-cis-linked, which are equally polar were separated by repeated silica gel column chromatography using benzene-diethyl ether (9:1) (FAB Mass, calculated for $C_{60}H_{45}N_4O_4Cl_8$ = 1158; observed m/z = 1156).

3.3.9 Preparation of para-xylyl strapped porphyrin

Dibenzaldehyde a or d (6.8 mmol) and pyrrole (13.6 mmol) in propionic acid (500 cm³) were heated under reflux for 2 h. The reaction mixture was set aside overnight and was filtered to remove the foam type material. The solvent was evaporated under reduced pressure and the resultant crude compound was chromatographed over silica gel (60-120 mesh) in benzene. The cross-trans-linked isomer was eluted first as a red band in benzene. This was rechromatographed over silica gel (60-120 mesh) using benzene. The pure product was obtained as a purple crystalline solid (3%). The other red fraction which was eluted with benzene-diethyl ether (19:1 v/v) was identified as a mixture of adjacent-trans and adjacent-cis-linked isomers. A clear separation of these two isomers has not yet been achieved. ✓

For both electron withdrawing substituted and unsubstituted para-xylyl strapped porphyrins, only cross-trans-isomer was obtained in the pure form (FAB Mass : for PSI, calculated for $C_{60}H_{42}N_4O_4 = 883$; observed $m/z = 883$ and for PSIBr₈, calculated for $C_{60}H_{32}N_4O_4Br_8 = 1514.18$; observed $m/z = 1514$).

3.3.10 Preparation of alkyl bridged porphyrins

These porphyrins were prepared by following the literature procedure⁶⁷. The required dialdehyde e, f and g (0.03 mmol) dissolved in 1.2 l. of freshly distilled propionic acid was put into a three-necked round bottomed flask equipped with a magnetic stirrer, reflux condenser, dropping funnel and air bubbler and heated to reflux. Pyrrole (0.065 mmol) dissolved in 50 cm³ of propionic acid was added dropwise. Air was bubbled through the solution, which turned from colourless to red to black. Total reflux time was 3 h. During the reflux, formation of the corresponding porphyrin products was monitored by UV-vis spectroscopy. After the mixture was cooled, the black precipitate was filtered off and discarded, and the filtrate was evaporated to dryness. The resulting black material was washed several times with portions of 50 cm³ of hot methanol to remove most of the black tar-like products. The remaining purplish solid was dissolved in a minimum amount of chloroform and loaded on a silica gel column. After elution with chloroform, the hexyl- and pentyl- bridged basket handle porphyrins showed three spots and butyl- bridged basket handle porphyrins showed only two spots on tlc. Further separation of isomers was done on a preparative tlc as outlined below.

For the hexyl bridged basket handle porphyrins, the three isomers were separated on a preparative tlc with hexane-toluene (1:3) as eluant and the three isomers of the pentyl bridged basket handle porphyrins were separated with toluene-methylene chloride (1:1) as eluent. Only isomers II and III of the butyl bridged basket handle porphyrins were separated on a silica gel column (methylene chloride - ethyl acetate, 1:1).

^1H NMR (CDCl_3)

3.3.10.1 Hexyl I : 8.75 ppm (8H, Py-H), 8.85 ppm (4H, o-Phenyl H), 7.58 ppm (8H, m and p-Phenyl H) 6.91 ppm (4H, m'-Phenyl H), -0.84 ppm (2H, N-H), 2.49 ppm (4H, O-CH₂), -1.13 ppm (4H, β -CH₂), -2.07 ppm (4H, γ -CH₂).

3.3.10.2 Hexyl II : 8.91, 8.69 ppm (8H, Py-H), 8.20 ppm (4H, o-phenyl H), 7.73 ppm (4H, p-phenyl H), 7.42 ppm (4H, m-phenyl H), 7.21 ppm (4H, m'-phenyl H), -2.58 ppm (2H, N-H), 3.73, 3.64 ppm (4H, O-CH₂), 0.90, 0.18 ppm (4H, β -CH₂), 0.18, 0.02 ppm (4H, γ -CH₂).

3.3.10.3 Hexyl III : 8.77, 8.68 ppm (8H, Py-H), 8.13 ppm (4H, o-phenyl H), 7.72 ppm (4H, p-phenyl H), 7.38 ppm (4H, m-phenyl H), 7.32 ppm (4H, m'-phenyl H), -2.54 ppm (2H, N-H), 3.81 ppm (4H, O-CH₂), 1.20, 0.66 ppm (4H, β -CH₂), 0.50, 0.45 ppm (4H, γ -CH₂).

3.3.10.4 Pentyl I : 8.80 ppm (8H, Py-H), 8.88 ppm (4H, o-phenyl H), 7.58 ppm (4H, p-phenyl H), 7.52 ppm (4H, m-phenyl H), 6.87 ppm (4H, m'-phenyl H), +0.18 ppm (2H, N-H), 0.88 ppm (4H, O-CH₂), -1.09 ppm (4H, β-CH₂), -2.44 ppm (2H, γ-CH₂).

3.3.10.5 Pentyl II : 9.04, 8.66 ppm (8H, Py-H), 8.36 ppm (4H, o-phenyl H), 7.72 ppm (4H, p-phenyl H), 7.43 ppm (4H, m-phenyl H), 7.15 ppm (4H, m'-phenyl H), -2.55 ppm (2H, N-H), 3.90, 3.78 ppm (4H, O-CH₂), 0.65, 0.55 ppm (4H, β-CH₂), 0.96, 0.87 ppm (4H, γ-CH₂).

3.3.10.6 Pentyl III : 8.69, 8.67 ppm (8H, Py-H), 8.30 ppm (4H, o-phenyl H), 7.73 ppm (4H, p-phenyl H), 7.40 ppm (4H, m-phenyl H), 7.21 ppm (4H, m'-phenyl H), -2.51 ppm (2H, N-H), 3.96, 3.86 ppm (4H, O-CH₂), 0.86, 0.76 ppm (4H, β-CH₂), 1.10, 1.06 ppm (2H, γ-CH₂).

3.3.10.7 Butyl II : 9.24, 8.40 ppm (8H, Py-H), 8.53 ppm (4H, o-phenyl H), 7.74 ppm (4H, p-phenyl H), 7.52 ppm (4H, m-phenyl H), 7.31 ppm (4H, m'-phenyl H), -2.22 ppm (2H, N-H), 3.90 ppm (4H, O-CH₂), 0.70, 0.25 ppm (2H, β-CH₂).

3.3.10.8 Butyl III : 8.82, 8.38 ppm (8H, Py-H), 8.47 ppm (4H, o-phenyl H), 7.74 ppm (4H, p-phenyl H), 7.48 ppm (4H, m-phenyl H), 7.30 ppm (4H, m'-phenyl H), -2.09 ppm (2H, N-H), 3.97,

3.87 ppm (4H, O-CH₂), 0.88, 0.60 ppm (2H, β-CH₂).

3.3.11 Synthesis of PSIBr₉

PSIBr₈ (60 mg, 0.0396 mmol) and NBS (8 mg, 0.0455 mmol) were refluxed in chloroform (20 cm³) for 3 h. The reaction mixture was evaporated under reduced pressure and residue was washed with methanol to remove green material. The product was purified over silica gel (60-120 mesh) column using benzene as the eluent, and a reddish green band separated which was identified as the product (62 mg, 98%) (FAB Mass : calculated for C₆₀H₃₁N₄O₄Br₉ = 1593.07; observed m/z = 1593).

3.3.12 Synthesis of PSIBr₁₂

PSIBr₈ (60 mg, 0.0396 mmol) and NBS (30 mg, 0.175 mmol) were refluxed in chloroform (30 cm³) for 3 h. Workup and purification as mentioned above gave the product (63 mg, 86%) (FAB Mass : calculated for C₆₀H₂₈N₄O₄Br₁₂ = 1829.8; observed m/z = 1830).

3.3.13 Synthesis of PSIBr₁₆

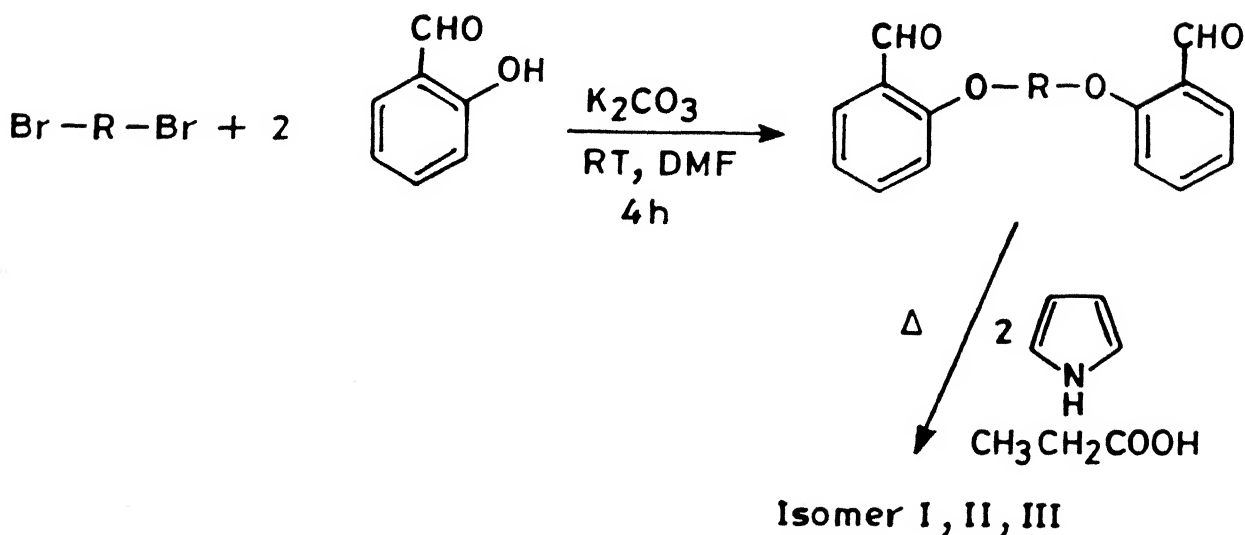
To a stirred solution of PSIBr₈ (25 mg, 0.0165 mmol) in 10 cm³ of CHCl₃/CCl₄ (1:1) was added 84.5 mg (0.027 cm³, 0.528 mmol) of liquid bromine in 4 cm³ of solvent mixture over a period of 30 min at 30°C. The stirring was continued for a period of 4 h. Pyridine 0.075 cm³ in 4 cm³ solvent mixture was added dropwise over a period of 30 min. The solution was stirred for another period of 12 h. The reaction mixture was treated with 20 cm³ of 20% aqueous sodium metabisulfite to destroy the excess bromine.

The organic layer was separated and washed with water (3 x 100 cm³) and dried over anhydrous Na₂SO₄ and the solvent was evaporated under reduced pressure to obtain the green product. The crude product was purified over silica gel (60-120 mesh) column using benzene as the eluent and the single dark green band was collected (9 mg, 26%) (FAB Mass : calculated for C₆₀H₂₄N₄O₄Br₁₆ = 2145.39; observed m/z = 2145).

3.4 RESULTS

3.4.1 SYNTHESIS :

The synthesis of various basket handle porphyrins reported here based on a combination of Adler's⁶⁸, Baldwin's⁶⁹ and Momenteau's⁶ synthetic route for sterically hindered porphyrins is outlined in Scheme-I.



For different R groups used, refer Fig. 3.1

The condensation of appropriate dialdehyde with pyrrole in molar ratio of 1:2 led to the formation of the crude basket handle

porphyrins which were obtained as a mixture of isomers. In order to minimize the formation of intermolecular polymerisation products and to increase the yield of crude material extremely, dilute conditions were employed. The crude porphyrins were separated by repeated column chromatography. Bromination at the pyrrole carbons of cross-trans-linked porphyrin, PSIBr_8 was achieved by following simple literature procedures⁷⁰. One and four bromines were introduced successively at the β -pyrrole carbons of PSIBr_8 by treating the porphyrin with appropriate equivalents of NBS and the octabromo substituted porphyrin was obtained directly with liquid bromine. FAB Mass and ^1H NMR data were used to confirm all the porphyrins synthesized in the present study.

3.4.2 ^1H NMR SPECTROSCOPY

The proton magnetic resonance spectral studies were informative about the structure of all compounds synthesized in the present study. The study is mainly governed by the symmetry properties of isomer I, isomer II and isomer III of basket handle porphyrins. The ^1H NMR spectra for three different isomers are shown in Fig. 3.2 and the data for all the compounds is presented in table 3.1. It is clear from Fig. 3.2 that isomer I shows very simple ^1H NMR relative to other two isomers. Specifically, in isomer I all eight pyrrole protons resonate as a sharp singlet, the eight protons of the methylene chain are equivalent and appear as a singlet and experience an upfield shift relative to the corresponding protons in free dialdehyde. The eight aromatic protons of two strap phenyl rings are equivalent and appear as a

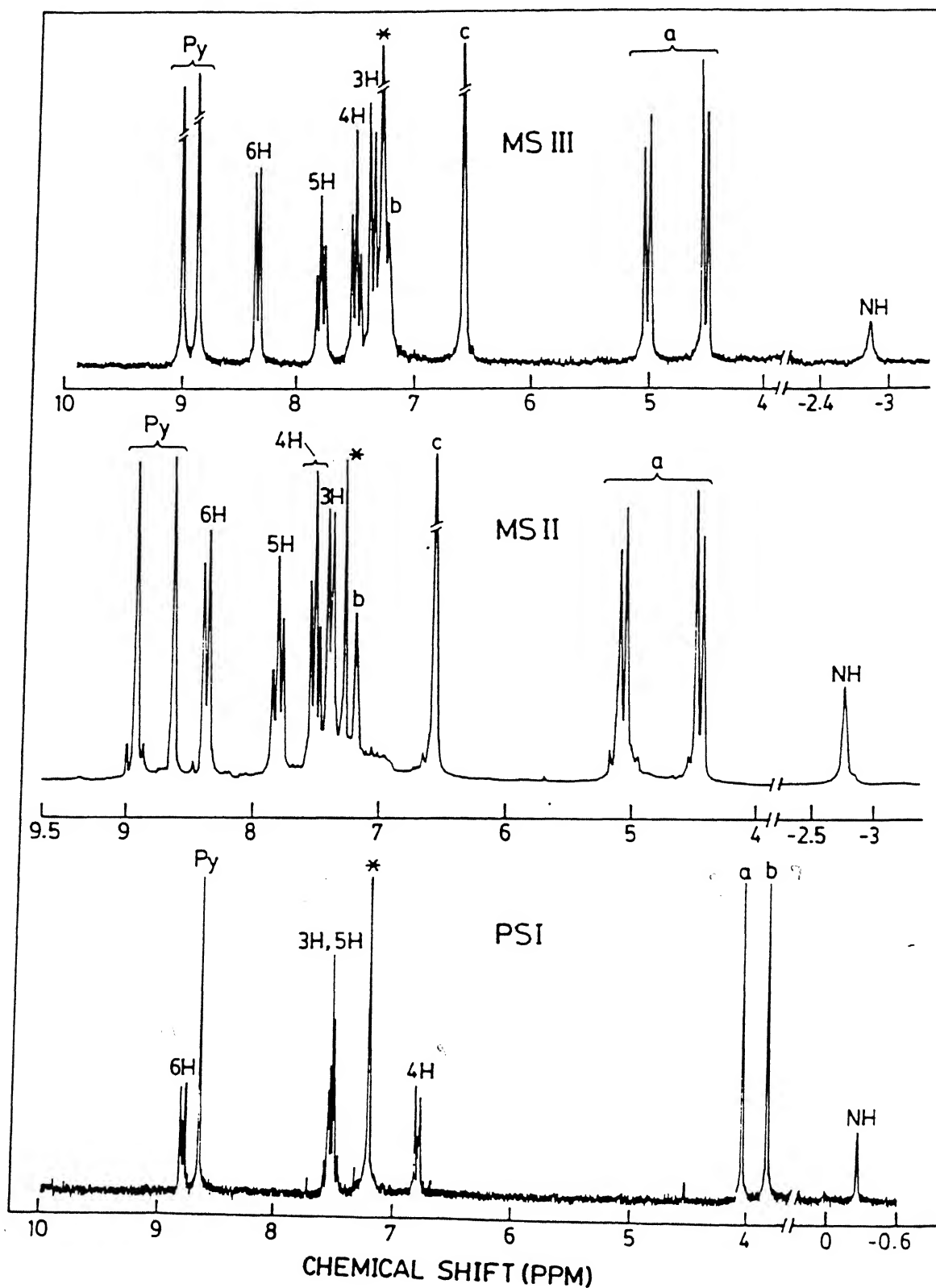


Fig. 3.2 : ^1H NMR spectra of (a) PSI, (b) MSII and (c) MSIII in CDCl_3 (concentration of the porphyrins used is $\sim 10^{-3} \text{ mol dm}^{-3}$). The asterisk corresponds to the CDCl_3 signal.

Porphyrin	Pyrrole	Phenyl (PORPHYRIN)			Strap CH ₂	Phenyl (strap)	-NH-
		6H	4H	3H	5H		
TMPP	8.73	8.00	7.75	7.35	-	-	-2.58 (s, 2H)
PSI	8.71 (s, 8H)	8.85 (m, 4H)	6.86 (m, 4H)	7.58 (m, 8H)	4.10 (s, 8H)	3.89 (s, 8H)	-0.27 (s, 2H)
MSII	8.92 (s, 4H) 8.62 (s, 4H)	8.37 (d, 4H)	7.49 (t, 4H)	7.37 (d, 4H)	7.80 (t, 4H)	AB quartet 5.06 (d, 4H) 4.45 (d, 4H)	-2.77 (s, 2H)
MSIII	8.86 (s, 4H) 8.99 (s, 4H)	8.34 (d, 4H)	7.50 (t, 4H)	7.35 (d, 4H)	7.80 (t, 4H)	AB quartet 5.02 (d, 4H) 4.53 (d, 4H)	-2.86 (s, 2H)
MSICl ₈	8.60 (s, 4H)	8.88 (m, 4H)	7.13 (m, 4H)	7.63 (m, 8H)	3.48 (s, 8H)	-	+0.88 (s, 2H)
MSIICl ₈	8.58 (s, 4H) 8.70 (s, 4H)	8.28 (d, 4H)	7.45 (m, 4H)	7.80 (t, 8H)	AB quartet 5.45 (d, 4H) 5.28 (d, 4H)	-	-3.08 (s, 2H)
MSIICl ₈	8.62 (s, 4H) 8.68 (s, 4H)	8.36 (d, 4H)	7.40 (m, 4H)	7.78 (t, 8H)	AB quartet 5.38 (d, 4H) 5.18 (d, 4H)	-	-3.05 (s, 2H)
PSIBr ₈	8.55 (s, 8H)	8.85 (m, 4H)	6.68 (m, 4H)	7.50 (m, 8H)	4.53 (s, 8H)	-	-0.43 (m, 2H)
PSIBr ₉	8.44-8.71 (complex multiplet, 7H)	8.84 (m, 4H)	6.69 (m, 4H)	7.49 (m, 8H)	4.56 (m, 8H)	-	-0.51 (m, 2H)
PSIBr ₁₂	8.59 (s, 4H)	8.82 (m, 4H)	6.77 (m, 4H)	7.56 (m, 8H)	4.64 (m, 8H)	-	-1.00 (s, 2H)
PSIBr ₁₆	-	8.89 (m, 4H)	6.79 (m, 4H)	7.57 (m, 8H)	4.75 (m, 8H)	-	-

singlet and are shielded by porphyrin anisotropy in comparison with the corresponding protons in free dialdehyde. This resonance is absent in PSIBr_8 and its pyrrole brominated derivatives. The $-\text{NH}$ protons are highly deshielded (~ 2.35 ppm) relative to tetra (o-methoxy phenyl) porphyrin (TMPP). Bromination at the β -pyrrole carbons is confirmed by monitoring the pyrrole resonances. A complex multiplet resonance and single resonance for pyrrole protons of monobromo (PSIBr_9) and symmetrically substituted tetrabromo (PSIBr_{12}) derivatives of PSIBr_8 respectively confirms the products obtained. Pyrrole resonance is completely absent in octabromo substituted derivative of PSIBr_8 as expected.

In contrast, isomers II and III gave a complex but clear ^1H NMR spectra. In these two isomers, the adjacent phenyl groups are linked by strapping groups and the straps are either on same side of the porphyrin ring as in isomer III or one strap is above the porphyrin plane and the other strap is below the porphyrin plane as in isomer II. Because the porphyrin is no more symmetric, the pyrrole protons show two resonances each corresponding to four equivalent protons carried by the opposite pyrrole groups. Also, the methylene chain protons appear as an AB quartet with negligible shielding relative to the corresponding free dialdehyde. The aromatic ring protons of the strapping group are confirmed by electron withdrawing groups substituted aromatic ring containing alkyl bridged porphyrins in which the signal is absent. These protons experience a small shielding in these isomers than TMPP in contrast to isomer I.

Furthermore, the chemical shifts of the ortho protons of meso

phenyl rings and inner NH protons has been used as a marker to assess the degree of distortion of the porphyrin core due to short bridging chain^{66,71}. A comparison of the chemical shifts of these two types of protons shown in table 3.2 for different cross-trans-linked isomers suggests a higher degree of distortion for meta-xylyl bridged porphyrin.

Table 3.2 : Chemical shift data of o-H and N-H protons of various cross-trans-linked basket handle porphyrins (in ppm)

Compound	o-H	N-H
Hexyl I	8.85	-0.84
PSI	8.85	-0.27
PSIBr ₈	8.85	-0.43
MSICl ₈	8.88	+0.88
TMPP	8.00	-2.58

Substitution of bromines at the β -pyrrole carbons of PSIBr₈ does not affect these two resonances (table 3.1)

3.4.3 VISIBLE ABSORPTION STUDIES

The absorption spectra of all three isomers differ considerably. The absorption spectra for Q-band and Soret region of MSICl₈, MSIICl₈ and MSIIICl₈ are shown in Fig. 3.3 and table 3.3 lists the UV-vis spectral data for all the compounds. For all the free-base compounds, the visible spectra shows the satellite bands I-IV characteristic for porphyrins and the Soret band in the region 425-455 nm. The following observations can be made from table 3.3.

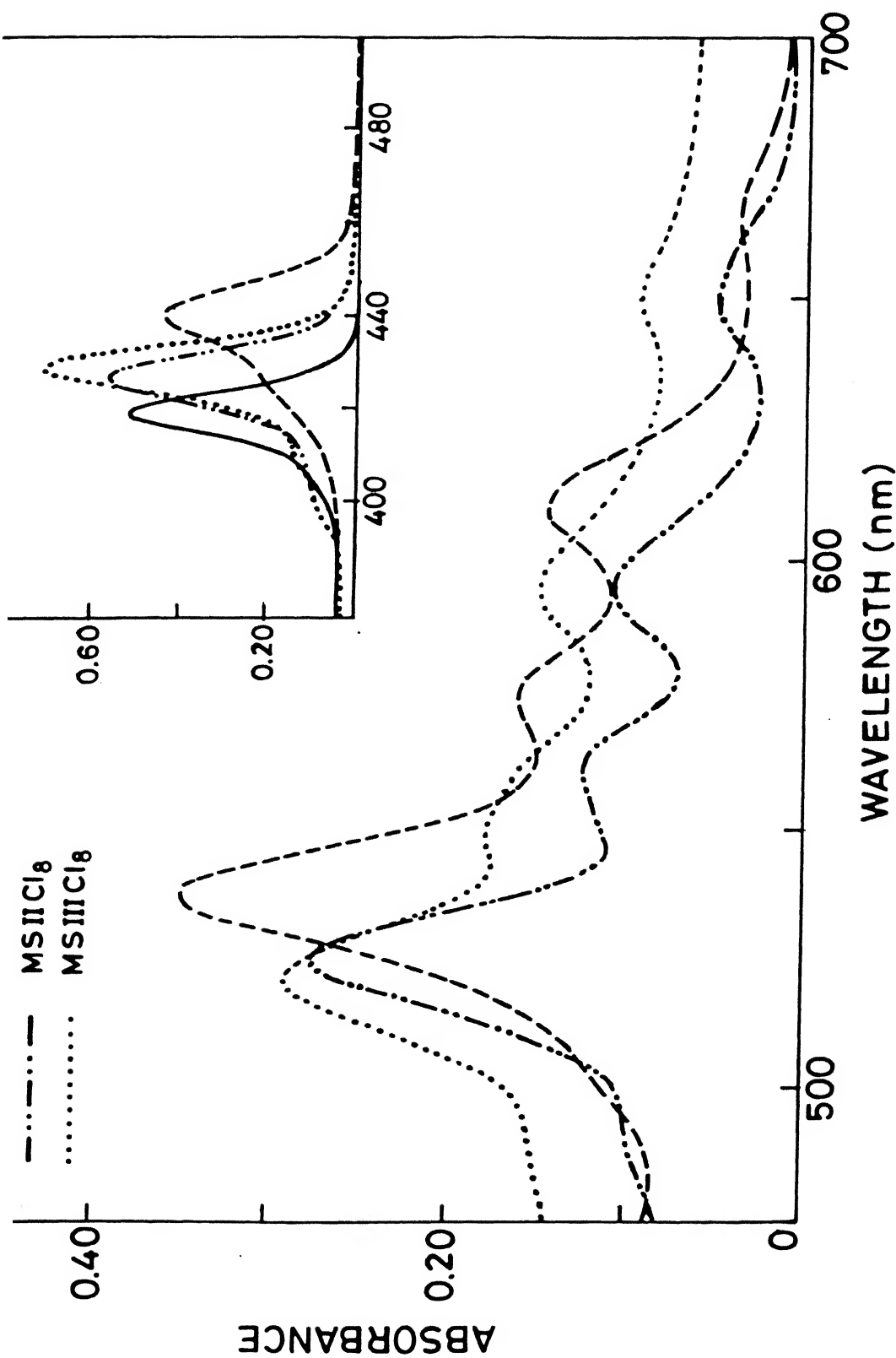


Fig. 3.3 : Comparison of Q-band absorption spectra of MSICl_8 , MSIICl_8 and MSIIICl_8 in chloroform. The inset shows the comparison of all three isomers along with H_2TPP for Soret band region. The concentrations used were $\sim 5 \times 10^{-5} \text{ mol dm}^{-3}$ for Q-bands and $\sim 5 \times 10^{-6} \text{ mol dm}^{-3}$ for Soret band.

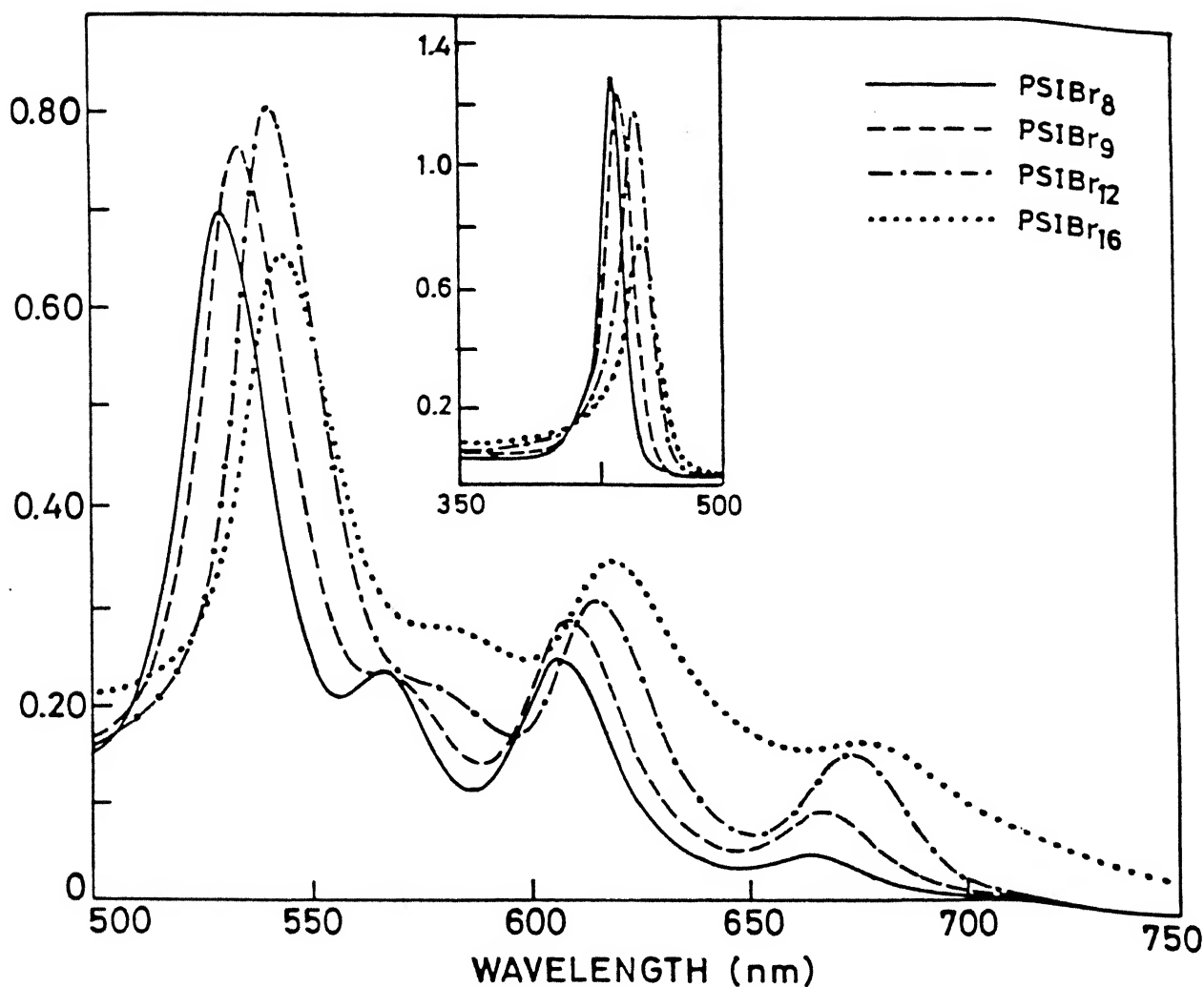
Table 3.3 : Electronic spectral data of short chain basket handle porphyrins in CHCl_3

PORPHYRIN	Soret Band $\lambda_{\text{max}}/\text{nm}$ $\epsilon \times 10^{-4} \text{ dm}^3 \text{ mol}^{-1} \text{ cm}^{-1}$ B(0, 0)	Q-bands $\lambda_{\text{max}}/\text{nm} (\epsilon \times 10^{-3} / \text{dm}^3 \text{ mol}^{-1} \text{ cm}^{-1})$			
		$Q_y (1, 0)$	$Q_y (0, 0)$	$Q_x (1, 0)$	$Q_y (0, 0)$
H_2TPP	419 (46.4)	515 (18.7)	548 (8.6)	592 (5.5)	647 (3.9)
MS II	432 (31.72)	526 (12.09)	566 (6.42)	601 (5.14)	657 (3.74)
MS III	428 (34.04)	520 (16.09)	552 (6.88)	602 (4.79)	661 (2.54)
PS I	433 (22.21)	529 (11.72)	566 (5.16)	605 (4.33)	663 (1.24)
MSICl_8	440 (14.7)	537 (11.7)	576 (6.4)	610 (4.8)	667 (1.3)
MSIICl_8	428 (23.7)	524 (11.92)	562 (6.20)	596 (5.24)	650 (3.68)
MSIIICl_8	426 (22.6)	520 (12.01)	549 (6.23)	595 (4.96)	651 (3.62)
PSIBr_8	436 (23.21)	532 (12.3)	568 (4.1)	606 (4.4)	663 (0.8)
PSIBr_9	440.5 (19.8)	536 (12.2)	571 (3.6)	610 (4.5)	667 (1.4)
PSIBr_{12}	450 (19.6)	544 (13.1)	579 (3.3)	616 (5.0)	674 (2.4)
PSIBr_{16}	453.5 (12.8)	546 (10.9)	583 (4.3)	620 (5.5)	676 (2.2)
Hexyl I	428 (22.8)	526 (11.5)	562 (5.1)	602 (4.5)	658 (1.7)
Hexyl II	420 (26.7)	516 (16.8)	548 (6.3)	592 (5.6)	646 (2.9)
Hexyl III	422 (25.1)	516 (13.7)	550 (5.0)	592 (4.3)	646 (2.1)
Pentyl I	438 (23.0)	536 (11.0)	576 (6.5)	610 (4.8)	668 (2.0)
Pentyl II	424 (27.1)	518 (17.4)	548 (7.5)	596 (5.9)	650 (2.9)
Pentyl III	424 (25.5)	520 (13.0)	552 (5.1)	594 (4.5)	648 (2.4)
Butyl II	426 (25.2)	520 (12.1)	556 (4.2)	604 (3.1)	662 (3.3)
Butyl III	426 (25.3)	520 (11.9)	556 (4.2)	604 (3.2)	662 (2.6)

- * Considerable red shift of both Soret and Q-bands.
- * A drastic reduction in the intensity of both Soret and Q-bands.
- * Magnitude of red shift of absorption bands and reduction in extinction coefficients depends on the nature of the isomer and bridging chain length.
- * Among three isomers, maximum effects were observed for cross-trans-linked isomer indicating the presence of maximum distortion in this isomer.
- * Among all cross-trans-linked basket handle porphyrins, $MSICl_8$ is found to be the most distorted one probably due to shorter bridging chain.
- * Introduction of electron withdrawing substituents at the β -pyrrole carbons of cross-trans-linked isomer result in further red shift of the absorption bands with reduction in intensity. The magnitude of red shifts and reduction in extinction coefficients depends on the number of bromines substituted (Fig.3.4). However, a plot (Fig 3.5) of magnitude of red shift versus the number of bromines substituted is non-linear suggesting that the magnitude of shifts are nonadditive.
- * Magnitude of red shift and reduction in intensity of isomers II and III are comparable and mainly depend on bridging chain length.

3.4.4 ELECTROCHEMISTRY

The distortion effects on the electrochemical behaviour of the porphyrins were monitored by cyclic voltammetry. A few



4 : Comparison of Q-band optical absorption spectra of various β -prrole brominated short chain basket handle porphyrins in chloroform. The inset shows the comparison of all the porphyrins for Soret band. The concentrations used were $\sim 5 \times 10^{-5} \text{ mol dm}^{-3}$ for Q-bands and $\sim 5 \times 10^{-6} \text{ mol dm}^{-3}$ for Soret band.

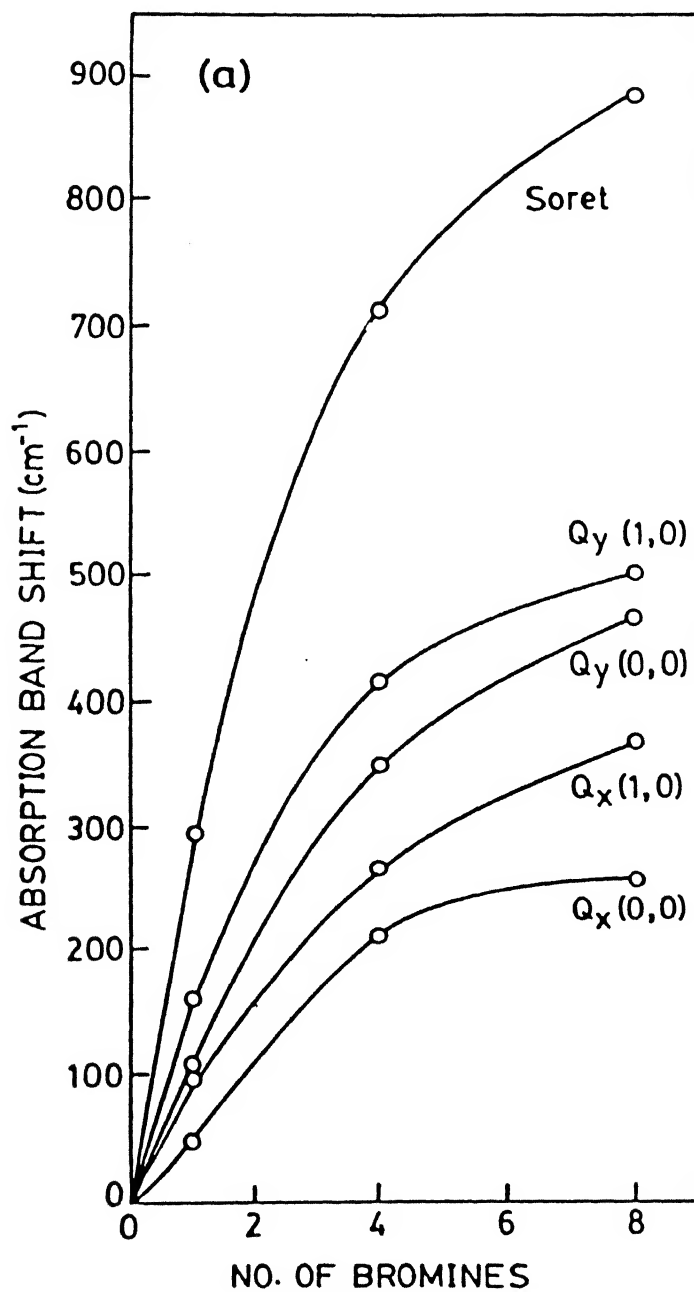


Fig. 3.5 : Plot of absorption band shift versus number of bromines of pyrrole brominated short chain basket handle porphyrins.

representative cyclic voltammograms of various porphyrins are presented in Fig. 3.6 and Fig. 3.7. All the free bases studied here exhibit two oxidations and two reductions and peak current ratio ($i_{pa}/i_{pc} = 1$) suggests a one electron process. Analysis of the data (table 3.4) suggests the following.

- * All oxidation potentials are shifted to lower positive values and reduction potentials to more negative values in deformed porphyrins compared to H_2TPP .
- * Maximum shift in redox potentials are observed for cross-trans-linked isomer relative to adjacent-trans and adjacent-cis isomers.
- * An additional reduction couple is observed for tetrabromo para-xylyl and tetrachloro m-xylyl bridged porphyrins. It is assigned to the reduction of the bridging phenyl ring containing electron withdrawing substituents.
- * Substitution of bromines at the β -pyrrole carbons results in harder oxidations and easier reductions. However, the shifts in the redox potentials are nonadditive and the specific potential shift induced per bromine decreases as the number of bromines on the porphyrin ring increases.

Thus the effect of deformation in the porphyrin skeleton is evident in the direction of redox potential shifts and maximum effects are observed for most deformed porphyrin systems.

3.4.5 MOLECULAR MECHANICS CALCULATIONS

The calculated structures of various deformed porphyrins studied here are determined with MOBY software and details of

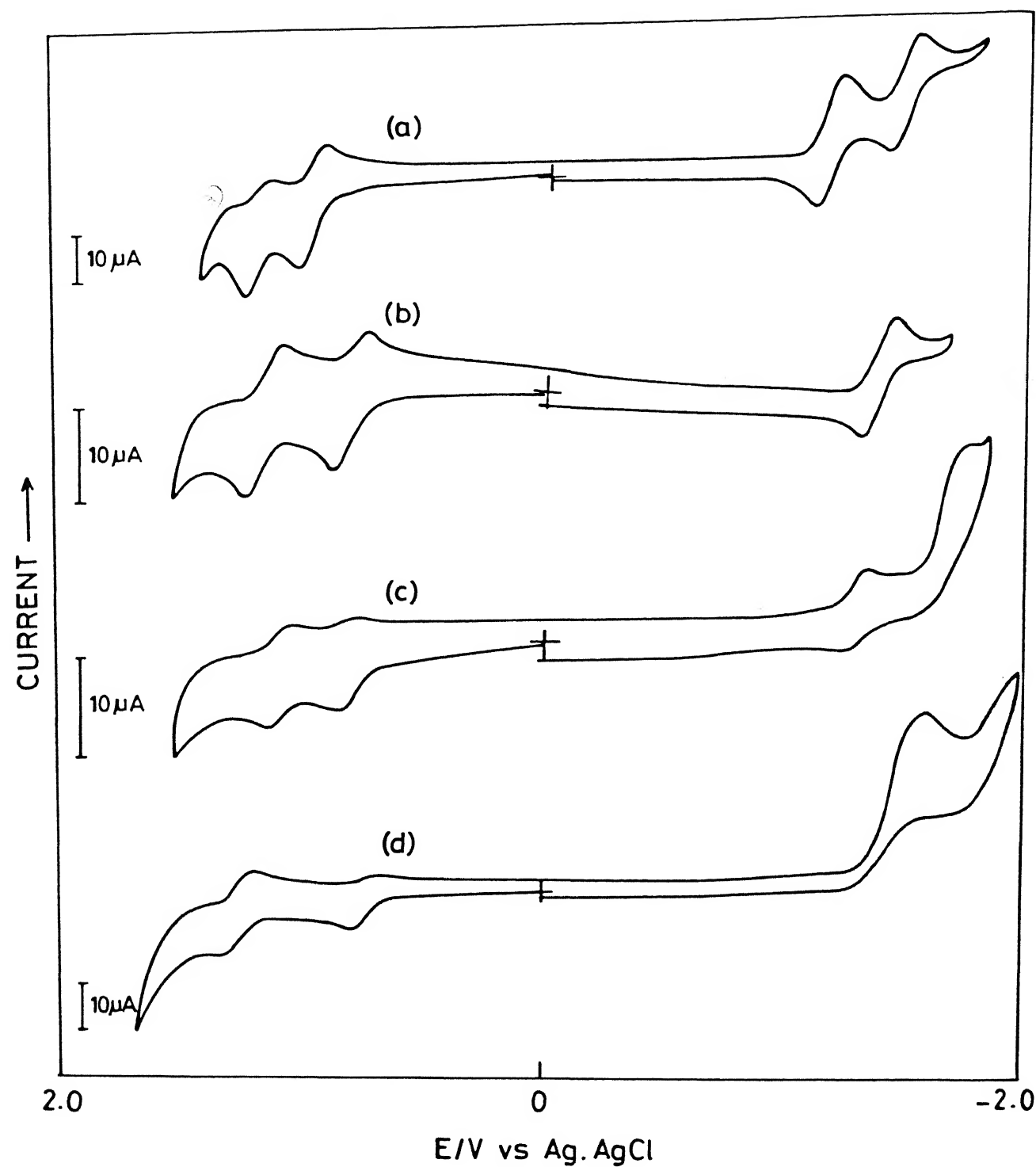


Fig. 3.6 : Cyclic voltammograms of (a) H_2TPP , (b) Hexyl I, (c) MSiCl_8 and (d) PSIBr_8 in dichloromethane containing 0.1 mol dm⁻³ TBAP. The concentrations used were $\sim 5 \times 10^{-3}$ mol dm⁻³. The Scan rate is 100mV/s.

Table 3.4 : Electrochemical redox data (V) of short chain basket handle porphyrins in dichloromethane containing 0.1 mol dm^{-3} TBAP.

PORPHYRINS	RING OXIDATION		BRIDGE PHENYL REDUCTION	RING REDUCTION	
	I	II		I	II
H ₂ TPP	1.03	1.30	-	-1.11	-1.52
Hexyl I	0.85	1.23	-	-1.40	-
Hexyl II	0.95	1.40	-	-1.34	-1.67
Hexyl III	0.93	1.24	-	-1.32	-1.65
Pentyl II	0.91	1.41	-	-1.34	-1.72
Pentyl III	0.91	1.26	-	-1.36	-1.67
Butyl II	0.91	1.32	-	-1.27	-1.61
MS II	0.84	1.20	-	-1.32	-1.67
MS III	0.90	-	-	-1.34	-1.67
MSICl ₈	0.85	1.32	-1.13	-1.45	-
MSIICl ₈	0.92	1.25	-1.14	-1.34	-1.69
MSIIICl ₈	0.95	-	-1.13	-1.34	-1.68
PS I	0.85	1.23	-	-1.39	-1.78

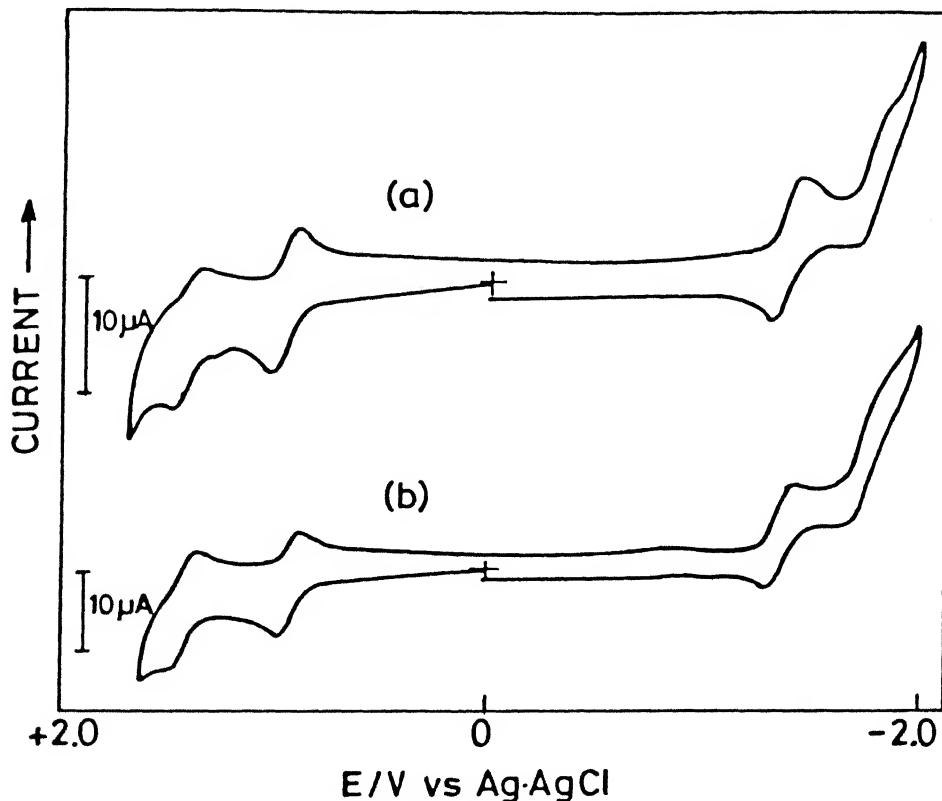
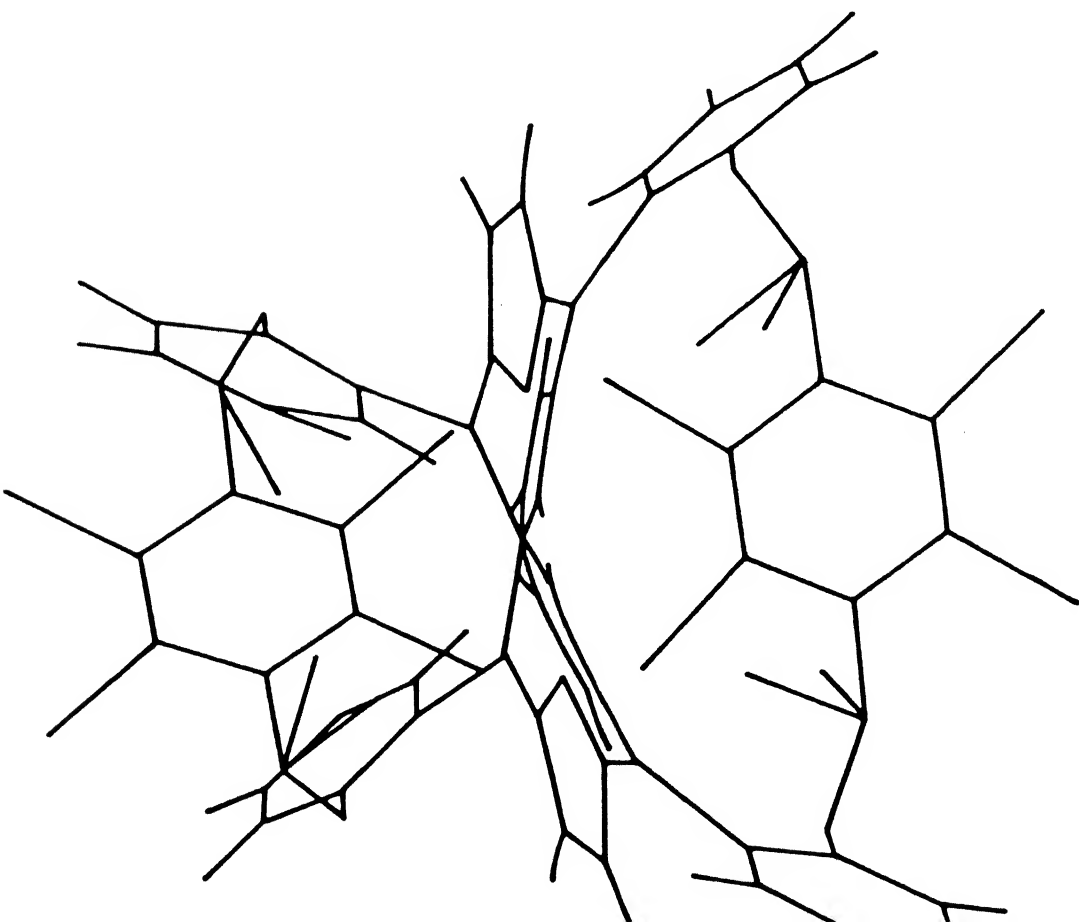


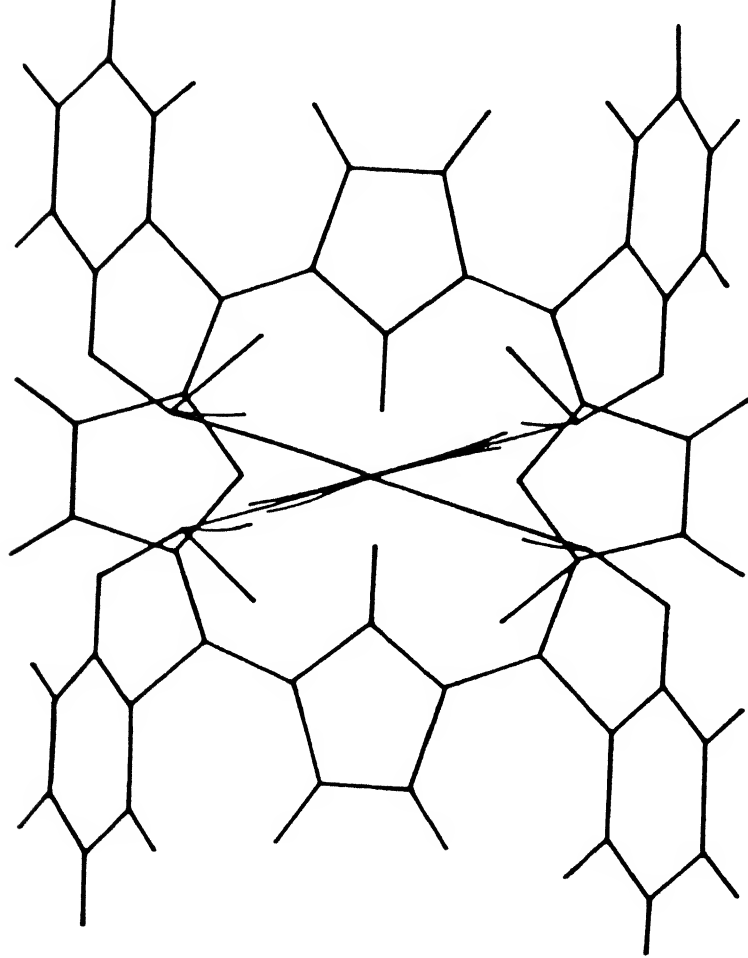
Fig. 3.7 : Cyclic voltammograms of (a) Hexyl II ($4.9 \times 10^{-4} \text{ mol dm}^{-3}$) and (b) Pentyl II ($5.5 \times 10^{-4} \text{ mol dm}^{-3}$) in dichloromethane containing 0.1 mol dm^{-3} TBAP at room temperature. The Scan rate is 100 mV/s.

the program are given in Chapter 2. These calculations are carried out for MSII, MSIII, MSICl_8 , PSI, PSIBr_8 and PSIBr_{12} . Various bond angles and bond lengths for these compounds are given as an appendix at the end of the thesis and some relevant bond angles and bond lengths affected due to distortion in the porphyrin ring of various deformed porphyrin systems are presented in table 3.5. The calculated structures shown in the Figs. 3.8-3.11 for various porphyrins reveals the enforced deformation of the porphyrin core due to covalent attachment of bridging groups. The following interesting observations can be made from the data :

* It is clear that in all isomers, the four pyrrole groups of



(a) SIDE VIEW



(b) TOP VIEW

Fig. 3.8 : Energy optimised calculated structure of PSIBr₈.

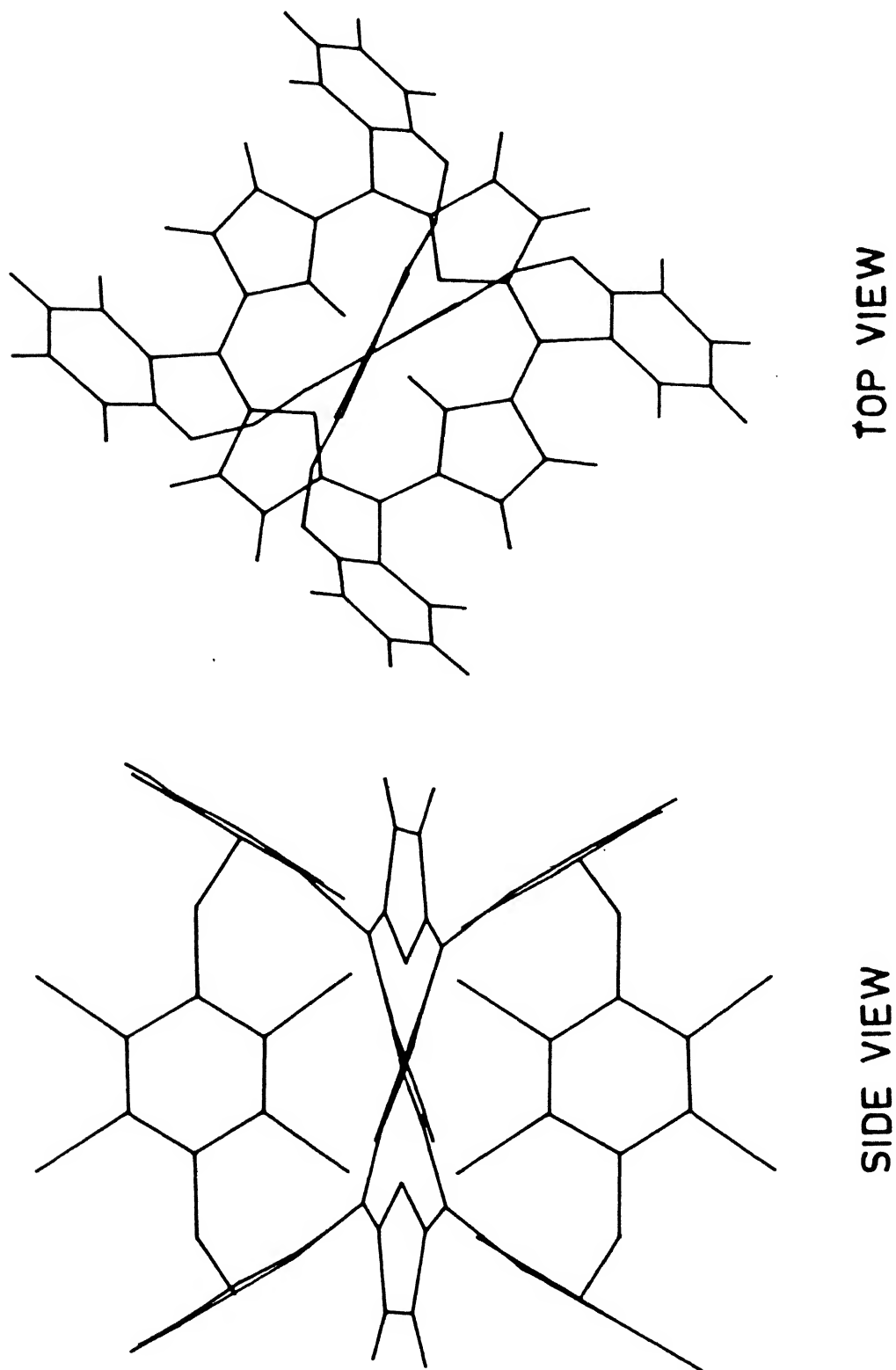


Fig. 3.9 : Energy optimised calculated structure of PSIBr₁₂.

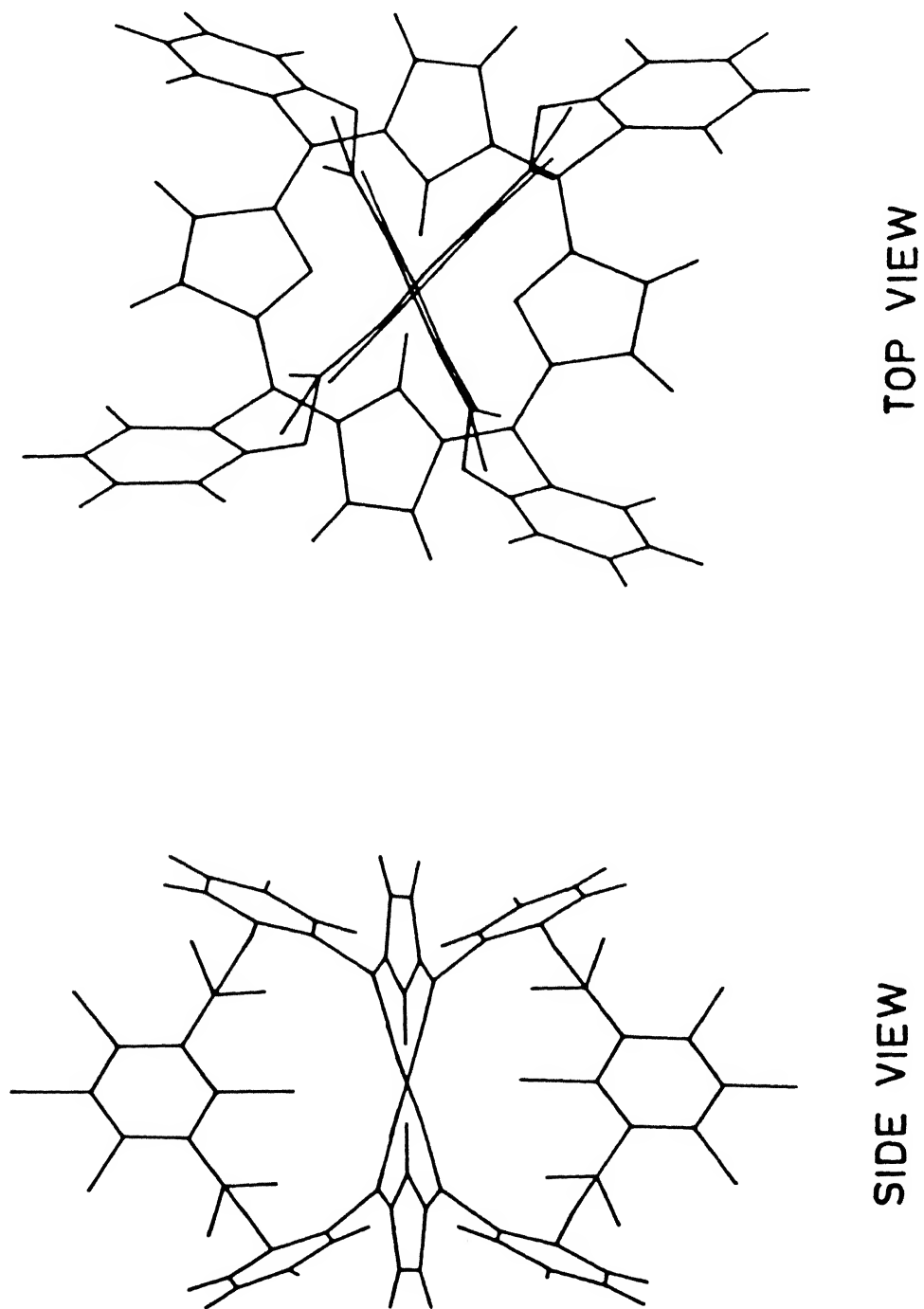


Fig. 3.10 : Energy optimised calculated structure of MSiCl₈.

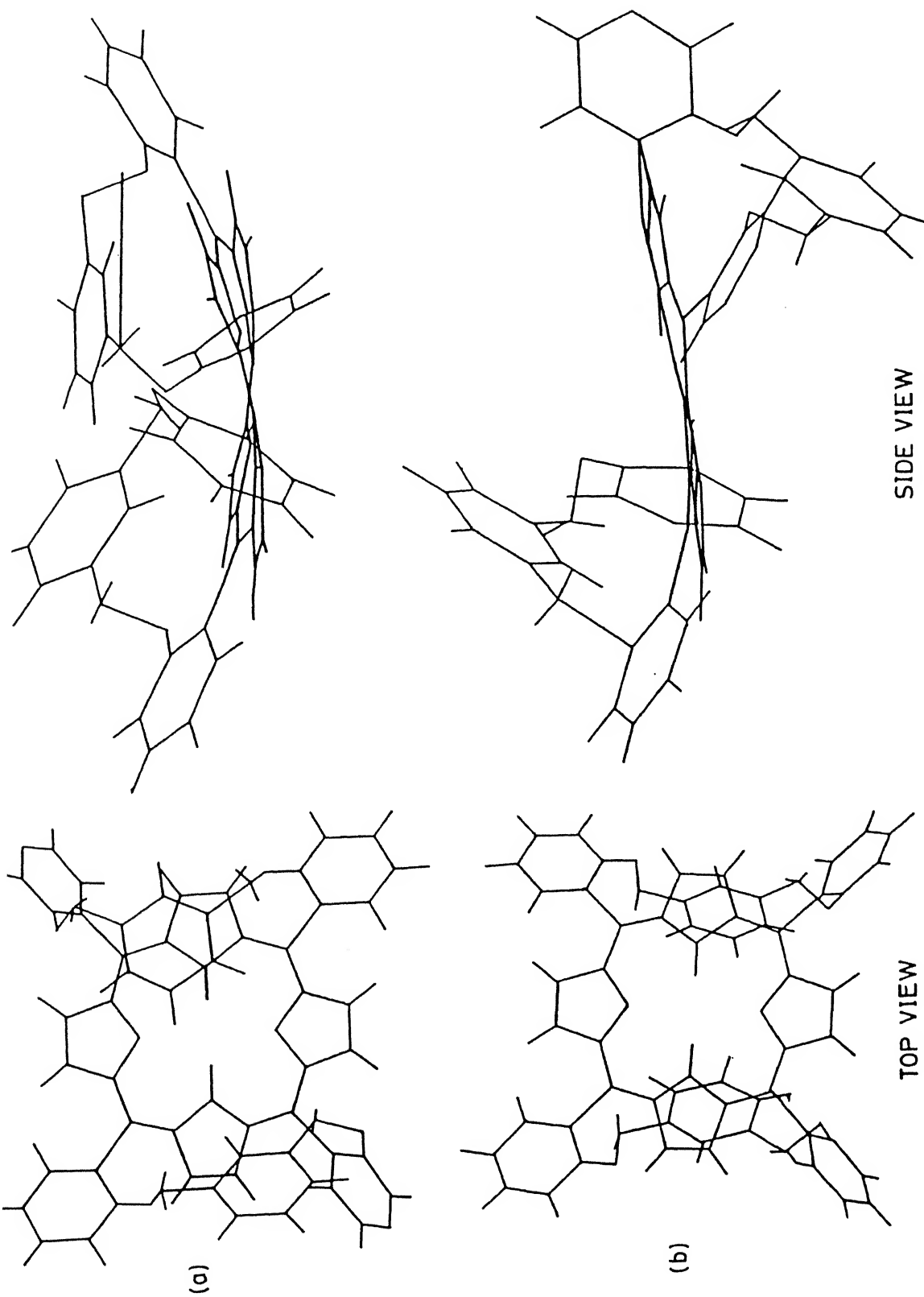


Fig. 3.11 : Energy optimised calculated structures for the adjacent cis (MS III) and adjacent trans (MS II) isomers of meta xylol linked porphyrins.

Table 3.5 : Selected bond angles and bond distances in short chain basket handle porphyrins.

Structural parameters	H ₂ TPP	MSII	MSIII	MSICl ₈	PSI	PSIBr ₈	PSIBr ₁₂
Bond angles (deg)							
C _α -N-C _α	105.6	105.6	105.7	108.3	108.2	108.0	108.1
C _α -C _m -C _α	124.7	124.4	123.9	122.0	122.9	121.9	122.4
C _α -N-H	-	126.1	126.2	125.9	125.9	126.0	126.0
N-C _α -C _β	110.1	110.1	109.9	107.9	108.1	108.2	108.1
C _α -C _β -C _β	107.1	107.1	107.2	107.9	107.1	107.8	107.8
N-C _α -C _m	125.2	-	-	124.7	124.0	122.7	124.0
C _α -N-N-C _α	3.472	-	-	5.81	14.19	11.31	10.86
	0.313	-	-	1.79	1.31	1.44	10.52
	2.202	-	-	4.55	12.29	12.16	10.09
	0.254	-	-	2.31	1.70	1.32	12.09
Bond lengths (Å)							
C _α -C _m	1.389	1.386	1.380	1.385	1.389	1.379	1.382
C _α -C _β	1.445	1.450	1.439	1.447	1.426	1.427	1.426
C _β -C _β	1.353	1.350	1.350	1.353	1.354	1.353	1.347

porphyrin ring are no more in one plane.

- * The orientation of the phenyl group of the bridging chain in para-xylyl linked and meta-xylyl linked porphyrin systems seems to be different with respect to the porphyrin plane.

It is evident that in para-xylyl linked porphyrin (Fig. 3.8 and 3.9), the phenyl group is slightly in parallel orientation and it is turning towards perpendicular orientation in meta-xylyl linked porphyrin (Fig. 3.10) with respect to porphyrin plane.

Furthermore, the degree of nonplanarity in the porphyrin ring can be accounted with the $C_{\alpha}-N-N-C_{\alpha}$ dihedral angle (Twist angle). It is indicative of the pyrrole twisting, defined by the dihedral angle between the planes of the opposite pyrrole rings. The higher values of $C_{\alpha}-N-N-C_{\alpha}$ in basket handle porphyrins relative to H_2TPP suggests the presence of nonplanarity in the porphyrin skeleton. Also, the increase of $C_{\alpha}-N-C_{\alpha}$ angle in these porphyrin systems relative to H_2TPP adds to the above conclusion.

3.5 DISCUSSION

3.5.1 1H NMR SPECTROSCOPY

The identification of three isomers was done by (i) using the symmetry concept proposed by Momenteau and coworkers⁶ (ii) comparing the NMR characteristics of the compounds synthesized in the present study with those of Simonis et.al.⁶⁷ synthesized alkyl bridged basket handle porphyrins. The isomer I is expected to show a relatively simple NMR spectrum because of the higher symmetry in which all the eight pyrrole protons, methylene chain protons and bridging phenyl protons resonate as three separate singlets indicating a highly symmetrical environment in this isomer. Because of the ring current of the porphyrin, all the resonances of the methylene chain protons and strap phenyl protons are significantly shifted to high field (~0.93 and ~3.53 ppm

respectively) relative to the corresponding dialdehydes, indicating that the linking chains are indeed above and below the porphyrin plane. The NMR data assigned for PSI, PSIBr₈ and MSICl₈ are consistent with these observations indicating that they are cross-trans-linked porphyrins.

In contrast, in isomer II and III, the symmetry is lowered hence these isomers show two pyrrole resonances and magnitude of separation between these resonances has been used to distinguish between these two isomers. An analysis of the peak separation for isomer II and isomer III for the hexyl, pentyl and butyl bridged porphyrins of Simonis et.al.⁶⁷ indicates that between these two isomers, always adjacent-trans-linked isomer shows a larger pyrrole peak separation relative to adjacent-cis-isomer in a given series. The data presented in table 3.6 supports this observation.

Table 3.6 : Chemical shift difference between two pyrrole signals
(in ppm)

Hexyl II	0.22	Hexyl III	0.09
Pentyl II	0.38	Pentyl III	0.02
Butyl II	0.84	Butyl III	0.44
MS II	0.30	MS III	0.13
MS II Cl ₈	0.12	MS III Cl ₈	0.06

The crystal structure solved from Zn Hexyl II⁶⁷ confirms the adjacent-trans-structure (Fig. 31.2). Similar observation was made by Momenteau and coworkers⁶⁶ for the larger alkyl chain bridged basket handle porphyrins. All the data confirms that the

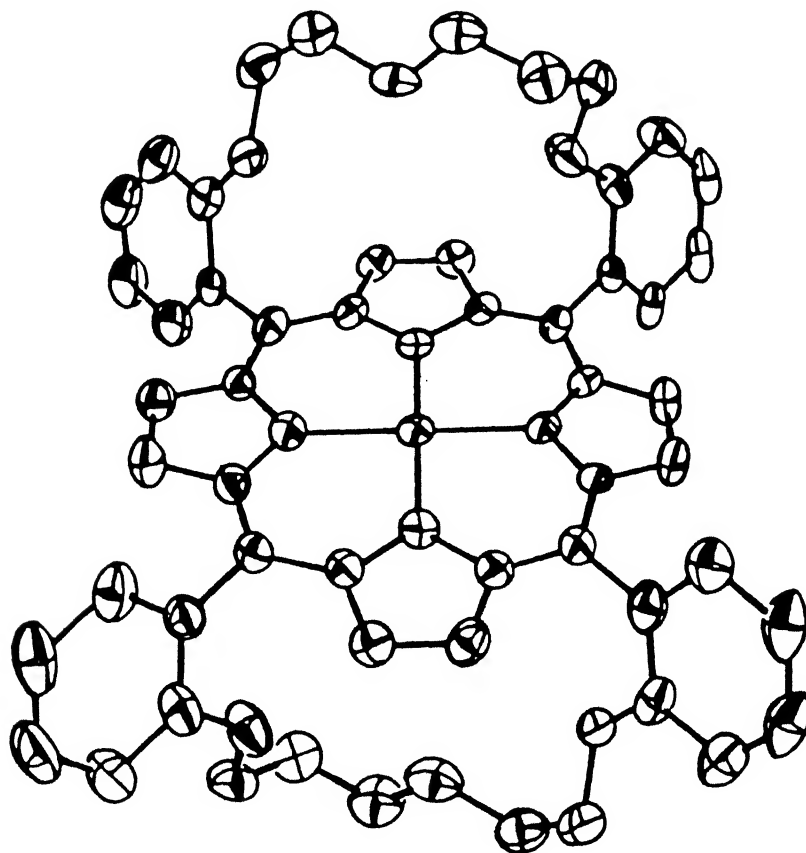


Fig. 3.12 : X-ray structure of Zn Hexyl II

compounds MSII, MSIICl_8 and MSIII, MSIIICl_8 have adjacent-trans and adjacent-cis structures respectively. The fact that the methylene chain protons and strap phenyl protons are no longer equivalent and exhibit negligible shielding relative to corresponding dialdehydes further supports the above conclusion. The ^1H NMR data for the pyrrole brominated porphyrins is in accordance with the number of bromines substituted.

The distortion in the porphyrin ring is clearly reflected in the up or down field shifts of various protons and magnitude of these shifts directly exposes the amount of distortion created by the linking chains. Momenteau and coworkers⁶⁶ used ring current model of Abraham and coworkers⁷² for their longer alkyl chain strapped porphyrins and came out with few interesting conclusions for cross-trans-linked isomer. They related the down field shift of ortho protons (6H) of phenyl ring and NH protons of pyrrole ring to the tension imposed on the porphyrin skeleton by the linking chains. The cross-trans-linked porphyrins described here show significant downfield shift for ortho phenyl protons (6H) and pyrrolic NH protons and comparison of different cross-trans-linked isomers suggests a higher degree of distortion for MSiCl_8 . The site of attachment of the bridging chain to the phenyl groups in this isomer results in shorter and hence tighter straps, relative to the alkyl or para xylyl bridged isomer and this is reflected in the higher deshielding of the ortho and NH protons. Bromination at the β -pyrrole carbons of PSIBr_8 does not have much influence on these two proton resonances. Also, the chemical shift of the pyrrole protons in this isomer is not altered much, suggesting very little disruption in peripheral ring current. In contrast, 6H, pyrrole and NH proton resonance shifts for isomer II and isomer III of different porphyrin systems described in the present study are less affected relative to isomer I (table 3.1) indicating a lower degree of distortion in these isomers.

The upfield shift of the bridging chain protons, methylene as well as strap phenyl protons in isomer I relative to the corresponding protons in the dialdehydes indicates that these

protons are present in the diamagnetic ring current zone of the aromatic nucleus. However, these protons in isomers II and III are not affected much suggesting that they are not in the ring current zone and this is clear from the calculated structures for these isomers. Thus, it has been possible to differentiate between isomers with ^1H NMR.

3.5.2 VISIBLE ABSORPTION STUDIES

Optical spectral studies exhibits large difference between the three isomers of basket handle porphyrins. All three isomers show significant red shifts of both Q-bands as well as Soret band (table 3.3) relative to unstrapped H_2TPP , indicating the presence of deformation in the porphyrin skeleton. Similar observations were made earlier in many sterically crowded porphyrins⁷³ and this was attributed to the nonplanarity of the porphyrin core. Furthermore, it should be noted here that the nonplanarity is not of the same magnitude in all three isomers as is evident from the difference in the magnitude of red shifts of optical bands. The cross-trans-linked isomer of various basket handle porphyrins show significant shifts of optical bands relative to other two isomers indicating the presence of higher degree of nonplanarity in the porphyrin cores.

An attempt has been made to explain the various optical absorption band shifts using Gouterman's four molecular orbital model⁷³. According to this, Soret and Q-bands in the visible absorption spectra of a porphyrin molecule, to a first approximation, are assigned to the transition between $A_{1u}(\pi) \rightarrow E_g(\pi^*)$ and $A_{2u}(\pi) \rightarrow E_g(\pi^*)$ molecular orbitals respectively. In

the free base porphyrins, due to symmetry and vibronic mixing, the Q-bands are further split into $Q_x(0,0)$, $Q_y(0,0)$, $Q_x(1,0)$ and $Q_y(1,0)$. Thus, any change in the energy of these absorption maxima in free base basket handle porphyrins relative to the corresponding unstrapped derivative indicates changes in the energies of A_{1u} , A_{2u} and E_g orbitals which are involved in the transition. In cross-trans-linked isomer, both the Soret and Q-bands are affected significantly and the magnitude of shifts of both Soret band and Q-bands are comparable. This indicates that the energy of $E_g(\pi^*)$ orbital of the porphyrin macrocycle is affected most in this isomer due to the introduction of the strap. The direction of the shift indicates a slight lowering of the energy of $E_g(\pi^*)$ orbital thus decreasing the energies of transition. However, by comparing the magnitude of red shifts in isomers II and III with that of isomer I, it appears that $E_g(\pi^*)$ orbitals are very less affected by the porphyrin ring distortion. In otherwords, the distortion created in the porphyrin skeleton by bridging adjacent phenyl groups is very less compare to the bridging of the opposite phenyl groups. Nevertheless, the magnitude of shifts of isomers II and III of meta xylyl bridged basket handle porphyrins described in the present study are comparable to those observed for the corresponding isomers of pentyl and butyl analogs suggesting similar degree of distortion in these isomers.

Pyrrole brominated cross-trans-linked porphyrins studied here showed further red shift of both Q- and Soret bands with reduction in intensity and their magnitude depends on the number of bromines substituted. This is because of the fact that the substituents on

pyrrole rings are known to decrease the energy of the transitions in the electronic absorption spectra⁷⁴. Theoretical IEH calculations⁷⁵ on relative effects of electron withdrawing β -substituents on meso-aryl porphyrins predict stabilisation of both HOMO $A_{1u}(\pi)$ and $A_{2u}(\pi)$ and LUMO $E_g(\pi^*)$ orbitals. However, the LUMO is slightly more stabilised relative to the HOMO. This is attributed to the weak "inductive" interactions with HOMO and strong "resonance" interactions with LUMO. Thus, the net result is decrease in the energy gap between the HOMO and the LUMO. INDO calculations^{30,32,76} on a series of nonplanar porphyrins predict destabilisation of porphyrin π -system upon distortion such that the HOMO level is principally raised more with a smaller perturbation in the LUMO, again decreasing the energy gap relative to the planar derivative. Thus, it clearly suggests that the red shifts observed upon β -substitution and distortion are due to different stabilisation/destabilisation mechanisms of the HOMO and the LUMO. A qualitative explanation is offered in the next chapter with the aid of spectroscopic energy shifts data.

Furthermore, the magnitude of red shifts with each bromine substitution at the pyrrole is nonadditive in contrast to a suggestion made by Callot^{74a}. From bromination study of H_2TPP , he has pointed out that each bromine substitution at the pyrrole position contributes a shift of 6 nm to the red region with respect to the bands observed for H_2TPP . However, in the present study the non-linear nature of the plot of magnitude of red shift versus the number of bromines substituted (Fig. 3.5) indicates that this prediction is not valid for bromo derivatives of cross-trans-linked isomer of basket handle porphyrins. This has

porphyrins (MSiCl_8 , MSiICl_8 and MSiIICl_8) and for PSIBr_8 and its pyrrole brominated derivatives. This couple is not observed for other strapped porphyrins and it is found to be reversible in all the cases when scanned separately. It is assigned to the reduction of bridging phenyl group having electron withdrawing substituents based on the electrochemical reduction of the corresponding dialdehyde under the same conditions. [(2,3,5,6-tetrabromo-p-phenylenedimethylenedioxy) dibenzaldehyde in CH_2Cl_2 exhibits a reversible couple at -1.015 V while the 2,4,5,6-tetrachloro-m-phenylenedimethylenedioxy) dibenzaldehyde shows an irreversible peak at -1.34 V]. This suggests that there is a possibility of intramolecular electron transfer from donor to acceptor in these kind of porphyrins which is of interest from the point of view of photoinduced electron transfer since the donor and the acceptor have a fixed orientation with respect to each other at a short distance.

A large body of data on electrochemistry of ring substituted porphyrins are well documented in literature^{73,74,77,79}. Generally, introduction of electron donating groups facilitates oxidation and hinders reduction at either metal center or porphyrin π -system. In contrast, introduction of electron withdrawing substituents at the porphyrin ring removes electron density and yields easier reductions and harder oxidations. Table 3.6 indicates a sudden change in the magnitudes of the ring centered oxidation and reduction potentials of pyrrole brominated derivatives of PSIBr_8 . It is observed that both ring oxidation and reduction peaks in brominated derivatives occurred at a more positive and less negative potentials respectively relative to

that found for PSIBr_8 . This supports the earlier conclusion⁸⁰ that the presence of electron withdrawing substituent bromine, at the β -pyrrole carbons makes the porphyrin ring easily reducible and difficult to oxidise. However, it shall be noted that, for a given substituent, the anodic shift is always smaller in oxidation than in reduction (table 3.6), namely, if

$$\Delta E_{1/2}^{\text{I(Ox)}} = E_{1/2}^{\text{I(Ox)}}(\text{PSIBr}_8(\text{Br})_n) - E_{1/2}^{\text{I(Ox)}}(\text{PSIBr}_8)$$

and

$$\Delta E_{1/2}^{\text{I(Red)}} = E_{1/2}^{\text{I(Red)}}(\text{PSIBr}_8(\text{Br})_n) - E_{1/2}^{\text{I(Red)}}(\text{PSIBr}_8)$$

$$n = 1, 4 \text{ and } 8 \quad \text{and} \quad \Delta E_{1/2}^{\text{I(Ox)}} < \Delta E_{1/2}^{\text{I(Red)}}$$

Thus the clear-cut difference between the oxidation and reduction behaviour, as a result of strong electron-withdrawing substituent bromine, may be ascribed primarily to a difference in the relevant reaction sites. The reductive electron transfer may be considered as a direct transfer to the π -electrons of the conjugated system⁸¹ with which the β -substituents are in direct resonance interaction⁸². On the contrary, the results obtained in oxidation preclude an electron transfer from the π -electron system and favour the interpretation that the lone electron pairs of the pyrrolic nitrogens are involved. As the potential shift due to bromine substitution are smaller in oxidation than in reduction, the pyrrolic nitrogens may indeed be the oxidative reaction site. Since the interactions of these nitrogens with the substituents are mostly inductive and inductive interactions are weaker than the conjugation (resonant) ones⁸³, the smaller effects observed in

Table 3.6 : Electrochemical data (V) for pyrrole brominated short chain basket handle porphyrins in dichloromethane containing 0.1 mol dm^{-3} TBAP

PORPHYRIN	OXIDATION			BRIDGE		REDUCTION		
	$E_{1/2}^I$	$E_{1/2}^{II}$	$\Delta E_{1/2}^I$	$E_{1/2}^{II}-E_{1/2}^I$	PHENYL REDUCTION	$E_{1/2}^I$	$E_{1/2}^{II}$	$\Delta E_{1/2}^{\text{Ox-Red}}$
PSIBr ₈	0.77	1.32	0	0.55	-1.14	-1.45	-	0 2.22
PSIBr ₉	0.89	1.32	0.12	0.43	-1.05	-1.34	-	0.11 2.23
PSIBr ₁₂	1.04 [*]	1.28 [*]	0.27	0.24	-0.92	-1.09	1.44	0.36 2.13
PSIBr ₁₆	1.11	-	0.34	0	-0.74	-0.99	-1.39	0.46 2.10

(*) Irreversible

oxidation than in reduction are expected. This interpretation is in agreement with the conclusions of Stanienda and coworkers⁸⁴ on the electrochemical reactivity of porphyrins.

An increased difficulty is observed for the oxidation of the porphyrin as the number of bromine substituents increases and the specific potential shift induced per bromine decreases as the number of bromines on the porphyrin ring increases. This weakening in the specific effect of the successive β -substituents may be rationalized in terms of antagonistic inductive effects of these substituents on the lone pairs of the pyrrolic nitrogens. As a consequence, the potential difference $\Delta E_{1/2}^{\text{I Ox-Red}}$ between the first oxidation wave and the first reduction wave of the porphyrin ligand decreases as the number of bromo substituents increases (table 3.6)

3.5.4 MOLECULAR MECHANICS CALCULATION

The calculated structures clearly reveal the nature of distortion created by linking the phenyl groups present at the periphery of the porphyrin system with various strapping groups. The porphyrin core shown in Fig 3.10 for adjacent-cis isomer can be compared to the "saddle conformation" described by Scheidt and Lee⁸⁵ in which the perpendicular displacement of pyrrole rings with respect to the mean plane of the porphyrin core are in the same direction and adjacent trans isomer to the "ruffled conformation" where the pyrrole rings are displaced alternatively above and below the mean plane of the porphyrin core. This is because both the straps are on same side in

adjacent-cis isomer which pulls the pyrrole rings upwards whereas the straps are on different side in adjacent-trans isomers which causes displacement of pyrrole rings alternatively up and down to the mean plane of the core. The different orientation of the strapping phenyl group in para and meta xylyl group suggests that short strap, because of the link at the meta position in MSICl_8 , forces the strapping phenyl group to adopt a slightly perpendicular orientation with respect to the porphyrin plane whereas in the para isomers (PSI and PSIBr_8) the relatively longer strap allows to turn towards parallel orientation with respect to the mean porphyrin plane. Furthermore, the bromines attached to the strap phenyl group in PSIBr_8 are almost touching the porphyrin core whereas chlorines in MSICl_8 are forced to move away from the porphyrin core due to short bridging group.

Table 3.7 : Bond distances (\AA) between pyrrolic nitrogen and hydrogens bonded to nitrogens.

PORPHYRIN	H.....H	N(A) ^aN(A)	N(B) ^bN(B)
H_2TPP	2.0477	4.0677	4.0133
MSII	1.9474	3.9682	4.0438
MSIII	2.0656	4.0545	4.0078
PSI	1.9684	3.9886	3.8821
PSIBr_8	1.8912	3.9107	3.9972
MSICl_8	1.7915	3.8116	3.9089

a: Nitrogens which are bonded to hydrogens

b: Nitrogens which are not bonded to hydrogens

The calculated bond distances between nitrogens of the

porphyrin core and hydrogens attached to nitrogens (table 3.7) show a considerable decrease in the distance relative to H_2TPP confirming the observed deformity in the porphyrin ring. In addition, the twist angle, $C_\alpha-N-N-C_\alpha$ gives a rough measure of degree of nonplanarity³²⁻³⁴. From table 3.5 it is clear that the twist angles are considerably larger for basket handle porphyrins than planar H_2TPP further proving the permanent deformation existing in the basket handle porphyrins. The increase of $C_\alpha-N-C_\alpha$ and decrease of $C_\alpha-C_m-C_\alpha$, $N-C_\alpha-C_\beta$ and $N-C_\alpha-C_m$ bond angles relative to H_2TPP also supports the above conclusion. Interestingly, introduction of bromines at the carbon of β -pyrroles does not alter the orientation of the strap phenyl in $PSIBr_{12}$. However, degree of distortion is increased by pyrrole bromination as evident by the large red shifts of optical bands. To estimate the relative distortions of $PSIBr_8$ and $PSIBr_{12}$, we made an attempt to calculate the bond distances between C_m and one of the carbon of the strap phenyl group with a view that if distortion is increased, the C_m 's will move more and more out of the plane of the porphyrin and hence their distance from the strap phenyl will also change. The increase of the bond distance of C_m and one of the carbon of the strap phenyl group in $PSIBr_{12}$ (4.823 \AA) relative to $PSIBr_8$ (4.746 \AA) is consistent with the above mentioned facts. Thus, the geometry optimized structure provides an explanation for the unusual spectral and electrochemical behaviour of basket handle porphyrins.

3.6 CONCLUSIONS

Short chain basket handle porphyrin systems reported here

provide unique opportunity to study many facets of porphyrin ring nonplanarity.

- * The short bridging chain results in considerable distortion in the porphyrin skeleton of basket handle porphyrins as is evident by spectroscopic and electrochemical behaviour.
- * Optical bands experience considerable red shift in comparison with unstrapped H_2TPP and a linear correlation is observed between the magnitude of the optical absorption band shifts and the degree of distortion present in short chain basket handle porphyrins.
- * Cyclic voltammetric studies indicate that basket handle porphyrins are better donors than planar H_2TPP . The easier oxidations and harder reductions relative to H_2TPP suggest that these shifts are structural rather than electronic in origin due to the nature of the bridging group.
- * Maximum shifts in optical bands and redox potentials are observed for cross-trans-linked isomer of basket handle porphyrins indicating that linking the opposite phenyls present at the periphery of the porphyrin ring induces considerable distortion relative to linking the adjacent phenyl groups by short bridging chains.
- * Introduction of electron withdrawing bromine substituents at the β -carbons of the pyrroles have large and different effects on the optical and electrochemical oxidation and reduction potentials. The bromine substituents produce dramatic shifts in the Soret and Q-bands of the porphyrins. This has been interpreted in terms of both inductive and conjugative effects induced by the bromine substituents. The

relative ease of reduction and difficulty in oxidation of the bromo substituted cross-trans-linked porphyrins relative to the parent unsubstituted cross-trans-linked porphyrins have been explained on the basis of substituent effects.

- * Molecular mechanics calculations reveal clearly the various modes of distortion present in different isomers of basket-handle porphyrins due to strapping of phenyl groups present at the periphery of the bridging chain. It offers an explanation for the unusual spectral and electrochemical shifts observed in the basket handle porphyrins relative to planar porphyrins.

CHAPTER 4

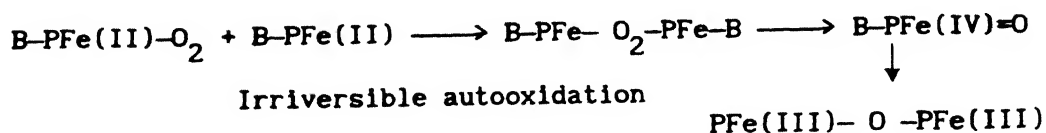
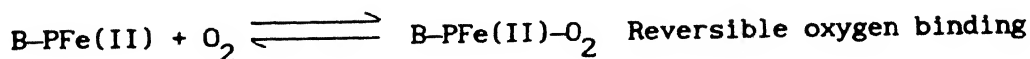
EFFECT OF METAL IONS (COPPER(II), IRON(III)) ON OPTICAL AND ELECTRONIC PROPERTIES OF SHORT-CHAIN BASKET HANDLE PORPHYRINS

4.1 INTRODUCTION

In the preceding chapter, the effect of nonplanarity on spectral and electrochemical properties of basket handle porphyrins is described. It is clear that the short straps used for linking the opposite or adjacent phenyls present at the periphery of the porphyrin have induced considerable distortion in the porphyrin ring. Three isomers are formed by condensation of appropriate dialdehyde and magnitude of distortion present in the porphyrin skeleton depends mainly on nature of the isomer. Spectroscopic and electrochemical studies on free base basket handle porphyrins confirmed that cross-trans-linked isomer showed maximum distortion relative to adjacent-trans or adjacent-cis-isomer. Although the studies related to deformation effect on physico-chemical properties of porphyrin ligands in free base basket handle porphyrins are quite useful in understanding

structure-function relationship, it is the study of metallo-porphyrins which gives ultimately a molecular level understanding of the properties and structure-function relationship occurring in the natural systems.

Since most of the natural porphyrins are iron containing porphyrins⁸⁶, many reports have appeared in recent years on supra-structural iron containing porphyrins⁸⁷. Most of the work has been done on synthetic models of heme containing proteins. The functional differentiations of heme proteins (hemoglobin, myoglobin, cytochromes, catalase and peroxidases) having the same prosthetic group (iron protoporphyrin-IX) arises from differences in the nature of axial ligation of the heme iron and from differences in the protein environment surrounding the heme. The first difficulty is the reproduction of the redox stability of the iron(II) upon exposure to dioxygen. In solution, simple iron(II) porphyrins cannot reversibly bind dioxygen, except at low temperature. At room temperature and in the absence of a large excess of nitrogenous ligands six coordinated, iron(II) oxygen complex is immediately converted to a μ -oxo-dimer via a μ -peroxo dimer and an iron(IV)-oxo species following a binuclear reaction. This reaction does not occur in hemoproteins because the polypeptide chain surrounding the heme prevents the close approach of two hemes and the subsequent oxidation.



To inhibit such an undesirable reaction, different modified porphyrins have been proposed. Each of these porphyrins is sterically encumbered on one side, thereby directing the binding of a nitrogenous base to the other side. Such an approach has been followed by many groups to produce an array of different model porphyrins : picket fence, cyclophane and capped⁸⁸. Thus, the bulky substituents cover one side of the heme in such a way that no irreversible autooxidation takes place as long as the other side is occupied by an axial ligand which favours reversible oxygenation. Steric encumbrance on both faces of the porphyrin, as in the "bis-pocket" porphyrin systems or basket handle porphyrins⁸⁸, may prevent this bimolecular oxidation pathway.

Momenteau and his colleagues⁸⁹ illustrated the degree of steric hindrance by the rates of metallation and oxidation of the various isomers of basket handle porphyrins. The adjacent -cis-linked isomer has one face hindered, and is easily metallated. In contrast the other isomers, where both faces are hindered, undergo iron insertion reluctantly. Either in the presence or in the absence of nitrogenous base, the iron(II) complexes of basket-handle porphyrins exhibit a remarkable redox stability towards oxidation when they are exposed to one atmosphere of dioxygen even at room temperature.

4.2 WORK DONE IN THE PRESENT STUDY

In the course of our investigations it is realized that it would be interesting to look at the deformation effect on the geometry around metal ion in all three isomers of basket handle

porphyrins. It would be interesting to see how the metal insertion into these distorted porphyrin systems effect their spectral and electrochemical properties. Simonis et.al. concluded that metal insertion into the most deformed isomer I is not possible due to steric hindrance provided by straps present above and below the plane of the porphyrin. However, we have been successful in introducing Cu^{2+} into the porphyrin core of isomer I (Fig. 4.1). This chapter gives the details of our studies on copper(II) derivatives of isomer I and high spin iron(III) derivatives of isomer II and III. The chapter is divided into two sections. In Section A the synthesis, spectral and electrochemical properties of copper(II) derivatives of various isomers I of basket handle porphyrins are described and Section B describes synthesis and preliminary studies on spectral and electrochemical properties of iron(III) derivatives of isomer II and isomer III.

SECTION A

SPECTRAL AND ELECTROCHEMICAL STUDIES ON COPPER(II) DERIVATIVES OF BASKET HANDLE PORPHYRINS

4.3 EXPERIMENTAL

Free base porphyrins were prepared as described in previous chapter.

4.3.1 General method for the synthesis of copper(II) porphyrins

The free base porphyrins and a two fold excess of copper(II) acetate in dimethylformamide was heated under reflux at 160°C for

8 h. The progress of the reaction was monitored by recording the absorption spectra of aliquots taken at different intervals of time. After completion of the reaction, the reaction mixture was concentrated to small volume and poured into a beaker containing water. Extraction with chloroform ($3 \times 100 \text{ cm}^3$) and drying over anhydrous sodium sulfate gave the crude product. This was purified by column chromatography using neutral alumina and chloroform as eluent.

FAB MASS :

4.3.2 Cu Hexyl I : Calculated for $\text{C}_{56}\text{H}_{48}\text{CuN}_4\text{O}_4$: 906.54

Observed : $m/z = 906$.

4.3.3 CuPSI : Calculated for $\text{C}_{60}\text{H}_{40}\text{CuN}_4\text{O}_4$: 946.56

Observed : $m/z = 946$.

4.3.4 CuMSICl₈ : Calculated for $\text{C}_{60}\text{H}_{32}\text{CuN}_4\text{O}_4\text{Cl}_8$: 1222

Observed : $m/z = 1220$.

4.3.5 CuPSIBr₈ : Calculated for $\text{C}_{60}\text{H}_{32}\text{CuN}_4\text{O}_4\text{Br}_8$: 1577.50

Observed : $m/z = 1577$

4.3.6 CuPSIBr₉ : Calculated for $\text{C}_{60}\text{H}_{31}\text{CuN}_4\text{O}_4\text{Br}_9$: 1657

Observed : $m/z = 1657$.

4.3.7 CuPSIBr₁₂ : Calculated for $\text{C}_{60}\text{H}_{28}\text{CuN}_4\text{O}_4\text{Br}_{12}$: 1897

Observed : $m/z = 1896$.

4.4 RESULTS

4.4.1 ELECTRONIC SPECTRA

A comparison of various deformed copper(II) porphyrins are shown in the Figs. 4.2 and 4.3 and the absorption data is listed in table 4.1. The following points are of interest from table 4.1:

- * A considerable red shift of soret and Q-bands with reduction in intensity relative to CuTPP.

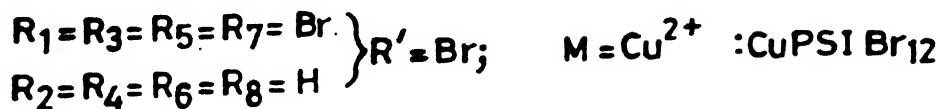
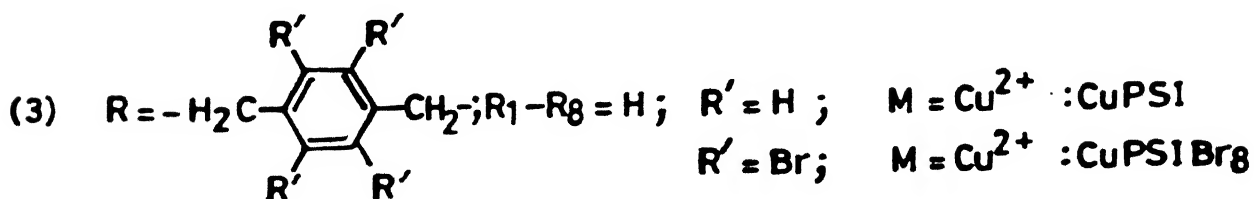
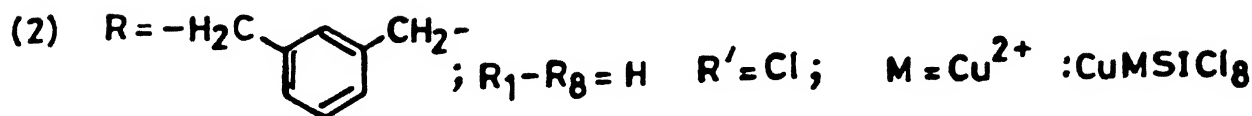
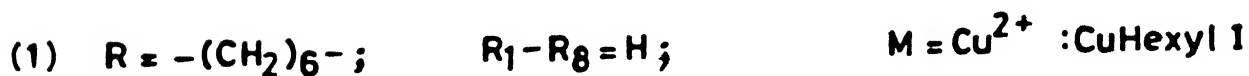
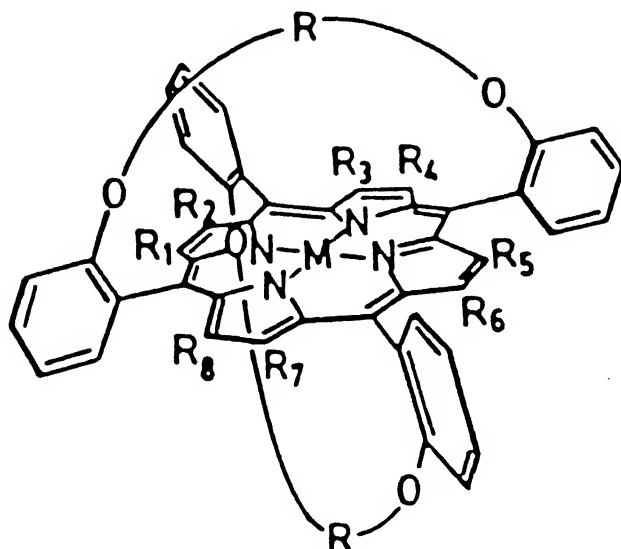


Fig. 4.1 : Structure of Copper(II) derivatives of cross-trans-linked isomer of various short chain basket handle porphyrins.

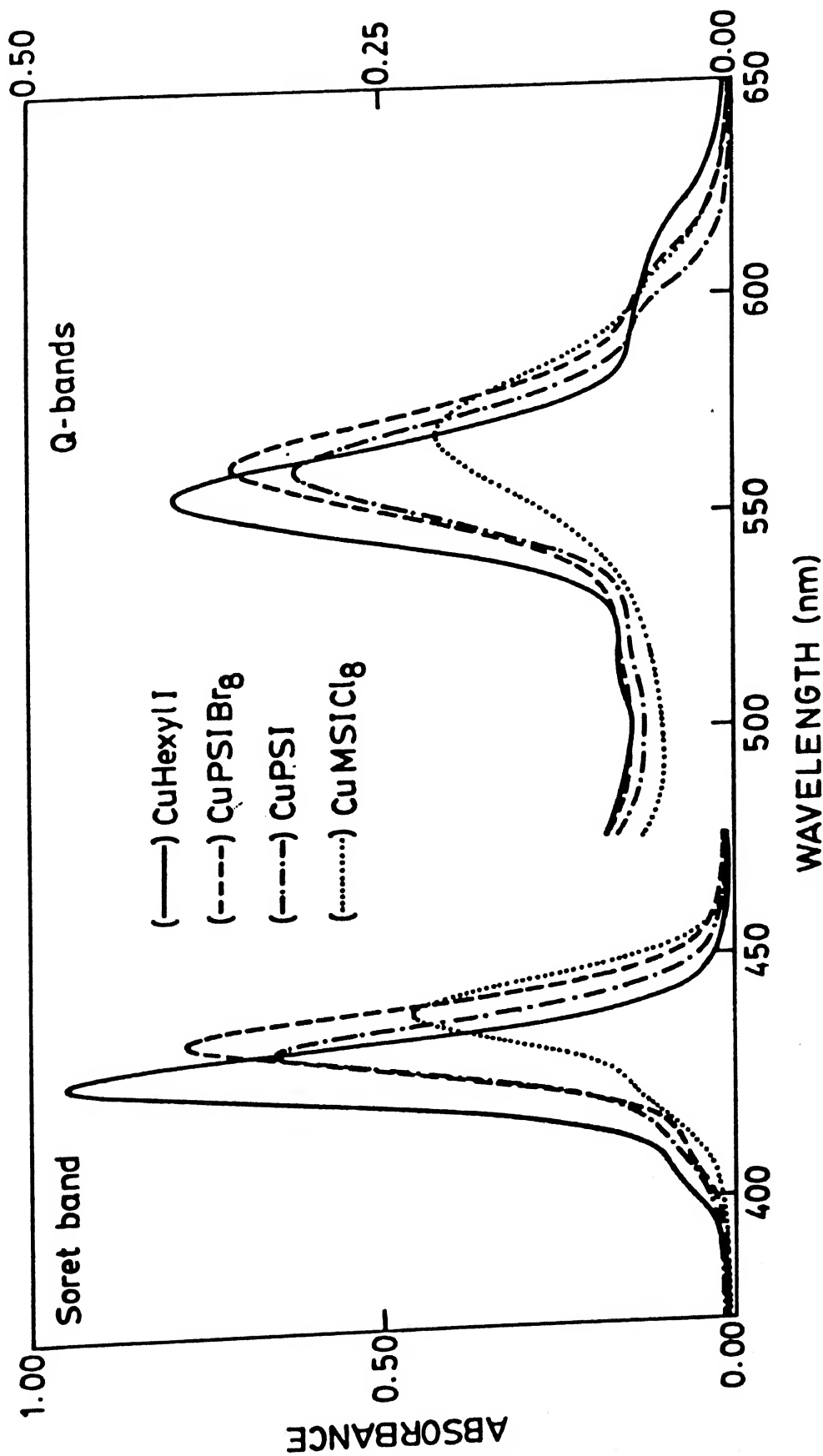


Fig. 4.2 : Comparison of optical absorption spectra of various Copper (II) porphyrins in chloroform for the Soret and Q-band region. The concentrations used were $\approx 5 \times 10^{-6} \text{ mol dm}^{-3}$ for Soret and $\approx 5 \times 10^{-5} \text{ mol dm}^{-3}$ for Q-bands.

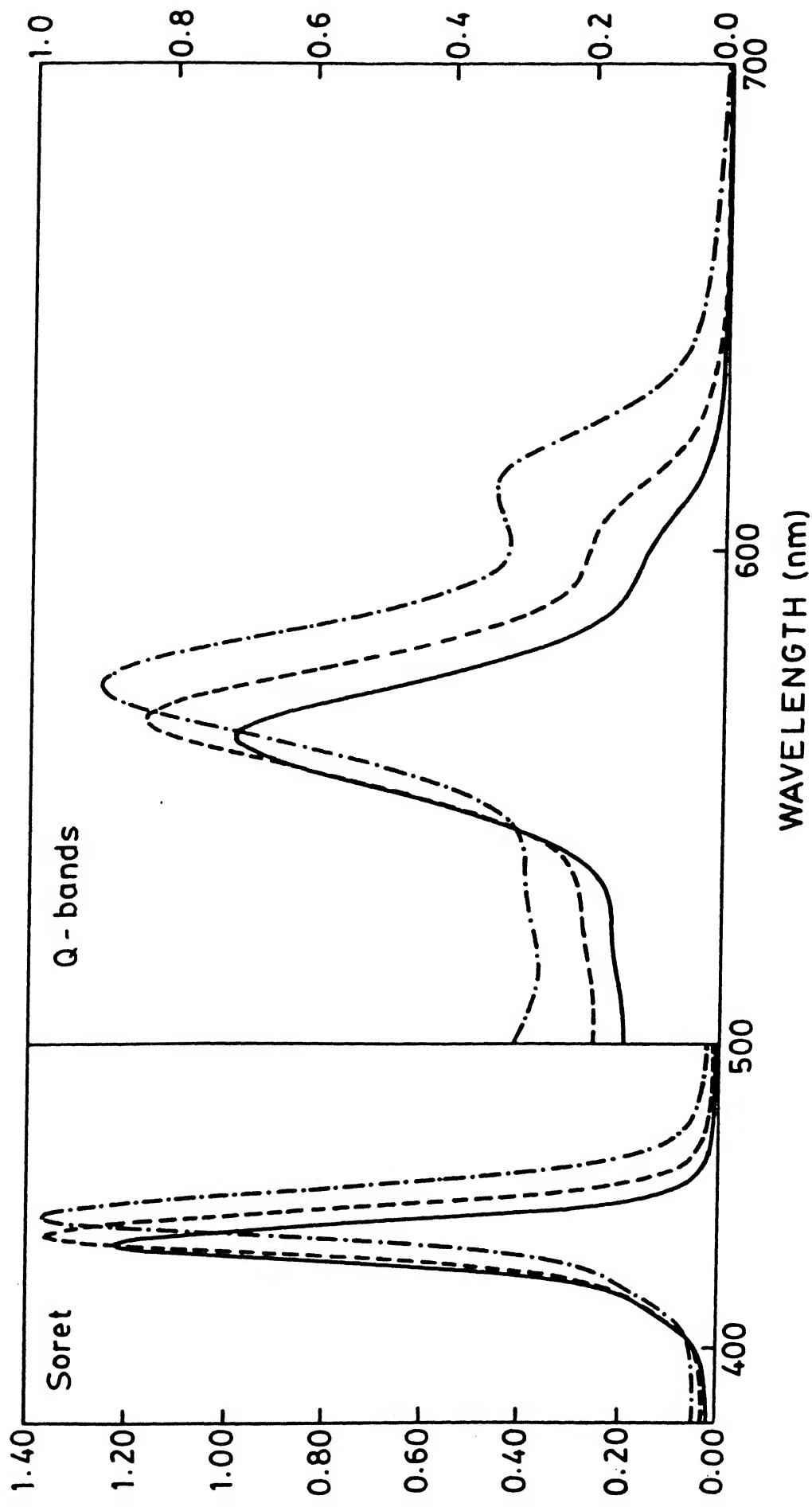


Fig. 4.3 : Comparison of absorption spectra of CuPSIBr₉ (----) and CuPSIBr₁₂ (-.-.-.-) relative to CuPSIBr₈ (—) in chloroform. Concentrations used were $\approx 5 \times 10^{-5} \text{ mol dm}^{-3}$ for Q-bands and $\approx 5 \times 10^{-6} \text{ mol dm}^{-3}$ for Soret band.

- * The magnitude of red shifts and intensity reduction depends on the length of the bridging chain.
- * Substitution of bromines at the β -positions of the pyrrole resulted in further red shift of all the bands and their magnitude depends on the number of bromines substituted. However, these shifts are nonadditive.
- * The effect of electron-withdrawing substituents on the phenyl ring of the bridging group is reflected in a further reduction in intensity of Soret and Q-bands. However, extinction coefficients are slightly higher upon β -substitution.

Table 4.1 : Electronic spectral data of Cu(II) derivatives of various cross-trans-linked basket handle porphyrins in chloroform

PORPHYRIN	Soret band	Q-bands	
	λ_{\max} (nm)	λ_{\max} (nm) ($10^{-3} \epsilon / \text{dm}^3 \text{mol}^{-1} \text{cm}^{-1}$)	
	($10^{-4} \epsilon / \text{dm}^3 \text{mol}^{-1} \text{cm}^{-1}$)	I	II
CuTPP	417 (41.69)	540 (19.5)	580
CuHexylII	427 (31.26)	556 (13.7)	594 (2.29)
CuPSI	432 (14.82)	562 (6.97)	600 (1.46)
CuMSICl ₈	440 (12.61)	569 (5.80)	611 (1.55)
CuPSIBr ₈	435 (21.53)	563 (19.52)	603 (2.06)
CuPSIBr ₉	437 (23.11)	566 (14.17)	605 (3.29)
CuPSIBr ₁₂	444 (20.99)	573 (13.80)	613 (5.11)

The magnitude of the band shifts for copper derivatives of

CHAPTER 4

present study relative to CuTPP⁹⁰ are comparable to the shifts observed for their corresponding free bases relative to unstrapped H₂TPP suggesting that the introduction of the Cu²⁺ ion does not alter the degree of distortion. In addition, from the absorption data it is clear that the degree of distortion mainly depends on the bridging chain length rather than the nature of the bridging group.

4.4.2 ELECTROCHEMISTRY

A comparison of cyclic voltammograms of copper(II) derivatives of various deformed porphyrins with that of planar CuTPP is shown in Fig.4.4 and cyclic voltammograms of CuPSIBr₈ and CuPSIBr₁₂ is shown in Fig 4.5. A comparison of the data (table 4.2) reveal the following effects :

- * Ist oxidation potential of Cu(II) derivative of basket handle porphyrins is found to be shifted to less positive value than CuTPP^{77,91}.
- * Ist reduction potential of Cu(II) derivative of basket handle porphyrins is shifted to more negative value relative to CuTPP.
- * An additional reduction couple at ~-1.14 V is present for CuMSICl₈, CuPSIBr₈ and its pyrrole brominated porphyrins. This couple is absent in CuHexyl I and CuPSI.
- * Pyrrole brominated derivatives exhibit harder oxidations and easier reductions relative to parent CuPSIBr₈. However, the shift in redox potentials is nonadditive and the specific potential shift induced per bromine decreases as the number of bromines on the porphyrin ring increases.

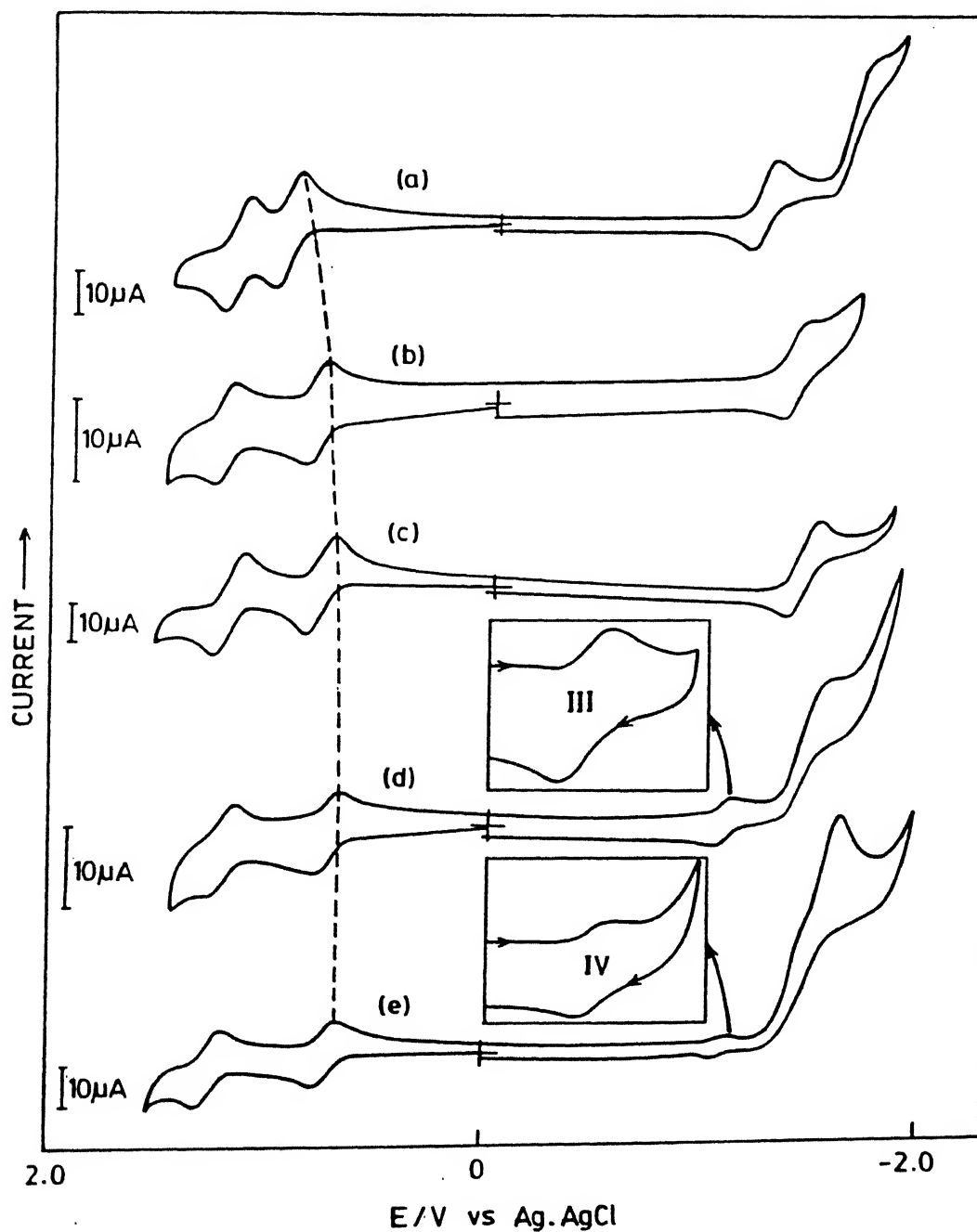
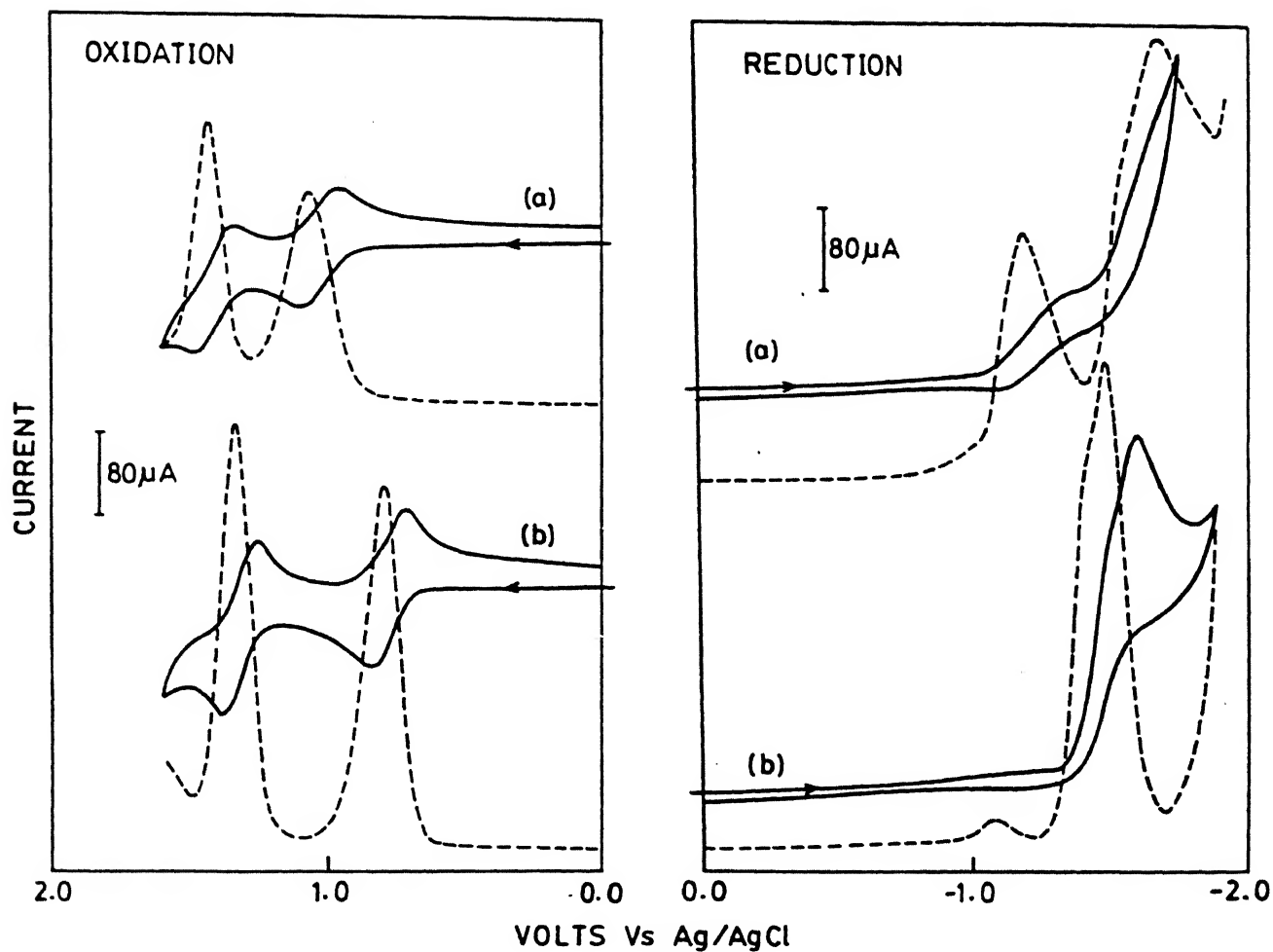


Fig. 4.4 : Cyclic voltammograms of (a) CuTPP, (b) CuPSI, (c) CuHexyl I, (d) CuMSICl₈ and (e) CuPSIBr₈. The concentrations used were $\approx 5 \times 10^{-4} \text{ mol dm}^{-3}$. The Scan rate is 100 mV/sec. The inset shows the reversible nature of bridging phenyl ring reduction. The potentials are versus Ag/AgCl with TBAP as the supporting electrolyte.



4.5 : Cyclic voltammograms of (a) CuPSIBr_8 ($6.3 \times 10^{-4} \text{ mol dm}^{-3}$) and (b) CuPSIBr_{12} ($7.6 \times 10^{-4} \text{ mol dm}^{-3}$) in dichloromethane containing 0.1M TBAP at room temperature (Scan rate : 200 mV/s). Dotted line corresponds to differential pulse voltammograms (Scan rate : 10 mV/s).

Table 4.2 : Electrochemical redox data (V) of Cu(II) derivatives of short chain basket handle porphyrins in dichloromethane containing 0.1 mol dm^{-3} TBAP

PORPHYRIN	RING OXIDATION		BRIDGE PHENYL REDUCTION	RING REDUCTION	
	I	II		I	II
CuTPP	1.06	1.31	-	-1.14	-1.74
CuHexylI	0.81	1.25	-	-1.50	-
CuPSI	0.85	1.50	-	-1.45	-
CuMSICl ₈	0.76	1.26	-1.14	-1.51	-
CuPSIBr ₈	0.74	1.30	-1.14	-1.66	-
CuPSIBr ₉	0.87	1.35	-1.05	-1.38	-
CuPSIBr ₁₂	1.07	1.43	-	-1.23	-1.70

4.4.3 ESR SPECTRAL STUDIES

In order to evaluate the changes in the electronic structure of Cu^{2+} upon β -substitution and distortion, ESR spectra of Cu^{2+} derivatives were recorded at room temperature and low temperature (Figs. 4.6 and 4.7) and the ESR data is tabulated in table 4.3. The room temperature spectra displays four resolved copper lines with superhyperfine structure observed for high field lines⁹². The low temperature spectra suggests an axial symmetry with resolved hyperfine couplings both in parallel and perpendicular fields. The ESR parameters of Cu^{2+} basket handle porphyrins (table 4.3) shows little variation from unstrapped CuTPP⁹² indicating that the nonplanarity of the porphyrin ring has little influence on the ESR spectra. However, the $A_{\parallel}^{\text{Cu}}$ and A_{O}^{Cu} decreases

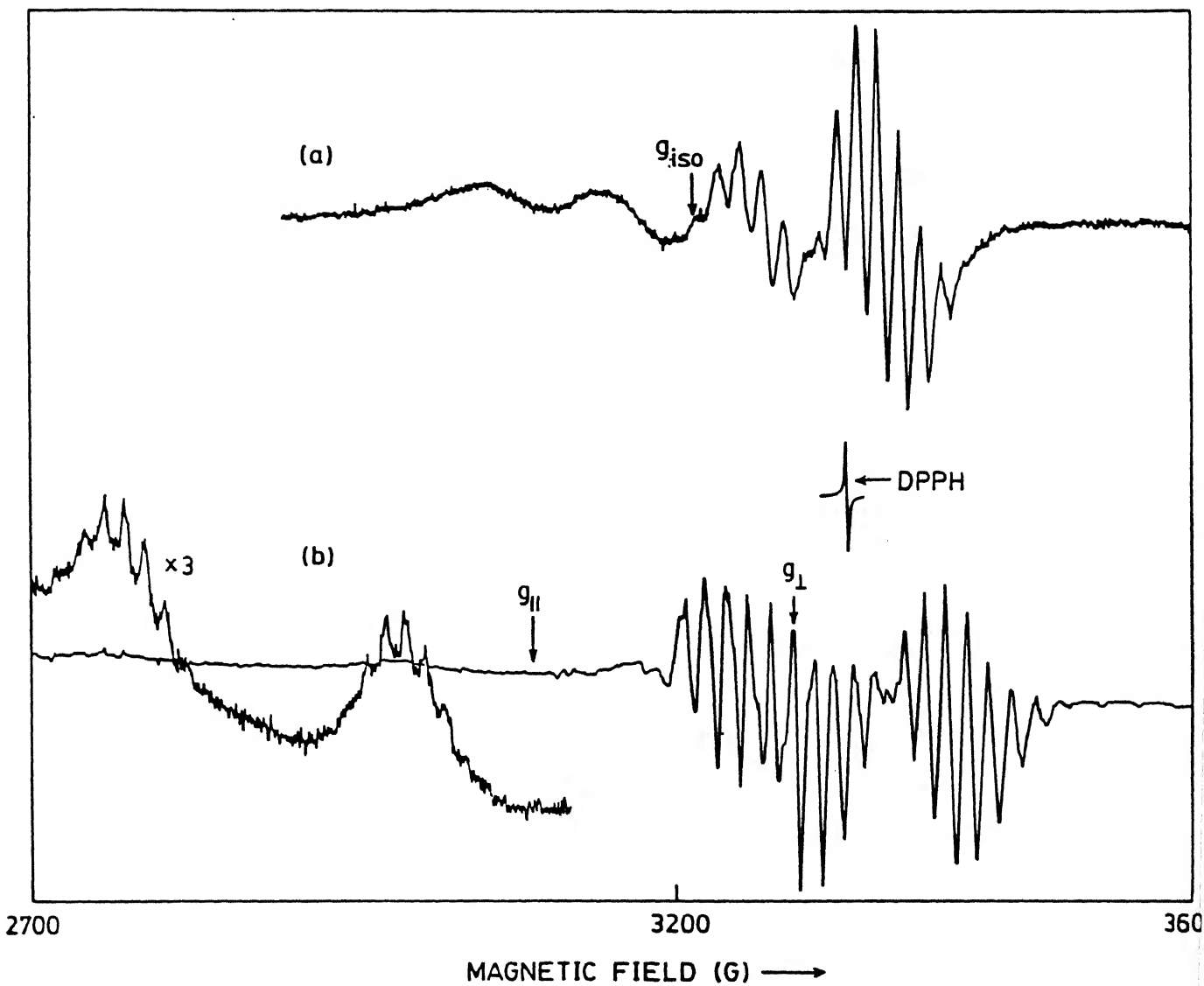


Fig. 4.6 : ESR spectra in chloroform:toluene (1:1) of
(a) CuHexyl I at 300 K and (b) CuPSIBr₈ at 130 K.

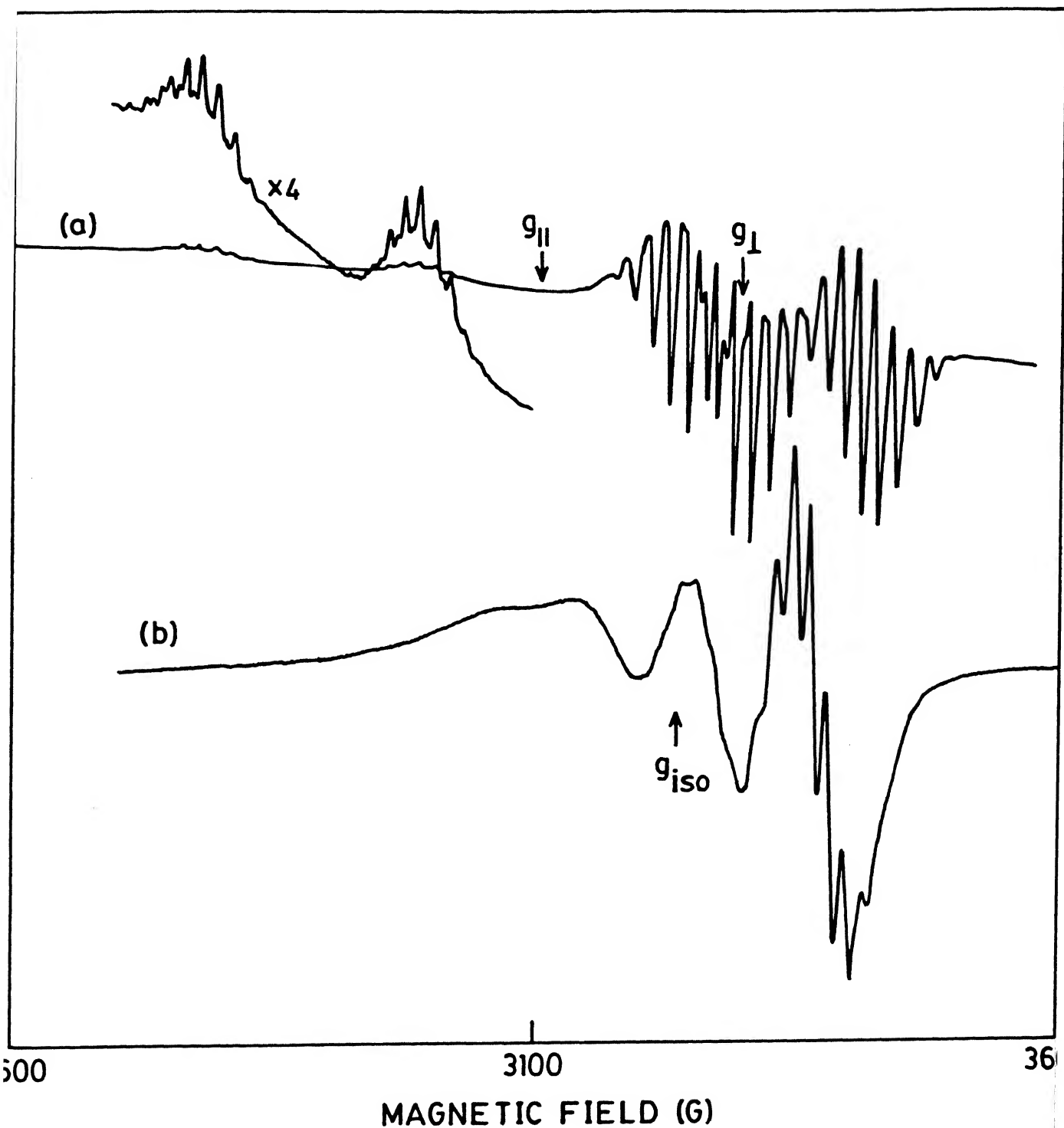


Fig. 4.7 : ESR Spectra of CuPSIBr_9 in toluene:chloroform (1:1)

(a) at 100 K and (b) at room temperature.

Table 4.3 : ESR data of Cu(II) derivatives of cross-trans-linked short chain basket handle porphyrins in chloroform : toluene (1:1)^{*}

PORPHYRIN	g_{\parallel}	g_o	Λ_{\parallel}^{Cu}	Λ_1^{Cu}	Λ_{11}^N	Λ_1^N	α^2	g_{Iso}	$\Lambda_0^{Cu} \times 10^4 \text{ cm}^{-1}$	$\Lambda_0^N \times 10^4 \text{ cm}^{-1}$
CuTPP	2.187	2.067	218	32.80	14.5	16.40	0.7500	2.17	97.7	15.90
Cuhexyl I	2.155	2.057	205	32.50	n.r.	16.25	0.7239	2.090	90.00	16.30
CuPSI	2.159	2.054	202	32.88	n.r.	16.44	0.7212	2.089	89.51	15.85
CuMSICl ₈	2.161	2.042	200	30.22	14.0	15.11	0.7234	2.081	86.96	16.30
CuPSIBr ₈	2.161	2.056	205	32.00	14.9	15.99	0.7332	2.091	89.70	15.85
CuPSIBr ₉	2.159	2.056	190	31.62	14.3	15.81	0.6485	2.081	87.8	15.80
CuPSIBr ₁₂	2.160	2.021	188	31.23	14.0	15.61	0.6347	2.082	86.2	15.20

(*) 'A' values in 10^{-4} cm^{-1} and the sign of 'A' is negative

gradually with increasing distortion relative to CuTPP probably indicating the expected nonplanarity around Cu^{2+} ion^{93,94}. The α^2 value which represents the strength of the Cu-N σ -bond⁹⁵ is calculated from experimental data. The small decrease in α^2 value indicates a weaker copper-nitrogen interaction in the distorted derivatives. Substitution of electron withdrawing groups at β -positions further weakens the Cu-N bond as evident from their decreased α^2 values.

4.5 DISCUSSION

4.5.1 ANALYSIS OF SPECTRAL AND ELECTROCHEMICAL SHIFTS

The magnitude of spectral and the redox potential shifts in the distorted copper(II) porphyrins relative to CuTPP suggests that the introduction of Cu^{2+} into the porphyrin core does not alter the degree of distortion. An attempt has been made here to understand these shifts using a treatment of Crossley and coworkers⁹⁰. The method relates the shifts observed in the center of gravity of Q- and B bands⁹⁶ in the absorption spectra (δE^{cg}) and the redox potentials ($\delta E_{\text{O}}^{\text{redI}}$ and $\delta E_{\text{O}}^{\text{oxI}}$) due to the substituent to the energy shifts of HOMO [$A_{1u}(\pi)$ and $A_{2u}(\pi)$] and LUMO [$E_g(\pi^*)$]. Using this method, the energy shifts in the A_{1u} , A_{2u} and the E_g orbitals of copper(II) derivatives of various deformed basket handle porphyrins are calculated by taking the data of planar CuTPP as reference. Thus, for the effect of distortion and the presence of electron withdrawing substituents on the n th oxidation or reduction potential, E_{O}^n , one can write

$$\Delta E_{\text{O}}^n(d) = E_{\text{O}}^n(d\text{-CuBHP}) - E_{\text{O}}^n(\text{CuTPP}) \quad 4.1$$

For a given reference electrode, these quantities are related to ionization potentials (I), electron affinities (A), and solvation energies (σ^{\pm}), as follows :

$$\delta E_{\text{o}}^{\text{red I}}(\text{d}) = (A - \alpha^{-})(\text{d-CuBHP}) - (A - \alpha^{-})(\text{CuTPP}) \quad 4.2$$

$$\delta E_{\text{o}}^{\text{ox I}}(\text{d}) = (I - \alpha^{+})(\text{d-CuBHP}) - (I - \alpha^{+})(\text{CuTPP}) \quad 4.3$$

At this level of approximation, the difference in solvation energy between deformed and planar porphyrins can be neglected and simplify equations 4.2 and 4.3 to

$$\delta E_{\text{o}}^{\text{red I}}(\text{d}) = A(\text{d-CuBHP}) - A(\text{CuTPP}) \quad 4.4$$

$$\delta E_{\text{o}}^{\text{ox I}}(\text{d}) = I(\text{d-CuBHP}) - I(\text{CuTPP}) \quad 4.4$$

In terms of the one electron scheme, the above equations can be written as

$$\delta E_{\text{o}}^{\text{red I}}(\text{d}) = -\delta \epsilon_{\text{k}}(\text{d}) \quad 4.5$$

$$\delta E_{\text{o}}^{\text{ox I}}(\text{d}) = -\delta \epsilon_{\text{j}}(\text{d}) \quad 4.6$$

where $\delta \epsilon_{\text{k}}$ corresponds to shift in the energy of the doubly degenerate E_{g} orbital and $\delta \epsilon_{\text{j}}$ corresponds to shift in the energy of either $A_{1\text{u}}$ or $A_{2\text{u}}$ orbital. For the calculation of energy shift in the remaining HOMO ($A_{1\text{u}}$ or $A_{2\text{u}}$) orbital, it is required to know the centre of gravity (E^{cg}) of the Q-B system, defined as

$$E^{\text{cg}} = 1/2 [E(\text{B}) + E(\alpha)] \quad 4.7$$

The centre of gravity E^{cg} of the Q and B bands of the metallo-porphyrin is given in a usual notation by

$$E^{CG} = \left[\epsilon_k - \frac{1}{2} (\epsilon_i + \epsilon_j) \right] - \frac{1}{2} \left[J_{ik} + J_{jk} - 2K_{ik} - 2K_{jk} \right] \quad 4.7$$

Thus, the shift of the Q-B center of gravity $\Delta E^{CG}(d)$ by deformation (d) is given by

$$\delta E^{CG}(d) = \delta \epsilon_k - \frac{1}{2} (\delta \epsilon_i + \delta \epsilon_j) \quad 4.8$$

where

$$\delta \epsilon_i = 2 \left(\delta E^{CG} + \delta \epsilon_k - \frac{1}{2} \delta \epsilon_j \right)$$

The values for $\delta \epsilon_k$, $\delta \epsilon_i$ and $\delta \epsilon_j$ so obtained are presented in table 4.4. The data of table 4.4 clearly shows the shifts of the frontier orbitals upon distortion and β -substitution on the porphyrin ring. Thus, on going from CuPSI to CuMSICl₈, the relative energies in $\delta \epsilon_k$, $\delta \epsilon_j$ and $\delta \epsilon_i$ increase suggesting destabilization upon increasing distortion. On the other hand, there is a gradual decrease in $\delta \epsilon_k$, $\delta \epsilon_j$ and $\delta \epsilon_i$ energies upon bromine substitution indicating relative stabilisation of these orbitals. Assuming that the β -substituent effect is approximately proportional to the β -density⁹⁰, the larger decrease in $\delta \epsilon_j$ and $\delta \epsilon_k$ relative to $\delta \epsilon_i$ can be rationalized provided that $\delta \epsilon_j$ and $\delta \epsilon_i$ are identified respectively with A_{2u} and A_{1u} orbital shifts. This is in conformity with the fact that $A_{2u} > A_{1u}$ in meso aryl porphyrins. Thus, this clearly suggests that the red shifts observed upon β -substitution and distortion are due to different stabilization/ destabilization mechanisms of the HOMO and the LUMO.

Table 4.4 : Spectroscopic energy shifts vs. redox potentials

PORPHYRIN	Electronic centre of gravity (E^{CG}) (eV)	I oxidn	I redn	(eV)		
				$\delta_{\epsilon i}$ <i>A_{1u}</i>	$\delta_{\epsilon j}$ <i>A_{1u}</i>	$\delta_{\epsilon k}$ <i>E_g</i>
CuTPP	0	0	0	0	0	0
CuHexylI	-0.06001	-0.25	-0.360	0.590	0.25	0.36
CuPSI	-0.08725	-0.21	-0.310	0.585	0.21	0.31
CuMSICl ₈	-0.12884	-0.30	-0.370	0.698	0.30	0.37
CuPSIBr ₈	-0.10228	-0.32	-0.340	0.565	0.32	0.34
CuPSIBr ₉	-0.11221	-0.19	-0.238	0.510	0.19	0.24
CuPSIBr ₁₂	-0.1461	-0.01	-0.087	0.476	-0.01	0.087

The plot in Fig.4.8 is quite revealing. It is inferred from the plot that the β -substitution by bromines increases the relative separation between A_{1u} and A_{2u} orbitals relative to CuTPP and the magnitude of increase is proportional to the number of bromines substituted. The free base derivatives also show the same trend. A similar conclusion was arrived at by Krishnan and Bhyrappa²¹ from their studies on metalloctabromotetraphenylporphyrin (MOBP). It has been shown that the relative separation between A_{1u} and A_{2u} increases in MOBP derivatives relative to the corresponding MTPP derivatives and the energy of the A_{2u} orbital is found to be dependent on the electronegativity of the metal while A_{1u} energy remain independent of the nature of the metal ion. It is pertinent to point out here that their data analysis is based on a different method developed by Shelnutt and Ortiz⁹⁷.

On the other hand, the relative increase in energy separation between A_{1u} and A_{2u} is considerably smaller upon distortion of the porphyrin plane (Fig. 4.8 Inset). This is not surprising considering the fact that the distortion is a steric effect while the β -substitution directly affects the porphyrin conjugation through a strong resonance interaction⁷⁸.

All copper(II) derivatives exhibit two separate one electron porphyrin ring centred oxidations corresponding to the formation of mono- and dications respectively. Both the oxidations are reversible with the ratio of peak currents close to unity. The one electron reductions of the porphyrin ring are observed in all the copper(II) derivatives suggesting the formation of monoanions. The oxidations are easier and reductions are harder reflecting the effect of nonplanarity on redox potentials in metalloderivatives as found in free base porphyrins. Furthermore, the extra reduction couple at $\sim -1.14V$ is also found in copper derivatives of tetrachloro or tetrabromo substituted meta or para xylyl bridged porphyrins only, which is assigned to the reduction of the phenyl ring having electron withdrawing substituents.

The direction of electrochemical potential shifts upon substitution of bromines are in agreement with the large body of the literature data on the substituent effects of porphyrins^{73,75,79,80,98}. Moreover, the magnitude of shifts are not additive both for oxidation and reduction. The optical absorption red shifts also follows the same trend. This has been ascribed in part to antagonistic inductive effects of substitution on the lone pair of the pyrrolic nitrogens⁷⁸. The steric effect

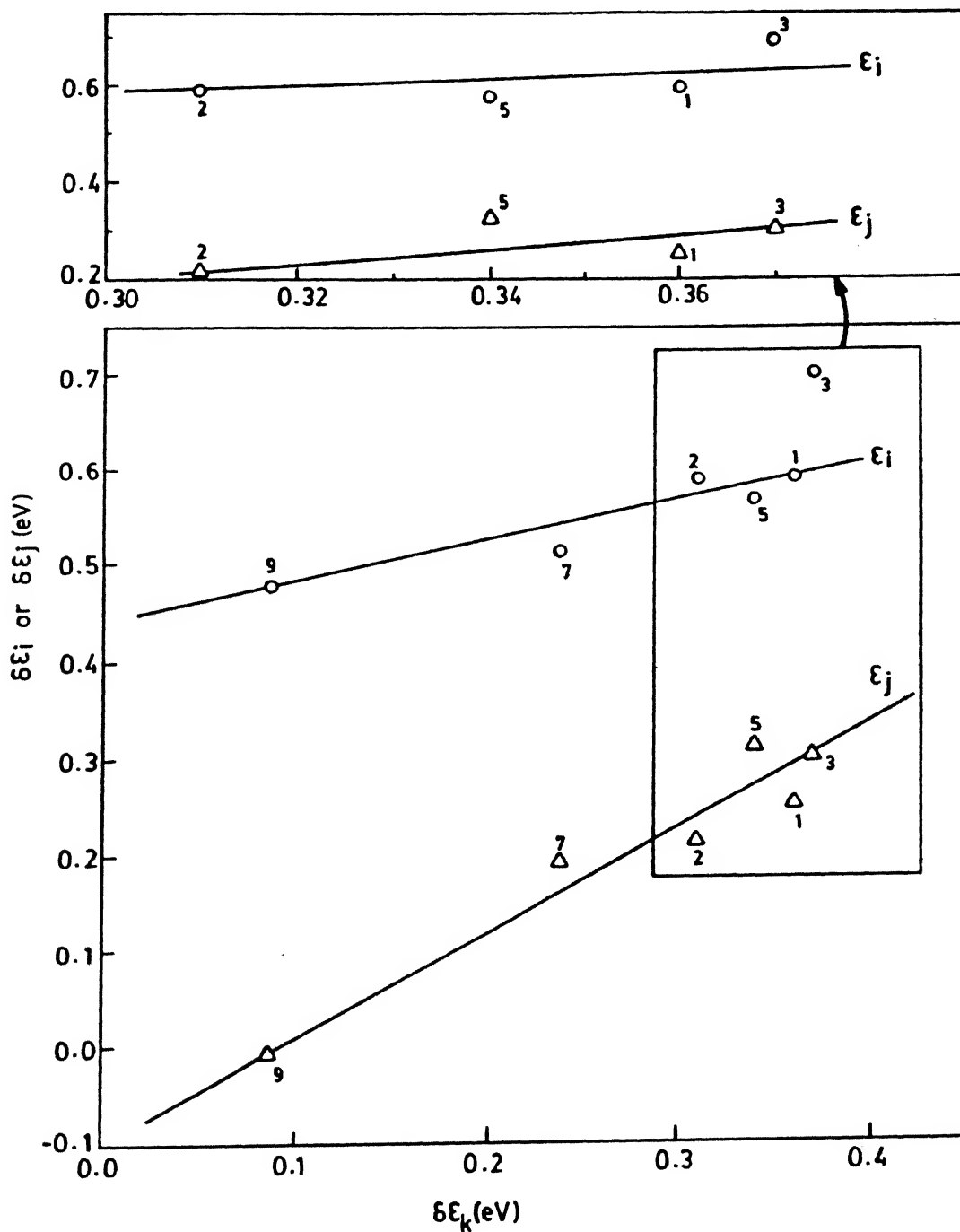


Fig. 4.8 : Shift of the highest occupied π -level energies [$(\Delta) \delta E_i$ and $(o) \delta E_j$] plotted against corresponding shifts for lowest unoccupied level [δE_k (eg)]. The inset shows the separation between A_{1u} and A_{2u} on distortion.

also contributes to this trend. The attachment of short chain across the periphery makes the porphyrin plane nonplanar with reduced dihedral angle between the porphyrin plane and the meso phenyl rings. Substitution of bulky bromine at the β -pyrrole positions results in the steric hindrance between β -substituent and the meso phenyl rings. Successive addition of more bromines enhances the steric hindrance thus increasing the nonplanarity of the porphyrin ring. Strong evidence for this conclusion comes from the X-ray structure of H_2OBP in which the porphyrin ring is found to be puckered relative to H_2TPP ²¹. Thus, the combined steric and antagonistic inductive effect accounts for the nonadditive nature of the potential shifts.

4.5.2 ESR SPECTRAL STUDIES

The ESR data (table 4.3) indicates that the principal tensor components of superhyperfine interaction between the pyrrolic nitrogens and unpaired electron in the metal are almost equal in parallel and perpendicular regions suggesting a predominantly isotropic interaction as expected for a CuN_4 moiety in an approximately tetragonal crystal field^{92,93}. Furthermore, the equally spaced nitrogen hyperfine lines (Figs. 4.6 and 4.7) indicate that the nonplanarity of the porphyrin ring has little influence on the ESR spectra and the unpaired electron is coupled equally to the four pyrrole nitrogens. This is not surprising as the nonplanarity observed in X-ray structural work on $CuTPP$ was not reflected in the ESR spectrum⁹².

Literature reports^{93,94} on structurally well characterised Cu^{2+} complexes with N, O, S donor ligands reveal inverse relationship between g_{\parallel} and $A_{\parallel}^{\text{Cu}}$ parameters. Generally, g_{\parallel} increases and $A_{\parallel}^{\text{Cu}}$ decreases upon increasing distortion. Even though g_{\parallel} values do not show any such trend, the $A_{\parallel}^{\text{Cu}}$ and A_{O}^{Cu} decreases gradually with increasing distortion relative to CuTPP probably indicating the expected nonplanarity around Cu^{2+} ion.

The α^2 value calculated from the spin Hamiltonian parameters represents the bonding coefficient of the b_1 molecular orbital and gives a qualitative idea about the strength of the Cu-N σ bond. The stronger the inplane σ -bond between Cu^{2+} and nitrogen, the higher is the energy of the b_1 molecular orbital because of its antibonding character. Thus, the gradual decrease observed (table 4.3) here indicates lowering of the energy of the b_1 molecular orbital relative to that of CuTPP and a weaker Cu-N interaction in the brominated distorted derivatives. A similar conclusion was arrived at to explain for higher value of α^2 for copper(II) phthalocyanine ($\alpha^2 = 0.79$; Cu-N bond length : 1.93 \AA) compared to CuTPP ($\alpha^2 = 0.75$; Cu-N bond length : 1.98 \AA)^{99,100}.

SECTION B

SPECTRAL AND ELECTROCHEMICAL PROPERTIES OF IRON(III) DERIVATIVES OF BASKET HANDLE PORPHYRINS

4.6 EXPERIMENTAL

Free base porphyrins were prepared as described in previous chapter.

4.6.1 FeMSIICl

A solution of free base porphyrin (0.100 g, 0.0001 mmol) and excess of freshly prepared anhydrous ferrous chloride in dry DMF was heated under reflux for 6 h in argon atmosphere. The progress of the reaction was monitored by absorption spectrum. The solution was filtered and evaporated to dryness under vacuo and the resultant solid was extracted with chloroform (100 ml). The organic layer was washed with dilute NaHCO_3 (3x100 ml) and evaporated to dryness. The crude iron(III) porphyrin was chromatographed over silicagel (60-120 mesh) using chloroform as the eluant. The fast moving unreacted free base porphyrin band was collected first. The required iron(III) derivative then moved slowly as a dark brown band and was collected. The solution was evaporated and the resultant solid was dried under high vacuum (0.060 g, 45%). The compound was recrystallised from chloroform-methanol.

FAB Mass : calculated for $\text{C}_{60}\text{H}_{40}\text{FeClN}_4\text{O}_4$ = 974.30; observed m/z = 974

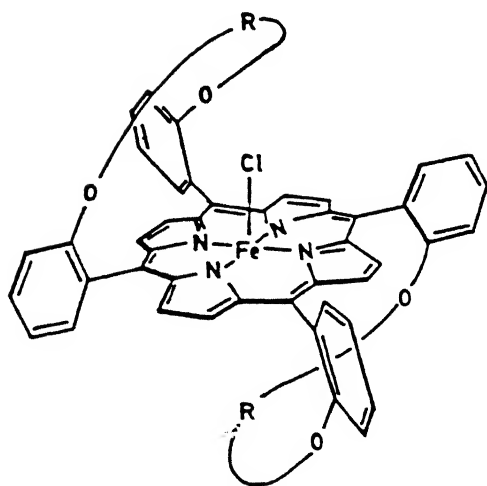
Anal. calcd. for $\text{C}_{60}\text{H}_{40}\text{N}_4\text{O}_4\text{FeCl}$: C, 73.89%; H, 4.10%; N, 5.75%
Found : C, 72.93%; H, 3.92%; N, 5.68%

The other iron derivatives were also synthesized as mentioned above (Fig. 4.9).

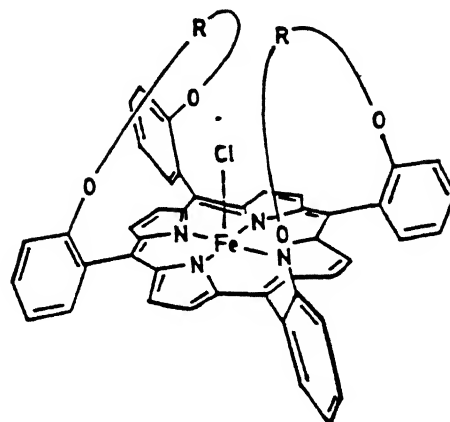
4.6.2 FeMSIIIICl

FAB Mass : calculated for $\text{C}_{60}\text{H}_{40}\text{FeClN}_4\text{O}_4$ = 974.30; observed m/z = 974

Anal. calcd. for $\text{C}_{60}\text{H}_{40}\text{N}_4\text{O}_4\text{FeCl}$: C, 73.89%; H, 4.10%; N, 5.75%
Found : C, 73.92%; H, 4.20%; N, 5.81%



II
ADJACENT-TRANS - LINKED



III
ADJACENT-CIS - LINKED

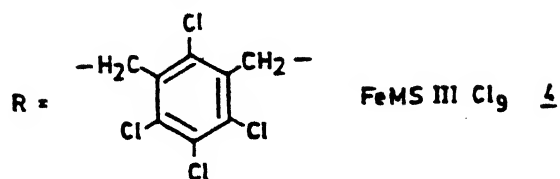


Fig. 4.9 : Structures of Iron(III) derivatives of adjacent-trans and adjacent-cis-linked isomers of short chain basket handle porphyrins.

4.6.3 FePIICl

FAB Mass : calculated for $C_{54}H_{44}FeClN_4O_4 = 904.27$; observed $m/z = 904$

Anal. calcd. for $C_{54}H_{44}N_4O_4FeCl$: C, 71.72%; H, 4.91%; N, 6.196%

Found : C, 71.5%; H, 4.82%; N, 6.26%

4.6.4 FeMSIIICl₉

FAB Mass : calculated for $C_{60}H_{32}FeClN_4O_4 = 1247.86$; observed $m/z = 1248$

Anal. calcd. for $C_{60}H_{32}N_4O_4FeCl_9$: C, 57.75; H, 2.59; N, 4.49

Found : C, 57.95; H, 2.63; N, 4.57

4.7 RESULTS

4.7.1 ¹H NMR

The pyrrole region of the ¹H NMR spectra of various deformed high spin Iron(III) porphyrins in CDCl₃ recorded on a 400 MHz spectrometer is displayed in Fig. 4.10 and the chemical shift data is presented in table 4.5. The notable features here are :

- * The multiplet structure for pyrrole protons, unlike singlet observed for unstrapped FeTPPCl
- * The chemical shift values in iron(III) basket handle porphyrins do not vary much relative to FeTPPCl.

Furthermore, the large downfield shift of pyrrole protons is associated with predominant σ -spin delocalisation in $d_{x^2-y^2}$ orbital.^{89, 101}

4.7.2 OPTICAL ABSORPTION STUDIES

The optical absorption spectral data of various high spin

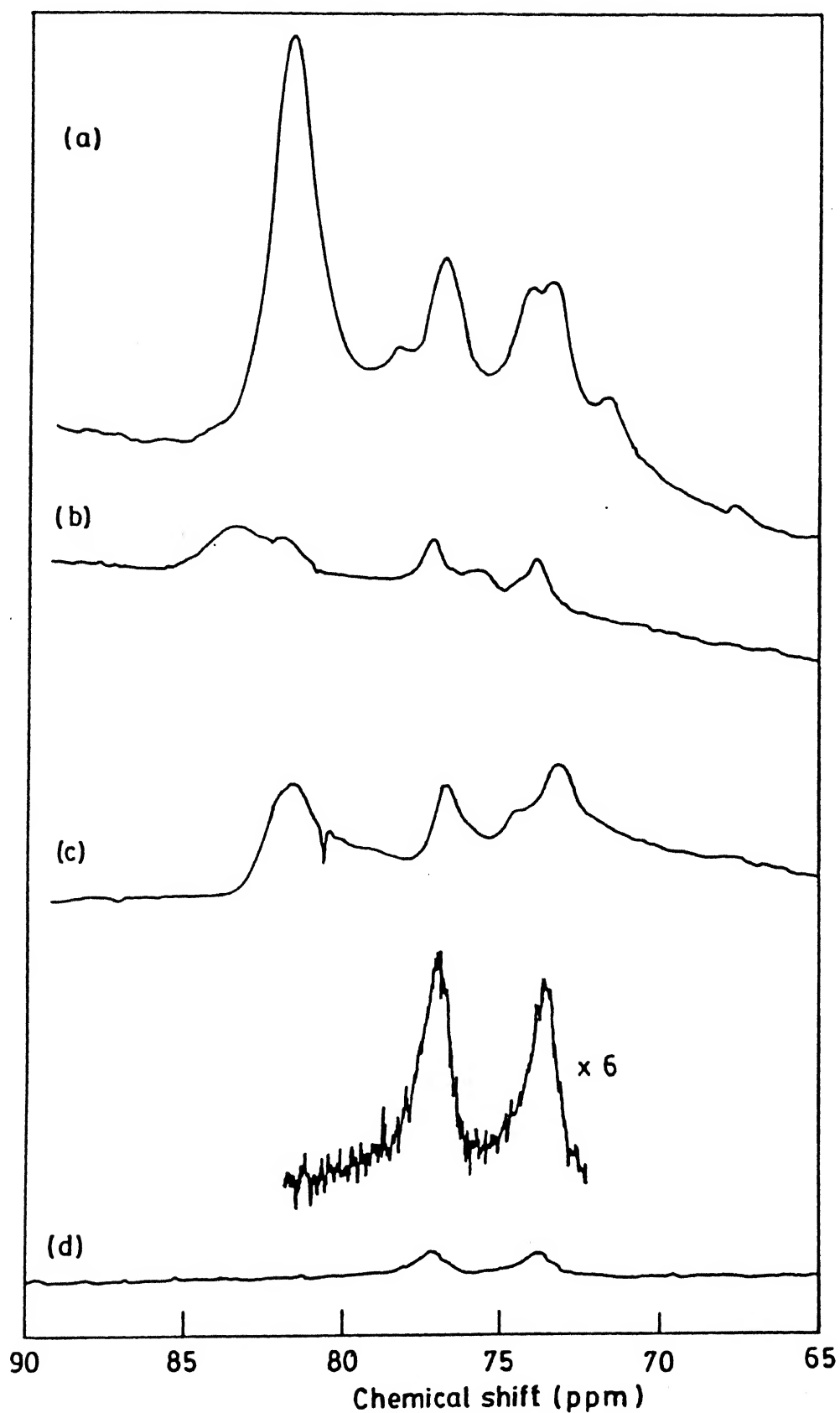


Fig. 4.10 : ^1H NMR spectra in pyrrole region of (a) FePIICl_2 ,

Table 4.5 : ^1H NMR chemical shifts (ppm) of high spin iron(III) porphyrins in CDCl_3

Porphyrin	Pyrrole	ortho	meta	para	$-\text{OCH}_2$
FeTPPCl	79.4	8.0, 5.0	13.3, 12.2	6.35	-
FePIICl	78.5 (m, 4H)	6.67 (m, 4H)	15.3(m, 4H) 12.7(m, 4H)	4.67 (m, 4H)	-4.5 (m, 10H)
FeMSIICl	75.8 (m, 8H)	7.50 (m, 4H)	13.3 (m, 8H)	4.83 (m, 4H)	-4.0 (m, 8H)
FeMSIIICl	78.3 (m, 8H)	6.90 (m, 4H)	13.6 (m, 8H)	4.65 (m, 4H)	-4.65 (m, 8H)
FeMSIIICl ₉	79.5 (m, 8H)	7.24 (m, 4H)	14.5 (m, 8H)	5.34 (m, 4H)	-3.45 (m, 8H)

iron(III) basket handle porphyrins presented in table 4.6 reveals a bathochromic shift of absorption maxima with reduction in extinction coefficients as compared to FeTPPCl. However, the red shifts observed due to ring deformation in various iron(III) basket handle porphyrins with respect to FeTPPCl are of comparable in magnitude to that of corresponding free bases relative to H_2TPP , suggesting that metallation does not alter the degree of deformation in the porphyrin skeleton.

4.7.2.1 AXIAL LIGATION STUDIES

Since in adjacent-trans-isomer, the straps being on both sides of the porphyrin ring, the entry of axial ligand may not be possible due to hindrance provided by straps. But in adjacent-cis-isomer, both the straps are on the same side of the porphyrin

ring and therefore the axial ligand can approach from the less hindered side of the porphyrin. To know the feasibility of axial ligation in Fe(III) derivative of adjacent-trans-isomer, the titration of ca. 5×10^{-5} mol dm $^{-3}$ of FeMSIICl with different

Table 4.6 : Electronic spectral data of various deformed iron(III) porphyrins in dichloromethane

PORPHYRIN	Soret band		Q-bands			
	B (0, 0)		λ_{\max}/nm			
	λ_{\max}/nm		$(10^{-3} \epsilon/\text{dm}^3 \text{mol}^{-1} \text{cm}^{-1})$			
	$(10^{-4} \epsilon/\text{dm}^3 \text{mol}^{-1} \text{cm}^{-1})$		I	II	III	IV
FeTPPCl	417(110)	511(13.4)	577(13.3)	658(2.8)	690(3.2)	
FePIICl	420(70.5)	512(11.03)	586(3.39)	656(2.30)	698(2.36)	
FeMSIICl	420(58.9)	513(7.24)	583(2.02)	656(1.51)	701(1.32)	
FeMSIICl	423(54.3)	511(8.34)	589(2.50)	657(1.68)	698(1.57)	
FeMSIICl ₉ ^a	420	511	589	656	697	

a : ϵ values are not evaluated due to poor solubility.

amounts of imidazole is carried out as shown in Fig. 4.11. Progressive addition of imidazole to the five coordinate iron(III) derivative in chloroform at room temperature results in red shift of Q-bands¹⁰² (UV-vis λ_{\max} (nm)(CH₂Cl₂) 425 and 551) with little change in Soret band maxima indicating the formation of hexa

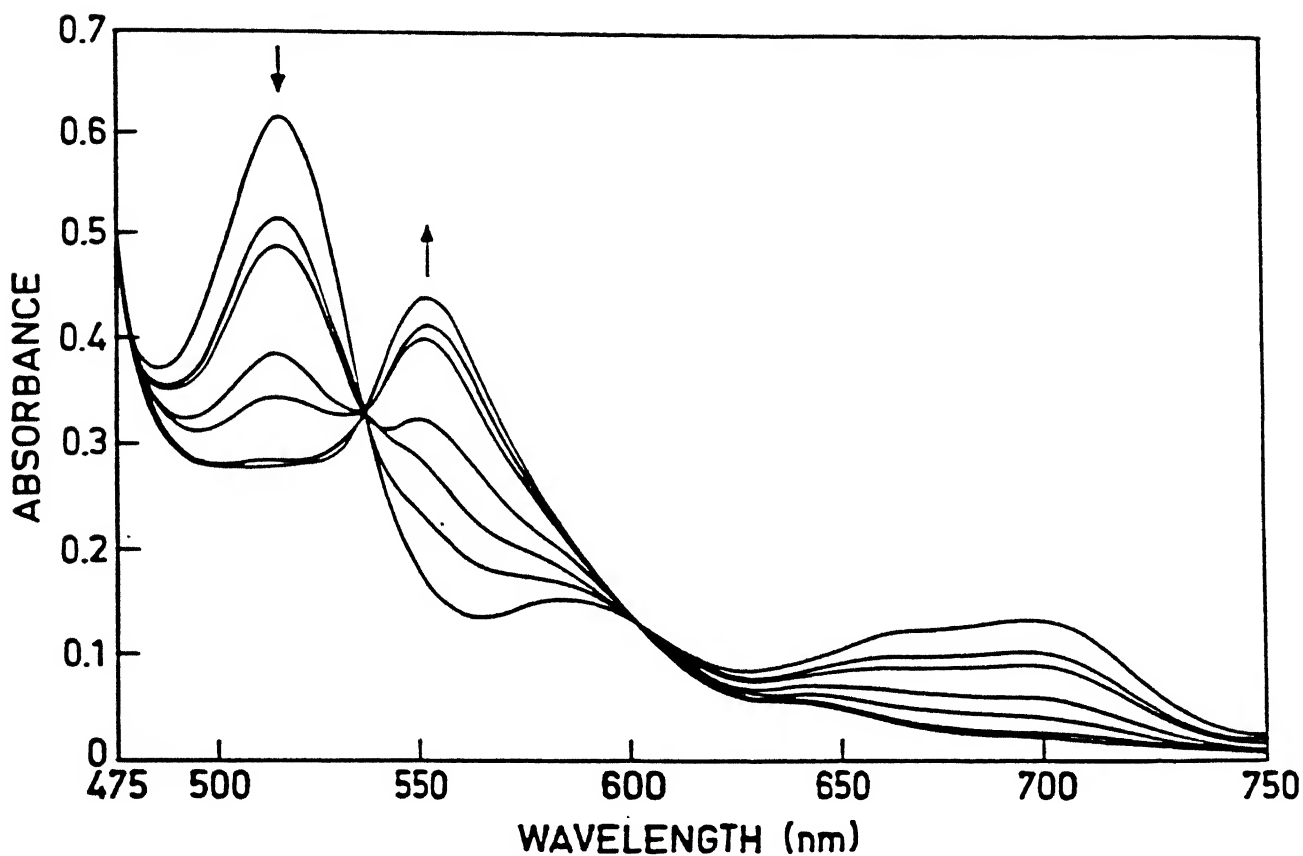


Fig. 4.11 : Absorption spectral changes of FeMSIICl ($7.2 \times 10^{-5} \text{ mol dm}^{-3}$) upon addition of increasing concentrations of imidazole. The concentrations of imidazole used were 2.2×10^{-5} , 4.4×10^{-5} , 6.6×10^{-5} , 1.5×10^{-4} and $2.0 \times 10^{-4} \text{ mol dm}^{-3}$. Arrows indicate the direction of spectroscopic change.

coordinate species due to binding of imidazole molecules to high spin iron(III) centre.

Similar spectral changes have been observed^{89,103} upon addition of imidazole to high spin Fe(II) derivative of basket handle porphyrins. The electronic spectral changes that accompany the reduction of Fe(III) to Fe(II) in FeMSIICl (UV-vis λ_{max} (nm)(CH₂Cl₂) 424 and 541) under argon atmosphere by sodium dithionate followed by the addition of imidazole is shown in Fig. 4.12 (UV-vis λ_{max} (nm) (CH₂Cl₂) for FeMSII(Im)₂: 426 and 553). The

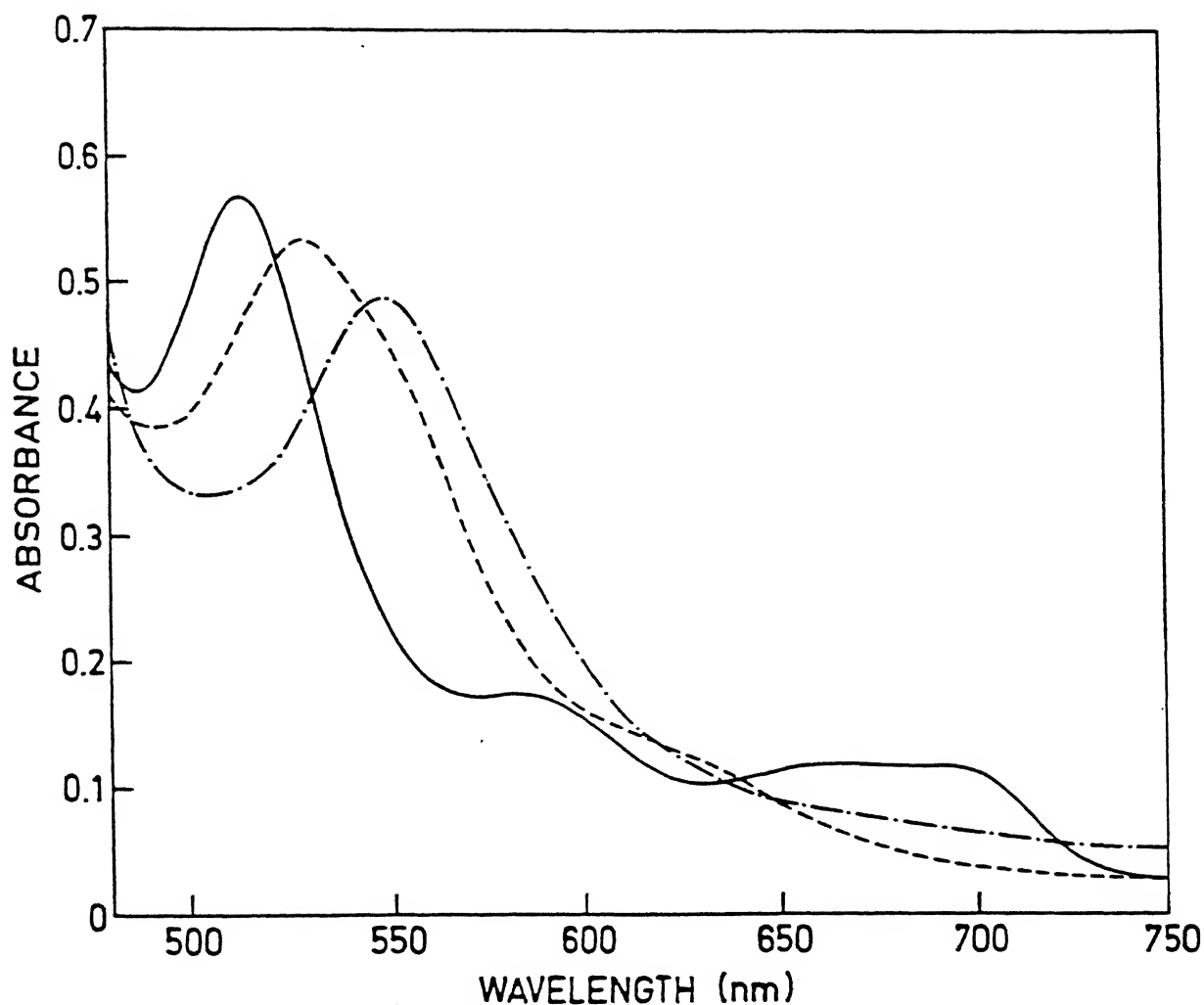


Fig. 4.12 : Absorption spectra of FeMSIICl ($\sim 5 \times 10^{-5}$ mol dm⁻³) in dichloromethane as Fe(III) derivative (—); after reduction with sodium dithionate [Fe(II) derivative] (----); after addition of (4×10^{-4} mol dm⁻³)imidazole (— · —).

red shift observed upon reduction of high spin $\text{Fe}(\text{MSIICl})$ is, due to formation of four coordinate iron(II) species which takes up two molecules of imidazole and forms a symmetric six coordinate species. The magnitude of red shifts observed upon addition of excess of imidazole to $\text{Fe}(\text{III})$ derivative as well as to $\text{Fe}(\text{II})$ derivative are the same, further confirming the formation of six coordinate species by binding imidazole molecules to iron centre.

4.7.3 ELECTROCHEMISTRY

Half-wave potentials measured for three iron(III) derivatives of basket handle porphyrins in four commonly used nonaqueous electrochemical solvents are presented in table 4.7 and a few representative cyclic voltammograms are shown in Figs. 4.13, 4.14 and 4.15 . Generally, the number of oxidations and reductions in iron(III) derivatives depends on the nature of the solvent. For e.g., in $\text{Fe}(\text{PIICl})$, two oxidations and two reductions are observed in dichloromethane whereas in DMSO, one oxidation and three reductions are observed. An inspection of the table 4.7 reveal the following observations :

- * Oxidation potentials are shifted towards less positive and reduction potentials to more negative values in iron(III) derivative of basket handle porphyrins compared to FeTPPCl^{104}
- * The potentials for the iron(III) oxidation are found to be independent of the nature of the solvent and reduction potentials appears to be solvent directed.

The first and second oxidation steps are assigned to the

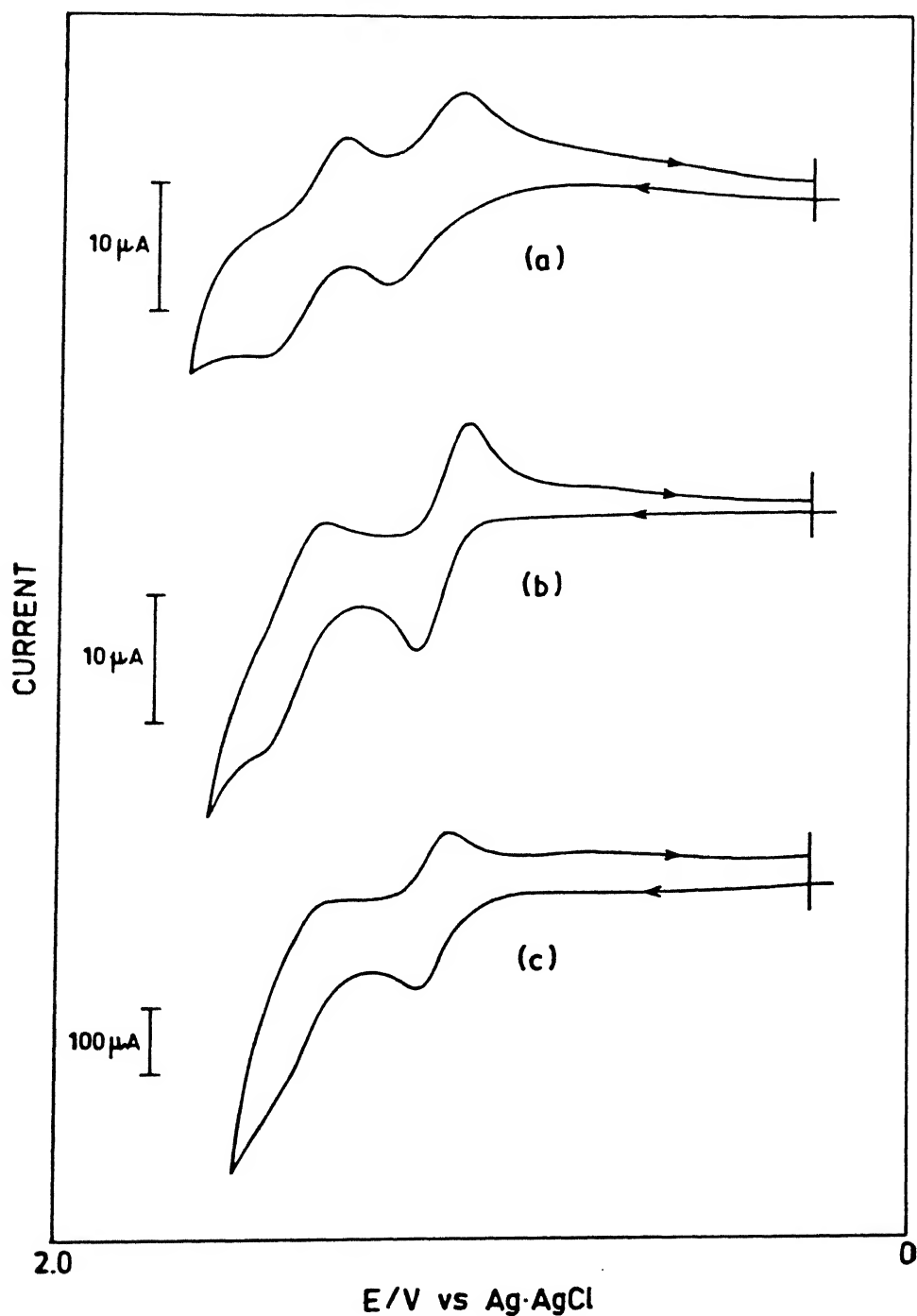


Fig. 4.13 : Cyclic voltammograms of (a) FePIIICl, (b) FeMSIICl and (c) FeMSIIICl in dichloromethane. The concentrations used were $\sim 5 \times 10^{-3} \text{ mol dm}^{-3}$. Scan rate is 100 mV/s. The potentials are versus Ag/AgCl with TBAP as the supporting electrolyte.

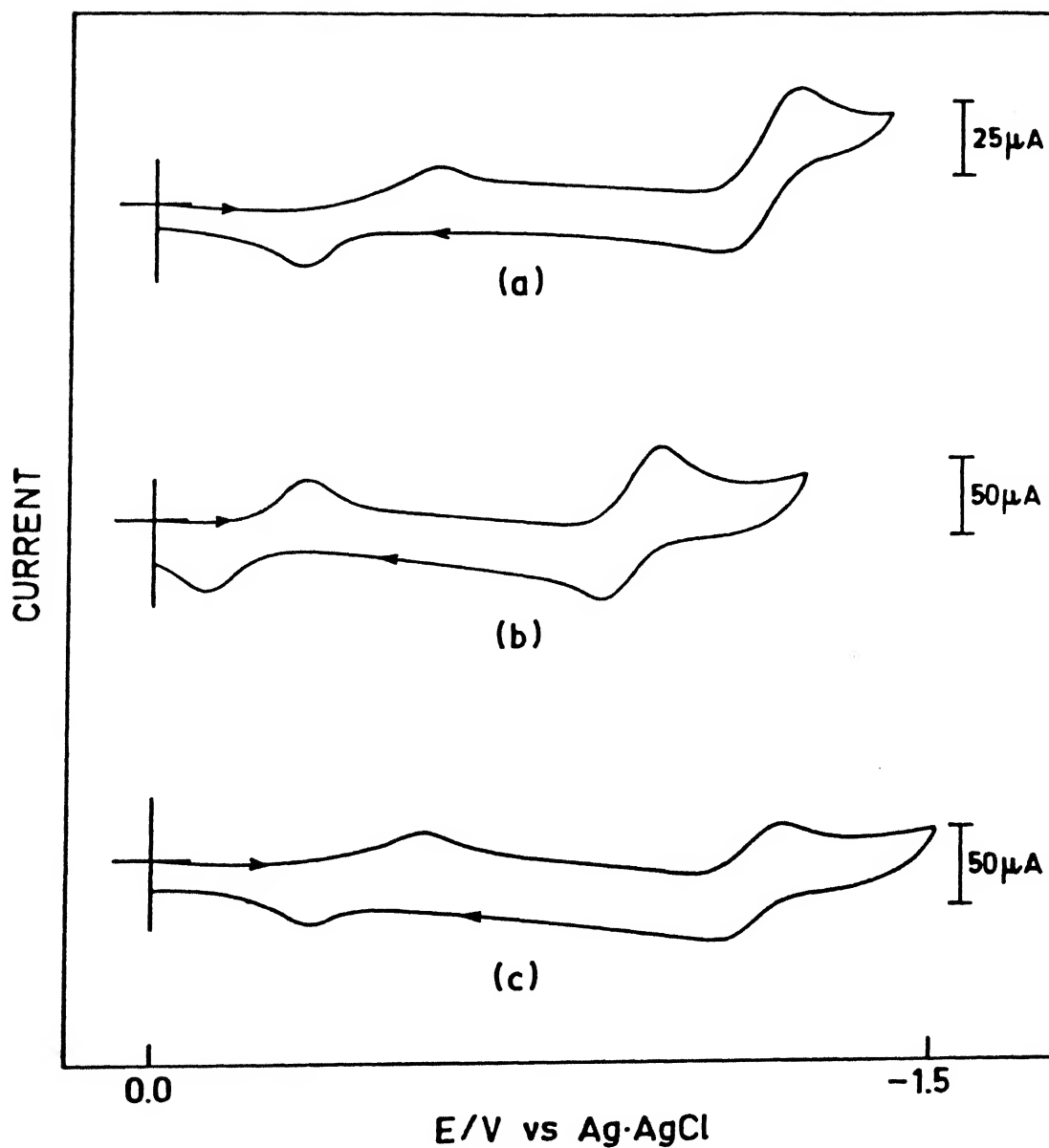


Fig. 4.14 : Cyclic voltammograms of (a) FePIICl, (b) FeMSIICl and (c) FeMSIIICl in dimethylformamide. The concentrations used were $\sim 5 \times 10^{-3} \text{ mol dm}^{-3}$. Scan rate is 100 mV/s. The potentials are versus Ag/AgCl with TBAP as the supporting electrolyte.

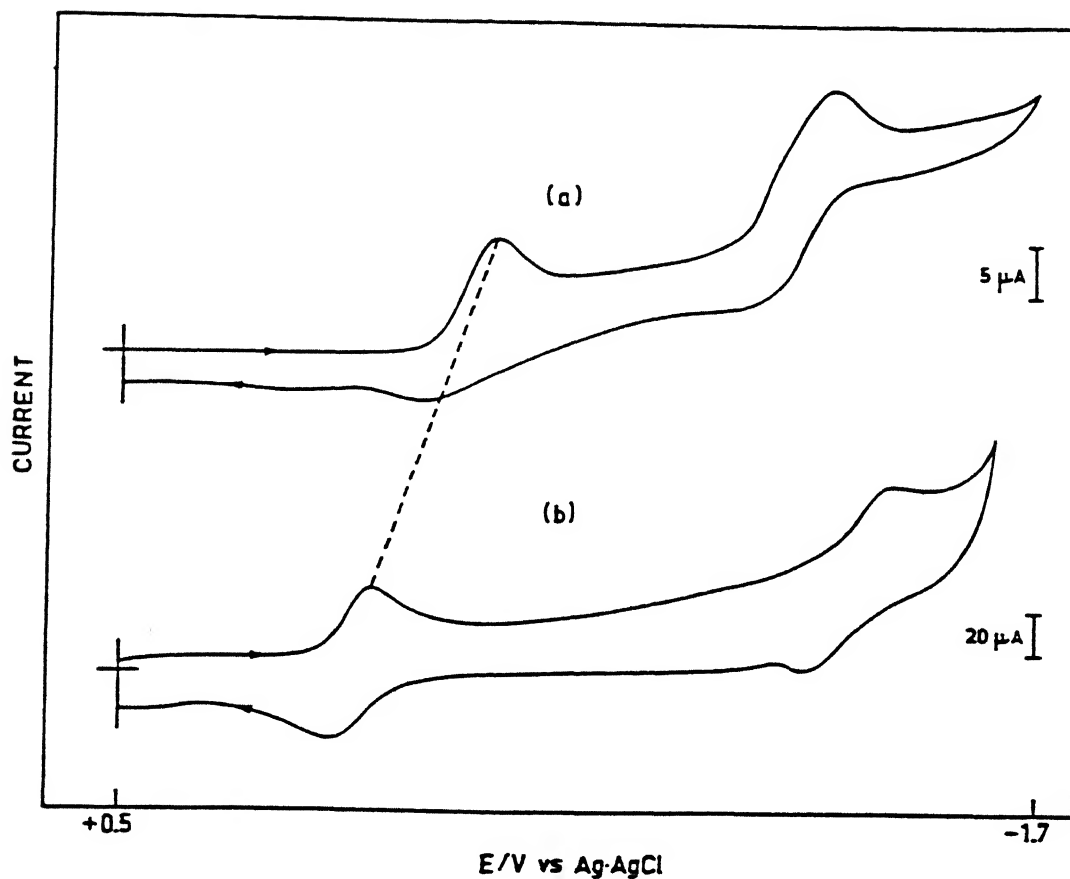


Fig. 4.15 : Cyclic voltammograms of FeMSIICl in (a) CH_2Cl_2 and (b) DMSO. The Scan rate is 100 mV/s . The potentials are versus Ag/AgCl with TBAP as the supporting electrolyte. The dotted line represents the shift in first reduction potential in two different solvents.

Table 4.7 : Electrochemical redox data(V) of iron(III) derivatives of short chain basket handle porphyrins in different solvents.

PORPHYRIN	SOLVENT	OXIDATION		REDUCTION		
		I	II	I	II	III
FeTPPCl	CH ₂ Cl ₂	1.14	1.40	-0.23	-1.07	-1.60
	CH ₃ -(CH ₂) ₂ -CN	1.14	-	-0.27	-1.05	-
	DMF	1.17	-	-0.19	-1.03	-1.61
	DMSO			-0.11	-1.14	-1.68
FePIICl	CH ₂ Cl ₂	1.09	1.40	-0.28	-1.18	-
	CH ₃ -(CH ₂) ₂ -CN	1.12	-	-0.26	-1.10	-
	DMF	1.11	-	-0.22	-1.12	-
	DMSO	0.98	-	-0.023	-1.31	-1.73
FeMSIICl	CH ₂ Cl ₂	1.04	1.46	-0.32	-1.16	-
	CH ₃ -(CH ₂) ₂ -CN	1.11	-	-0.31	-1.04	-
	DMF	1.00	-	-0.25	-1.11	-
	DMSO	0.98	-	-0.030	-1.35	-
FeMSIIICl	CH ₂ Cl ₂	1.02	1.44	-0.39	-1.19	-
	CH ₃ -(CH ₂) ₂ -CN	1.12	-	-0.28	-1.10	-
	DMF	1.08	-	-0.20	-1.10	-
	DMSO	0.98	-	-0.030	-1.35	-

formation of Fe(III) porphyrin cation radical and dication and the two reduction process to the formation of Fe(II) and Fe(I) porphyrin derivatives respectively. The extra reduction observed

for FePIICl in DMSO is due to formation of Fe(I) porphyrin anion radical. These assignments are based on similar reactions observed for FeTPPCl in the respective solvent systems.

4.8 DISCUSSION

4.8.1 ^1H NMR

The contact shift contributions appear as a result of unpaired spin delocalisation through either σ or π molecular orbitals, or both. For direct σ -spin delocalisation, contact shifts are expected in a downfield direction and the observed large downfield shift of pyrrole protons in iron(III) porphyrins is thus attributed to σ -spin delocalisation in $d_{x^2-y^2}$ orbital^{89,101}. Observed multiplet structure for pyrrole protons suggests that all four pyrrole rings are not in the same environment and are displaced up and down from the mean plane due to deformation created in the porphyrin ring by the bridging meso phenyl groups with short chains. Furthermore, similar asymmetry in the porphyrin skeleton is also noted in the corresponding free bases. The splitting of pyrrole signal in free base porphyrins suggest that there is retainment of deformation in the porphyrin ring upon insertion of iron(III) metal ion into its core. However, the shifts are minor relative to FeTPPCl indicating that the tension imposed by the bridging adjacent phenyl groups is not effective. The support for this observation comes from the spectral and electrochemical properties of the corresponding free bases relative to H_2TPP , as described in previous chapter.

4.8.2 OPTICAL ABSORPTION STUDIES

The observed red shifts in the optical spectra for various iron(III) derivatives of basket handle porphyrins relative to FeTPPCl suggests that there is retainment of deformation in the porphyrin skeleton in solution.

Addition of increasing concentrations of imidazole to chloroform solutions of chloroiron(III) basket handle porphyrins result in dramatic visible region spectral changes. The Q-bands are shifted towards higher wavelength with well defined isosbestic points indicating the existence of equilibrium between the two species. Since prior to addition of imidazole ligand, the iron(III) derivative is penta coordinate, certainly the species formed with the addition of imidazole is hexa coordinate due to binding of imidazole ligands to iron(III) centre. Furthermore, the addition of imidazole to ferrous form which is obtained by *in situ* reduction of ferric derivative with aqueous dithionate, also result in similar spectral changes with comparable magnitude of red shifts further supports the formation of symmetrical hexa coordinate species. These studies clearly suggest that the strapping groups present on both sides of the porphyrin ring do not hinder the entry of nitrogenous ligand from binding to the iron centre.

Thus, the preliminary optical studies reported here indicates that the straps present over the porphyrin skeleton not only prevent the μ -oxo dimer formation but also allow the incoming axial ligands. This suggests that reactions with small molecules

such as O_2 and CO will be certainly helpful in understanding the mechanism by which oxygen carrier heme proteins regulate dioxygen and carbon monoxide binding. Such studies are in progress.

4.8.3 ELECTROCHEMISTRY

The easier oxidations and harder reductions observed for iron(III) derivatives of basket handle porphyrins relative to FeTPPCl is consistent with the earlier observations. The optical data and calculated structures of corresponding free base derivatives are also in line with this observation. This point is well elaborated in the preceding section.

The electrochemical data clearly demonstrates that solvent has a marked effect on the redox potentials of iron(III) basket handle porphyrins. The potential shifts seem to be dependent on the coordinating ability of the solvent and site of reaction. The effect of the electrochemical solvent on half-wave potentials has been discussed in the literature for a number of simple metal ions and organometallic complexes. For iron porphyrins, shifts of half-wave potentials are generally attributed to solvent binding at the axial coordination position of the oxidised or reduced forms of the complex.

The electrode reactions observed for the oxidation and reduction of iron(III) derivatives of porphyrins are carried out in nonaqueous solvents with dielectric constants ranging from 8.9 (CH_2Cl_2) to 46 (DMSO). As seen from the table 4.7 that the half-wave potentials for oxidation of iron(III) basket handle porphyrins are invariant and this is assigned to porphyrin ring

centred oxidation rather than metal centred oxidation. The support for above conclusion comes from the observed negligible magnitude of shift in the oxidation potentials even though the coordinating ability of the solvent has increased. However, the reduction potentials for iron(III) derivatives significantly shift as a function of solvent⁷⁷. The first electrode reaction corresponds to Fe(III)/Fe(II) and second reduction is assigned to Fe(II)/Fe(I). A third reduction couple observed only for FePII in DMSO is due to the formation of porphyrin anion radical. The effects of different solvents on reduction potentials are clearly reflected from table 4.7. For e.g., the first reduction is observed at -0.023 V in DMSO for FePIICl, but in CH₂Cl₂, it is shifted to -0.28 V. The easier reduction in DMSO compared to CH₂Cl₂ suggests the stabilisation of Fe(II) over Fe(III) since DMSO is a strong coordinating solvent and therefore can act as a axial ligand. It binds axially to iron centre by displacing counter ions and forms a symmetrical six coordinate iron(II) species. However, the second reduction which is attributed to Fe(II)/Fe(I) appears to be insensitive to changes in the solvent, presumably because Fe(I) is noncomplexing¹⁰⁴. In addition, it is interesting to note here that the difference in half-wave potentials between the first and second reductions in all iron(III) derivatives remain same in dichloromethane, butyronitrile and DMF (~ 900 mV). This difference in redox potentials between various solvents further reflects different stabilisation effects of various solvents on reduced forms of iron(III) derivatives reported here.

4.9 CONCLUSIONS :

- * Introduction of a metal into the porphyrin core does not effect the degree of distortion.
- * An analysis of optical absorption and electrochemical studies indicate significant changes in the energies of HOMO [$A_{1u}(\pi)$ and $A_{2u}(\pi)$] and LUMO [$E_g(\pi^*)$] of porphyrin ring upon β -substitution and distortion. Specifically : (a) Both distortion and β -substitution decreases the energy gap between HOMO and LUMO due to different stabilization/destabilization mechanisms and (b) The magnitude of separation between $A_{1u}(\pi)$ and $A_{2u}(\pi)$ is large for β -substitution while it is small for distortion relative to the corresponding planar unsubstituted derivative.
- * ESR spectral studies indicate weakening of the Cu-N σ -bond without much change in the electronic structure of Cu^{2+} ion.
- * Electrochemistry of iron(III) porphyrins in different solvent systems suggests the stabilisation of iron(II) and iron(I) over iron(III) in strong coordinating solvents.

CHAPTER 5

EFFECT OF PORPHYRIN RING DISTORTION ON THE SINGLET AND TRIPLET EXCITED STATE PROPERTIES

5.1 INTRODUCTION

The biological importance of variety of nonplanar conformations in several biomolecules of diverse functions are described in Chapter 1. Since the primary step in photosynthesis is the transfer of electrons from special pair in the singlet excited state to the plastoquinone molecule¹⁰⁵, the studies on the excited state properties of various model systems reported to date have been limited to simple porphyrins linked to one or more acceptors¹⁰⁶. Although, the importance of nonplanarity at the reaction centre of photosynthesis process was noted much before, only few reports on the excited state properties of nonplanar porphyrins have appeared. Barkigia et.al.³²⁻³⁴ synthesized various nonplanar porphyrins with varying degrees of steric crowding introduced at the periphery of the porphyrin ring to produce different degree of nonplanarity and looked superficially

into their emission properties. These porphyrins were found to be weakly fluorescent which was accounted in terms of distortion.

Recently, Tsuchiya and coworkers¹⁰⁷ have reported that a nonplanar meso-tetrakis (pentafluorophenyl) porphyrin gives weak fluorescence which was explained in terms of intramolecular electron transfer between the electron donating porphyrin rings and the electron deficient pentafluorophenyl groups. Later, Takeda and others¹⁰⁸ observed similar magnitude of emission for dodeca- phenyl porphyrins which was accounted in terms of enhancement of rate of non-radiative processes (internal conversion or intersystem crossing) because of severe distortion of the dodecaphenyl porphyrins. Furthermore, except one report¹⁰⁹ from our laboratory on the triplet excited state properties of nonplanar porphyrins, there is no other report on such studies.

5.2 WORK DONE IN THE PRESENT STUDY

The important problems which need to be investigated in the direction of nonplanarity effect of porphyrin ring on its excited state properties are :

- * Need of systematic study on excited state properties of additional nonplanar model compounds.
- * Relation of structural deformation in the porphyrin ring to its excited state properties.
- * Combined effect of distortion and introduction of electron withdrawing groups on the excited state properties of porphyrins.

Thus, in this chapter, a systematic investigation on the photophysical properties of various short chain basket handle porphyrins (Fig. 5.1) is described with the aid of fluorescence

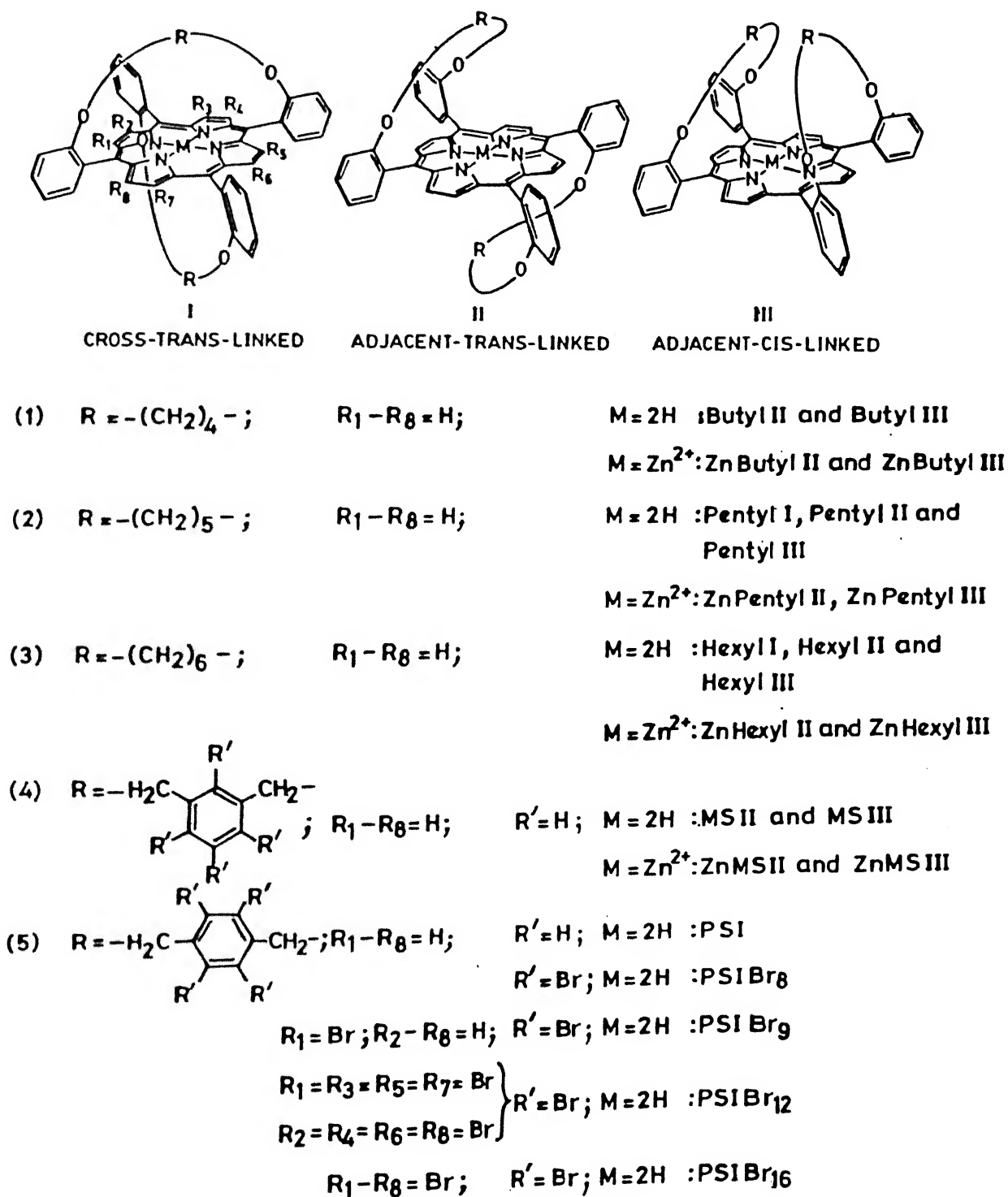


Fig. 5.1 : Structures of various free base short chain basket handle porphyrins and their Zn^{2+} derivatives.

and triplet ESR spectral method. This chapter is divided into two sections. In section A, the singlet excited state properties of a series of distorted basket handle porphyrins, their dications and Zn^{2+} derivatives are described with the aid of fluorescence spectra. The triplet excited state properties of various basket handle porphyrins and their Zn^{2+} derivatives by photoexcited triplet ESR spectra are presented in section B. The results and discussion are given in the forthcoming sections.

SECTION A

SINGLET EXCITED STATE PROPERTIES OF BASKET HANDLE PORPHYRINS

5.3 RESULTS

5.3.1 FREE BASE PORPHYRINS

Three different sets of comparison of the emission spectra of distorted porphyrins with planar H_2TPP are shown in Figs. 5.2, 5.3, and 5.4 respectively. Fig. 5.2 shows a comparison of the emission spectra of dilute solutions of (3×10^{-6} m) Hexyl II, Pentyl II and Butyl II with H_2TPP . Emission spectra of the three isomers of meta xylyl linked porphyrins (MSICl_8 , MSIICl_8 and MSIIICl_8) and PSIBr_8 along with H_2TPP are shown in Fig. 5.3 whereas Fig. 5.4 shows a comparison of emission spectra of β -halogen substituted porphyrins, PSIBr_9 , PSIBr_{12} and PSIBr_{16} with PSIBr_8 . Table 5.1 lists the complete emission data evaluated. The changes in the singlet excited state potentials estimated from the ground state redox potentials and singlet excited state are also included in table 5.1. From this table the following observations can be made :

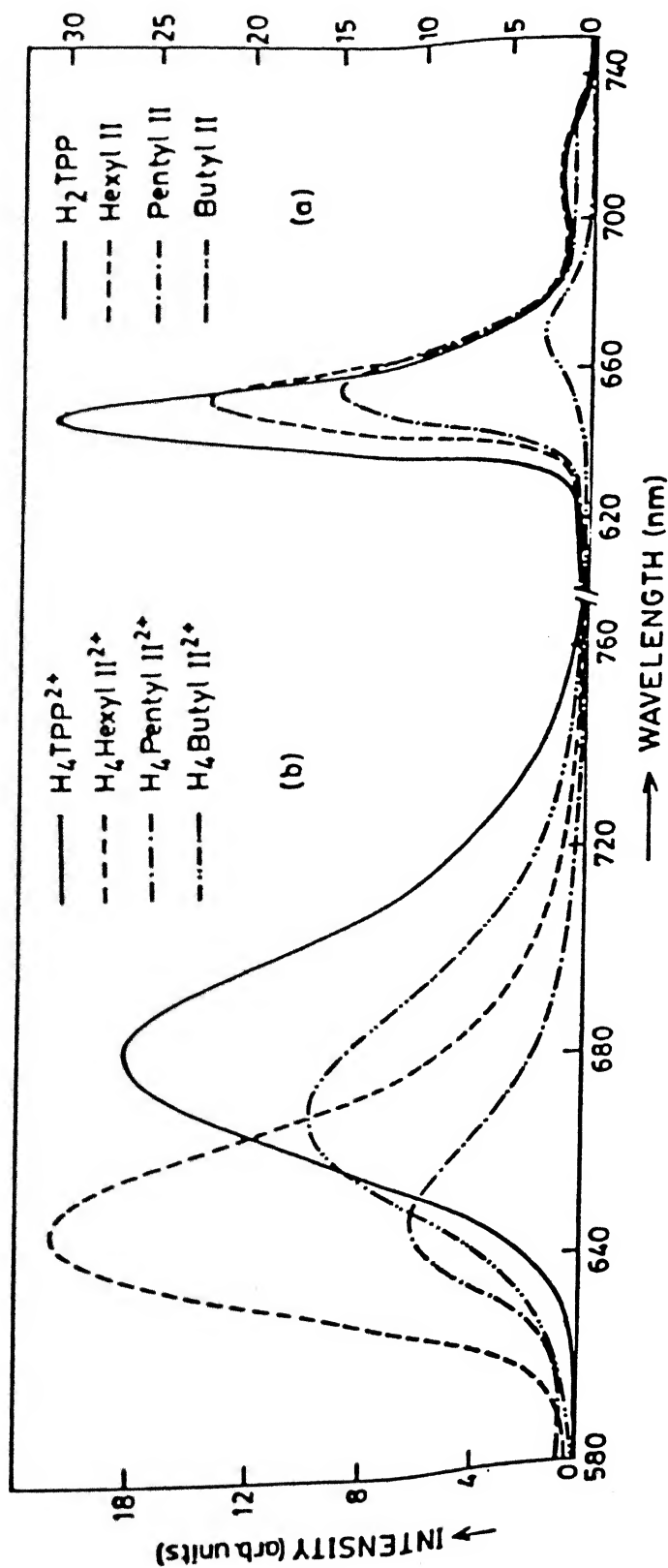


Fig. 5.2 : (a) Comparison of fluorescence spectra of Hexyl II, Pentyl II and Butyl II with H_2TPP in benzene. The concentrations used were $\sim 2 \times 10^{-6}$ mol dm^{-3} . All spectra were recorded at $25^\circ C$ and $\lambda_{exc} = 515$ nm. (b) Emission spectra of protonated derivatives of H_2TPP , Hexyl II, Pentyl II and Butyl II in benzene at $25^\circ C$. The excitation and emission slit widths were 10 and 15 nm respectively and $\lambda_{exc} = 440$ nm.

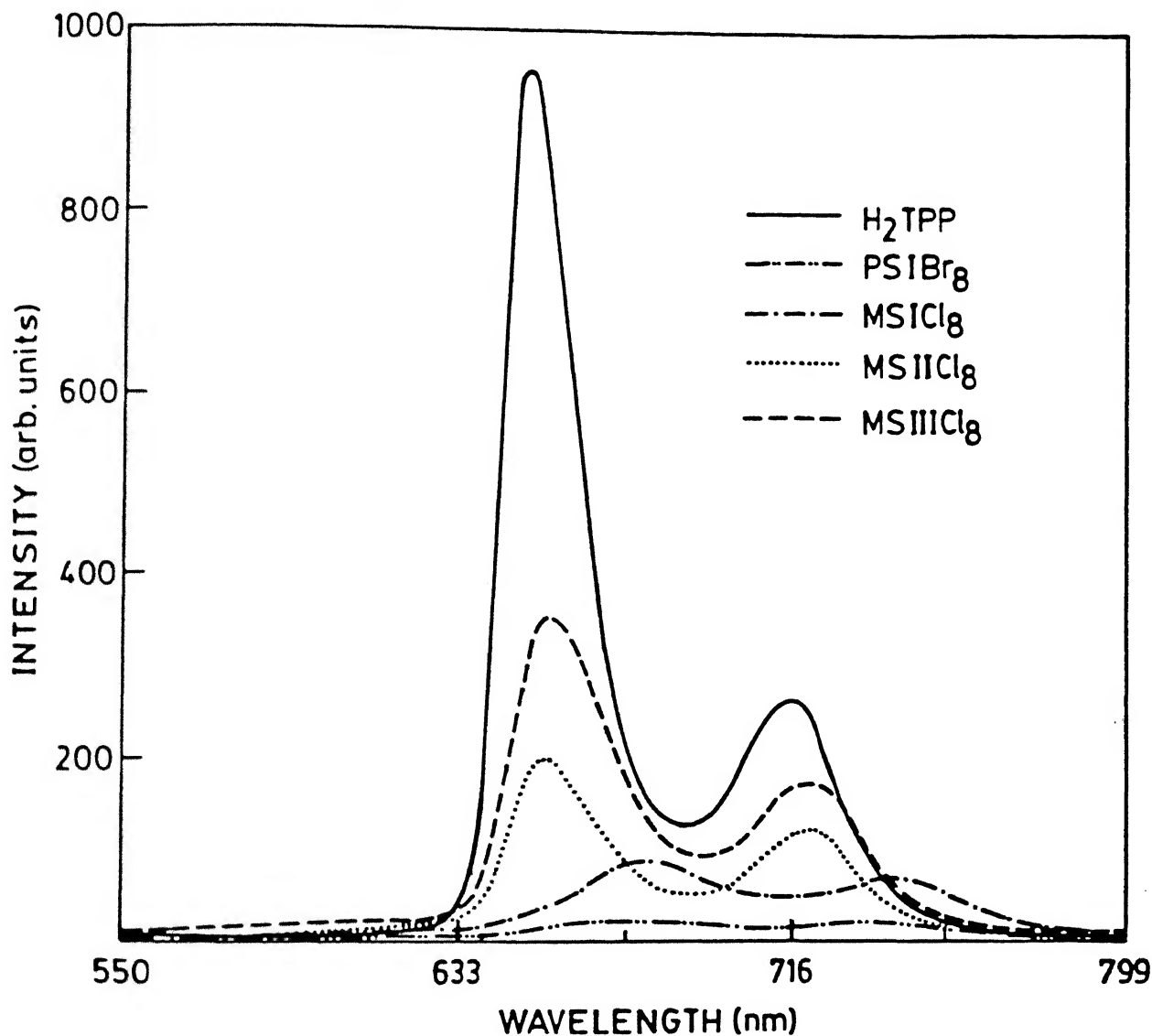


Fig. 5.3 : Comparison of emission spectra of H₂TPP, PSIBr₈, MSICl₈, MSIICl₈ and MSIIICl₈ in chloroform. The concentrations used were $\approx 5 \times 10^{-6}$ mol dm⁻³. All spectra were recorded at 25°C and $\lambda_{\text{exc}} = 515$ nm.

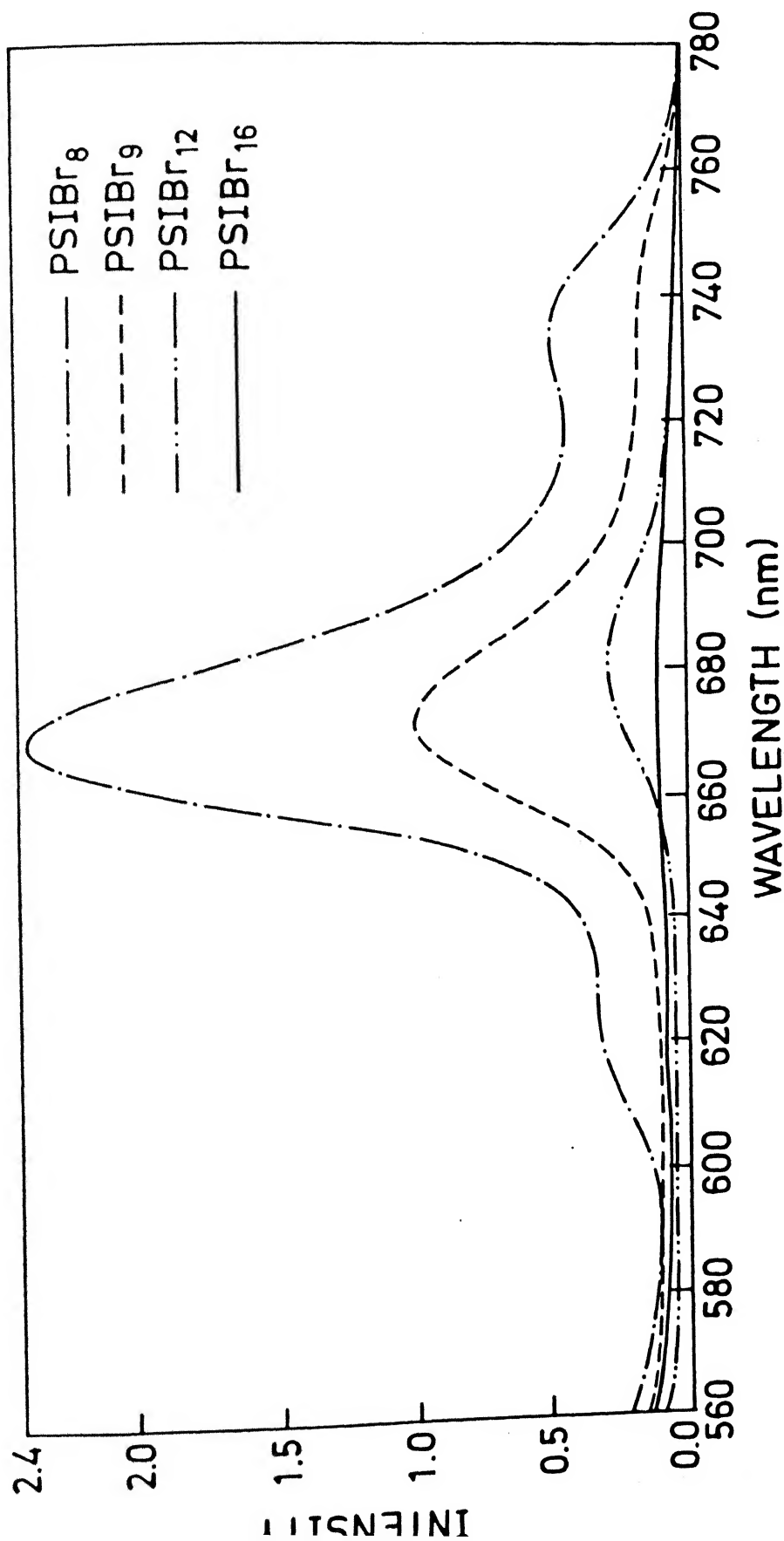


Fig. 5.4 : Comparison of emission spectra of various pyrrole

brominated porphyrins relative to PSIBr₈ in chloroform.

The concentrations used were $\approx 2 \times 10^{-6}$ mol dm⁻³ and

$\lambda_{\text{exc}} = 515$ nm.

Table 5.1 : Singlet excited state parameters of free base basket handle porphyrins in chloroform

PORPHYRIN	Q(0,0) λ_{\max} (nm)	Q(0,1) λ_{\max} (nm)	ϕ_f	$E_{0-0}(P-P^*)$ (eV)	$^*E^0(P^+/P^*)$ (V)	$^*E^0(^*P/P^-)$ (V)
H ₂ TPP	653	717	0.110	1.900	-0.870	0.670
Hexyl I	678	734	0.057	1.829	-0.979	0.429
Hexyl II	654	719	0.100	1.896	-0.946	0.556
Hexyl III	654	717	0.086	1.896	-0.966	0.576
Pentyl II	657	724	0.043	1.887	-0.977	0.547
Pentyl III	659	724	0.060	1.881	-0.971	0.521
Butyl II	667	-	0.040	1.859	-0.949	0.589
Butyl III	662	-	0.041	1.873	-	-
PS I	672	739	0.012	1.845	-0.995	0.445
MS II	665	727	0.039	1.864	-1.024	0.544
MS III	663	727	0.032	1.870	-0.970	0.530
MSICl ₈	679	745	0.028	1.826	-0.976	0.496
MSIICl ₈	658	723	-	1.884	-0.964	0.544
MSIIICl ₈	656	723	0.023	1.890	-0.940	0.540
PSIBr ₈	669	736	0.010	1.853	-1.083	0.353
PSIBr ₉	673	736	-	1.842	-0.952	0.502
PSIBr ₁₂	682	-	-	1.818	-0.778	0.728
PSIBr ₁₆	686	-	-	1.807	-0.697	0.833

* Both Q (0,0) and Q(0,1) emission bands of distorted porphyrins are shifted to higher wavelength relative to

- * Broadening of the emission bands with significant quenching of fluorescence intensity leading to a decrease in the quantum yields relative to H_2TPP .
- * Presence of electron withdrawing groups (ex : Br^-) on β -pyrrole carbons result in further red shift of the emission bands with reduction in intensity.
- * Magnitude of red shift and reduction in fluorescence yields are dependent on the nature of the isomer, chain length and presence of electron withdrawing substituents.
- * Maximum red shift and intensity quenching of fluorescence bands are observed for cross-trans-linked isomer in the order : alkyl bridged porphyrins < aryl bridged porphyrins < porphyrins with electron withdrawing groups on the bridging phenyl < porphyrins with electron withdrawing groups on β -pyrrole carbons and bridging phenyl.
- * Magnitude of red shift and reduction in fluorescence yields of isomer II and III of alkyl and aryl bridged porphyrins are comparable and depends on the length of the bridging chain.
- * All distorted porphyrins excluding β -halogen substituted porphyrins are found to be better donor in the singlet excited state relative to H_2TPP .
- * Among different isomers, cross-trans-linked isomer exhibits better donating ability in the singlet excited state.
- * Substitution of electron withdrawing groups at β -pyrrole carbons results in reduction of electron density in the porphyrin ring and makes it poor electron donor compared to H_2TPP in the singlet excited state.

Thus, various factors such as nature of isomer, chain length and presence of electron withdrawing substituents have profound influence on excited state properties of basket handle porphyrins. Furthermore, the orientation of bridging phenyl groups also affect fluorescence yields as shown for MSiCl_8 and PSiBr_8 . Although MSiCl_8 is more distorted compared to PSiBr_8 due to shorter bridging chain, the quantum yield of MSiCl_8 is 20% higher than PSiBr_8 because of different orientations of the bridging phenyl groups in MSiCl_8 and PSiBr_8 . The reversal in the excited state potential trend in β -substituted porphyrins shows the effect of electron withdrawing groups which are in direct conjugation with porphyrin π -system.

5.3.2 DICATIONS

The room temperature emission spectra of protonated derivatives of adjacent trans linked derivatives of varied chain length ($n = 4, 5, 6$) alkyl bridged porphyrins and different meta xylyl linked isomers, together with H_2TPP dication are shown in Figs. 5.2(b) and 5.5 respectively. The emission data evaluated for protonated derivatives of all the basket handle porphyrins along with $\text{H}_4\text{TPP}^{2+}$ is listed in table 5.2. In particular, the following spectral changes are observed for basket handle porphyrin dications in comparison with $\text{H}_4\text{TPP}^{2+}$.

- * A blue shift, broadening and reduction in intensity of emission bands in contrast to red shift observed for dication of H_2TPP .
- * Reduction in quantum yields; maximum effects are observed for cross-trans-linked isomer.

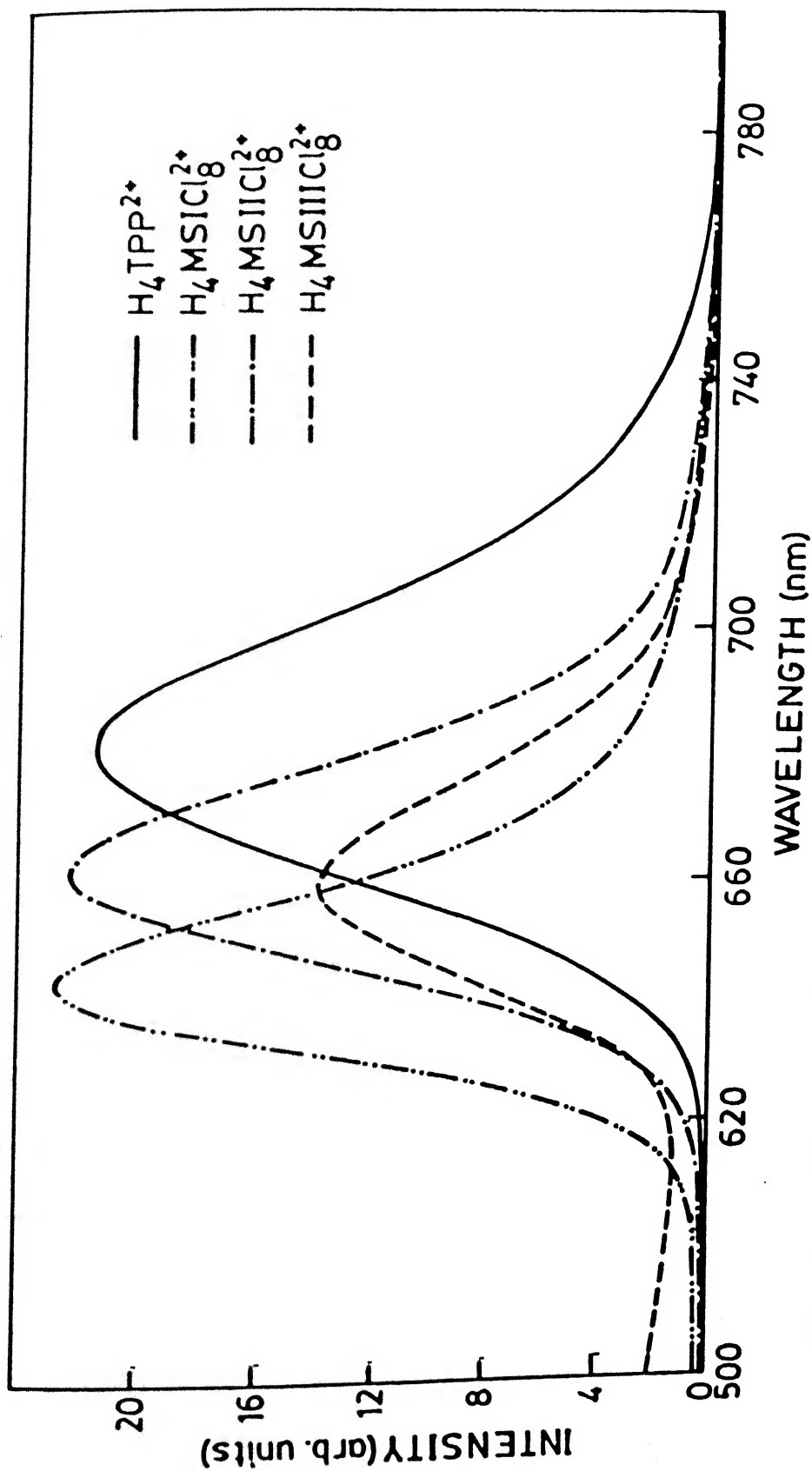


Fig. 5.5 : Emission spectra of dications of H_2TPP , $MSICl_8$, $MSIICl_8$ and $MSIIICl_8$ in benzene. The dications were generated by addition of a drop of trifluoroacetic acid to $\sim 5 \times 10^{-6}$ mol dm^{-3} porphyrin. Spectra were recorded at $25^\circ C$ and $\lambda_{exc} = 440$ nm with excitation and emission slit widths were 10 and 15 nm respectively.

Table 5.2 : Emission data of dications of basket
handle porphyrins

PORPHYRIN	Q(0,0) λ_{\max} (nm)	ϕ_f
H ₄ TPP ²⁺	683	1.4x10 ⁻³
H ₄ Hexyl I ²⁺	643	-
H ₄ Hexyl II ²⁺	647	-
H ₄ Hexyl III ²⁺	653	-
H ₄ Pentyl II ²⁺	649	-
H ₄ Pentyl III ²⁺	666	-
H ₄ Butyl II ²⁺	670	-
H ₄ Butyl III ²⁺	671	-
H ₄ PS I ²⁺	663	4.7x10 ⁻⁵
H ₄ MS II ²⁺	665	9.1x10 ⁻³
H ₄ MS III ²⁺	649	-
H ₄ MSICl ₈ ²⁺	662	7.3x10 ⁻³
H ₄ MSIICl ₈ ²⁺	644	-
H ₄ MSIIICl ₈ ²⁺	655	1.3x10 ⁻⁴
H ₄ PSIBr ₈ ²⁺	659	5.1x10 ⁻³
H ₄ PSIBr ₉ ²⁺	658	-
H ₄ PSIBr ₁₂ ²⁺	662	-
H ₄ PSIBr ₁₆ ²⁺	660	-

Similar spectral changes were observed for protonated tetraalkyl porphyrins and ortho-substituted tetraphenyl porphyrins¹¹⁰. These spectral effects are due to lack of resonance type of interaction which is very well recognised for dications of H₂TPP.

5.3.3 Zn^{2+} DERIVATIVES

The Zn^{2+} derivatives of the porphyrins showed emission from both the S_1 and S_2 excited states. Fig. 5.6 shows the comparison of the emission spectra from the S_1 and S_2 excited states of Zn^{2+} derivatives of adjacent-trans-linked isomers of hexyl, pentyl and butyl bridged porphyrins along with that of ZnTPP. The excitation spectra were recorded, in particular for the S_2 emission, and the inset in Fig. 5.6 shows a comparison of the emission and excitation spectra for the Zn pentyl II isomer. Similarly, the room temperature S_1 and S_2 emission spectra of the Zn^{2+} derivatives of various aryl bridged porphyrins together with ZnTPP are given in Fig. 5.7 and the inset shows the mirror image relationship between the Soret fluorescence and the Soret absorption for the ZnMSII isomer. The emission data for the Zn^{2+} derivatives is listed in table 5.3. The salient features as evident from this table are as follows :

- * A red shift in both the S_1 and S_2 emission maxima relative to ZnTPP,
- * A reduction in the S_1 and S_2 fluorescence yields, and a small reduction in energy gap between the S_2 and S_1 excited states in the distorted porphyrins relative to ZnTPP.

A knowledge of ground state potentials is essential for the evaluation of excited state potentials. Hence, we performed cyclic voltammetric experiments on various Zn^{2+} derivatives of basket handle porphyrins and estimated singlet excited state redox potentials by following literature method.⁶⁰

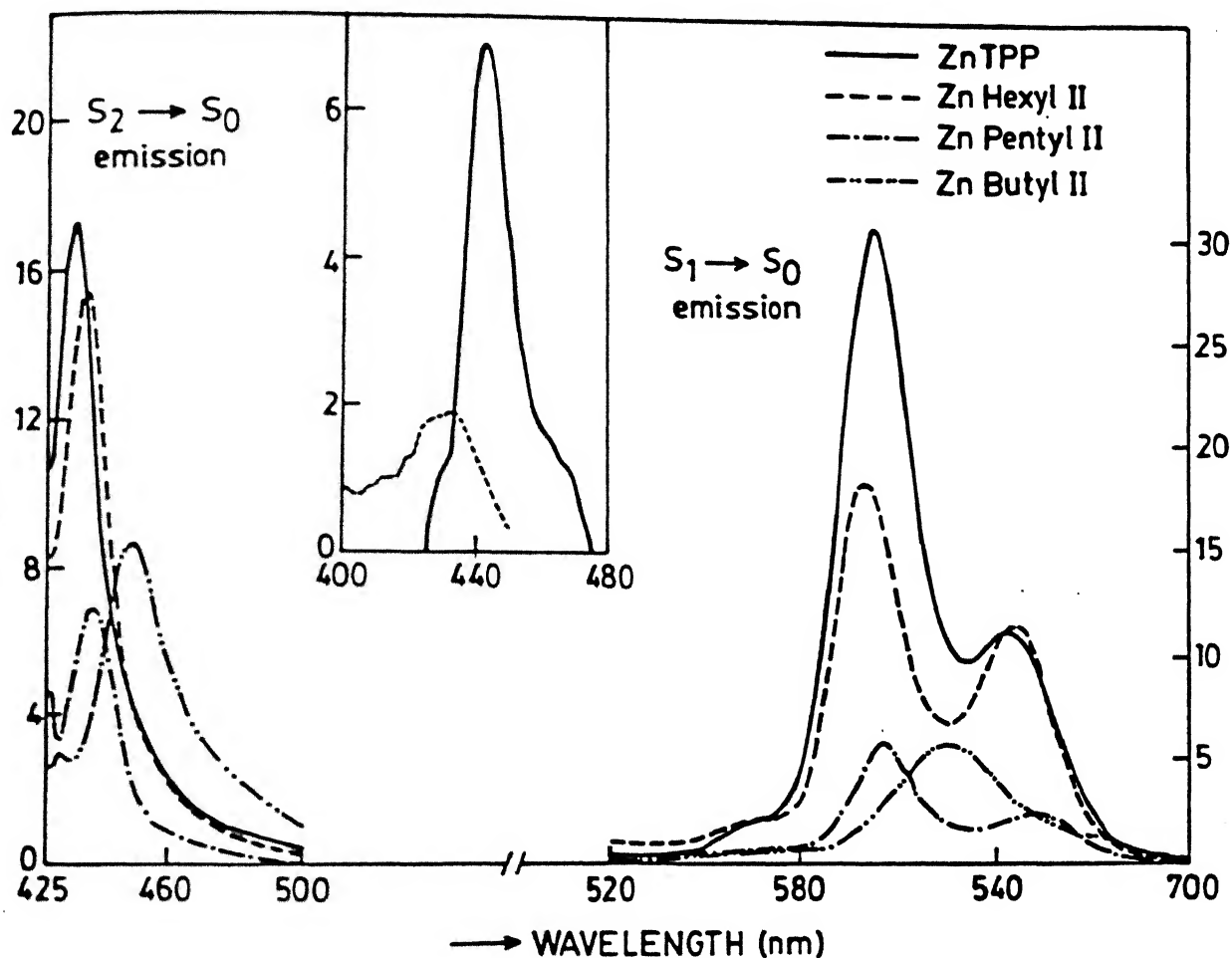


Fig. 5.6 : Emission spectra of various Zn^{2+} derivatives of alkyl bridged basket handle porphyrins and ZnTPP in benzene. The concentrations used were $\sim 2 \times 10^{-6} \text{ mol dm}^{-3}$. (a) Emission from S_1 excited state (b) Emission from S_2 excited state The excitation wavelength for both S_1 and S_2 emissions being 415 nm. The inset shows the emission (—) ($\lambda_{\text{exc}} = 415 \text{ nm}$) and excitation (....) ($\lambda_{\text{emi}} = 460 \text{ nm}$) spectra of ZnPentyl II.

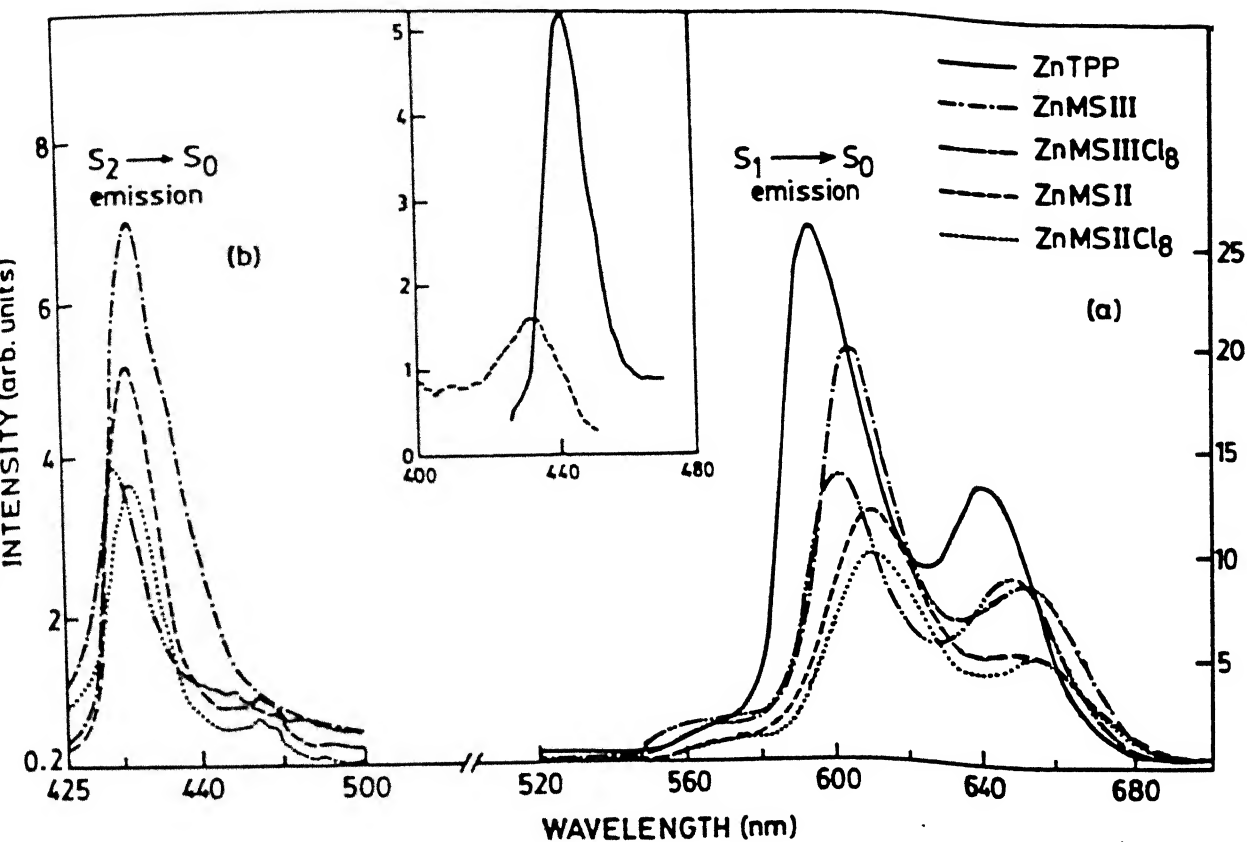


Fig. 5.7 : Fluorescence spectra in benzene of various Zn^{2+} derivatives of basket handle porphyrins and ZnTPP. The concentrations used were $\sim 2 \times 10^{-6} \text{ mol dm}^{-3}$. (a) Emission from S_1 excited state, $\lambda_{\text{exc}} = 431 \text{ nm}$. (b) Emission from S_2 excited state, $\lambda_{\text{exc}} = 415 \text{ nm}$. The inset shows the emission (—) ($\lambda_{\text{exc}} = 415 \text{ nm}$) and excitation (....) ($\lambda_{\text{emi}} = 460 \text{ nm}$) spectra of ZnMSII.

Table 5.3 : S_1 and S_2 emission data for Zn^{2+} derivatives of various short chain basket handle porphyrins in benzene

PORPHYRIN	S_2 emission		S_1 emission			$\Delta E_{(S_2-S_1)}$ ($\times 10^3 \text{ cm}^{-1}$)
	B(0,0)	$\phi_f \times 10^4$	Q(0,0)	Q(0,1)	$\phi_f \times 10^3$	
	$\lambda_{\text{max}} \text{ (nm)}$		$\lambda_{\text{max}} \text{ (nm)}$	$\lambda_{\text{max}} \text{ (nm)}$		
Zn TPP	433	3.9	598	647	0.033	6.69
Zn Hexyl II	436	3.7	599	647	0.028	6.24
Zn hexyl III	437	3.1	603	646	0.024	6.30
Zn Pentyl II	440	3.5	613	653	0.023	6.23
Zn Pentyl III	442	3.6	609	652	0.024	6.15
Zn Butyl II	448	3.2	626	-	0.019	6.35
Zn Butyl III	444	3.0	620	-	0.021	6.39
Zn MS II	443	3.4	618	660	0.022	6.39
Zn MS III	444	-	610	660	-	6.13
Zn MSIICl ₈	443	2.9	612	654	0.019	6.23
Zn MSIIICl ₈	439	-	602	649	-	6.17

A representative cyclic voltammograms of a few Zn^{2+} derivatives in CH_2Cl_2 at room temperature are shown in Fig. 5.8. Zn^{2+} derivatives, like free bases, show two oxidation waves with peak separation $\Delta(E_a - E_c)$ in the range 80-120 mV. Both the oxidations are one electron processes ($I_{Pa}/I_{Pc} = 1$) and are ascribed to the formation of monocations and dications of the porphyrin ring. Upon scanning to negative potentials, the Zn^{2+} derivatives show only one ring reduction, corresponding to the formation of the monoanions. The ground and excited state potentials of the Zn^{2+} derivatives are listed in table 5.4. An inspection of the table indicates easier oxidations and difficult

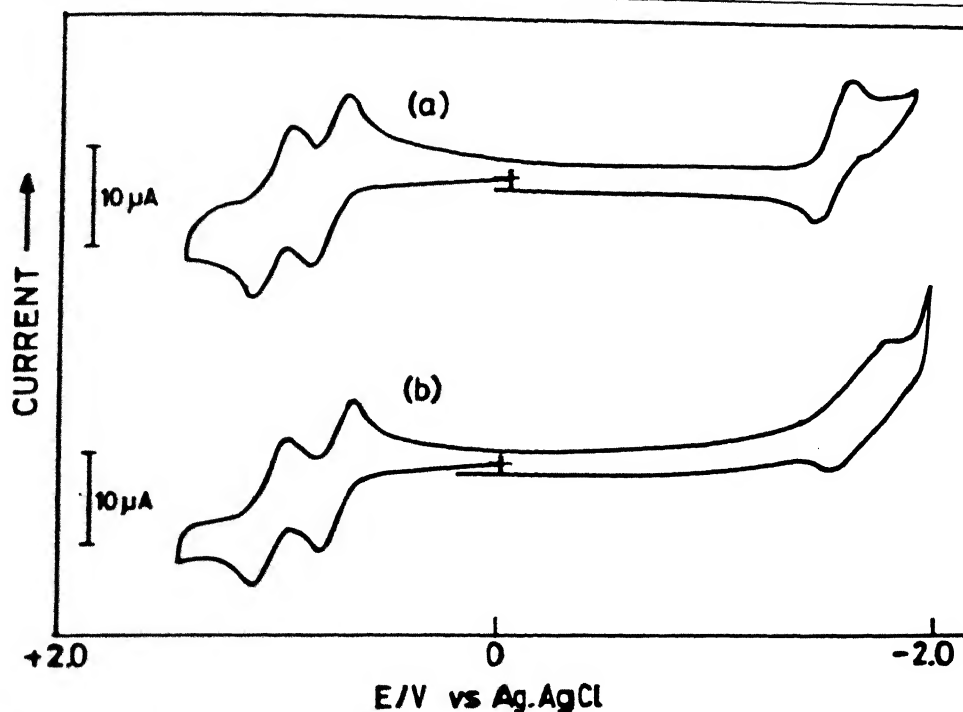


Fig. 5.8 : Cyclic voltammograms of (a) ZnHexyl II and (b) ZnPentyl II in CH_2Cl_2 containing 0.1 mol dm^{-3} TBAP at room temperature. The concentrations used were $\sim 5 \times 10^{-4} \text{ mol dm}^{-3}$. The Scan rate is 100 mV/s .

Table 5.4 : Ground and excited state redox potential (V) of Zn^{2+} derivatives of basket handle porphyrins in CH_2Cl_2

PORPHYRIN	$E^\circ_{(\text{P}/\text{P}^+)}$		$E^\circ_{(\text{P}/\text{P}^-)}$		$^*E^\circ_{(\text{P}^+/\text{P}^*)}$	$^*E^\circ_{(\text{P}^*/\text{P}^-)}$
	I	II	I	II		
ZnTPP	0.77	1.08	-1.35	-1.71	-1.200	0.760
Zn Hexyl II	0.77	1.04	-1.46	-	-1.270	0.610
Zn Hexyl III	0.76	0.99	-1.46	-	-1.296	0.596
Zn Pentyl II	0.72	1.02	-1.62 ^a	-	-	-
Zn Pentyl III	0.74	0.99	-1.48	-	-1.326	0.556
Zn Butyl II	0.71	0.96	-1.42	-	-1.271	0.561
Zn Butyl III	0.71	1.00	-1.43	-	-1.289	0.570

a : peak potential

reductions in the porphyrin ring of Zn^{2+} derivatives. However, Zn^{2+} derivatives are found to be poor oxidants and reductants than free base derivatives, both in the ground and excited states.

5.4 DISCUSSION

5.4.1 FREE BASE PORPHYRINS

It has been shown in earlier chapters 3 and 4 that distortion in the porphyrin ring results in reduction of energy gap between HOMO and LUMO and this is reflected in red shifts of absorption peak maxima. These effects mainly depend on the nature of isomer, chain length of the bridging group and presence of electron withdrawing substituents. Maximum effects are observed for most distorted porphyrin derivatives as discussed in earlier chapters. The fluorescence band shifts are in congestion with these observations.

The inspection of the quantum yield data in table 5.1 indicates significant quenching in the distorted porphyrins relative to planar H_2TPP . The quenching is maximum for cross-trans-linked isomer relative to other two isomers. The important factors which contribute to this quenching are as follows : (1) The ortho substituent effect¹¹⁰ on the meso-phenyl ring of H_2TPP decreases the quantum yield by about 10% relative to unsubstituted porphyrins; (2) The heavy atom effect of the substituted halogens decreases the quantum yield by about 60% by increasing the rate of intersystem crossing; (3) The orientation of the bridged phenyl ring with respect to the porphyrin plane and (4) The decay of the S_1 state through internal conversion leads to a decrease in the quantum yield. Generally, internal conversion

accounts for about 20% decay in porphyrins. In the absence of quantitative data on the rates of intersystem crossing, internal conversion and the quantum yield of the triplet state, it is difficult to determine the individual contributions of these effects to fluorescence quenching, but the decrease in the quantum yield can be attributed to their combined effect.

Despite the fact that MSiCl_8 is more distorted than PSiBr_8 , the quantum yield of MSiCl_8 is about 20% higher than that of PSiBr_8 . This difference is ascribed to the difference in the orientation of the bridging phenyl groups in MSiCl_8 and PSiBr_8 . The steric constraints impose a near perpendicular orientation of the phenyl group with respect to the porphyrin plane in MSiCl_8 , whereas a parallel orientation is observed in PSiBr_8 . Both the phenyl groups act as electron acceptors because of the electron withdrawing nature of their substituent, leading to quenching of the fluorescence of the porphyrin; the quenching is favourable when the donor (porphyrin) and acceptor are in a parallel orientation¹¹¹. It is pertinent to note that the addition of first electron results in the reduction of the bridging phenyl group rather than the porphyrin macrocycle, confirming the electron- accepting nature of the bridging phenyl ring.

5.4.1.1 EXCITED STATE POTENTIALS

The singlet excited state potentials were estimated with the assumption that the excited states are not very much distorted relative to the ground state. The details of the calculation of potentials are described in Chapter 2. This method has been used

earlier for porphyrin systems^{112,113}. The changes in the singlet excited state potentials estimated from the ground state redox potentials and the singlet excited state energy (Fig. 5.9) reveal the following features :

- * The distorted porphyrins are better oxidants in the singlet excited state relative to planar H_2TPP .
- * Among the three isomers, cross-trans-linked isomer is better donor.
- * Among the cross-trans-linked isomer derivatives, $PSIBr_8$ is a relatively strong donor ($\Delta E = 317$ mV) compared to $MSICl_8$ ($\Delta E = 174$ mV) reflecting the effect of bridging group orientation.

Among alkyl bridged series, Hexyl I is the most distorted, hence the maximum of excited state reduction potential shifts to a less positive value (241 mV) followed by that for Butyl II (149mV) relative to H_2TPP . Furthermore, it was noted that the donor ability of the most deformed cross-trans-linked isomer of basket handle porphyrin is completely reversed upon introduction of bromines at β -pyrrole carbons relative to unsubstituted cross-trans-linked derivatives. This indicates that the presence of electron withdrawing substituents at β -pyrrole carbons induces a decrease in the electron density of the conjugated tetrapyrrole ring since electron withdrawing substituents are in direct conjugation with the porphyrin π -system and makes the porphyrin ring, a weak donor in the ground and singlet excited state. This is evident from the shifts in the excited state reduction potentials to a more positive value compared to H_2TPP (table 5.1).

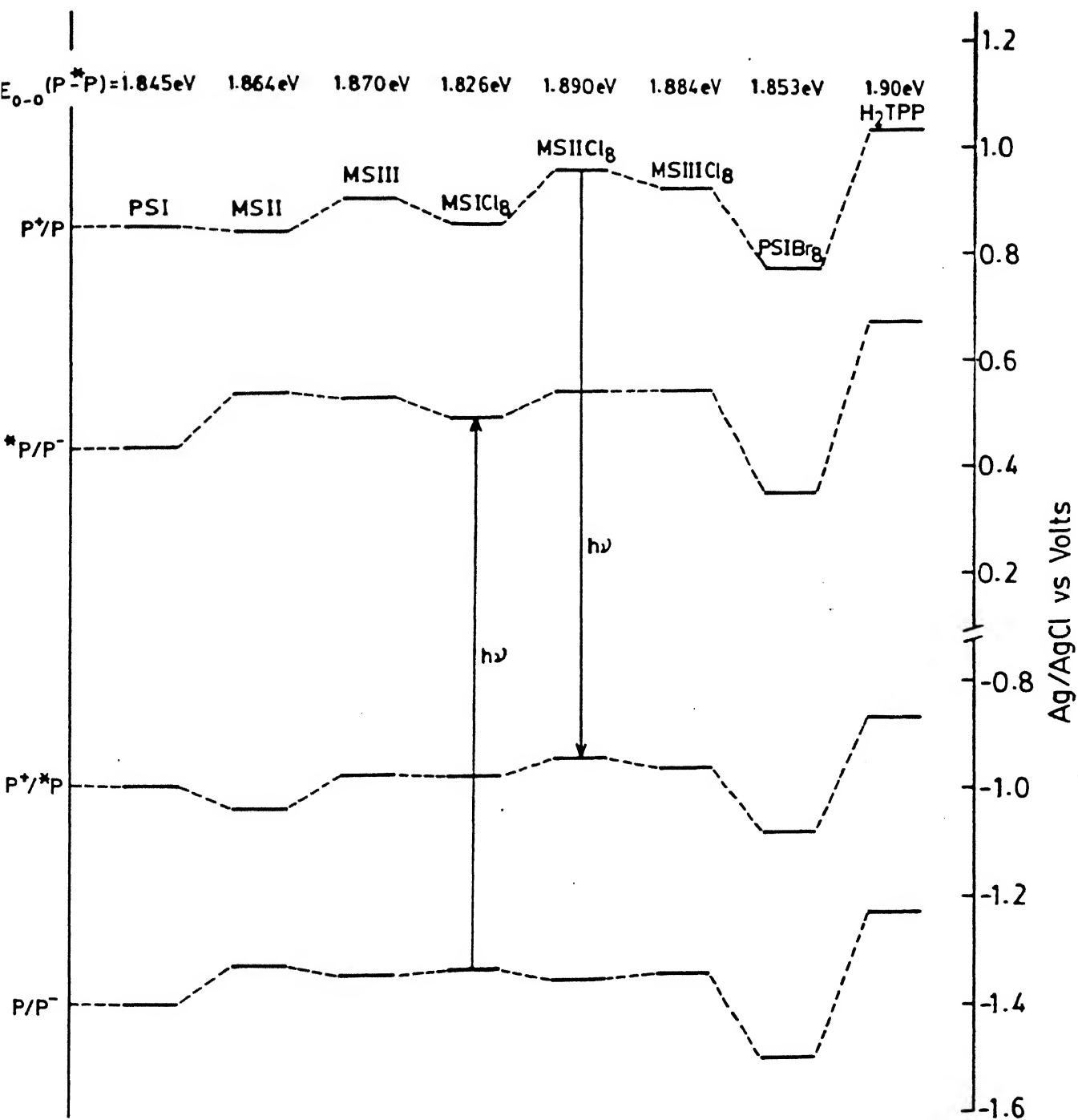


Fig. 5.9 : Comparison of ground and excited state redox potentials of various free base basket handle porphyrins with H_2TPP .

5.4.2 DICATIONS

It is well known fact that, on protonation, the free base tetraaryl porphyrins undergo a structural change by releasing the repulsive interaction between the ortho hydrogens of the meso-phenyl rings and the adjacent pyrrole protons. This results in the phenyl rings becoming more coplanar with the porphyrin plane, facilitating the delocalisation of π -electrons into the phenyl rings by resonance interaction¹¹⁴ and this is reflected in the large red shifts in the Q- and Soret-bands in the optical and emission spectra. On the other hand, free base tetraalkyl porphyrins exhibit a spectral blue shift on protonation due to the lack of resonance interaction¹¹⁰. The substitution of the bridging chain at the ortho position of the meso-phenyl rings in the basket handle porphyrins described here restrict the free rotation around the porphyrin-phenyl bond, thus preventing the extension of the conjugation between the phenyl rings and the porphyrin plane. This accounts for the observed blue shift of the emission bands on protonation (table 5.2). As expected, the quantum yield of the dications are less than the neutral derivatives and the effects are at a maximum for the cross-trans-linked basket handle porphyrin systems.

5.4.3 Zn^{2+} DERIVATIVES

5.4.3.1 S_1 EMISSION

The introduction of the Zn^{2+} ion into the porphyrin core does not affect the degree of distortion of the porphyrin ring. This is reflected in the red shift of both the Q (0,0) and Q (0,1) emission bands relative to planar ZnTPP (table 5.3). The Zn^{2+}

derivatives of cross-trans-linked isomer could not be synthesized because of the steric hindrance of the strapping phenyl ring from both faces of the porphyrin plane. A comparison of the magnitude of the red shift for the adjacent-trans-linked and adjacent-cis-linked isomers indicates slightly larger distortion for the adjacent-trans-linked isomer. The ground state absorption data reveal the same. Furthermore, the magnitude of red shift in Zn^{2+} derivatives which directly gives the degree of distortion in the porphyrin ring, mainly depends on the bridging chain length.

The introduction of the Zn^{2+} ion into the porphyrin core is expected to quench the fluorescence yield due to spin-orbit coupling¹¹⁵ and this is reflected in the reduced quantum yield for Zn^{2+} derivatives relative to free base derivatives. The quenching is found maximum for butyl derivatives among alkyl bridged Zn^{2+} basket handle porphyrins indicating the presence of more deformation in this porphyrin core. This is also supported by large red shifts observed for butyl derivatives than pentyl and hexyl derivatives in emission spectra. The additional quenching effect from the eight electron-withdrawing chlorine substituents is evident in the further reduction of the quantum yield for ZnMSIICl_8 relative to ZnMS II . The poor solubility of ZnMS III and ZnMSIICl_8 prevented the accurate determination of the quantum yields for these isomers.

5.4.3.2 S_2 EMISSION :

Detection of Soret fluorescence is difficult because of the scattered incident light and the reabsorption by the intense Soret absorption band. These problems can be minimised by excitation at

wavelengths considerably shorter than the Soret absorption maximum and by the use of very dilute solutions¹¹⁶. The Soret fluorescence spectra shown in Figs. 5.6 and 5.7 for various alkyl and aryl bridged Zn^{2+} derivatives respectively were recorded in benzene ($\sim 2 \times 10^{-6}$ M) by excitation at 415 nm, a 25 nm shorter than the Soret absorption maxima. In all the cases, S_2 emission spectrum is a mirror image of the Soret absorption band which is characteristic of S_2 emission in metalloporphyrins¹¹⁷. Furthermore, the fact that the S_2 emission is only observed when excited through the Soret absorption rules out any thermal repopulation of S_2 from S_1 . The effect of distortion is reflected in the slight red shift of the emission bands and the reduced quantum yields relative to ZnTPP. The magnitude of red shift and reduction of fluorescence yield is higher for butyl derivatives among alkyl bridged porphyrins indicating higher degree of deformation present in the porphyrin core in these derivatives. Presence of electron withdrawing groups reduces the quantum yields of Soret fluorescence as evident by lower fluorescence yields in ZnMSIICl_8 than ZnMSII.

The ability of deformed porphyrins to emit from the Soret band level suggests the following :

- * The two common (π, π^*) excited configurations, $^1(A_{1u} E_g)$ and $^1(A_{2u} E_g)$ are accidentally degenerate and the energy surfaces of the S_1 and S_2 excited states are parallel. This retards $S_2 \rightarrow S_1$ intramolecular relaxation.
- * There is no triplet excited state between S_1 and S_2 excited states¹¹⁸.

considered to predominate at relatively low values of the excitation densities. However, the contribution of the mechanism [C] was not determined experimentally. Though for the deformed Zn^{2+} porphyrins studied here, mechanism [B] is the most possible one, an optical-optical double resonance study is required to explore the actual mechanism for the population of S_2 state. Furthermore, S_2 fluorescence is not observed for free base basket handle porphyrins and their dications. This could be due to rapid $S_2 \rightarrow S_1$ internal conversion.

A comparison of the oxidation potential shifts for the Zn^{2+} derivatives of deformed porphyrins with ZnTPP indicates lesser distortion in these isomers. The easier oxidations and harder reductions are observed in all Zn^{2+} derivatives relative to ZnTPP as observed in free base basket handle porphyrins in comparison with H_2TPP essentially suggesting that the introduction of the Zn^{2+} ion does not alter the degree of distortion. The excited state potential data suggests that the distortion of the porphyrin plane leads to better electron donating ability in the singlet excited state as observed for free bases. However, Zn^{2+} derivatives are found to be poor donors than free base derivatives in the singlet excited state.

SECTION B

PHOTOEXCITED TRIPLET ESR STUDIES ON BASKET HANDLE PORPHYRINS

5.5 INTRODUCTION

In this section a brief outline of the general principles of the photoexcited triplet ESR¹²⁰ is presented before a detailed

discussion on the results obtained for basket handle porphyrins.

Electron paramagnetic resonance (EPR) spectroscopy covers transition energies of the order of $0.3\text{--}1\text{ cm}^{-1}$, compared to $10^4\text{--}5\times 10^7\text{ cm}^{-1}$ in optical spectroscopy. In addition, the conspicuous variation of EPR line widths reflects dynamic processes which may be studied over a wide range of time, i.e., $10^{-4}\text{--}10^{-10}\text{ s}$. These two properties make the EPR method very powerful in the unique determination of molecular structure and many inter- and intramolecular dynamic processes.

In a magnetic field the photoexcited triplet energy will become field dependent as shown by Fig. 5.10. The spin Hamiltonian must now include the Zeeman term

$$H = -\beta H \cdot \hat{g}s + \mathcal{H}_d$$

where \hat{g} is a second rank tensor. In many cases its isotropic value almost coincides with the free electron g_e factor 2.0023. The detailed analysis of the Hamiltonian will not be treated here except for summarizing the useful and relevant points.

When the external magnetic field is along one of the principal axes, one state remains always stationary with respect to the field strength. The other two states diverge in opposite directions as the strength of magnetic field increases (Fig. 5.10a). In general, the high field ESR spectrum of randomly oriented triplet state molecules consists of three pairs of symmetrically disposed lines, each pair corresponding to those molecules for which one of the magnetic axes is nearly parallel to the applied magnetic field¹²⁰. The two lines in each pair correspond to the transition between high field spin states; $|0\rangle$

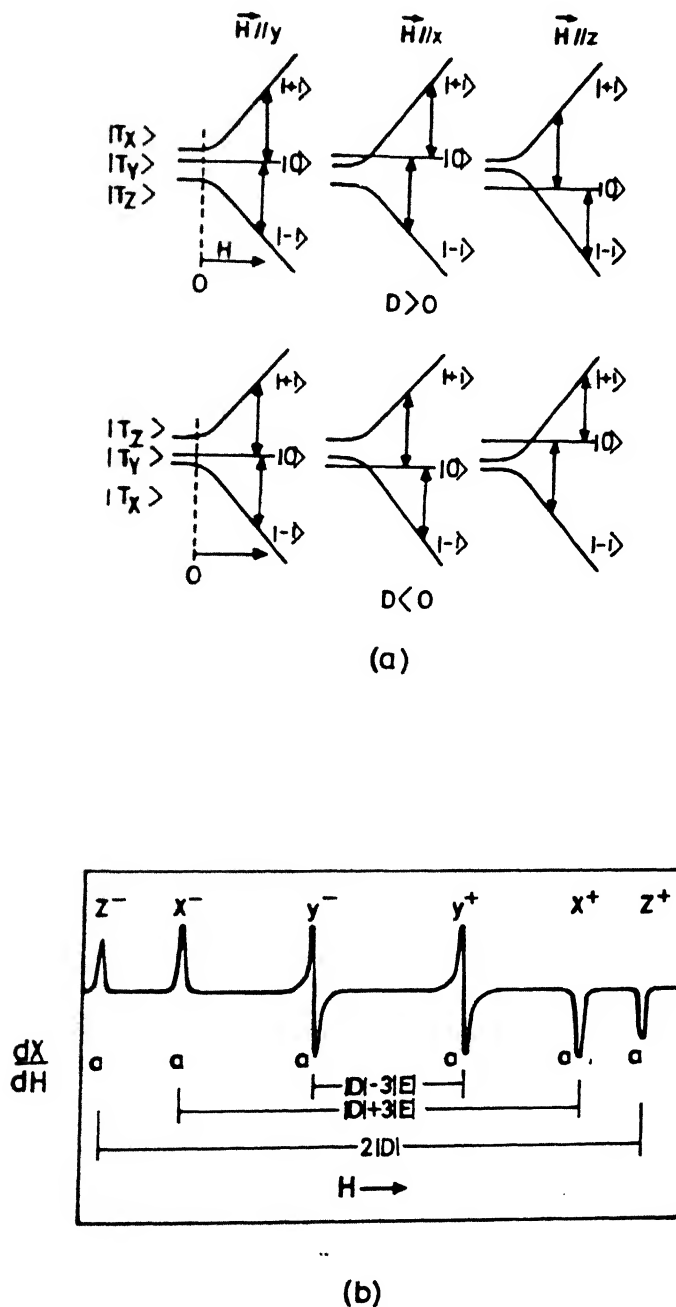


Fig. 5.10 : (a) Magnetic field dependence of the spin energy levels for the three canonical orientations. The upper trace is the energy level diagram for $D > 0$, whereas the lower trace is for $D < 0$. (b) First derivative of a randomly oriented triplet having $|D| > 3|E|$. The line shape and peak intensities are typical of a triplet state that is in thermal equilibrium; all signal intensities are in the absorption mode indicated by 'a'.

$\longleftrightarrow |+\rangle$ and $|0\rangle \longleftrightarrow |-\rangle$. First derivative of a randomly oriented triplet ESR spectra is shown in Fig. 5.10b. The separation between the pairs of lines are given by $2D$ and $D \pm 3E$ where D and E are zero field splitting (ZFS) parameters¹²¹.

It is the magnitude of $|D|$ and $|E|$ which determines whether one should be able to apply EPR spectroscopy to detect the triplet state. Thus, a necessary condition for EPR triplet detection is that the ZFS parameter $|D|$ and $2|E|$ should be smaller than the external magnetic field.

5.6 RESULTS

5.6.1 FREE BASE PORPHYRINS

A comparison of EPR spectra of triplets of Hexyl I, Hexyl II and Hexyl III randomly oriented in toluene : ethanol (4:1) at -160°C and without modulation is presented in Fig. 5.11 whereas Fig. 5.12 and Fig. 5.13 shows the ESR spectra of triplets MSICl_8 , MSIICl_8 and PSIBr_8 at two different temperatures (-106°C and -160°C) with modulation respectively. Table 5.5 presents the zero field splitting parameters (ZFS) D and E and spin polarization pattern obtained from the spectra including the data of planar H_2TPP . In general, the data in table 5.4 indicates;

- * In a given basket handle porphyrin series, the isomer I experiences a significant ($48\text{--}97 \text{ cm}^{-1}$) decrease in the D value relative to planar H_2TPP .
- * Among isomer I of basket handle, porphyrin systems MSICl_8 shows maximum decrease probably reflecting the highest degree of distortion.

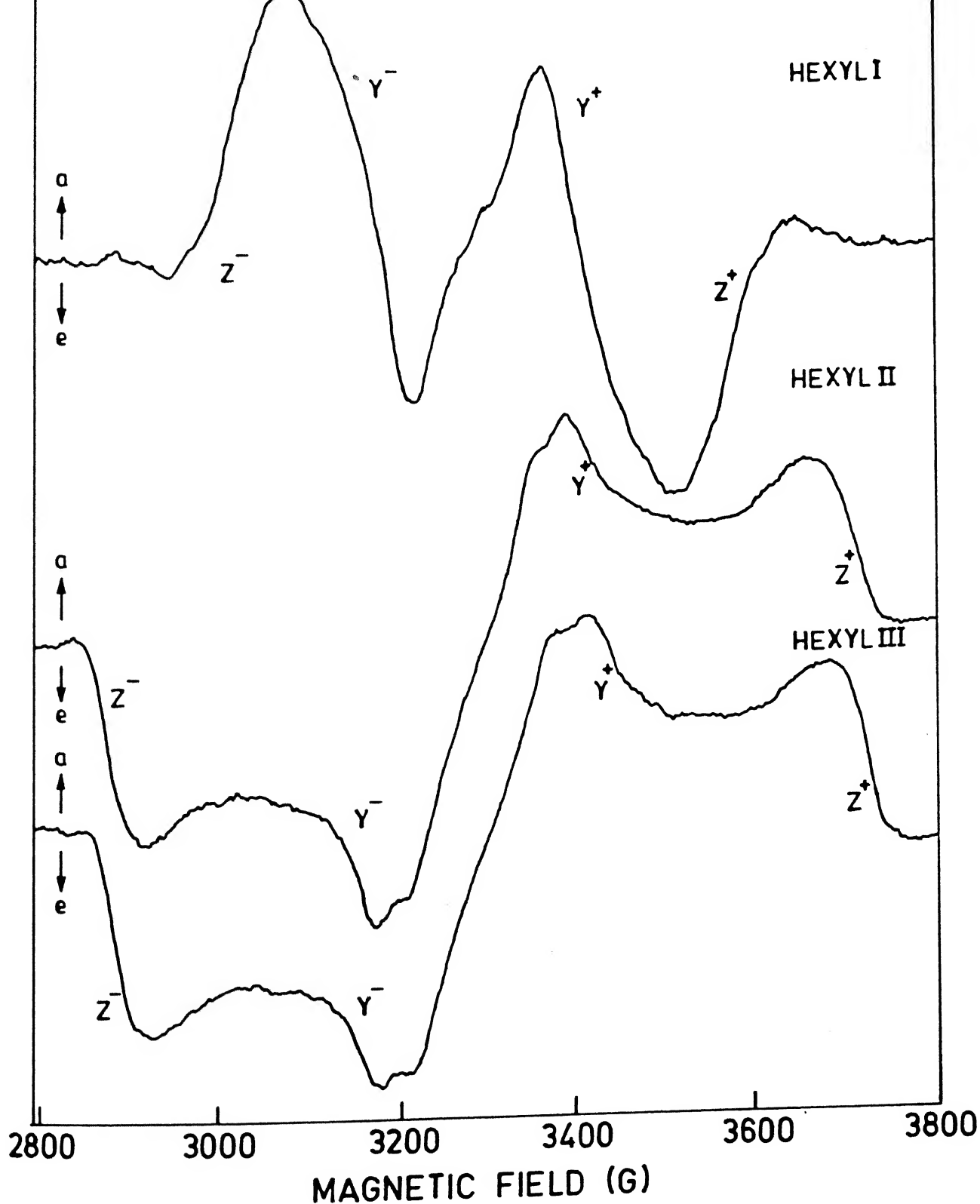


Fig. 5.11 : Triplet ESR spectra of (a) Hexyl I, (b) Hexyl II and (c) Hexyl III in a 4:1 toluene/ethanol mixture at 100 K. Microwave power 5 mW and without field modulation and excitation with pulsed laser (560 nm). Absorption and emission peaks are labelled 'a' and 'e'

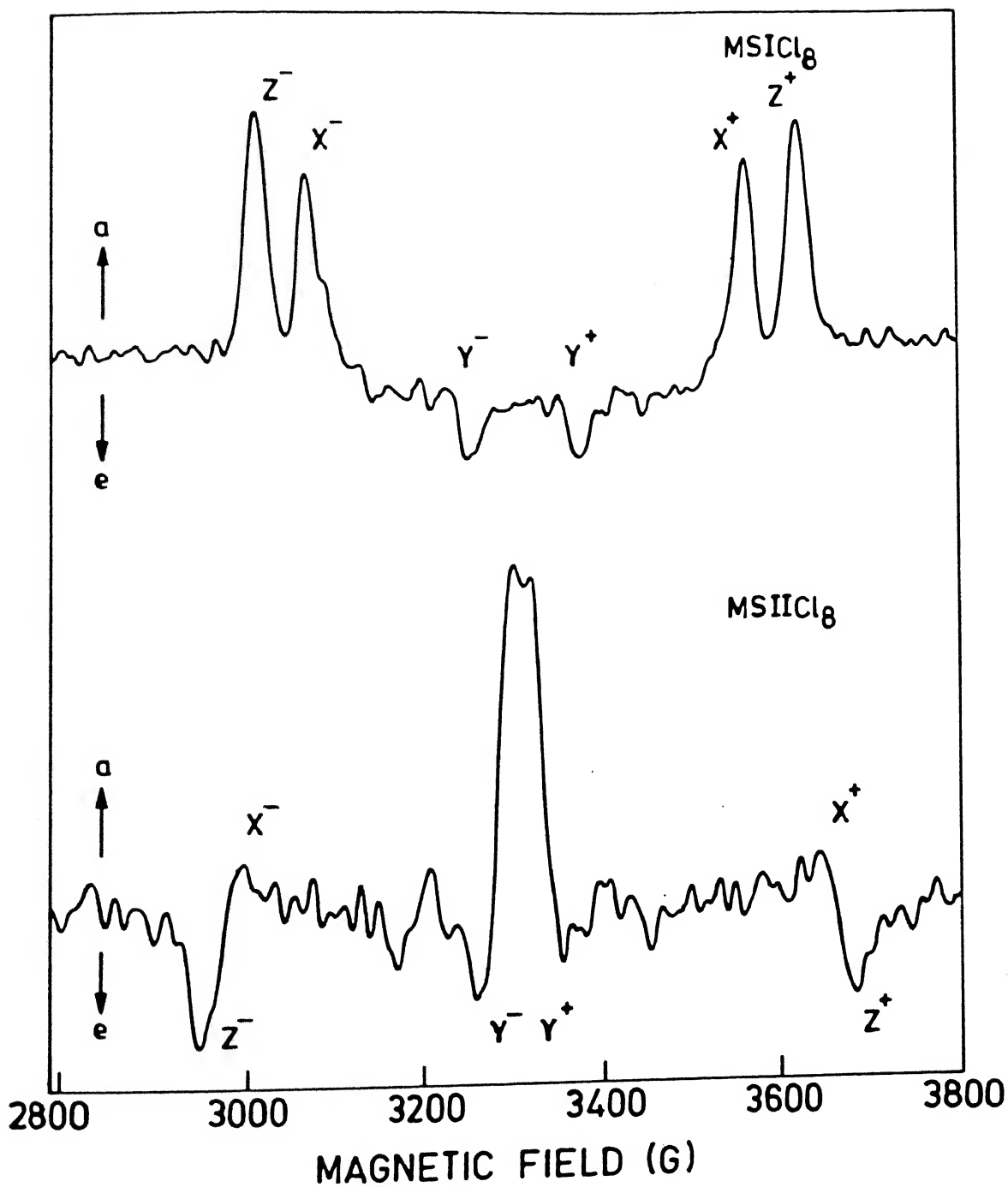


Fig. 5.12 : ESR spectra of photoexcited triplets of (a) MSICl_8 and (b) MSIICl_8 in toluene:ethanol (4:1) at about 100 KHz recorded with light modulation and excitation at 560 nm with pulsed radiation. Absorption and emission peaks are labelled as 'a' and 'e' respectively.

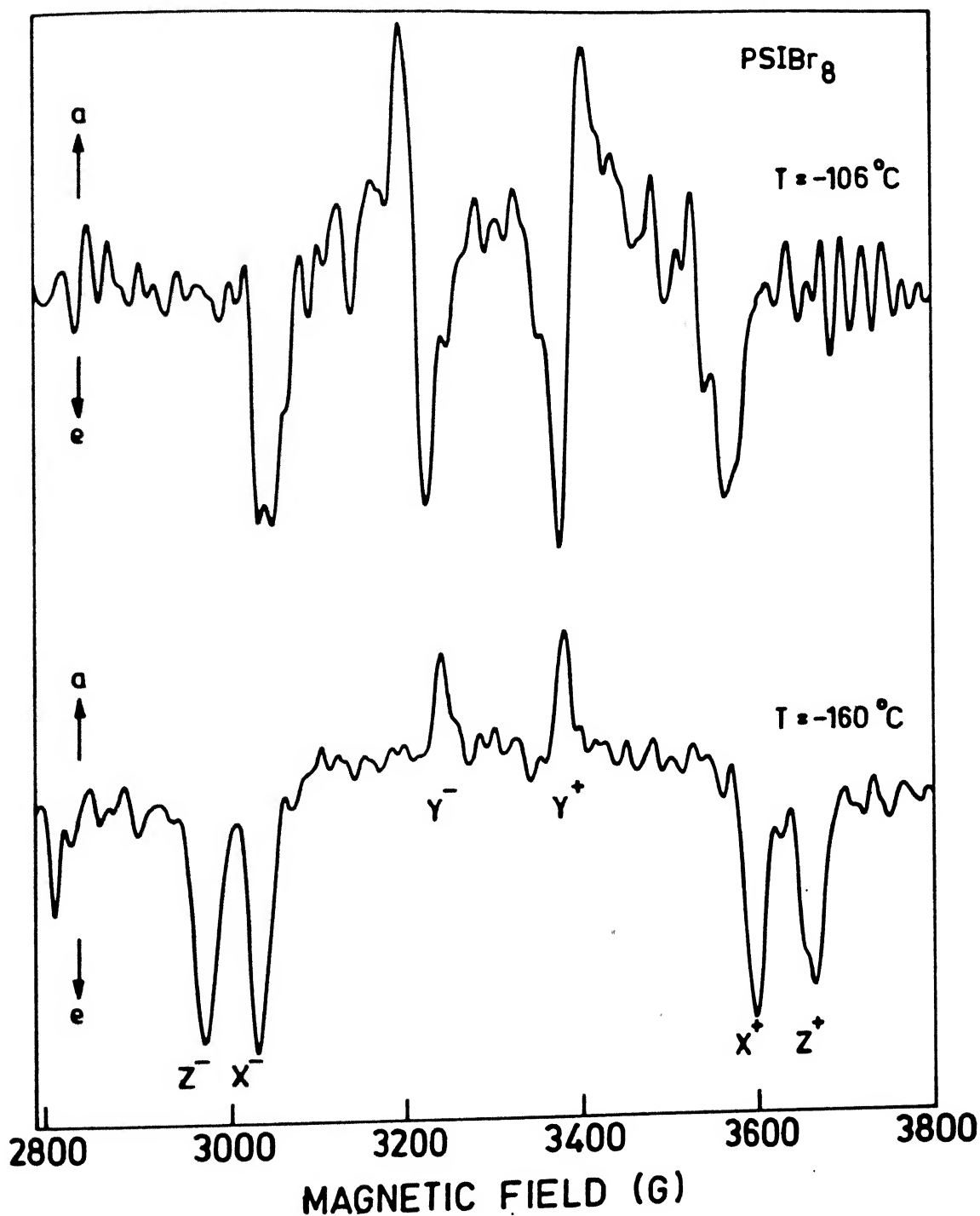


Fig. 5.13 : Triplet ESR spectra in toluene:ethanol of PSIBr_8 at (a) -106°C and (b) -160°C . Microwave power 5 mW, Field modulation 100 KHz. Excitation at 560 nm with pulsed radiation. Absorption and emission peaks are labelled as 'a' and 'e' respectively.

- * No significant change in the D value seen for isomer II and isomer III relative to H_2TPP .

Table 5.5 : Zerofield splitting parameters of various free base short chain basket handle porphyrins

PORPHYRIN	$D/cm^{-1} \times 10^{-4}$	$E/cm^{-1} \times 10^{-4}$	Polarisation pattern
Hexyl I	335	62	eaeaea
Hexyl II	390	50	eaeaea
Hexyl III	388	96	eaeaea
Pentyl I	321	80	eaeaea
Pentyl II	388	92	eaeaea
Pentyl III	357	90	eaeaea
MS II	347	84	eaeaea
MS III	369	85	eaeaea
$MSICl_8$	286	58	aaaeae
$MSIICl_8$	344	92	eaeaea
PS I	295	61	eaeaea
$PSIBr_8$	325	66	eeaeaa (-160°C)
$PSIBr_8$	329	53	eeaeaa (-106°C)
H_2TPP	383	78	eaeaea
H_2TPPS	391	75	eaeaea

- * The E value do not show any definite variation but for a small change in the magnitude.

- * The polarization pattern for all the porphyrin systems described here except $MSICl_8$ and $PSIBr_8$ remain same (eaeaea)

as observed for H_2TPP^{122} . However, the polarization pattern for $MSiCl_8$ shows on aaaaae behaviour while for $PSiBr_8$ it is found to be dependent on temperature at which the spectrum is recorded and the solvent used. For e.g., at $-160^\circ C$ $PSiBr_8$ shows an eaeaaa pattern while at $-106^\circ C$ an eaeaaa behaviour is observed. This signifies that the triplet kinetics is a sensitive function of temperature in this isomer.

5.6.2 Zn^{2+} PORPHYRINS

A comparison of ESR spectrum of triplet state $ZnButyl$ II, $ZnPentyl$ II and $ZnHexyl$ II in toluene : ethanol (4:1) is shown in Fig. 5.14 and the data of all Zn^{2+} derivatives is presented in table 5.5. Zn^{2+} derivatives of isomer I could not be obtained because of the steric hindrance of the strapping phenyl ring from both the faces of the porphyrin plane. An inspection of the data reveal the following :

Table 5.6 : Zerofield splitting parameters of various Zn^{2+} derivatives of basket handle porphyrins

PORPHYRIN	$D/cm^{-1} \times 10^{-4}$	$E(cm^{-1} \times 10^{-4})$	Polarisation pattern
$Zn Hexyl$ II	325	84	aaaaee
$Zn Hexyl$ III	329	108	aaaaee
$Zn Pentyl$ II	322	83	aaaaee
$Zn Butyl$ II	286	86	aaeaae
$ZnMSiCl_8$	306	93	aaeaae
$ZnTPP$	298	98	aaaaee
$ZnTPPS$	323	95	aaaaee

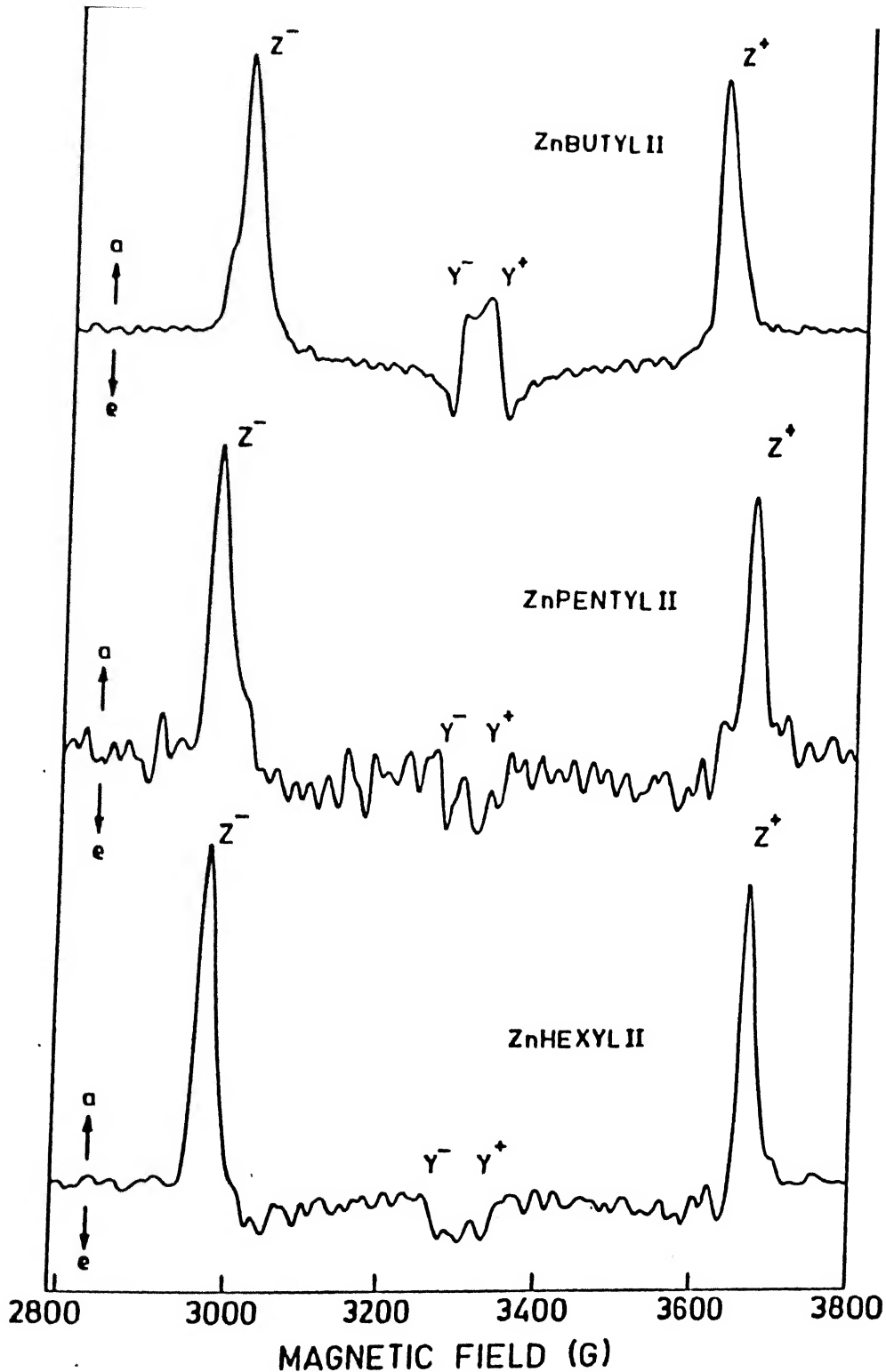


Fig. 5.14 : ESR spectra of photoexcited triplets of (a) ZnButyl II, (b) ZnPentyl II and (c) ZnHexyl II in toluene:ethanol (1:1) at about 100 KHz recorded with field and light modulation using pulsed radiation with excitation at 560 nm. Absorption and emission peaks are labelled as 'a' and 'e' respectively.

- * A small change in D and E values compared to planar ZnTPP
- * The spin polarization pattern remains same as in ZnTPP¹²³ except for Zn Butyl II and ZnMSIICl₈.

5.7 DISCUSSION

5.7.1 FREE BASE PORPHYRINS

An inspection of D values given in table 5.4 shows that, in general, there is a decrease in D value for all basket handle porphyrins relative to that of the parent H₂TPP, suggesting an increase in the average separation between the unpaired electrons. This observed reduction in D value is probably due to the fact that the porphyrin ring is not a rigid structure so that its geometry can be modified by intermolecular interactions. In TPP systems, as pointed out by van der Waals et.al.¹²³, a lowering of the D value is expected on (i) delocalization of the π electrons in the phenyl groups and (ii) when the porphyrin ring becomes nonplanar. ¹H NMR studies of these porphyrins have indicated that the meso-phenyl ring is under considerable strain at least in the isomer I because of the tension imposed by the bridging chain. This might reduce the dihedral angle between the phenyl and porphyrin plane, thus allowing increased spin delocalization in the phenyl rings. The large red shifts of both the Soret and Q-bands in the optical spectrum relative to H₂TPP supports this possibility. Thus, it is likely that, at least in the isomer I, spin delocalization in the phenyl ring is increased, which would account in part for the observed reduction in the D value. Furthermore, the calculated structures of all the porphyrins as well as X-ray structure of a free base capped porphyrin (which has

a similar bridging group) have indicated that the porphyrin skeleton is markedly nonplanar with buckling of the porphyrin plane^{124,125}. Thus, the structural change upon introduction of a short bridging chain and the spin delocalization in the phenyl groups accounts for the reduction in D values.

Table 5.5 indicates small differences in the magnitude of E values for the different isomers relative to H₂TPP. Thus the observed small decrease and increase in E values for isomer I and isomer II, isomer III, respectively, suggests a smaller deviation of the axial symmetry for isomer I relative to isomer II and isomer III.

The intersystem crossing (ISC) generating the triplets, and the triplet decay process are known to be spin selective¹²⁶. For porphyrins, at 100 K in dilute frozen solution, the relative magnitude of the triplet lifetime and electron spin relaxation time (T_1) are such that, even under steady state illumination, thermal equilibrium is not established. With light modulation coupled with synchronous detection using a lock-in amplifier the spin polarization effect is enhanced strongly. This accounts for the observation of absorption (a) as well as emission (e) signals in the ESR spectra.

A correlation has been obtained between the relative polarization patterns of EPR and the initial population or depopulation rates¹²⁷ as shown in the table 5.7 by following the convention; the order of energy levels is chosen $T_x > T_y > T_z$.

Thus, the spin polarization pattern (eaeaea) observed in all

porphyrins except MSICl_8 and PSIBr_8 , corresponds to that found in the parent H_2TPP . From table 5.7 it is clear that the middle (Y) zero-field spin level is most active in the triplet state $T_1 \rightarrow S_0$ intersystem crossing in the basket handle porphyrins relative to the other states (X and Z). A small value of D and different spin polarization pattern (aaaaee) observed for MSICl_8 could be

Table 5.7 : Polarization patterns predicted from relative zero field population : depopulation rates^a

Relative Population : depopulation rate ^b			Polarization at canonical orientations ^c					
K_x	K_y	k_z	Z^-	X^-	Y^-	Y^+	X^+	Z^+
1	0	0	e	e	a	e	a	a
0	1	0	e	a	e	a	e	a
0	0	1	a	a	a	e	e	e
1	1	0	e	e	e	a	a	a
1	0	1	a	e	a	e	a	e
0	1	1	a	a	e	a	e	e
2	1	0	e	e	-	-	a	a
2	0	1	-	e	a	e	a	-
1	2	0	e	-	e	a	-	a
0	2	1	-	a	e	a	e	-
1	0	2	a	-	a	e	-	e
0	1	2	a	a	-	-	e	e

^aThis table gives representative population : depopulation rates for spin-orbit intersystem crossing (isc) for isolated molecules and is not all inclusive.

^bValid if certain restrictions can be made in the value of T_{1e} (electron spin lattice relaxation time) relative to the population:depopulation rate constants.

^cThe assignments are made assuming $D > 0$ (the usual case for $\pi\pi^*$ triplet states) and $D > -3E > 0$.

due to larger distortion created in the porphyrin skeleton by short bridging groups. A large red shift in absorption and emission bands seen for $MSiCl_8$ relative to other cross-trans-linked porphyrin derivatives and the calculated structure supports the above observation. The spin polarization pattern observed for $MSiCl_8$ suggests the redirection of spin sublevel activity from inplane Y sublevel to out of plane Z sublevel due to distortion in the porphyrin skeleton by attachment of short bridging group.

The compound that shows the most interesting behaviour is $PSiBr_8$. The triplet spectrum of this compound is dependent on solvent and temperature. A comparison of the graphs of the two spectra at two different temperatures (-106°C and -160°C) suggests that the spectrum at higher temperature is more narrow and the polarization for the Y-peaks are the reverse of the one at lower temperatures. This would lead to the conclusion that at higher temperatures some charge-transfer takes place. However, calculations show that the D values for the two spectra must be the same and that the apparent narrowing of the spectrum is due to the disappearance of the Z-peak polarization without a change in their position. An alternative reasoning may be the transfer of single electron might occur and the back reaction thus generates a

triplet with polarization that is different from the polarization from intersystem crossing. Another possibility is that changes in temperature or solvent favour different configurations of the molecule thereby changing the intersystem crossing rates from the singlet to each of the three triplet sublevels. The spectra measured in tetrahydrofuran show that polarization patterns are in between the two extremes in ethanol. This spectrum is temperature dependent to a lesser extent than those in ethanol.

5.7.2 Zn^{2+} Derivatives

The Zn^{2+} derivatives described here lack a four fold symmetry axis unlike ZnTPP^{123} is expected to give rise to a small rhombic contribution ($E \neq 0$). The zero field splitting parameters presented in table 5.6 clearly suggests the existence of such a rhombic distortion and this contribute to the E value. It is pertinent to point out here that the ZnTPP triplet ESR spectrum is found to be dependent on temperature. For e.g., at 100 K, ZnTPP shows a triplet spectrum which is characteristic of axial symmetry ($E=0$) but at lower temperature (~ 10 K), the triplet spectrum is characteristic of a rhombic symmetry with nonvanishing E value. This temperature effect has been attributed to rapid interconversion processes between various distorted configurations due to the Jahn-Teller distortion. However, in the present case, this explanation may not be valid since the Zn^{2+} derivatives of basket handle porphyrins are expected to lack axial symmetry because of the short bridging chain.

The data for Zn^{2+} derivatives of adjacent-trans and adjacent-

cis-isomers indicate that the zero field splitting parameter D is little affected relative to planar ZnTPP. This is probably due to less constraint on the normal possible motions of the porphyrin by connecting adjacent phenyl groups. The less red shifts observed for adjacent-trans and adjacent-cis isomers in absorption bands also suggests the presence of less deformation in the porphyrin skeleton. Furthermore, slightly higher values of D for hexyl and pentyl bridged porphyrins are attributed to the presence of two species. It was observed earlier that the longer alkyl chains are apparently flexible enough to interconvert and hence there may be an equilibrium between two distinct configurations for these compounds. The greater reduction in D values in Zn Butyl II and ZnMSIICl₈ indicate the presence of relatively higher deformation in these porphyrins due to shorter bridging chain.

Generally, in chlorophylls¹²⁸ and free base porphyrin systems, the observed polarization pattern suggest the dominance of X and Y (inplane molecular axes) spin sublevels with respect to population and decay of triplet states. This data suggest that the intersystem crossing may be described in terms of models advanced for the non-radiative transitions in planar aromatic hydrocarbons¹²⁹. Furthermore, in chlorophylls, it signifies negligible contributions to spin-orbit coupling from the central magnesium atom¹³⁰. In contrast, the introduction of Zn²⁺ ion into the porphyrin or chlorophyll core changes the spin sublevel intersystem crossing activity drastically (aaaaaa) suggesting the dominance of the Z-sublevel (outerplane molecular axis) with respect to population and decay. This is due to the large

contribution to spin-orbit coupling integral from mixing of zinc atom with the porphyrin orbitals¹³¹. The spin polarization pattern for Zn^{2+} derivatives of basket handle porphyrins except ZnButyl II and ZnMSIICl_8 is in accordance with this. However, different spin polarization pattern observed for Zn Butyl II and ZnMSIICl_8 (aaeae) is attributed to structural change in the porphyrin skeleton due to attachment of short bridging groups which changes the population and decay of spin sublevels. The ESP pattern aaeae for Zn Butyl II and ZnMSIICl_8 suggest that both inplane (Y spin sublevel) and out of plane (Z spin sublevel) molecular axes are dominant unlike other Zn^{2+} derivatives where Z spin sublevel is more active.

5.8 CONCLUSIONS

The following conclusions can be drawn from the present study :

- * Distortion in the porphyrin plane leads to better donating ability in the singlet excited state. However, introduction of bromines at the β -pyrrole carbons make the porphyrin ring a poor donor than H_2TPP in the singlet excited state.
- * Singlet excited state parameters depend more on the length of the bridging chain than on the nature of the chain.
- * The reduction in D value observed for free base basket handle porphyrins and their Zn^{2+} derivatives indicates the retainment of the deformation even in the triplet state.
- * The temperature dependent ESR spectrum observed for PSIBr_8 suggests the possibility of electron transfer from porphyrin ring to bridging aryl group having electron withdrawing substituents.

CHAPTER 6

MAGNETIC INTERACTIONS IN π -CATION RADICALS OF COPPER(II) AND HIGH SPIN IRON(III) DERIVATIVES OF SHORT CHAIN BASKET HANDLE PORPHYRINS

6.1 INTRODUCTION

From the literature survey data presented in Chapter 1, it is clear that the magnetic interaction between the unpaired electron in the paramagnetic metal and the unpaired electron in the porphyrin ring depends on the structure of the porphyrin core. The limited data available in literature correlating the spin system and the nature of the magnetic coupling suggests that the planar core leads to ferromagnetic coupling and the nonplanar core leads to antiferromagnetic coupling^{45,47,50,51}. Especially, in the MTPP⁺ type cation radicals it has been shown that the dimerization is suggested to be a requirement. However, a number of examples of metalloporphyrin radicals having different kind of nonplanar structure are required to substantiate such a conclusion. The porphyrin systems in this thesis have unique structure in terms of their nonplanarity, therefore it is of interest to study magnetic interactions in these porphyrins. Two

points of interest which have emerged from the literature survey are : (1) Most of the $\text{MTPP}^{\cdot+}$ cation radicals are found to be dimeric in solid state and the porphyrin core is saddle shaped^{49,50}. (2) Difference in magnetic coupling behaviour in solid and solution phases. For example, $\text{CuTPP}^{\cdot+}$ is found to be dimeric and ruffled in the solid state and it is monomeric and planar in solution⁴⁹. Thus, the observed antiferromagnetic coupling in solid state and independent spins in solution are accounted to its structural difference existing in solid and solution phase. This clearly suggests that porphyrin systems which can have permanent deformation in both the phases will be interesting to study the anomalous magnetic behaviour in solid and solution phase in paramagnetic metalloporphyrin π -cation radicals.

6.2 WORK DONE IN THE PRESENT STUDY

In this chapter, the magnetic interactions in doubly strapped paramagnetic metalloporphyrin π -cation radicals are presented. The purpose of choosing these porphyrin systems is

- (1) Existence of permanent deformation in the porphyrin skeleton due to attachment of short bridging chains across the porphyrin periphery as shown in the preceding chapters.
- (2) The presence of straps prevent the dimer formation in oxidised porphyrins which is responsible for the unusual saddle shaped core conformation observed in several π -cation radicals reported till date.

The studies are carried out with two metallo derivatives, copper(II) and high spin iron(III) derivatives, with a view that

if antiferromagnetism is observed between unpaired electron of the metal and unpaired electron of the porphyrin ring in both solid and solution phase due to deformed porphyrin core, the copper(II) derivatives will be totally diamagnetic whereas high spin iron(III) derivatives will be paramagnetic with net magnetic moment for four unpaired electrons.

This chapter is divided into two sections : section A describes the studies on π -cation radicals of copper(II) derivatives of basket handle porphyrins (Fig. 6.1) and section B describes the studies on π -cation radicals of high spin iron(III) derivatives of basket handle porphyrins (Fig. 4.8). The experimental results and discussion are given in the following sections.

SECTION A

π -CATION RADICALS OF COPPER(II) DERIVATIVES OF BASKET HANDLE PORPHYRINS

6.3 EXPERIMENTAL

The syntheses of all copper(II) derivatives studied here are described in Chapter 4.

6.3.1 SYNTHESIS OF $[\text{CuPSIBr}_8] [\text{SbCl}_6]$

CuPSIBr_8 (0.010 g, 0.006 mmol) in CH_2Cl_2 (10 cm^3) was stirred for 10 minutes under argon atmosphere and 1.1 equivalent of tris (p-bromophenyl) ammonium hexachloroantimonate (0.006 g, 0.069 mmol) was added slowly to it. A deep green color developed

immediately and stirring was continued for four hours. The progress of the reaction was monitored with UV-vis spectrophotometer. After filtration, the solvent was evaporated under vacuo and the green powder obtained was dissolved in a minimum amount of CH_2Cl_2 and precipitated with hexane. The product was filtered and washed several times with dichloromethane-hexane (1:9) solvent mixture, dried and stored under vacuo (yield 0.010 g, 80%).

Anal. Calcd. $\text{C}_{60}\text{H}_{32}\text{CuCl}_6\text{Br}_8\text{N}_4\text{O}_4\text{Sb}$: C, 37.69%; H, 1.69%; N, 2.92%.

Found : C, 37.02%; H, 1.85%; N, 2.75%.

Similar procedure was followed for the synthesis of other oxidized derivatives.

6.3.2 [CuHexyl I'] [SbCl₆]

Anal. Calcd. $\text{C}_{54}\text{H}_{48}\text{N}_4\text{O}_4\text{CuCl}_6\text{Sb}$: C, 53.38%; H, 3.98%; N, 4.61%.

Found : C, 52.79%; H, 3.89%; N, 4.52%.

6.3.3 [CuPSI'] [SbCl₆]

Anal. Calcd. $\text{C}_{60}\text{H}_{40}\text{CuCl}_6\text{N}_4\text{O}_4\text{Sb}$: C, 56.34%; H, 3.15%; N, 4.38%.

Found : C, 55.78%; H, 2.93%; N, 4.29%.

6.3.4 [CuMSICl₈'] [SbCl₆]

Anal. Calcd. $\text{C}_{60}\text{H}_{32}\text{CuCl}_{14}\text{N}_4\text{O}_4\text{Sb}$: C, 46.35%; H, 2.07%; N, 3.60%.

Found : C, 45.55%; H, 1.96%; N, 3.52%.

6.3.5 [CuMSIICl₈'] [SbCl₆]

Anal. Calcd. $\text{C}_{60}\text{H}_{32}\text{CuCl}_{14}\text{N}_4\text{O}_4\text{Sb}$: C, 46.35%; H, 2.07%; N, 3.60%.

Found : C, 45.09%; H, 1.89%; N, 3.49%.

6.4 RESULTS

6.4.1 ELECTRONIC SPECTRA

The absorption spectra of neutral CuPSIBr_8 and its cation radical $[\text{CuPSIBr}_8] [\text{SbCl}_6]$ in CH_2Cl_2 is presented in Fig. 6.2.

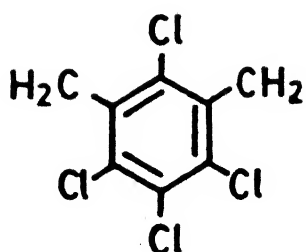
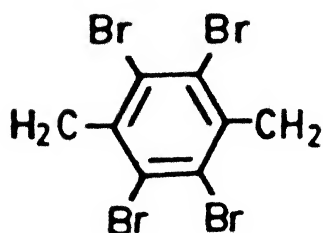
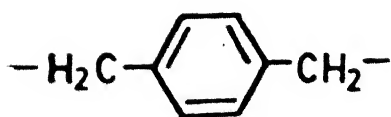
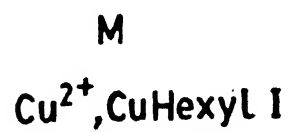
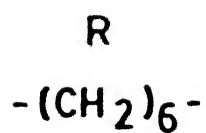
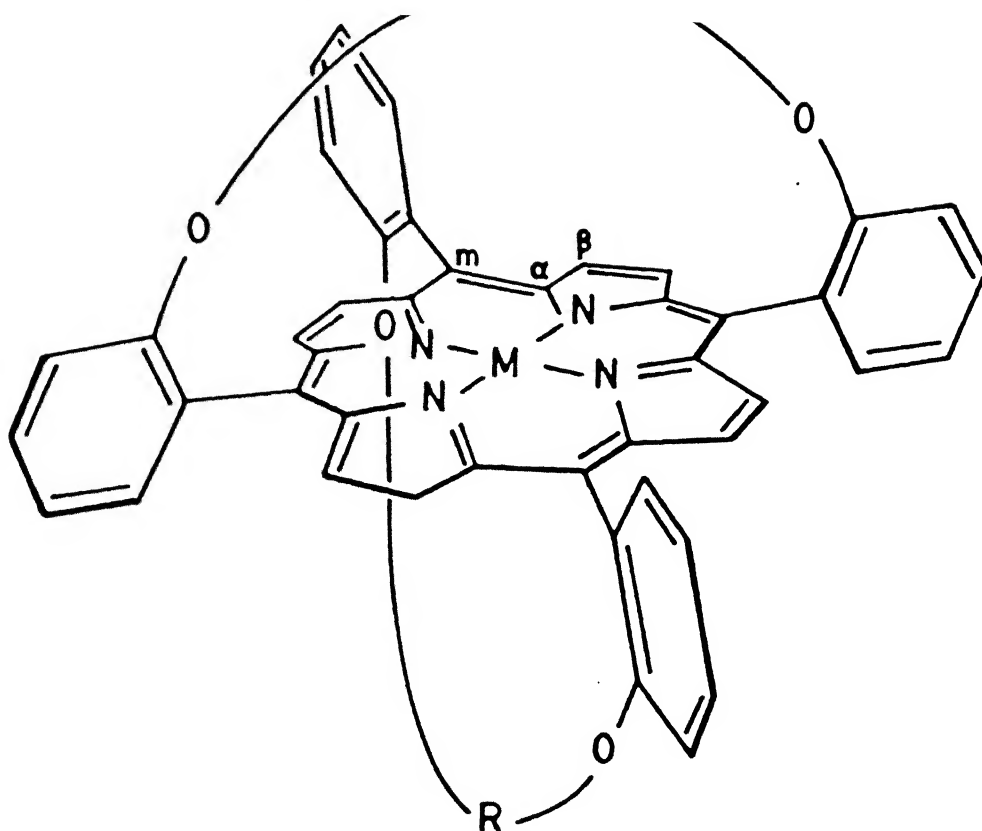


Fig. 6.1 : Structure of Copper(II) derivatives of cross-trans-

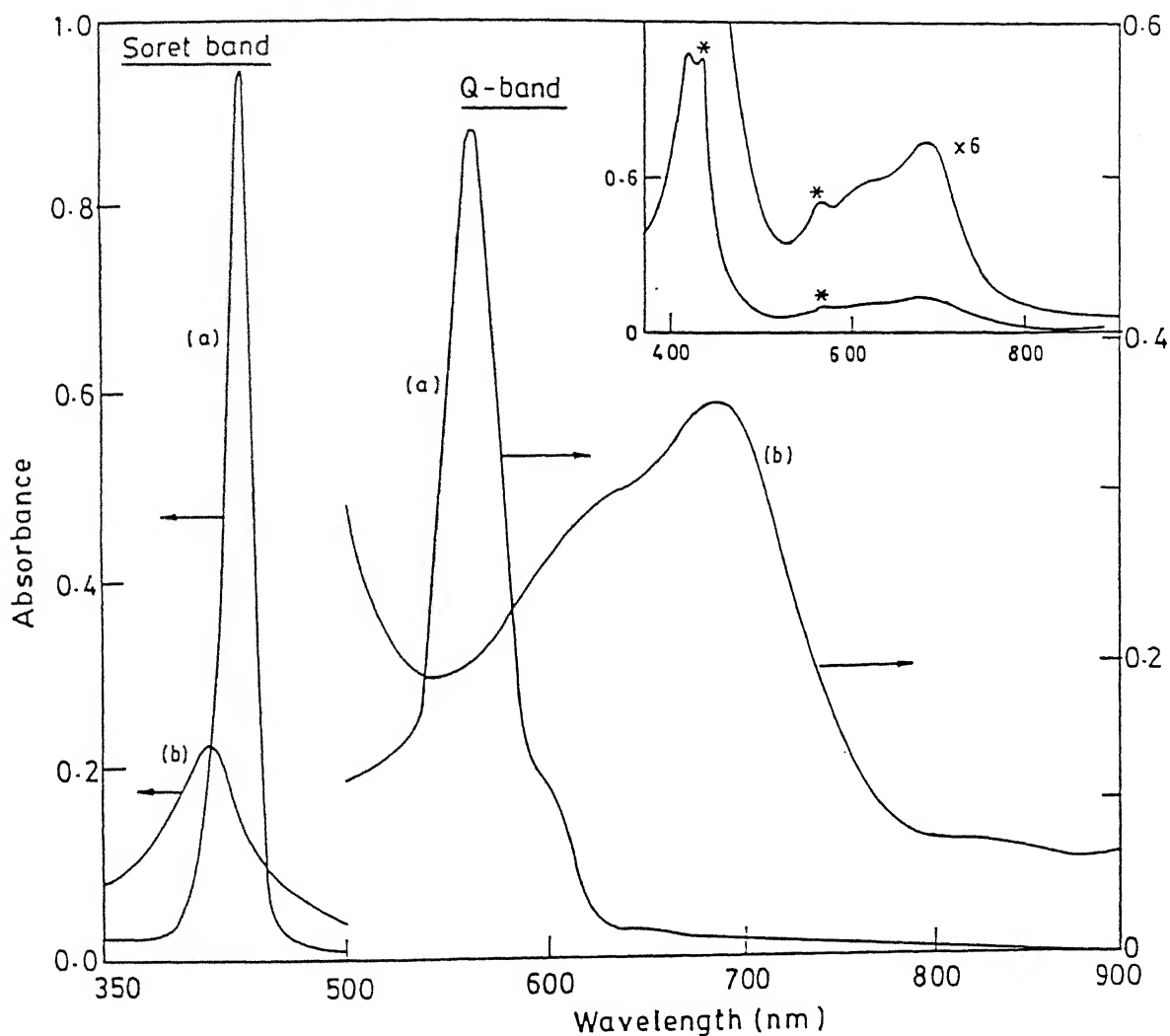


Fig. 6.2 : Comparison of the optical absorption spectra of (a) $[\text{CuPSIBr}_8]$ and (b) $[\text{CuPSIBr}_8][\text{SbCl}_6]$ in dichloromethane. The concentrations used were $\approx 2 \times 10^{-5} \text{ mol dm}^{-3}$ for Q-bands and $\approx 2 \times 10^{-6} \text{ mol dm}^{-3}$ for Soret. The inset shows the optical spectrum of coulometrically oxidised species of CuPSIBr_8 . (*) indicates the presence of some unoxidised CuPSIBr_8 .

The electrochemically generated optical spectra of $\text{CuPSIBr}_8^{\cdot+}$ by controlled potential coulometry at +0.96 V in CH_2Cl_2 with 0.1 M TBAP is included in inset. The similarity between two spectra confirms the purity of the radical species isolated. The broad featureless red shifted Q-bands and blue shifted Soret bands with reduced intensity of the oxidised species are in conformity with the oxidation of the ring rather than metal center^{132,133}. The optical data of both neutral and radical species are tabulated in table 6.1. A comparison of the data of π -cation radicals of

Table 6.1 : Electronic Spectral data of various deformed copper(II) porphyrins and their cation radicals in CH_2Cl_2 .

PORPHYRIN	Soret band	Q-bands	
	B(0,0)	$\lambda_{\text{max}}/\text{nm}$	
	$\lambda_{\text{max}}/\text{nm}$	$(10^{-3} \epsilon/\text{dm}^3 \text{ mol}^{-1} \text{ cm}^{-1})$	
	$10^{-4} \epsilon/\text{dm}^3 \text{ mol}^{-1} \text{ cm}^{-1}$	I	II
CuTPP [*]	417	540	580 (sh)
[CuTPP][SbCl ₆] [*]	408	600 (sh)	630
Cuhexyl I	426	556	594 (sh)
[CuhexylI][SbCl ₆]	410	614 (sh)	684
CuPSI	432	562	600 (sh)
[CuPSI][SbCl ₆]	414	610	686
CuMSIBr ₈	435	563	603 (sh)
[CuMSIBr ₈][SbCl ₆]	412	618 (sh)	687
CuMSICl ₈	440	569	611 (sh)
[CuMSICl ₈][SbCl ₆]	414	-	701
CuMSIICl ₈	419	544	-
[CuMSIICl ₈][SbCl ₆]	408	-	606

deformed copper(II) porphyrins with their corresponding neutral derivatives reveals the following :

- * A large blue shift of Soret band upon oxidation.
- * The magnitude of red shift of Q-bands are larger upon oxidation of deformed porphyrins relative to oxidation of CuTPP.

Furthermore, the optical bands of radical cations of basket handle porphyrins are red shifted relative to $\text{CuTPP}^{\cdot+}$ indicating the retainment of distortion in solution upon oxidation. However, the magnitude of blue shift of Soret band and red shift of Q-bands upon oxidation of adjacent-trans-linked isomer, CuMSIICl_8 are very less compared to oxidised products of cross-trans-linked copper porphyrins further suggesting that the trend of deformation observed for neutral copper porphyrins are retained in their cation radicals.

6.4.2 INFRARED SPECTRA

A diagnostic π -cation radical band at $\sim 1285 \text{ cm}^{-1}$ was observed in all the derivatives confirming the oxidation of the ring rather than metal⁴³. The origin of this mode is not yet clear but it is tentatively assigned to strongly IR allowed porphyrin ring mode.

6.4.3 RESONANCE RAMAN SPECTRA

Resonance Raman spectra of CuPSIBr_8 and CuHexyl I and their corresponding cation radicals in CH_2Cl_2 in the region $800\text{--}1800 \text{ cm}^{-1}$ are shown in Fig. 6.3 and Fig. 6.4 and the frequencies of important modes are listed in table 6.2. The assignments of

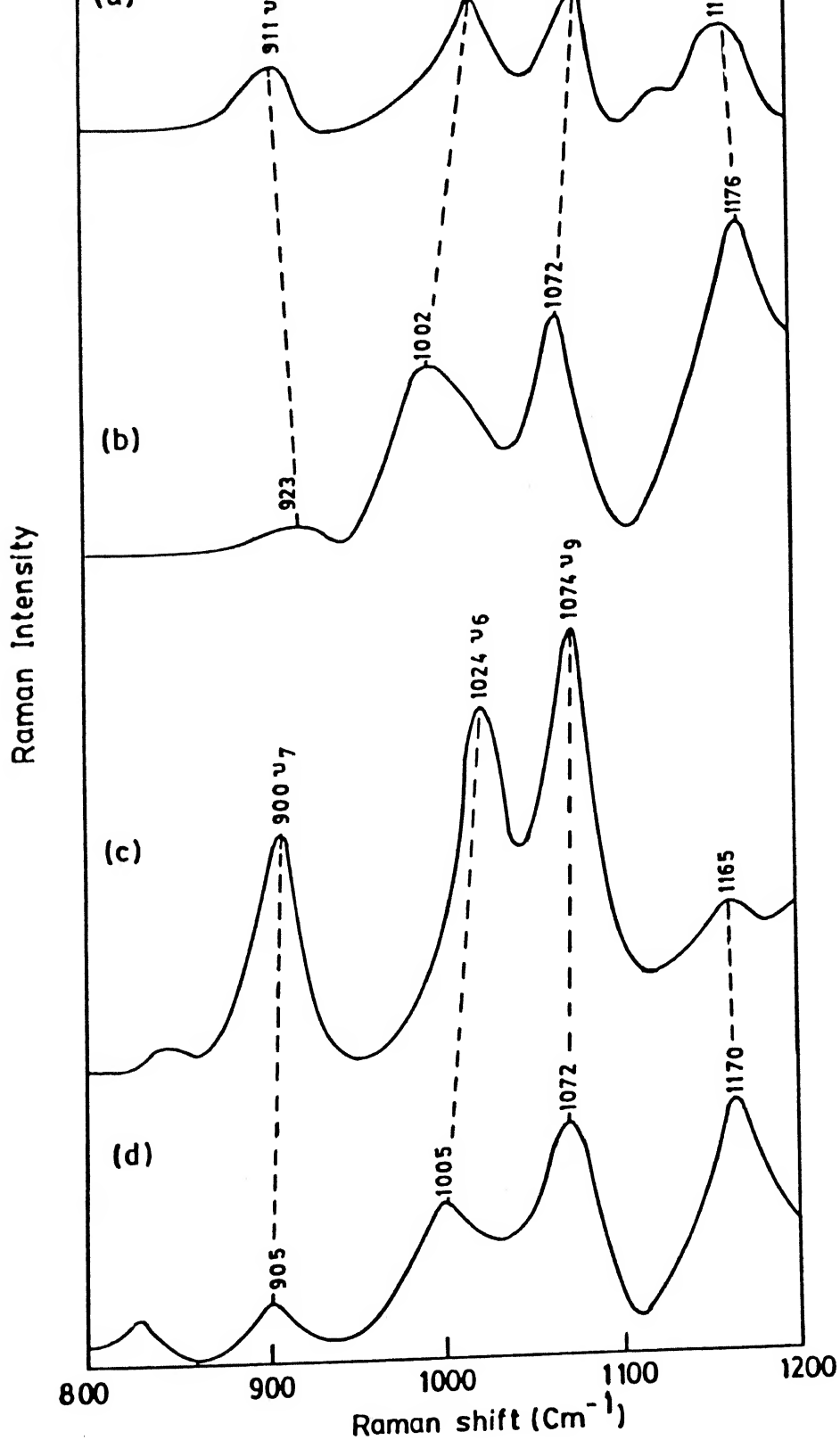


Fig. 6.3 : Resonance Raman spectra in the lower frequency region of (a) CuHexyl I, (b) $[\text{CuHexyl I}'] [\text{SbCl}_6]$, (c) $[\text{CuPSIBr}_8]$ and (d) $[\text{CuPSIBr}_8'] [\text{SbCl}_6]$ with excitation with 457.9 nm. Samples were dissolved in dry dichloromethane. The

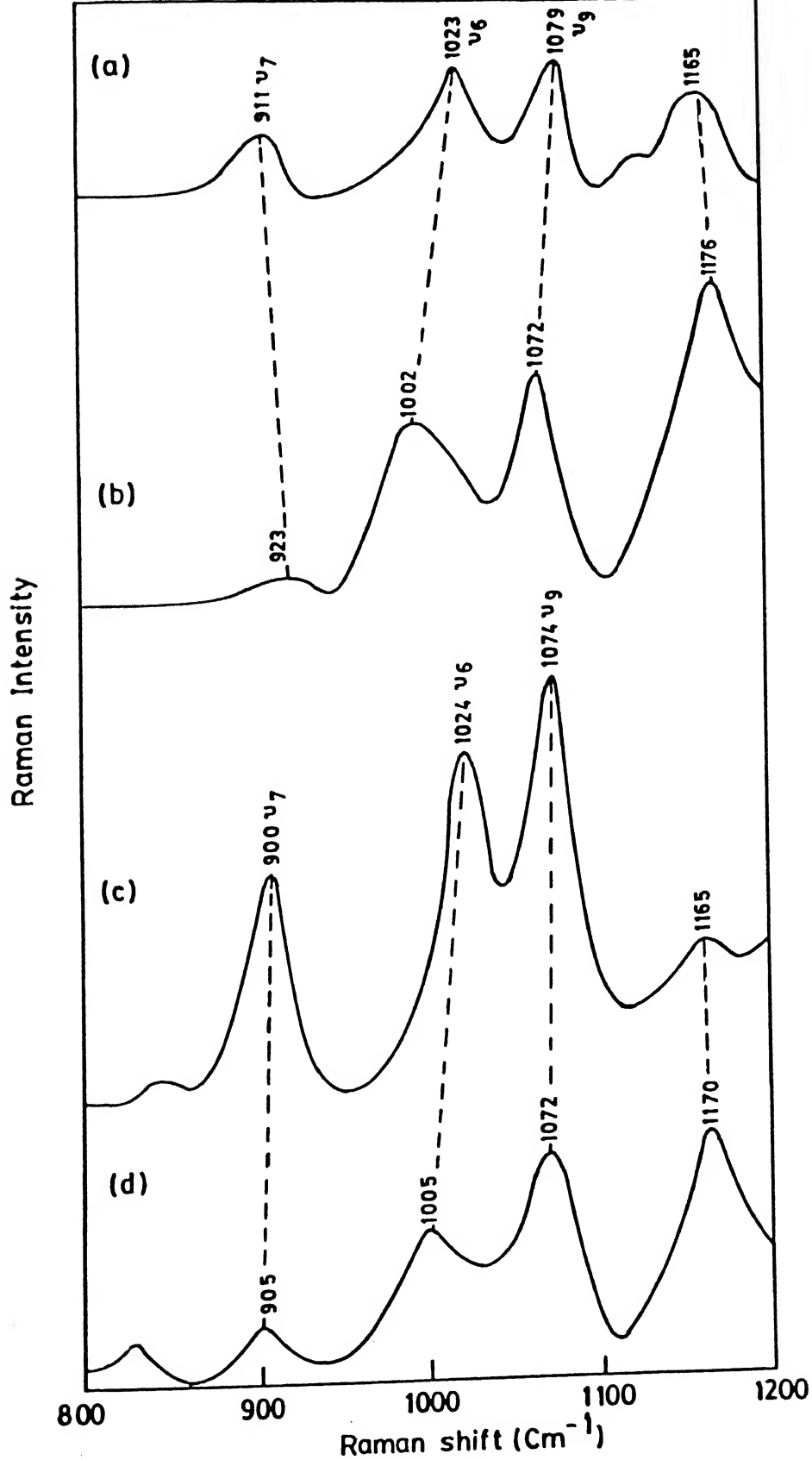


Fig. 6.3 : Resonance Raman spectra in the lower frequency region of (a) CuHexyl I , (b) $[\text{CuHexyl I}'] [\text{SbCl}_6]$, (c) $[\text{CuPSIBr}_8]$ and (d) $[\text{CuPSIBr}_8'] [\text{SbCl}_6]$ with excitation with 457.9 nm.

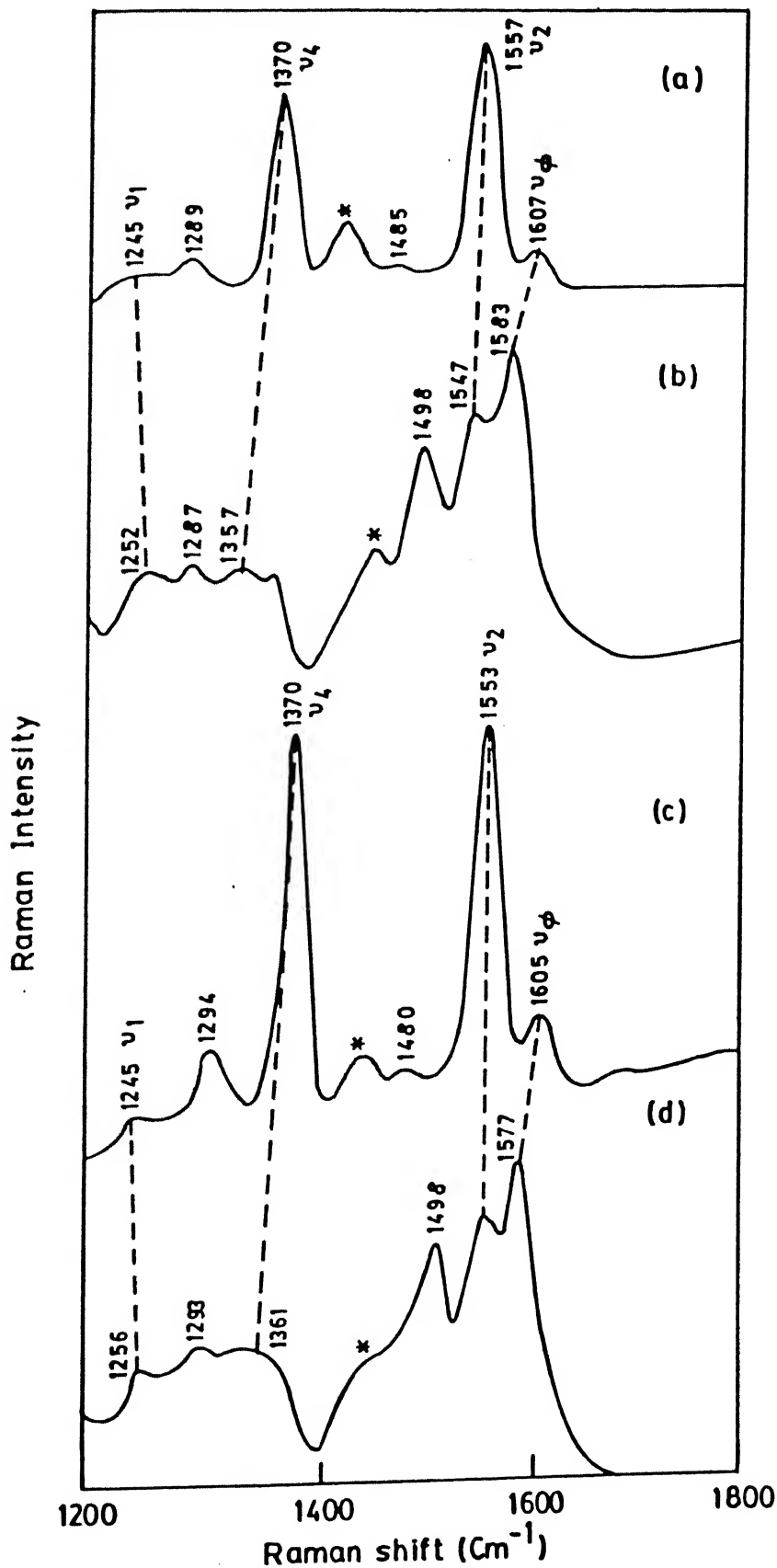


Fig. 6.4 : Resonance Raman spectra in the higher frequency region with excitation at 457.9 nm in dry dichloromethane of (a)

Table 6.2 Comparison of resonance Raman frequencies [cm^{-1}] of CuPSIBr_8 and CuHexyl I and their cation radicals with CuTPP and its cation radical.

Mode No.	Description	[CuTPP]	[CuTPP] $^{\cdot+}$	[CuPSIBr $_8$]	[CuPSIBr $_8$] $^{\cdot+}$	CuHexyl I	[CuHexyl I] $^{\cdot+}$
ν_ϕ	$\nu_{\text{C-C Phenyl}}$	1599	1595	1605	1577	1607	1583
ν_2	$\nu_{(\text{C}_\beta-\text{C}_\beta)\text{sym}}$	1562	1530	1553	1545	1557	1547
ν_{11}	$\nu_{(\text{C}_\beta-\text{C}_\beta)\text{asym}}$	1501	-	1480	-	1485	-
ν_4	$\nu_{(\text{pyr. half ring})\text{sym}}$	1365	1355	1370	1361	1370	1357
ν_1	$\nu_{(\text{C}_m-\text{C}_\phi)}$	1237	1234	1245	1256	1245	1252
ν_9	$\delta_{(\text{C}_\beta-\text{H})\text{sym}}$	1080	1077	1074	1072	1079	1072
ν_6	$\nu_{(\text{Pyr. breathing})}$	1008	1002	1024	1005	1023	1002
ν_7	$\delta_{(\text{Pyr. def})\text{sym}}$	886	884	900	905	911	923

important vibrational modes were done following the latest normal mode analysis of metallo tetraphenylporphyrins by Spiro and coworkers³⁷. The effect of deformation in Cu(II) derivatives of basket handle porphyrins resulted in the shifts and changes in structurally sensitive modes compared to CuTPP. The following major changes were noted.

- * The $C_{\beta}-C_{\beta}$ stretching modes ν_2 and ν_{11} shift to lower frequency.
- * The oxidation state marker band ν_4 slightly shifts to higher frequency.
- * ν_1 mode ($\delta_{C_m-C_{\phi}}$) shifts to higher frequency.
- * The phenyl mode, ν_{ϕ} , experiences a small shift to higher frequency ($\sim 6-8 \text{ cm}^{-1}$).

The spectra of radical cations are much weaker than those given by the neutral porphyrin (Figs. 6.3 and 6.4). The following changes were noted by comparison of neutral derivatives with those of corresponding π -cation radicals :

- * ν_2 and ν_4 modes shift to lower frequency and the magnitude of shifts vary from $10-30 \text{ cm}^{-1}$.
- * ν_1 shifts to the higher frequency ($\approx 10 \text{ cm}^{-1}$) while ν_9 to lower frequency ($\approx 7 \text{ cm}^{-1}$).
- * The relative intensities of the Raman bands also change; for e.g., the ν_{ϕ} gains intensity while ν_2 and ν_4 modes lose intensity.

The results mentioned above explain that the deformation in porphyrin skeleton affects the delocalisation of π electrons of porphyrin ring resulting in changes in the force constants of

porphyrin ring as well as peripheral substituent modes in neutral and cation radicals. In addition to this, the shifts of ν_2 and ν_4 in cation radicals reflect the A_{2u} nature of radical for these porphyrins.

6.4.4 EPR SPECTRA

The oxidised products of copper(II) porphyrins studied here were found to be EPR silent in solid state and in chloroform : toluene (1:1) solvent mixture over a temperature range 300-77 K. The lack of an EPR signal has also been observed in CuOEC^+ and CuTPP^+ ⁴⁴ which has been interpreted in terms of an aggregation effect resulting in intermolecular π - π spin coupling in the former and line broadening due to triplet ground state ($s = 1$) in the latter respectively. Aggregation effect is ruled out in the present study due to presence of bridging chains across the porphyrin periphery which prevents dimer formation and magnetic susceptibility measurements ruled out the possibility of triplet ground state. The diamagnetism observed here may be due to intramolecular d- π coupling as supported by variable temperature magnetic susceptibility measurements.

6.4.5 MAGNETIC MEASUREMENTS

Solution magnetic measurements on various oxidised copper(II) porphyrins were performed by the NMR (Evan's) method in CD_2Cl_2 and on powder sample by variable temperature magnetic susceptibility measurements over a temperature range 300-80 K. Measurements were made in CD_2Cl_2 on four separate preparations of each sample. The measurements indicate a small magnetic moment $\sim 0.235 \mu_B$ in all

samples. This value may be contrasted with $2.4 \mu_B$ measured for $\text{CuTPP}^{\cdot+}$ ⁴⁴ and $2.9 \mu_B$ for $\text{CuTMP}^{\cdot+}$ ⁵¹ in CD_2Cl_2 at 300K (table 6.3). Magnetic susceptibility measurements (Faraday method) on the powder samples showed normal temperature independent diamagnetism over the temperature range 300-80K. The diamagnetism

Table 6.3 : Magnetic moment data of various copper(II) porphyrin cation radicals

PORPHYRIN	$\mu_{\text{eff}}(\text{CD}_2\text{Cl}_2)$		$\mu_{\text{eff}}(\text{solid})$		Ref
	μ_B	Nature of coupling	μ_B	Nature of coupling	
$(\text{CuTPP})^{\cdot+}$	2.4	Independent spins	0	Antiferromagnetic	37
$(\text{CuTMP})^{\cdot+}$	2.9	Ferromagnetic	2.9	Ferromagnetic	51
$(\text{CuBHP})^{\cdot+}$	~0.235	Antiferromagnetic	0	Antiferromagnetic	This work

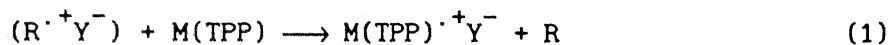
observed for all $(\text{Cu(II) BHP})^{\cdot+}$ studied here are due to d- π coupling of unpaired spins present on the metal centre and porphyrin ligand respectively.

6. 5 DISCUSSION

6.5.1 SYNTHESIS

Since the porphyrins studied here are highly deformed, simple electrochemical methods for the *insitu* generation of oxidised metalloporphyrins are not feasible due to highly unstable nature of porphyrin π -cation radicals in solution. Moreover, the isolation of analytically pure materials is difficult because of

the difficulty in removing large molar excess of electrolyte. Gans et.al.⁴² recently developed a clean and convenient synthetic method which lead to isolable crystalline solids of analytical purity. The idea employed here was to find a simple organic radical cation salt, $(R^{\cdot+})Y^-$, whose $R/R^{\cdot+}$ redox couple matched with that of the required metalloporphyrin redox reaction. A range of such redox reagents would represent the synthetic equivalent of controlled potential electrolysis. Ideally, a simple stoichiometric reaction (eq. 1) would occur.



The choice of $R^{\cdot+}$ should be such that the reduction potential, R is nonligating and noninterfering. R is usually phenoxathiin, thianthrene or tris (p-bromophenyl)amine, since their radical cations are readily synthesized and isolated as perchlorate, hexachloroantimonate or hexafluoroantimonate salts. They can be weighed out for stoichiometric use and moreover, since the cations $R^{\cdot+}$ are intensely blue but the neutral R is colourless, they are titrable and also they are nonligating. The $R/R^{\cdot+}$ redox potentials are all ca. 1.20 V relative to SCE. The oxidation potentials for CuHexyl I, CuPSI, CuPSIBr₈, CuMSICl₈ and CuMSIICl₈ are 0.81, 0.85, 0.74, 0.76 and 0.90 V respectively under the same conditions, so that both redox reagents are appropriately matched for both oxidations. The final choice of tris(p-bromophenyl) ammonium hexachloroantimonate for the oxidation of copper porphyrins was based on the ease with which crystalline, analytically pure product could be obtained. Dichloromethane was chosen as the solvent for these reactions since nucleophilic solvents react with both the $R^{\cdot+}$ reagents and the porphyrin

radical cation products. Analytically pure materials of oxidised copper porphyrin products were obtained by this methodology as confirmed by different spectroscopic techniques and magnetic susceptibility measurements.

6.5.2 ELECTRONIC SPECTRA

Electronic spectroscopy provides a ready means of identifying the site of oxidation : porphyrin centred versus metal centred. The observed broadened α , β region, a new band at lower energy and a dramatically broadened, low intensity blue shifted Soret band in oxidised species are characteristic features of porphyrin ring centred rather than metal^{132,133}. This is confirmed by absorption spectra of controlled potential electrolysis at porphyrin ring centred oxidation potential +0.96 V in CH_2Cl_2 matches exactly with the chemically oxidised species. It has been shown earlier in Chapter 4 that all the neutral copper porphyrins taken for study here are highly deformed as reflected by large red shifts with reduction in extinction coefficients compared to CuTPP and it is accounted in terms of destabilisation of HOMO resulting in reduction in energy gap between HOMO and LUMO. The magnitude of absorption shifts are related to amount of distortion which is maximum for CuMSiCl_8 due to short straps compared to CuHexyl I, CuPSI and CuPSiBr_8 . Upon abstraction of an electron, the magnitude of shifts in Q-bands as well as Soret band are maximum in these porphyrins compared to oxidised CuTPP and the maximum effects were seen for oxidised CuMSiCl_8 . Furthermore, a comparison of the absorption maxima of $\text{CuTPP}^{\cdot+}$ (630, 600 (sh), 408 nm) with the $\text{CuPSiBr}_8^{\cdot+}$, CuHexyl I $^{\cdot+}$, $\text{CuMSiCl}_8^{\cdot+}$ and $\text{CuPSI}^{\cdot+}$

suggests considerable (1370, 485, 238; 1254, 380, 119; 1608, 355; 1296, 273, 355 cm^{-1} respectively) red shifts of Q- and Soret bands in the basket handle porphyrin radical cations suggesting the retainment of deformation in oxidised basket handle porphyrins in solution. As noted earlier, an adjacent-trans-linked CuMSIICl_8 , which is less deformed compared to all cross-trans-linked copper porphyrins, upon oxidation exhibits less optical band shifts suggesting that the trend of deformation observed for neutral copper porphyrins are retained in their cation radicals.

Two π -cation radical types A_{1u} and A_{2u} have been characterized for metallo porphyrins by Dolphin and coworkers^{36a} (Fig. 6.5). Their numerous studies on electronic spectra of oxidised metalloporphyrins have led to the compilation of few empirical rules that help to distinguish between A_{1u} and A_{2u} type

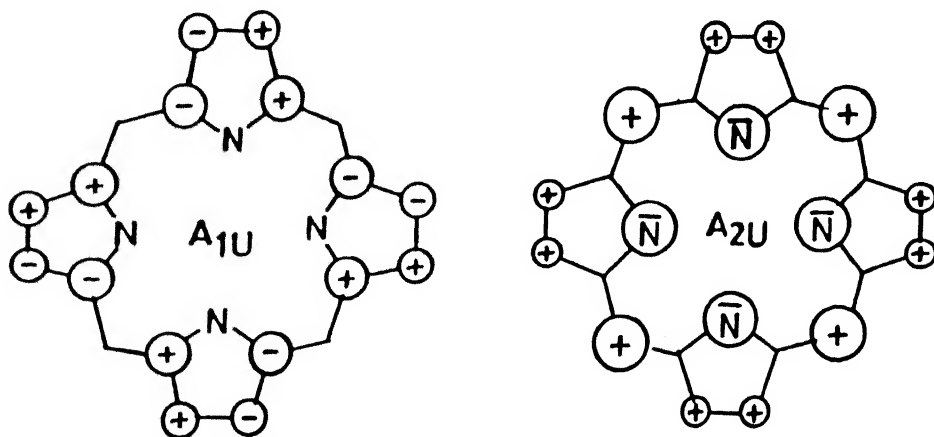


Fig. 6.5 : Molecular orbital diagram for the A_{1u} and A_{2u} orbitals of porphine. The atomic orbital coefficients are proportional to the size of the circles.

radicals. SCF-MO calculations on metalloporphyrins showed that the highest filled orbitals of porphyrin, A_{1u} and A_{2u} are almost degenerate in the unoxidised species and π -cation radicals produced by abstraction of electron from one of these orbitals would lead to either A_{1u} or A_{2u} ground state with an energy gap of 2000 to 3000 cm^{-1} . This small energy gap is very sensitive to the peripheral substituents on the porphyrin ring, the metal or its axial ligands. The electron density distribution varies in these two orbitals. The A_{1u} orbital is associated with high electron density on pyrrolic α - and β -carbons while meso carbons and pyrrolic nitrogens have high electron density in A_{2u} orbital (Fig. 6.5). The optical spectra of radical cations produced by abstraction of electron from any of these orbitals are different and can distinguish between these two types. The spectrum shown in Fig. 6.2 suggests that the radical cations described here have a hole in the A_{2u} orbital. This is not surprising since the ortho substituent on the meso phenyl ring should raise the energy of the A_{2u} orbital relative to A_{1u} via the interaction of the filled phenyl and porphyrin π -orbitals¹¹⁵.

6.5.3 INFRARED SPECTRA

A recent paper by Goff, Reed and coworkers⁴³ concluded that a characteristic infrared band in the 1270-1295 cm^{-1} can be used as a diagnostic tool for porphyrin ring oxidation in metallo tetraphenylporphyrins. Deuteration studies indicated that this particular mode is insensitive to phenyl deuteration but found to be sensitive to pyrrole deuteration suggesting that this new band arises from a strongly IR allowed porphyrin ring mode. The

oxidised derivatives of all copper basket handle porphyrins showed a strong IR band at $\sim 1290\text{ cm}^{-1}$ further confirming porphyrin ring oxidation.

6.5.4 RESONANCE RAMAN SPECTRA

Distortion of the porphyrin core is known to weaken the bonding in the macrocycle, thus lowering the frequencies of stretching vibrations of the core. The neutral copper basket handle porphyrins are highly deformed by covalent attachment of the short bridging chains across the porphyrin. Furthermore, because the chains are linked at the ortho-position of the meso phenyl rings, the dihedral angle between the phenyl rings and the porphyrin plane is reduced making the phenyl rings more coplanar with the porphyrin plane facilitating the delocalisation of electrons into the phenyl rings. This effect is clearly reflected in shifts of porphyrin skeletal modes ν_2 and ν_{11} to lower frequencies relative to planar CuTPP. The observed small ($5\text{--}7\text{ cm}^{-1}$) higher frequency shifts of phenyl mode (ν_ϕ) and $\delta_{\text{C}_m\text{--C}_\phi}$ (ν_1) mode in the neutral derivatives relative to CuTPP further reflects the strengthening of the C-C bond of meso phenyl rings as well as $\text{C}_m\text{--C}_\phi$ via the extended π -delocalisation.

Resonance Raman spectroscopy provides a promising tool for studying molecular and electronic structure in porphyrin radicals. The direction of the shifts of the porphyrin skeletal modes upon radical formation are suggested to be diagnostic of the predominant orbital character (A_{1u} and A_{2u})³⁸. As noted earlier, on the basis of SCF-MO calculations, the porphyrin radicals with

predominantly A_{2u} character have high electron densities located on the C_m and N atoms and this orbital is bonding with respect to the $C_\beta-C_\beta$ and $C_\alpha-C_m$ bonds while it is slightly antibonding with respect to $C_\alpha-N$ and $C_\alpha-C_\beta$ bonds. Removal of an electron should weaken $C_\beta-C_\beta$ and $C_\alpha-C_m$ bonds and decrease their frequencies while it should enhance the bonding character of the $C_\alpha-N$ bonds with concomitant increase in these frequencies (table 6.4). In case of A_{1u} type porphyrin radicals, the electron density is high on pyrrolic α - and β -carbons and this orbital is antibonding with respect to $C_\beta-C_\beta$ but bonding with respect to $C_\alpha-C_\beta$ bonds (table 6.4). Removal of an electron is expected to increase the $C_\beta-C_\beta$ bond strength and raise the stretching frequency whereas it lowers the $C_\alpha-C_\beta$ frequency.

Table 6.4 : Qualitative values of $\Delta\nu_{ox}$, the wave number shift due to porphyrin oxidation, for internal stretching coordinates of the metalloporphyrin.

Coordinate	Predicted	
	A_{1u}	A_{2u}
$\nu_{C_\alpha-C_m}$	negative	negative
$\nu_{C_\alpha-C_\beta}$	negative	positive
$\nu_{C_\alpha-N}$	negative	positive
$\nu_{C_\beta-C_\beta}$	positive	negative

In all the cation radicals studied here, the ν_2 mode, which involves $C_\beta-C_\beta$ stretching mainly and some contribution from $C_\alpha-C_m$,

shifts to lower frequency suggesting the abstraction of electron from an A_{2u} orbital since A_{2u} orbital is bonding with respect to these bonds as described above. The nature of the absorption spectra (Fig. 6.2) also supports this conclusion^{36a}. The 13 cm^{-1} shift of the ν_4 mode assigned to pyrrole symmetric half ring stretch to lower frequency is consistent with the observed $4\text{--}18\text{ cm}^{-1}$ lower frequency shifts for many MTPP radical cations having an A_{2u} ground state^{38e}. The large shift ($20\text{--}25\text{ cm}^{-1}$) to lower frequencies of ν_ϕ mode in cation radicals suggests the disruption in the delocalisation pathway^{38e}. The intensity increase in the phenyl modes in the π -cations is attributed to phenyl porphyrin mode mixing and it has been shown earlier that such mixing between ν_2 and ν_ϕ modes is possible due to the favourable orientation of the coordinates¹³⁴.

6.5.5' EPR SPECTRA

All the oxidised copper(II) basket handle porphyrins are EPR silent in solid phase and in dichloromethane:toluene mixture (1:1) over a temperature range $300\text{--}77\text{ K}$. The absence of EPR signal in these porphyrins may be because of any of the following reasons:

- * Aggregation resulting in intermolecular $\pi\text{--}\pi$ spin coupling.
- * Line broadening due to triplet ground state ($s = 1$).
- * Single electron localized on the porphyrin ring will couple via an exchange interaction with spin localised on the metal.

Aggregation is a common phenomenon observed in many metallo-porphyrin π -cation radicals⁴⁴⁻⁴⁸. The lack of the EPR signal in

$\text{CuOEC}^{\cdot+}$ ⁴⁴ was explained on the basis of intermolecular spin-spin coupling only. This type of aggregation is not possible for the copper(II) basket handle porphyrins due to the presence of short straps across the porphyrin. Since one strap is above and the other strap is below, the dimerization is completely prevented. Hence, the intermolecular π - π spin coupling reasoning for absence of ESR signal is ruled out. The presence of triplet ground state ($s = 1$) is not true for these porphyrins as confirmed by magnetic susceptibility measurements which showed normal temperature independent diamagnetism over the temperature range 300-80 K. This proves that the lack of EPR signal here is due to coupling of single electron localised on the porphyrin with spin localised on the metal via an exchange interaction.

6.5.6 MAGNETIC MEASUREMENTS

When $s = 1/2$ porphyrin radical moiety is coordinated to $s = 1/2$ copper(II) center, there are three possible descriptions of the overall spin state : (a) Antiferromagnetic coupling of unpaired electrons give $s = 0$ diamagnetic state. (b) Ferromagnetic coupling of unpaired spins with spin only magnetic moment $\mu_s = 2.83 \mu_B$ results in $s = 1$ state. (c) Noninteracting spins with $\mu_s = 2.45 \mu_B$ give independent $s = 1/2$ and $s = 1/2$ states. The planarity versus ruffling of metalloporphyrin cation radical species has been judged to be important in determining spin state. The generalisation is that in planar environment of such symmetry, $\text{Cu}^{\text{II}}(\text{porph})^{\cdot+}$ would have orthogonal metal ($d_{x^2-y^2}$) and ligand (A_{1u} or A_{2u}) magnetic orbitals and is expected to show a ferromagnetic coupling with $s = 1$ (i.e. triplet) ground state. On the other

hand, the loss of D_{4h} symmetry by ruffling of the porphyrin ring destroys the orthogonality of the ligand A_u and metal $d_{x^2-y^2}$ magnetic orbitals, thereby providing an overlap pathway for antiferromagnetic coupling with $s = 0$ (i.e., singlet) ground state. Thus, it is quite possible that by a fortuitous accident the distortion is just enough to balance the opposing effects of antiferromagnetism and ferromagnetism and essentially noninteracting system results.

Previous magnetic studies on $\text{CuTPP}^{\cdot+}$ ⁴⁴ radical indicates that the radical cation is completely diamagnetic in solid state and paramagnetic ($s = 1$) in solution. The diamagnetism in solid state was explained on the basis of X-ray crystal structure of the radical cation. An important factor of the solid state structure is the appearance of tightly associated pairs of cations with a Cu-Cu separation of 5.43 \AA (Fig. 6.6). Furthermore,

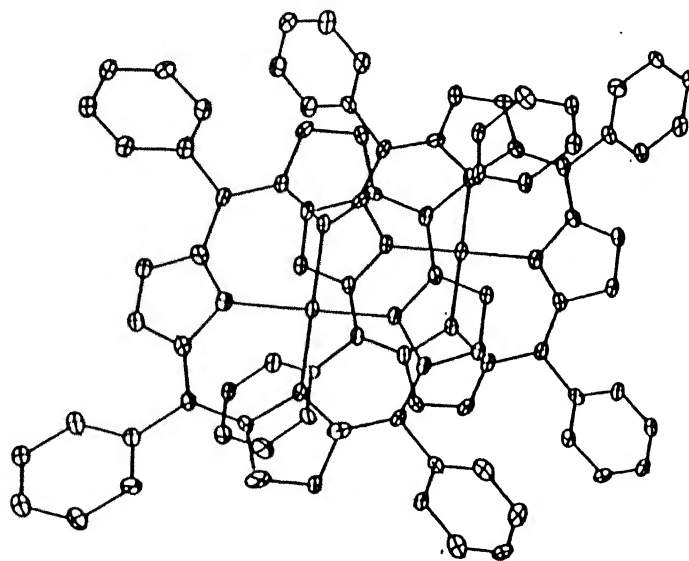


Fig. 6.6 : View of the solid state interaction between two $[\text{CuTPP}^{\cdot}]^+$ ions. The lower (left-hand) ion is drawn such that its mean plane is parallel to the plane of the paper; the centrosymmetric relationship between the two ions ensures that the upper mean plane core is

because of the ruffled core the orthogonality of the ligand A_u and metal $d_{x^2-y^2}$ magnetic orbitals are destroyed providing a pathway for intermolecular $d-\pi$ coupling within each $\text{CuTPP}^{\cdot+}$ molecule accounting for observed diamagnetism. In solution, however, it was assumed that the $\text{CuTPP}^{\cdot+}$ is monomeric with planar core where strict orthogonality of magnetic orbitals prevents the $d-\pi$ coupling giving rise to the paramagnetic state. The X-ray crystal structure of $[\text{CuTMP}^{\cdot}][\text{SbCl}_6]^{49}$ which is monomeric and planar, is in accordance with this argument. In this, the ortho-methyl substituent on the TMP ligand were expected to provide adequately bulky peripheral substituents to prevent saddle conformation arising out of $\pi-\pi$ type of solid state aggregation. The magnetic moment of $[\text{CuTMP}^{\cdot}][\text{SbCl}_6]$ ($\mu_{\text{eff}} = 2.9 \mu_B$) is consistent with the conclusion of strong intramolecular ferromagnetic coupling and is rationalised by orthogonality of the copper and ring magnetic orbitals.

However, for the porphyrins described here, dimer formation is completely ruled out because of the bridging chain above and below the porphyrin plane. Thus, the observed diamagnetism has to be explained in terms of the deformation of the porphyrin core caused by attachment of short bridging chain. This deformation can be compared to the so called ruffling of the porphyrin core in which opposite pyrrole rings are alternately displaced up and down relative to the mean plane. The calculated structures described in Chapter 3 clearly display this ruffling. The effect of this ruffling is to remove the orthogonality between the metal $d_{x^2-y^2}$ orbital and the porphyrin $A_{2u}(\pi)$ orbital allowing intramolecular

d- π coupling necessary for antiferromagnetic exchange. Furthermore, the observed diamagnetism in solution also should be attributed to antiferromagnetic coupling unlike $\text{CuTPP}^{\cdot+}$. This is possible only when the ruffling is retained in solution since it is well established that the planar porphyrin cores leads to ferromagnetic coupling. This clearly suggests that the bridging chain across the porphyrin periphery prevents the flexibility of the molecule to interconvert between the ruffled to planar core on going from solid state to solution phase as observed for $\text{CuTPP}^{\cdot+}$.

SECTION B

Π -CATION RADICALS OF HIGH SPIN IRON(III) DERIVATIVES OF BASKET HANDLE PORPHYRINS

6.6 EXPERIMENTAL

The synthesis of neutral high spin iron(III) porphyrins are described in chapter 4.

6.6.1 SYNTHESIS OF $[\text{FeMSIICl}][\text{SbCl}_6]$

A solution of FeMSIICl (0.010 g, 0.0102 mmol) in dichloromethane was stirred under argon for five minutes. 1.1 equivalent of tris (p-bromophenyl) ammonium hexachloro antimonate (0.0092g, 0.0113 mmol) dissolved separately in dry CH_2Cl_2 was added slowly to the porphyrin solution. A light greenish colour which developed at initial stages of addition disappeared upon progress of the reaction. Stirring was continued under argon for a further period of 3 h. Completion of the reaction was monitored by absorption spectrum. The reaction mixture was filtered and the

solvent was concentrated to minimum amount under vacuum and the product was precipitated with hexane. The compound was filtered and washed several times with hexane and recrystallised from chloroform-hexane. The dark black crystals were dried and stored in vacuum (0.006 g, 45%).

Anal. Calcd. for $C_{60}H_{40}FeCl_7N_4O_4Sb$: C, 54.99%; H, 3.08%; N, 4.27%

Found : C, 54.23%; H, 3.10%; N, 4.36%

Similar procedure was used for the synthesis of other oxidised high spin iron(III) derivatives of basket handle porphyrins.

6.6.2 $[FeMSIIICl][SbCl_6]$

Anal. Calcd. for $C_{60}H_{40}N_4O_4FeCl_7Sb$: C, 54.99%; H, 3.08%; N, 4.27%

Found : C, 55.05%; H, 3.01%; N, 4.21%

6.6.3 $[FePIICl][SbCl_6]$

Anal. Calcd. for $C_{54}H_{44}N_4O_4FeCl_7Sb$: C, 52.34%; H, 3.58%; N, 4.52%

Found : C, 52.23%; H, 3.42%; N, 4.41%

6.6.4 $[FeMSIIICl_9][SbCl_6]$

Anal. Calcd. for $C_{60}H_{32}N_4O_4FeCl_{15}Sb$: C, 45.54%; H, 2.04%; N, 3.54%

Found : C, 45.62%; H, 2.13%; N, 3.63%

6.7 RESULTS

6.7.1 ELECTRONIC SPECTRA

A comparison of optical spectra of $FeMSIIICl$ and its cation radical in CH_2Cl_2 is shown in Fig. 6.7 and the data for all high spin iron(III) derivatives and their cation radicals is tabulated in table 6.5. A closer look of the data given in the table 6.5 reveals the following :

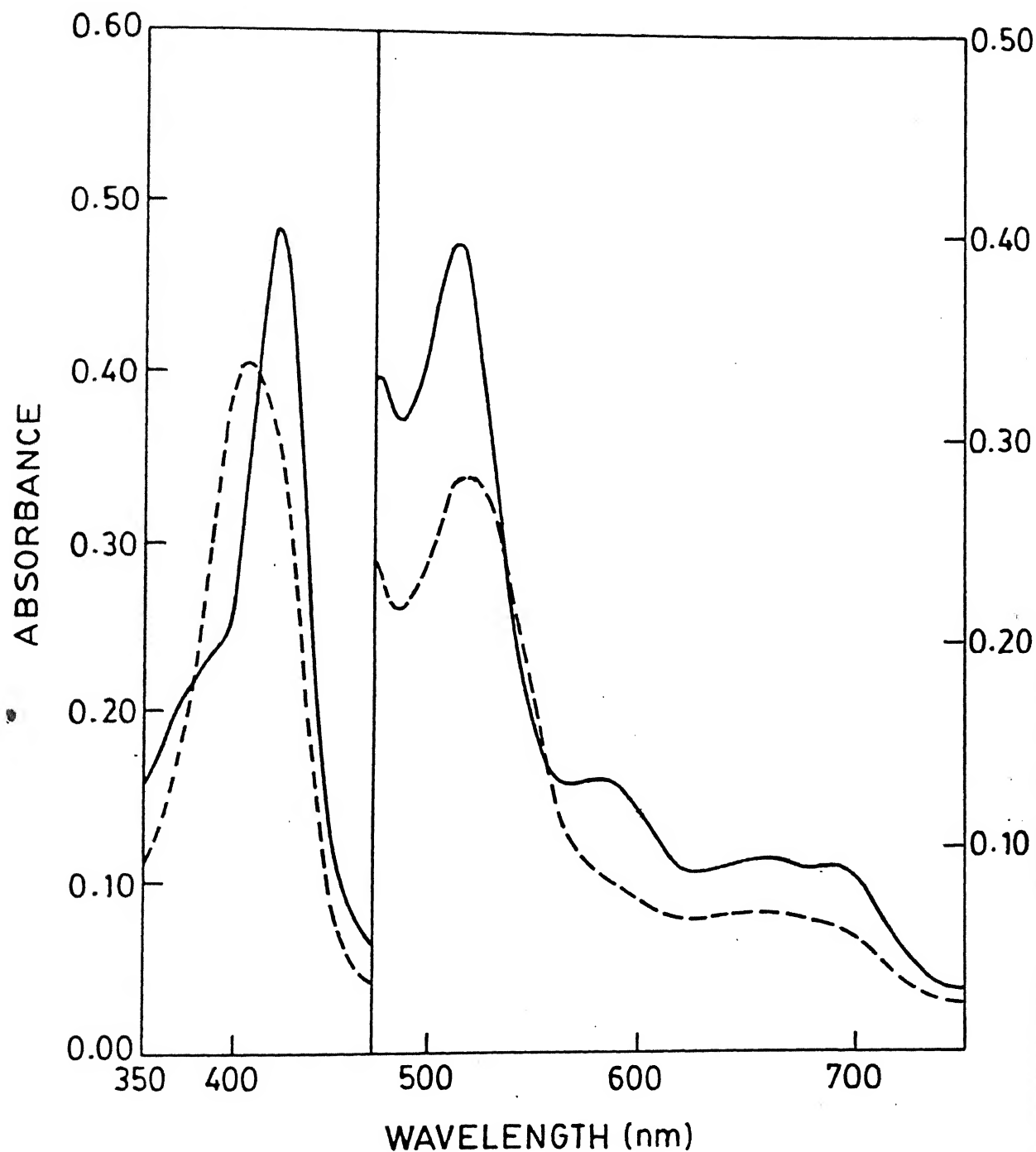


Fig. 6.7 : Comparison of the optical absorption spectra of FeMSIIICl (—) and its cation radical (....) in dichloromethane. The concentrations used were $\approx 2 \times 10^{-5}$ mol dm $^{-3}$ for Q-bands and $\approx 2 \times 10^{-6}$ mol dm $^{-3}$ for Soret.

- * The absorption maxima of neutral iron(III) basket handle porphyrins are red shifted relative to FeTPPCl and
- * Upon oxidation, the Soret band shifts to blue (8-10 nm) with reduction in intensity and broadening with only small perturbations in the Q-bands.

Table 6.5 : Electronic spectral data of various deformed iron(III) porphyrins and their cation radicals in CH_2Cl_2 .

PORPHYRIN	Soret band B (0,0) $\lambda_{\text{max}}/\text{nm}$ ($10^{-4} \epsilon/\text{dm}^3$ $\text{mol}^{-1} \text{cm}^{-1}$)	Q-bands $\lambda_{\text{max}}/\text{nm}$ ($10^{-3} \epsilon/\text{dm}^3 \text{mol}^{-1} \text{cm}^{-1}$)			
		I	II [†]	III [†]	IV [†]
FeTPPCl	417(110)	511(13.4)	577(13.3)	658(2.8)	690(3.2)
[FeTPPCl ^{•+}][SbCl ₆]	387	533	615	-	750
FeMSIICl	420(58.9)	513(7.24)	583(2.02)	656(1.51)	701(1.32)
[FeMSIICl ^{•+}][SbCl ₆]	408(36.9)	520(4.83)	586(1.68)	658(1.09)	698(0.82)
FeMSIIICl	423(54.3)	511(8.34)	589(2.50)	657(1.68)	698(1.57)
[FeMSIIICl ^{•+}][SbCl ₆]	412(38.3)	521(4.99)	590(1.49)	661(1.19)	694(0.95)
FePIICl	420(70.5)	512(11.03)	586(3.39)	656(2.30)	698(2.36)
[FePIICl ^{•+}][SbCl ₆]	414(43.8)	515(11.02)	-	-	703(2.19)
FeMSIIICl ₉	420	511	589	656	697
[FeMSIIICl ₉ ^{•+}][SbCl ₆]	412	515	589	-	702

† - shoulder peaks

The absorption shifts indicate that the amount of distortion present in these adjacent-trans and adjacent -cis-linked metallo porphyrins and their cation radicals are less compared to

cross-tans-linked metalloporphyrins and their cation radicals studied in the previous section.

6.7.2 INFRARED SPECTROSCOPY

The confirmation for the ring oxidation rather than iron(III) came from infrared spectroscopy⁴³. The IR spectra of all the oxidised species in KBr pellet showed the diagnostic band in the region $1280-1290\text{ cm}^{-1}$ characteristic of oxidation of the porphyrin ring.

6.7.3 MAGNETIC MEASUREMENTS

Magnetic moment measurements were done in both solid phase and CD_2Cl_2 solution. Fig. 6.8 shows the Curie and magnetic moment plot versus temperature for $[\text{FeMSII}'][\text{SbCl}_6]$ in the accessible temperature range 300-80 K. The solid line represents a linear least square fit. The measured magnetic moment vary from 4.9 to $5.1\ \mu_B$ for various oxidised iron porphyrins (table 6.6) at 300 K

Table 6.6 Magnetic moment data for various iron(III) deformed porphyrin cation radicals

Compound	μ_{eff} (300K) in CD_2Cl_2 (μ_B)	μ_{eff} (80K) (Solid) (μ_B)	μ_{eff} (300K) (Solid) (μ_B)	$\theta(\text{K})$
$[\text{FeTPPCl}'][\text{SbCl}_6]$	6.1	-	4.8	-7.5
$[\text{Fe}(\text{OClO}_3)_2][\text{SbCl}_6]$	6.9	-	6.9	-
$[\text{FeMSIICl}'][\text{SbCl}_6]$	4.8	4.84	5.1	-18.9
$[\text{FeMSIIICl}'][\text{SbCl}_6]$	4.9	4.78	4.9	-19.8
$[\text{FePIICl}'][\text{SbCl}_6]$	4.9	4.82	5.1	-19.6
$[\text{FeMSIIICl}_9'][\text{SbCl}_6]$	5.0	4.80	5.1	-20.2

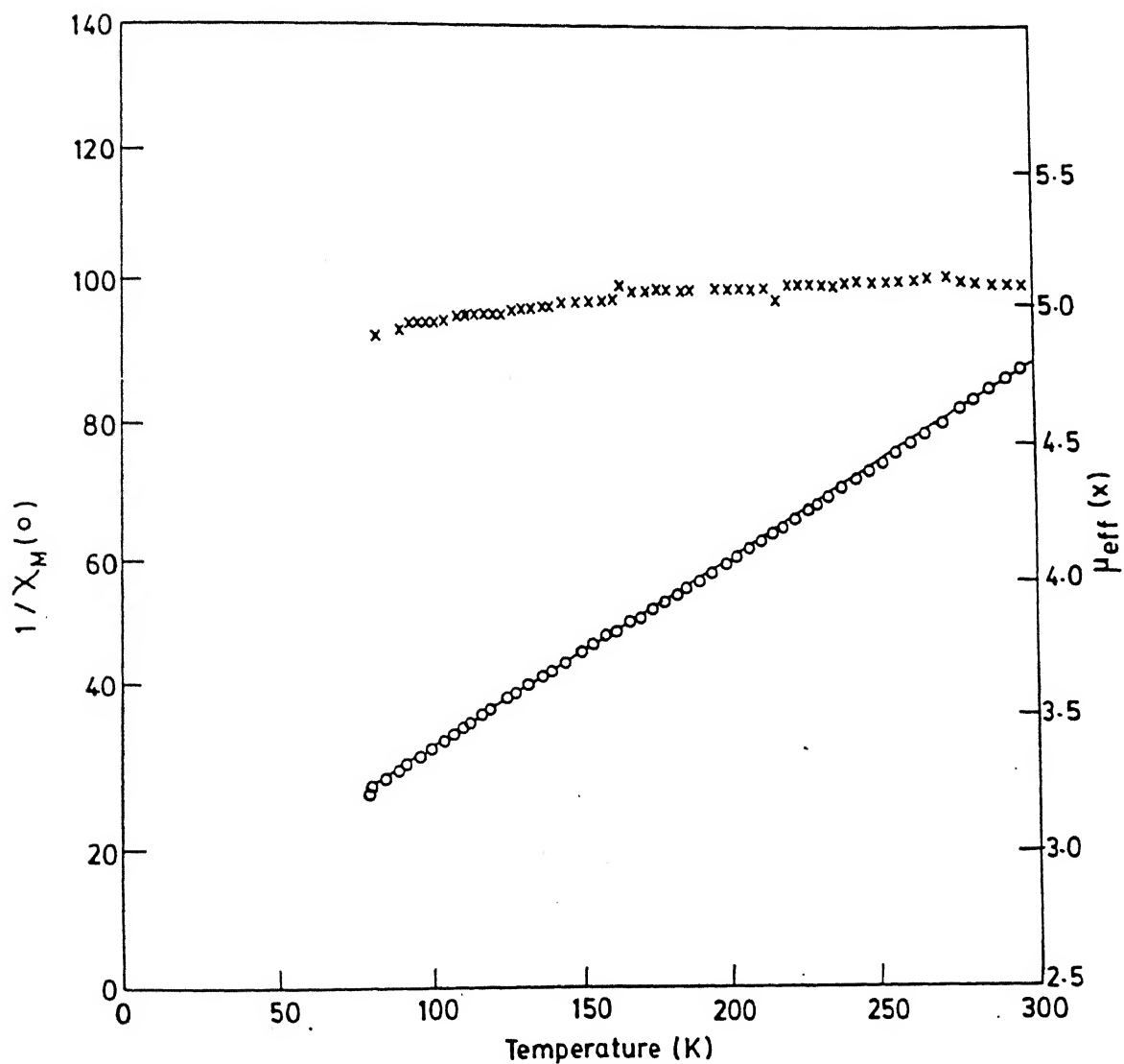


Fig. 6.8 : Curie plot (o) of the reciprocal molar susceptibility and μ_{eff} (x) vs. temperature for $[\text{FeMSIIICl}'] [\text{SbCl}_6]$.

both in solid phase and CD_2Cl_2 solution. Theoretically calculated magnetic moment for high spin iron(III) with $s = 5/2$ and the porphyrin radical with $s = 1/2$ are given in table 6.7. Thus, the measured magnetic moment imply an antiferromagnetic coupling

between the metal and porphyrin ring electrons to give an overall $s = 2$ state for all the iron porphyrin cation radicals.

Table 6.7 : Expected magnetic moment for various types of coupling in high spin iron(III) porphyrin cation radicals.

Type of coupling	Expected Magnetic moment μ_B
Independent spin	6.16
Ferromagnetic	6.93
Antiferromagnetic	4.89

6.7.4 ^1H NMR SPECTRA

^1H NMR spectroscopy probe the environment of protons at the extreme periphery of the ligand. The chemical shifts of these protons are strongly influenced by the spin state of the metal atom.

Table 6.8 : ^1H NMR data of various high spin iron(III) porphyrins and their cation radicals in CDCl_3 .

PORPHYRIN	Pyrrole	Ortho	meta	para	$-\text{CH}_2-$	Nature of coupling
FeClTPP	79.4	8.0, 5.0	13.3, 12.2	6.35		
$[\text{FeClTPP}^+][\text{SbCl}_6^-]$	68.8	42.2	-12.3	35		Anti-ferro-magnetic
$[\text{Fe}(\text{OCIO}_3)_2(\text{TPP})]$	31.1	-19.3	35.0	-13.2		Ferro-magnetic
FePIICl	78.5	6.67	15.3, 12.7	4.67	-4.5	-
$[\text{FePIICl}^+][\text{SbCl}_6^-]$	69	46	-14.0	26.2	-3.66	Anti-ferro-magnetic

Preliminary ^1H NMR studies were carried out on FePIICl and its cation radical to understand the nature of the coupling between the high spin iron(III) with $s = 5/2$ and porphyrin cation radical with $s = 1/2$. The resonances are tabulated in table 6.8. Since the cation radicals studied here are of A_{2u} type which exhibit large unpaired spin density at the meso carbon position and as a consequence, phenyl proton NMR signals are shifted to extreme upfield and downfield positions. The pyrrole region of the ^1H NMR spectra of FePIICl and its cation radical unlike FeTPPCl and its radical showed the multiplet structure due to the inequivalence of pyrrole protons thus revealing the presence of deformation in solution in both neutral and oxidised species. The large downfield shift of pyrrole protons is indicative of one electron occupancy of the $d_{x^2-y^2}$ orbital.

Extensive studies on neutral high spin iron(III) porphyrins and their cation radicals^{40d,42,47,52} have led to two major generalizations for oxidised iron(III) porphyrins. Firstly, there are large paramagnetic shifts of the phenyl protons in π -cation radical complexes. Downfield ortho and para resonances and upfield meta resonances may be a general signature of antiferromagnetic coupling whereas ferromagnetic coupling with metal spin gives rise to upfield ortho, para resonances and downfield meta resonances in metallo TPP cation radicals. Thus the direction and magnitude of shifts of the pyrrole, ortho, meta and para phenyl protons in $[\text{FePIICl}'][\text{SbCl}_6]$ relative to FePIICl is consistent with the antiferromagnetic coupling observed for five coordinate, high spin Fe(III) porphyrin cation radicals.

6.8 DISCUSSION

6.8.1 SYNTHESIS

The oxidation of (chloro)(porphyrinato) iron(III) with tris (P-bromophenyl) ammonium hexachloroantimonate in CH_2Cl_2 afforded a black crystalline radical cation which by elemental analysis was shown to have a composition of $[\text{Fe}(\text{BHPCl}')][\text{SbCl}_6]$. Same tris(P-bromophenyl) ammonium hexachloroantimonate was used as oxidant for oxidation of all iron(III) porphyrins studied here for the advantages described in the previous section for the oxidation of copper(II) porphyrins. The first ring oxidation in cyclic voltammetry occurs at 1.02, 1.04 and 1.05 V for FeMSIICl , FeMSIICl and FePIICl in CH_2Cl_2 respectively. The oxidant, $\text{R/R}^{\cdot+}$ redox potential in CH_2Cl_2 is Ca. 1.20 V relative to SCE which conveniently put it just above all $\text{Fe}(\text{Cl})(\text{BHP})/\text{Fe}(\text{Cl})(\text{BHP})^{\cdot+}$ potentials indicating that they are appropriately matched for oxidation reactions. The elemental, spectroscopic and magnetic susceptibility measurements confirm the purity of all oxidised porphyrins synthesized by following this methodology.

6.8.2 ELECTRONIC SPECTRA

Electronic spectra of all the oxidised iron(III) basket handle porphyrins is similar to those of other iron(III) porphyrin cation radicals described in the literature^{40c,42,47} displaying broad Q-bands with reduction in intensity and blue shift, broad with decrease in extinction coefficients of Soret band confirming the oxidation of the ring. An additional evidence came from the oxidation of iron(III) basket handle porphyrins at the first cyclic voltammetric wave which can be compared favourably with

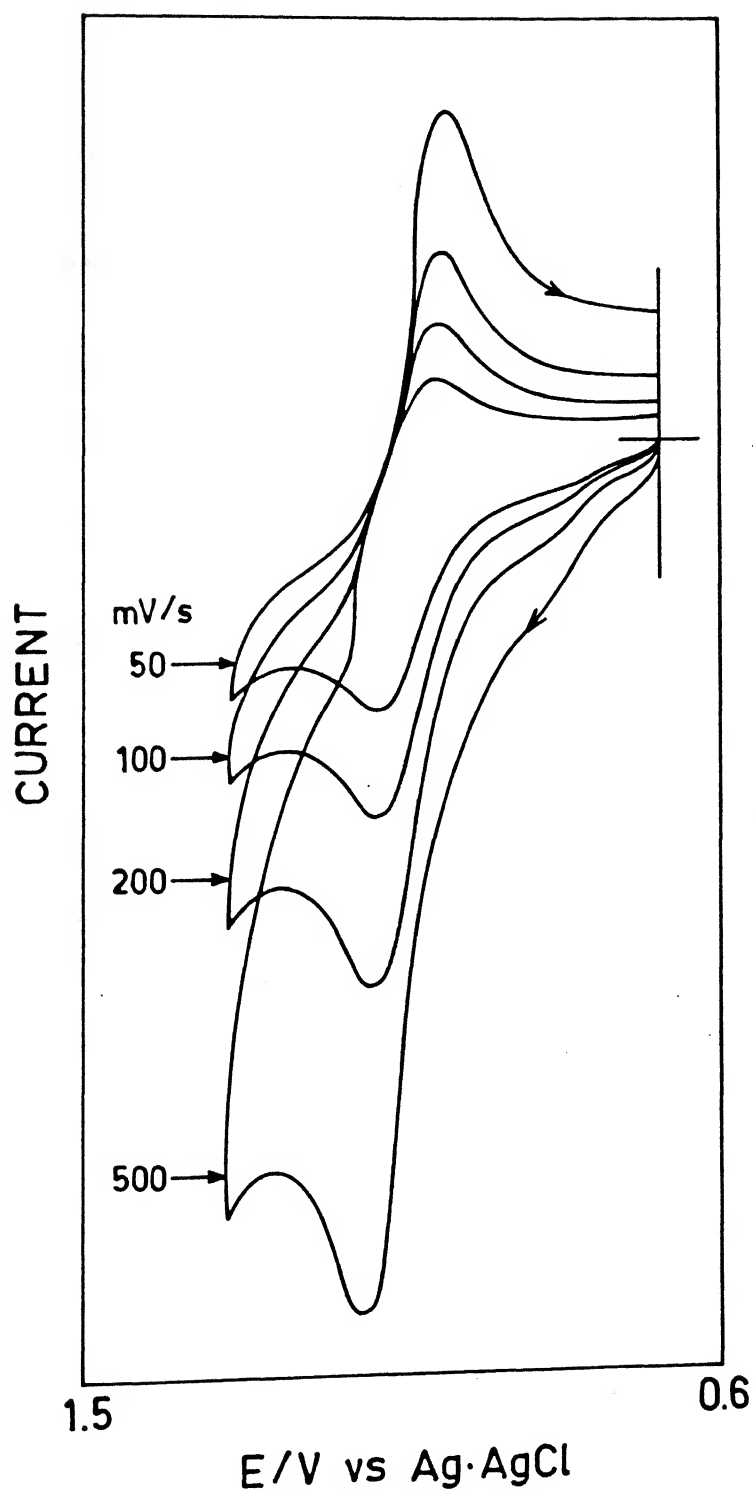


Fig. 6.9 : Cyclic voltammograms of FeMSIIICl in dichloromethane at different Scan rates. The concentration used was $6 \times 10^{-3} \text{ mol dm}^{-3}$. The potentials are versus Ag/AgCl with TBAP as the supporting electrolyte.

1.10 ± 0.01 V observed for a series of TPPFeX compounds for the ring oxidation. The reversibility of the first ring oxidation as shown in Fig. 6.9 for FeMSIICl is observed for all other Fe(III) basket handle porphyrins at scan rates ranging from 50 to 500 mV/sec. This reversibility nature of the couple over a range of scan rates suggests that coordination number of the parent iron(III) and oxidised iron(III) porphyrin species must be the same.

The optical red shifts of both Soret ($171\text{--}340\text{ cm}^{-1}$) and Q-band ($76\text{--}354\text{ cm}^{-1}$) of FePIICl, FeMSIICl, FeMSIICl and FeMSIICl₉ relative to FeTPPCl (table 6.5) are consonant with the distortion of the porphyrin macrocycle.

Furthermore, the absorption shifts also indicate the amount of distortion present in these adjacent -trans and adjacent -cis-linked isomers of iron(III) derivatives and their cation radicals are less compared to cross-trans-linked copper(II) porphyrins and their cation radicals studied in the previous section.

6.8.3 MAGNETIC MEASUREMENTS

When $s = 1/2$ porphyrin radical moiety is coordinated to $s = 5/2$ high spin iron(III) center there are three possible descriptions of the overall spin state. Firstly, antiferromagnetic coupling would lead to an $s = 2$ ground state. If the magnitude of coupling constant ($-2J$) is several hundred wave numbers, then there would be no population of the higher multiplicity $s = 3$ state at room temperature. Simple Curie-Weiss law magnetic data consistent with four unpaired electrons (spin

only $\mu_{\text{eff}}^{300\text{K}} = 4.9 \mu_B$) would be expected. Secondly, ferromagnetic coupling would lead to an $s = 3$ ground state. A spin only magnetic moment of $6.9 \mu_B$ would be expected if the magnitude of coupling constant ($+2J$) is very large. Smaller values of $2J$ would lead to thermal population of the lower multiplicity $s = 2$ state at higher temperatures, and hence lower magnetic moments and curvature of the Curie plot would result. Thirdly, if the iron spin was noninteracting with the porphyrin spin, then the $s = 5/2$, $s = 1/2$ spin systems would be expected to show magnetic moments given by the square root of the sum of the squares of the individual moments. The spin only value at 25°C would be $6.17 \mu_B$.

Reed and coworkers⁴⁷ from an elegant study on the π -cation radicals of $[\text{FeTPPCl}'][\text{SbCl}_6]$ and $[\text{Fe}(\text{OCIO}_3)_2\text{TPP}]$ have related their contrasting behaviour to the structure of the porphyrin core. X-ray structures of $[\text{FeClTPP}]^{+\cdot}$ and $[\text{Fe}(\text{OCIO}_3)_2\text{TPP}]$ ⁴⁷ reveals that the former has a ruffled core while the latter has a planar or flat core with effective D_{4h} symmetry on the iron centre. Because the magnetic orbitals in metal $\left[d_{x^2-y^2} (B_{1g}), d_{z^2} (A_{1g}), d_{xz} (E_g), d_{yz} (E_g) \text{ and } d_{xy} (B_{2g}) \right]$ and the half filled porphyrin ring (A_{2u}) have different symmetry, strict orthogonality is maintained between these orbitals leading to the alignment of all the spins in a parallel position resulting in a lowest energy $s = 3$ state. However, if the core is ruffled, the D_{4h} symmetry at the iron center is lowered probably to C_{2v} reducing the symmetry of the iron d-orbitals to A_1, A_1, B_1, B_2 and A_2 and the half filled porphyrin A_{2u} orbital to A_1 . Thus, an overlap of A_1 orbital on metal and A_1 orbital of porphyrin results in pairing of

the electrons suggesting an $s = 2$ ground state. From this, a theory has been proposed that the presence of planar or flat core leads to a ferromagnetic coupling while that of ruffled core results in an antiferromagnetic coupling. The measured magnetic moments for the two radical species are in excellent agreement with this conclusion.

The magnetic moments measured for the radical species generated in the present study in solid phase and in CD_2Cl_2 solution (table 6.6) suggest an antiferromagnetic coupling between the iron and the porphyrin unpaired electrons. The calculated structures of adjacent-cis and adjacent-trans show clearly the enforced deformation of the porphyrin core due to the covalent attachment of short bridging groups. As described in Chapter 3, the porphyrin core in adjacent-cis isomer can be compared to the saddle conformation described by Scheidt in which the perpendicular displacement of pyrrole rings with respect to mean plane of the core are in the same direction and that of adjacent-trans isomer to the ruffled conformation where the pyrrole rings are displaced alternately above and below the mean plane of the core. Apparently, this type of deformed cores present in the iron porphyrins described here destroys the orthogonality between the d-orbitals of iron and the half filled porphyrin A_{2u} orbital allowing an intramolecular d- π coupling necessary for the antiferromagnetic exchange. It is pertinent to point out here that Goff and coworkers⁴⁰ on the basis of NMR and magnetic moment measurements concluded that the oxidised five coordinate Fe(III)TPPX complexes with weak axial ligands such as

ClO_4^- and SO_3CF_3^- retained the spin admixed $s = 5/2, 3/2$ configuration in solution. However, the similar magnitude of magnetic moment values in solid phase and in CD_2Cl_2 solution and larger value of θ ($\theta \approx -20\text{K}$ measured on extrapolation of the plot shown in Fig. 6.8) (table 6.6) relative to that of $[\text{FeClTPP}]^{\cdot+}$ ($\theta = -7.5\text{ K}$) leads us to rule out the possibility of presence of admixed spin configuration for the radical cations discussed here.

Furthermore, the observed antiferromagnetism in solution indicates the retainment of ruffled porphyrin core in solution since from above study it is clear that only ruffling core leads to antiferromagnetic exchange. This clearly suggests that the bridging chain prevents the flexibility of the molecule to interconvert between the deformed to planar core on going from solid state to solution state.

6.8.4 ^1H NMR SPECTRA

^1H NMR spectra of FePIICl and its one electron oxidised product showed multiplet structure for pyrrole protons suggesting the inequivalence of all pyrroles due to deformed porphyrin core present in these species. Furthermore, the data also gives clue about metal vs. ring centered oxidation since metal centred oxidation yielding an iron(IV) center would be associated with depopulation of the $d_{x^2-y^2}$ orbital and consequent upfield shifts of the pyrrole proton NMR signal is expected. From table 6.8 it is noted that the pyrrole proton resonance for FePIICl is at 78.5 ppm comparable to high spin FeClTPP (79.4 ppm). The pyrrole proton signal is shifted downfield as a consequence of predominant

σ spin delocalisation from the $d_{x^2-y^2}$ orbital. Thus, existence of iron(IV) in these species is ruled out.

Goff and coworkers⁴⁰ used ^1H NMR technique for understanding magnetic interactions in several oxidised iron porphyrins. Their extensive studies on ruffled $[\text{FeCl}(\text{TPP})]^{+\cdot}$ and planar $[\text{Fe}(\text{OCIO}_3)_2\text{TPP}]$ observed that the direction of ortho, para and meta protons is completely reversed between these two. The downfield ortho, para protons (42, 35 ppm) and upfield meta protons (-12 ppm) in $[\text{FeCl}(\text{TPP})]^{+\cdot}$ contrast sharply with the upfield ortho, para protons (-19, -13 ppm) and downfield meta protons (35 ppm) in $[\text{Fe}(\text{OCIO}_3)_2\text{TPP}]$. This feature was explained on the basis of spin flip in the porphyrin radical moiety. There is a different type of magnetic coupling in these two species; antiferromagnetic in $[\text{FeCl}(\text{TPP})]^{+\cdot}$ and ferromagnetic in $[\text{Fe}(\text{OCIO}_3)_2\text{TPP}]$. This means that the natural atom by atom alteration of spin inherent to a π -spin delocalisation mechanism is reversed on going from $[\text{FeCl}(\text{TPP})]^{+\cdot}$ to $[\text{Fe}(\text{OCIO}_3)_2\text{TPP}]$. In fact, it is apparent that all axially symmetric iron porphyrin radical cations show ferromagnetic coupling and unsymmetric iron porphyrins show antiferromagnetic coupling.

As noted earlier at different places, the porphyrins studied here are deformed and hence the metal and ligand orbitals won't be orthogonal, and antiferromagnetic coupling is expected. The direction and magnitude of shifts of the pyrrole, ortho, meta and para phenyl protons in $[\text{FePIICl}][\text{SbCl}_6]$ relative to FePIICl is consistent with the antiferromagnetic coupling observed for five coordinate, high spin iron(III) porphyrin cation radicals.

6.9 CONCLUSIONS

Following conclusions can be drawn based on present investigations :

- * The optical and resonance Raman spectral data suggests that the π -cation radicals of basket handle metalloporphyrins studied here are of A_{2u} type.
- * The degree of deformation present in the neutral metallo derivatives of basket handle porphyrins in solution is retained in their π -cation radicals.
- * π -cation radicals of Cu(II) and Fe(III) basket handle porphyrins are antiferromagnetically coupled due to the coupling of unpaired electrons in the metal and porphyrin ring facilitated through the deformation of the porphyrin core.
- * The diamagnetism observed for copper(II) basket handle porphyrins in CD_2Cl_2 is in contrast to the paramagnetic behaviour observed for other copper meso aryl porphyrin cation radicals. To the best of our knowledge this is the only report where diamagnetism has been observed in solution.
- * The present study substantiating the emerging generality between the structure of the macrocycle and the metal-ligand magnetic interactions in metallo basket handle porphyrin cation radical complexes that ruffled cores lead to antiferromagnetic coupling while the planar or flat core results in ferromagnetic coupling as proposed by Reed and coworkers. However, this study also reveals that the presence of ruffled cores need not necessarily lead to

dimerization of the porphyrin, a suggestion made by Reed and coworkers based on X-ray structures of many MTPP radical cations.

CHAPTER 7

DIMERIZATION EFFECTS ON SPECTROSCOPIC PROPERTIES OF WATER-SOLUBLE PORPHYRINS IN AQUEOUS AND MICELLAR MEDIA

7.1 INTRODUCTION

The importance of chlorophyll dimers has already been highlighted in Chapter 1 and present chapter describes our studies on aggregation behaviour of water-soluble porphyrins.

Previous investigations have been concerned with concentration dimers¹³⁵⁻¹³⁸ by spontaneous aggregation of porphyrins and phthalocyanins and covalently linked systems¹³⁹⁻¹⁴¹. The latter have an advantage that the dimer geometry is fairly well defined due to the constraints imposed by the linking groups. This offers an opportunity to study the relationship between structure and spectroscopic properties. However, it is well known that there is no covalent linkage between two chlorophyll molecules in bacteriochlorophyll dimer and also it is evident that the relationship of structure and

spectroscopic properties can be affected by covalent links. For instance, the links can modify the geometry of the tetrapyrrole cores. Also, functional groups in the links may interact with the rings. In both cases, the electronic structure of the ring systems will be modified. The effect may become more pronounced as the chainlength of the bridges is reduced. For this reason, it is also of interest to study dimers without covalent links. Tetracrowned porphyrins and phthalocyanins¹⁴²⁻¹⁴⁷ and water-soluble porphyrins¹⁴⁸ are suitable for concentration dimers study. Addition of alkali metal ions promotes dimerization in these systems.

7.2 WORK DONE IN THE PRESENT STUDY

The present study has been carried out keeping following points in mind :

- * The presence of different metal ions in the porphyrin cavity.
- * The presence of different crown ethers of variable cavity size.
- * The presence of organized media on the monomer and dimer equilibrium.

Two water-soluble porphyrins, 5,10,15,20-tetrakis (4-carboxy phenyl) porphyrin (H_2tCPP^{4-}) and 5,10,15-20-tetrakis (4-sulfonato phenyl) porphyrin (H_2tPPS^{4-}) and divalent metal derivatives (Cu^{2+} , Ni^{2+} and Zn^{2+}) (Fig. 7.1) have been chosen to study the dimerisation equilibrium. The crown ethers used were 1,4,7,10,13,16-hexaoxacyclooctadecane (18-crown-6), 1,4,7,10,13-pentaoxacyclooctadecane (15-crown-5) and 1,4,7,10-tetraoxacyclododecane (12-crown-4) and the surfactants chosen were anionic sodium dodecyl sulfate (SDS).

Cationic cetyltrimethylammonium bromide $[\text{NMe}_3(\text{C}_{16}\text{H}_{33})\text{Br}]$ and neutral Triton X-100 (TX-100). Results and discussion are given in the following sections.

7.3 RESULTS

7.3.1 ELECTRONIC SPECTRA

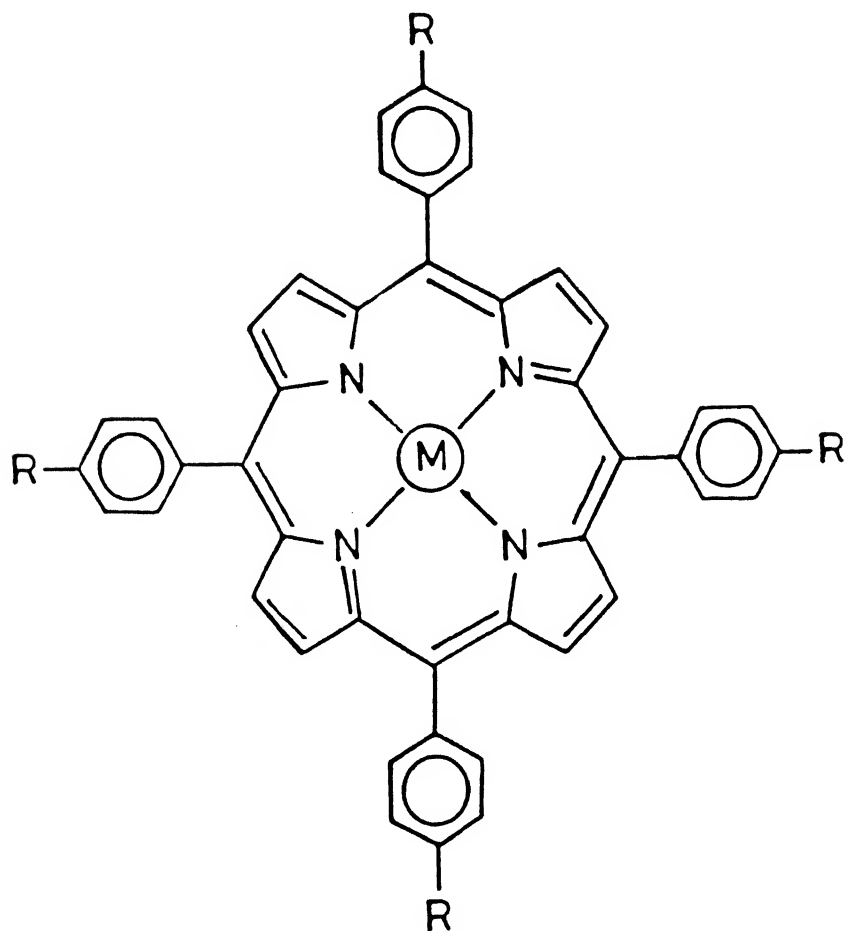
The absorption spectra of $\text{H}_2\text{tCPP}^{4-}$ in the presence of fixed concentration of 18-crown-6 and increasing amounts of K^+ in aqueous medium are shown in Fig. 7.2 and the data is presented in tables 7.1 and 7.2. The dimerization resulted in the following major changes :

- * Reduction in absorbance and broadening of all Q-bands.
- * A red shift of Q-bands with well defined isosbestic points. The magnitude of the intensity decrease and the red shift depends on the nature of cation and crown ether added.
- * No Soret band shift for free bases, blue shift for Cu^{2+} and Ni^{2+} derivatives and red shift for Zn^{2+} derivatives.
- * Dimerization is observed in only anionic micellar medium (SDS) and porphyrins remain monomeric in cationic (CTAB) as well as neutral (TX-100) micellar media.

7.3.2 EMISSION SPECTRA

The room temperature fluorescence spectrum of $\text{H}_2\text{tCPP}^{4-}$ in the presence and absence of 18-crown-6 and K^+ ions in aqueous and micellar media is shown in Fig. 7.3 and data is tabulated in table 7.3. The following changes were noted :

- * Red shift with reduction in intensity.
- * Magnitude of red shifts for Zn^{2+} derivatives is very less



(i) $R = \text{COO}^-$, $M = 2\text{H}$; H_2TCPP
 $M = \text{Zn}^{+2}$; ZnTCPP
 $M = \text{Cu}^{+2}$; CuTCPP
 $M = \text{Ni}^{+2}$; NiTCPP

(ii) $R = \text{SO}_3^-$, $M = 2\text{H}$; H_2TPPS
 $M = \text{Zn}^{+2}$; ZnTPPS
 $M = \text{Cu}^{+2}$; CuTPPS
 $M = \text{Ni}^{+2}$; NiTPPS

Fig. 7.1 : Molecular structures of various water-soluble porphyrin derivatives.

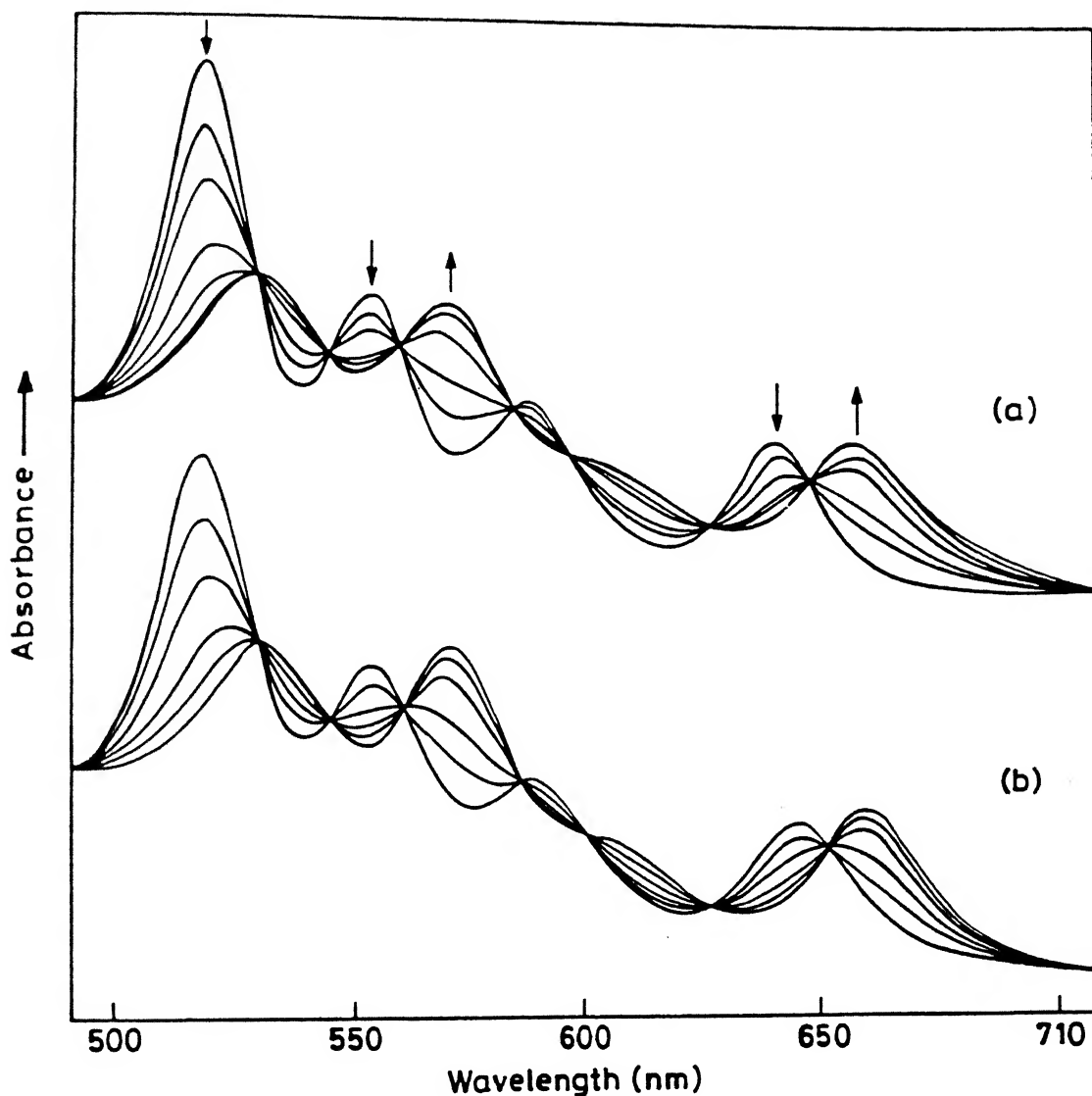


Fig. 7.2 : Visible absorption spectra of $\text{H}_2\text{tcp}^{4-}$ in aqueous medium under different conditions (a) Effect of addition of increasing amounts of K^+ ions on the absorption spectra of $\text{H}_2\text{tcp}^{4-}$ solution ($4.81 \times 10^{-5} \text{ mol dm}^{-3}$) containing (0.05 mol dm^{-3}) of 18C6 at 25°C in sds medium. The concentrations of K^+ are 4×10^{-3} , 9.3×10^{-3} , 2.3×10^{-2} , 6.3×10^{-2} , 1.7×10^{-1} and $1.9 \times 10^{-1} \text{ mol dm}^{-3}$. Arrows indicate the direction of spectroscopic change. (b) Effect of temperature on spectra of $\text{H}_2\text{tcp}^{4-}$ [$4.81 \times 10^{-5} \text{ mol dm}^{-3}$] containing (0.05 mol dm^{-3}) 18C6 and [$1.9 \times 10^{-1} \text{ mol dm}^{-3}$] K^+ ions. The temperatures are 10° , 20° , 30° , 40° , 50°

Table 7.1 : Dimerization induced absorption band red-shifts (nm)
for free base porphyrins in the presence of
cation-crown-ether complexes*

System	Medium	Q-bands			
		I	II	III	IV
$H_2tcpp^{4-} + 18\text{-crown-6} + K^+$	Aqueous	20	-	16	13
$H_2tcpp^{4-} + 18\text{-crown-6} + NH_4^+$	Aqueous	23	-	15	13
$H_2tcpp^{4-} + 18\text{-crown-6} + NH_4^+$	sds	21	-	15	12
$H_2tcpp^{4-} + 15\text{-crown-5} + Na^+$	sds	21	-	13	10
$H_2tcpp^{4-} + 12\text{-crown-4} + Li^+$	sds	14	-	9	6
$H_2tpps^{4-} + 18\text{-crown-6} + K^+$	Aqueous	22	18	13	9
$H_2tpps^{4-} + 18\text{-crown-6} + NH_4^+$	sds	22	18	15	12
$H_2tpps^{4-} + 15\text{-crown-5} + Na^+$	sds	19	10	10	7
$H_2tpps^{4-} + 12\text{-crown-4} + Li^+$	sds	11	6	6	4

* concentrations : Porphyrin, $\approx 5 \times 10^{-5}$; crown ether, 0.05;
cation, 0.19 mol dm^{-3} .

Table 7.2 : Dimerization induced absorption band shifts^a (nm) and the exciton coupling parameter, V (cm^{-1}) for metalloporphyrins in the presence of cation-18-crown-6 complexes

System ^b	Medium	Q-band(s)		Soret band	V
		I	II		
$[\text{Cu}(\text{tcpp})]^{4-} + \text{K}^+$	Aqueous	12	12	-8	1856
$[\text{Cu}(\text{tcpp})]^{4-} + \text{NH}_4^+$	sds	14	13	-6	1727
$[\text{Ni}(\text{tcpp})]^{4-} + \text{K}^+$	Aqueous	8	-	-9	2659
$[\text{Ni}(\text{tcpp})]^{4-} + \text{NH}_4^+$	sds	7	-	-7	1986
$[\text{Zn}(\text{tcpp})]^{4-} + \text{K}^+$	Aqueous	1	1	+1	-
$[\text{Zn}(\text{tcpp})]^{4-} + \text{NH}_4^+$	sds	11	9	+7	-
$[\text{Cu}(\text{tpps})]^{4-} + \text{K}^+$	Aqueous	11	12	-4	2924
$[\text{Cu}(\text{tpps})]^{4-} + \text{NH}_4^+$	sds	10	12	-6	2727
$[\text{Ni}(\text{tpps})]^{4-} + \text{K}^+$	Aqueous	8	-	-5	4308 ^c
$[\text{Ni}(\text{tpps})]^{4-} + \text{NH}_4^+$	sds	7	-	-3	4124 ^c
$[\text{Zn}(\text{tpps})]^{4-} + \text{K}^+$	Aqueous	2	2	+1	-
$[\text{Zn}(\text{tpps})]^{4-} + \text{NH}_4^+$	sds	9	6	+7	-

(a) A positive value indicates a red shift. (b) In the presence of 0.05 mol dm^{-3} 18-crown-6; $\sim 5 \times 10^{-5} \text{ mol dm}^{-3}$ metalloporphyrin, 0.19 mol dm^{-3} cation (c) The Soret bands were too broad in these cases to calculate the half band width thereby increasing $\Delta\lambda$ values.

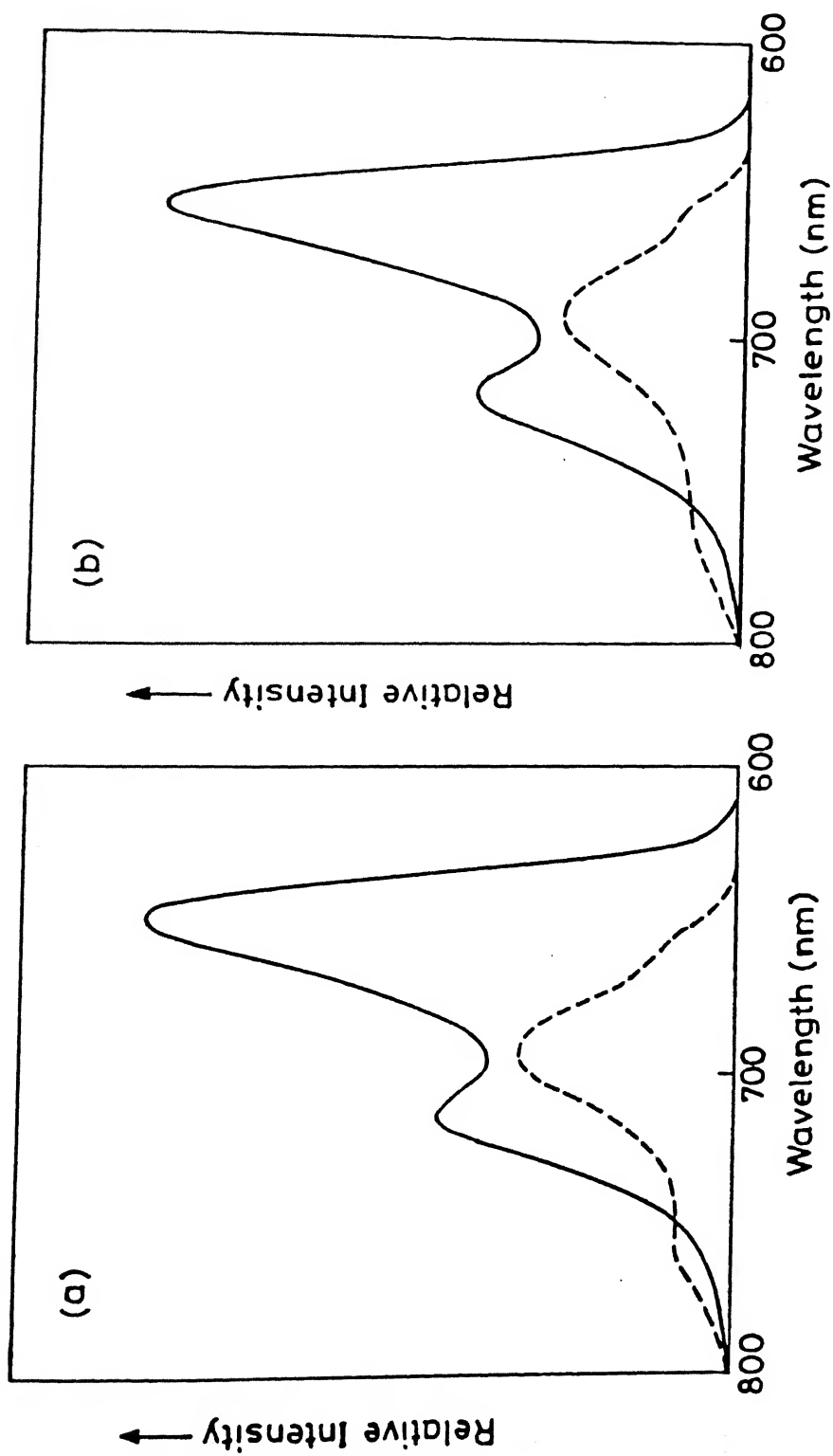


Fig. 7.3 : Fluorescence spectra of $\text{H}_2\text{tcpP}^{4-}$ [2.4×10^{-5} mol dm^{-3}] (solid line) and $\text{H}_2\text{tcpP}^{4-} + 18\text{C6} + \text{NH}_4^+$ (dotted line) in (a) aqueous medium and (b) 0.1 mol dm^{-3} sds containing 30 mM tris at 25°C .

Table 7.3 : Emission data of free base and metallo porphyrin monomers and dimers *

PORPHYRIN	Medium	$Q_{(0,0)}/nm$	$Q_{(0,1)}/nm$	$I_{(0,0)}/I_{(0,1)}$
H_2tcpp^{4-}	Aqueous	644	702	2.01
	sds	649	710	2.17
	$NMe_3(C_{16}H_{33})Br$	649	710	2.41
$[H_2(tcpp)]_2^{8-}$	Aqueous	681	751	4.00
	sds	680	750	3.65
	$NMe_3(C_{16}H_{33})Br$	651	716	2.37
$[Zn(tcpp)]^{4-}$	Aqueous	610	659	1.76
	sds	610	660	1.34
	$NMe_3(C_{16}H_{33})Br$	613	664	2.35
$[Zn(tcpp)]_2^{8-}$	Aqueous	614	662	1.82
	sds	614	663	2.11
	$NMe_3(C_{10}H_{33})Br$	613	664	2.31
$[Zn(tpps)]^{4-}$	Aqueous	605	652	1.66
	sds	607	658	1.34
$[Zn(tpps)]_2^{8-}$	Aqueous	608	659	1.33
	sds	614	661	1.53

* Dimers were generated by addition of K^+ and 18-crown-6. Concentrations : H_2tcpp^{4-} , 2×10^{-5} ; $[Zn(tcpp)]^{4-}$, $[Zn(tpps)]^{4-}$, 2×10^{-5} ; 18-crown-6, 0.05; cation, 0.19 mol dm^{-3} . compared to free bases.

* No appreciable red shifts in cationic and neutral micellar media and large red shifts observed in anionic micellar medium.

7.3.3 EVALUATION OF DIMER FORMATION CONSTANTS (K) IN THE PRESENCE OF CATION-CROWN ETHER COMPLEXES

The progressive decrease in absorbance of a prominent Q-band with increasing addition of cation-crown ether complex is made use of to evaluate the extent of dimer formation using a method described previously^{142a}.

According to this method, the cation-crown ether induced dimerization can be represented by equn. (7.1)



where P stands for porphyrin molecule, C^+ represents the cation-crown ether complex and n is the number of cation-crown ether complexes incorporated. The value of n was varied from 1 to 4. A maximum of four was chosen since there are four negative groups in the periphery of porphyrin. The overall formation constant of 7.1 is given as

$$K = [(P_2C_n)^{n+}] / ([P]^2 [C^+]^n) \quad (7.2)$$

If it is assumed that x mol of the dimer is formed at any instant, then it can be shown that

$$K = x / ((P_t - 2x)^2 (C_t - n_x)^n) \quad (7.3)$$

where P_t and C_t denote the total concentration of porphyrin and cation respectively.

The absorbance value of the monomeric porphyrin is designated as A_p while the absorbance of pure dimer is represented as A_d .

The cation addition results in dimer formation, leading to a decrease in the absorbance values of the monomeric porphyrin. This decrease in absorbance is designated as A_n and is composed of the absorbance of the dimer formed and the absorbance of free monomeric porphyrin that is present in the mixture at equilibrium 7.1. This can be represented as

$$A_n = A_p + A_d \quad (7.4)$$

Since the absorbance is equivalent to ϵcl where ϵ is the molar absorption equivalent and c is the concentration and l is the path length, Eq. (7.4) can be rewritten as

$$A_n = \epsilon_p (P_t - 2x)l + \epsilon_d xl$$

where ϵ_p and ϵ_d are the molar absorption coefficients of the monomeric porphyrin and cation-crown ether induced dimer respectively. The path length, l , was unity and remained invariant throughout the absorbance measurements.. In such situations, the difference between the absorbance values of the monomeric porphyrin and those of the dimer produced by addition of cation-crown ether complex can easily be shown to be

$$A_p - A_n = \Delta OD = x(2\epsilon_p - \epsilon_d)$$

Using above method, by assuming different values of K and computing the theoretical values of x , the amount of dimer formed and ΔA , the decrease in absorbance at each concentration of cation added using experimentally known parameters such as the porphyrin concentration, the concentrations of cations added, the decrease in absorbance at each cation concentration added and the molar

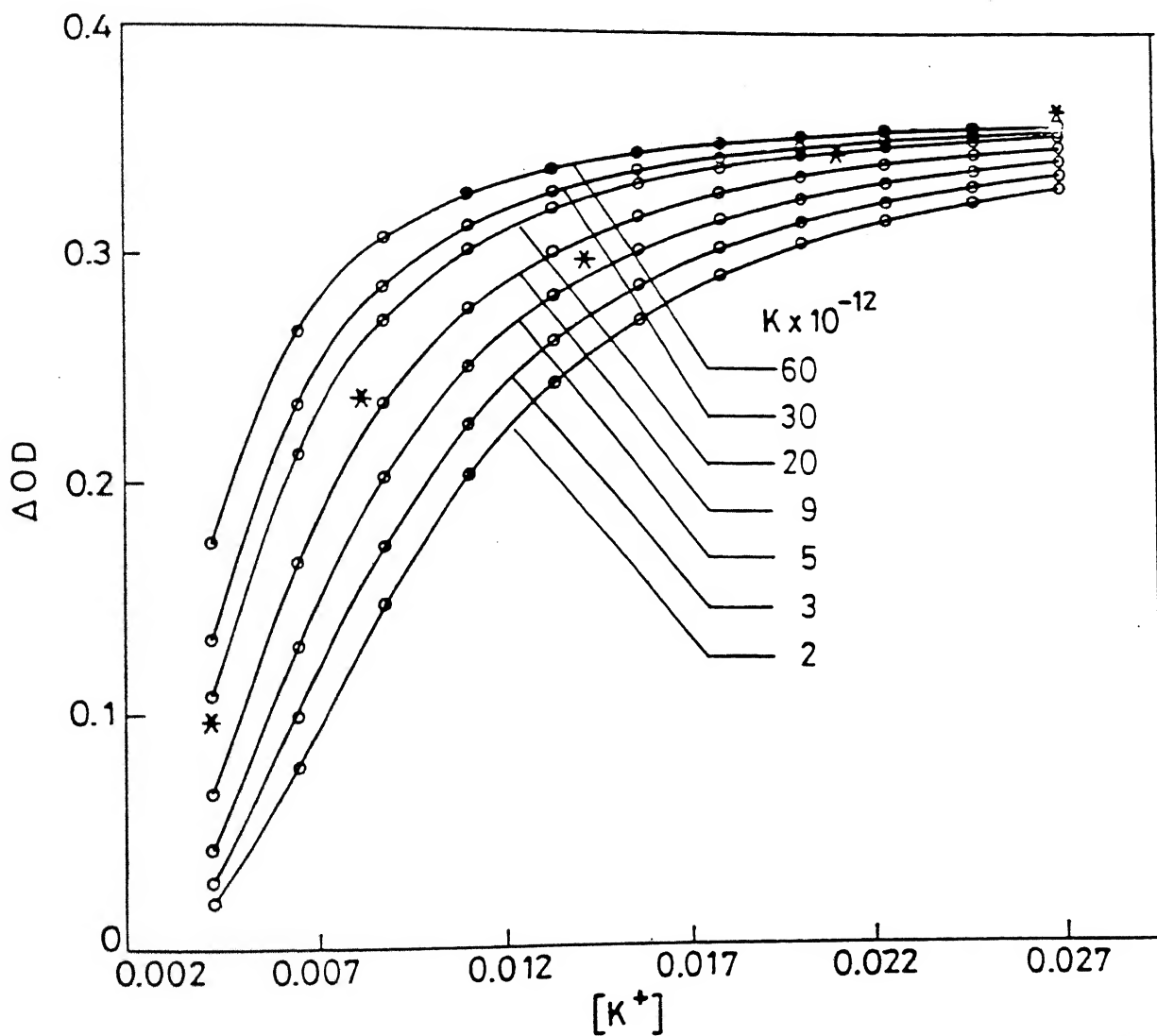


Fig. 7.4 : Difference in absorbance values (ΔOD) versus the concentrations of K^+ ions added for various assumed values of K for Cutpps⁴⁻ dimerization (for $n = 4$, See text). (o) Corresponds to theoretical points and (*) corresponds to experimental points.

absorption values of monomer and dimer (the absorption values of the dimer being calculated from the spectrum run at 5°C). A computer program was devised to carry out the calculations using Newton-Raphson iterative method. Theoretical plots of ΔA vs. concentration of the cation added for various values of K were constructed. The experimental points were then mapped into this plot and the best fit chosen for the overall formation constant of the dimer. Calculations were performed using the value of n from 1 to 4 and in all the cases the best fit is observed when $n = 4$ suggesting that four cation-crown ether complexes are involved per dimer. A representative plot for the K^+ -18-C-6 induced dimer of $[Cu(tPPS)]^{4-}$ for $n = 4$ is given in Fig. 7.4 and the K values are tabulated in table 7.4. Dimerization constants reported in literature for dimers formed by concentration effects in the presence of electrolyte are also included for comparison. It is clear from table 7.4 that dimerization constants of present study is very much higher than those reported in literature^{135,136a}. However, the general trend of stabilities follows the same order in both instances.

7.4 DISCUSSION

7.4.1 ELECTRONIC SPECTRA

All water-soluble porphyrins studied here obey Beer's law in the concentration range $5 \times 10^{-4} - 5 \times 10^{-7} \text{ mol dm}^{-3}$ indicating that they are existing as monomers. Addition of K^+ to a solution

Table 7.4 : Formation constants of Porphyrin dimers induced by cation-crown ether complex in aqueous medium at 25°C.

PORPHYRIN	log K	log K ^a
H ₂ tcpp ⁴⁻	11.0 ± 1.5	4.66
[Cu(tcpp)] ⁴⁻	12.5 ± 1.8	5.23
[Ni(tcpp)] ⁴⁻	12.8 ± 1.8	5.20
[Cu(tpps)] ⁴⁻	12.9 ± 1.8	4.61, 4.83
[Ni(tpps)] ⁴⁻	12.2 ± 1.5	-
[Zn(tcpp)] ⁴⁻	10.0 ± 1.0 ^b	c
[Zn(tpps)] ⁴⁻	10.0 ± 1.0 ^b	c

(a) These values are taken from refs. 135 and 136

(b) In 0.1 mol dm⁻³ sds solution.

(c) under the conditions described in refs. 135 and 136 dimerization does not occur.

containing H₂tcpp⁴⁻ and 18-crown-6 resulted in red shifts in Q-bands, no shift in Soret band with clear isosbestic points. These results suggest the existence of two species in equilibrium. The porphyrin exists as a monomer under our experimental conditions in the absence of cation and crown ether and addition of these two induces dimerization resulting in existence of equilibrium between monomer and dimer. In the absence of cation, the close approach of two porphyrin monomers is not favoured due to repulsion of the negative charges on the periphery of the porphyrins. The added cation reduces this electrostatic repulsion by shielding the negative charges and facilitating the close approach of two porphyrin rings to form a dimer through the π - π

interaction. It is observed¹⁴⁸ that the cation-crown ether complex is much more effective in driving the equilibrium to the dimer side than to the cation alone. This could be due to the exclusion of some water molecules from the solvation shell of the cation on complexation with the crown ether making the environment of the cation less polar allowing the cation to approach the porphyrin more closely than can a completely solvated cation. The effect of temperature on the monomer-dimer equilibrium is apparent from Fig. 7.2. Evidently, small changes in temperature have a large effect on the extent of dimerization with lower temperatures favouring the formation of the dimer while higher temperatures shift the equilibrium towards the monomer.

Spectral titrations of crown ether-cation complexes with metalloporphyrins show a similar effect as observed for the free base porphyrins. However, the decrease in magnitude of intensity and red shift were found to be dependent on the metal ion present in the porphyrin (Fig. 7.5). Well defined isosbestic points were observed in all the spectra and no shift in these were seen upon addition of higher concentrations of potassium ion. However, the shape of the curves in Fig. 7.5 reveal that the process of formation of the dimer involves more than one step. Two types of dimer can be visualised upon addition of cation-crown ether complex; a "side-by-side" dimer of the type (tcpp)M-(cation-crown ether)-M(tcpp) involving only one cation-crown ether complex per dimer and a cofacial dimer which involves two or more cation-crown ether complexes per dimer. When K^+ ions are added to a solution of $[M(tcpp)]^{4-}$ ($M = Ni^{2+}, Cu^{2+}$ or Zn^{2+}), the intensity decrease is sharp at lower concentrations of K^+ [$<0.025 \text{ mol dm}^{-3}$] probably

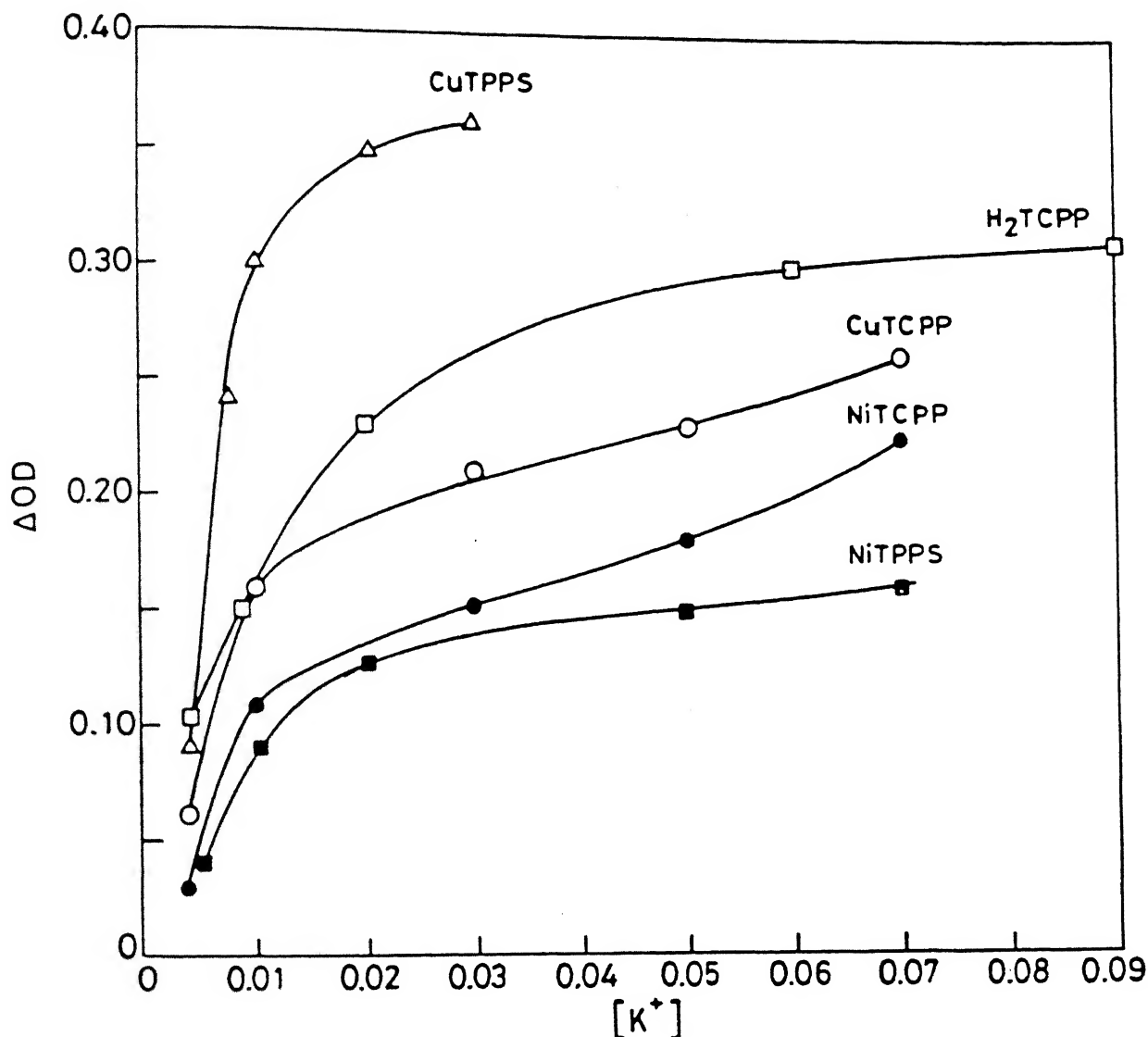


Fig. 7.5 : Intensity changes of a prominent Q-band of porphyrins [$\sim 5 \times 10^{-5} \text{ mol dm}^{-3}$] containing [0.05 mol dm^{-3}] 18C6 and increasing amount of K^+ ions in aqueous medium.

indicating the formation of a side-by-side dimer with a very high formation constant. At higher concentration of K^+ , a transformation of side-by-side dimer to a cofacial dimer occurs by encapsulating a second cation-crown ether complex. Since two more sites are still available in the cofacial dimer for saturation, it

is possible that the encapsulation continues at higher concentrations until the two porphyrin units bind four cation-crown ether moieties in the metalloderivatives. However, Fig. 7.5 indicates a different stoichiometry for H_2tcpp^{4-} . We believe that in this instance the cofacial dimer involves only two cation-crown ether complexes per dimer probably because of the different symmetry of free H_2tcpp^{4-} from those of its metal derivatives.

An additional feature in the metalloderivatives is the shift of the Soret band. The complexes $[Cu(tcpc)]^{4-}$, $[Cu(tpps)]^{4-}$, $[Ni(tcpc)]^{4-}$ and $[Ni(tpps)]^{4-}$ show a blue shift of the Soret band on addition of 18-crown-6 and K^+ while $[Zn(tcpc)]^{4-}$ and $[Zn(tpps)]^{4-}$ show a red shift [Fig. 7.6a]. The Ni^{2+} and Cu^{2+} derivatives of both the porphyrins show a strong dimerization induced shift while for the Zn^{2+} derivatives only a small shift is observed in the optical spectra (table 7.2). It is known that the Ni^{2+} and Cu^{2+} derivatives have a planar structure with the four co-ordinate metal ion at the centre of the porphyrin core whereas in the Zn^{2+} complexes the metal is out of the plane of the porphyrin core and an axial water molecule is incorporated in the co-ordination sphere^{135,136}. The planar nature of the Ni^{2+} and Cu^{2+} derivatives shows the close approach of the two porphyrin rings leading to a stronger $\pi-\pi$ interaction and resulting in a large red shift of the Q-bands. The presence of axial ligands in Zn^{2+} derivatives however hinders the close approach of the two rings with the consequent reduced $\pi-\pi$ interaction resulting in only a small red shift of the Q-bands in aqueous medium. In fact literature data suggest that the Zn^{2+} derivatives do not actually

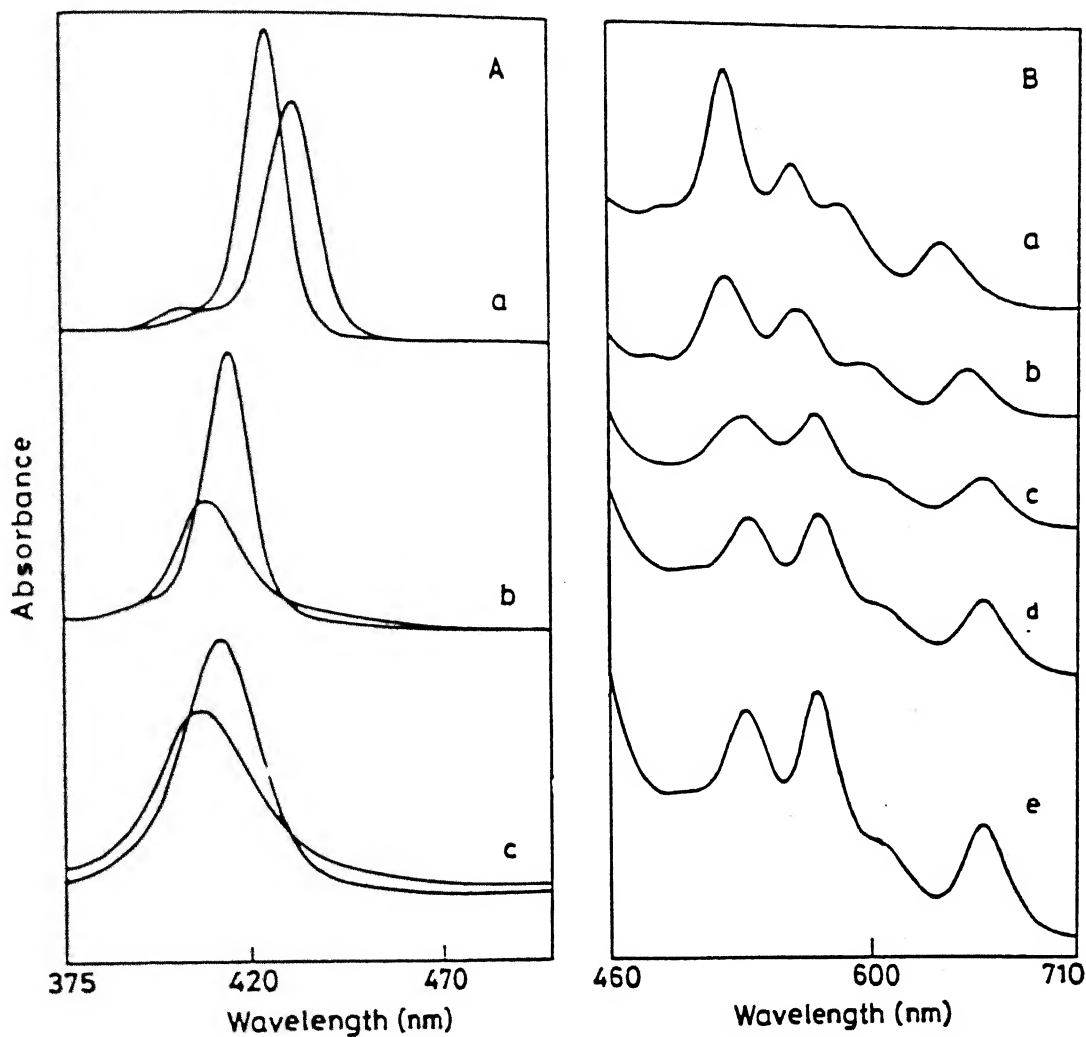


Fig. 7.6 : Visible absorption spectra of free base and metalloporphyrins under different conditions in 0.1 mol dm^{-3} sds containing 30 mM Tris. (A) Comparison spectra of monomer and dimer of (a) ZnTcPP^{4-} , (b) CuTcPP^{4-} and (c) NiTcPP^{4-} in Soret region at 25°C . Spectra with reduced absorbance values corresponds to dimer. (B) Optical spectra in the Q-band region of (a) $\text{H}_2\text{TcPP}^{4-}$, (b) $\text{H}_2\text{TcPP}^{4-} + 12\text{C4} + \text{Li}^{2+}$, (c) $\text{H}_2\text{TcPP}^{4-} + 15\text{C5} + \text{Na}$, (d) $\text{H}_2\text{TcPP}^{4-} + 18\text{C6} + \text{K}^+$, and (e) $\text{HtcPP}^{4-} + 18\text{C6} + \text{NH}_4^+$ at 5°C .

dimerize in aqueous solutions in the presence of an electrolyte^{135,136}.

7.4.2 STUDIES IN MICELLAR MEDIA

To know the effect of micellar media on the aggregation properties of water-soluble porphyrins studied here, we carried out dimerization studies in cationic, anionic and neutral micellar media. Porphyrins showed aggregation behaviour only in anionic sodium dodecyl sulfate and remained monomeric both in cationic cetyltrimethylammonium bromide and neutral Triton X-100.

A comparison of optical spectra of H_2tcpp^{4-} and its metal derivatives ($5 \times 10^{-5} \text{ mol dm}^{-3}$) in aqueous medium and in 0.1 mol dm^{-3} sds solution containing 30 mmol Tris [tris(hydroxymethyl) methylamine] shows small decrease in molar absorption values and slight blue shift (4-5 nm) of Soret bands in 0.1 mol dm^{-3} sds. This indicates that in 0.1 mol dm^{-3} sds the porphyrins show a tendency to aggregate probably due to the presence of free Na^+ ions in sds solution. Addition of cations and crown ether produces similar effects on the optical bands of the porphyrins as found in the aqueous solutions (Fig. 7.6b) indicating that the equilibrium is shifted to dimer formation. This observation suggests that H_2tcpp^{4-} and its metal derivatives do not reside at the hydrophobic region of the sds micelle. On the other hand addition of crown ethers and cations did not produce any appreciable changes in the spectra of the porphyrins in $NMe_3(C_{16}H_{33})Br$ or TX-100 solutions suggesting that the porphyrin derivatives remain monomeric in these micelles. This could be due to the solubilization of the porphyrin derivatives into the

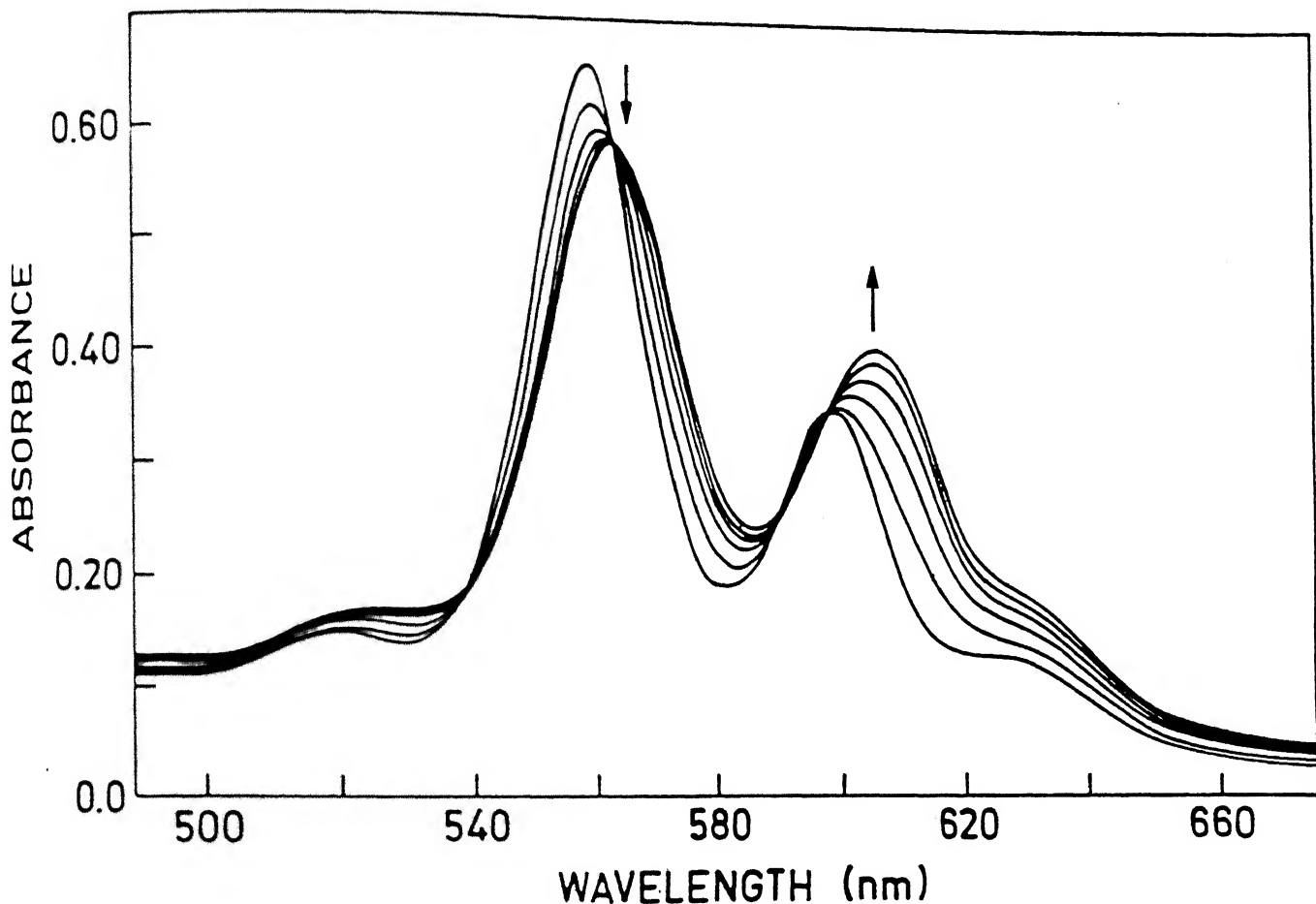


Fig. 7.7 : Effect of addition of increasing amounts of K^+ ions on the absorption spectra of $Zntcpp^{4-}$ solution ($\sim 5 \times 10^{-5} \text{ mol dm}^{-3}$) containing (0.05 mol dm^{-3}) of 18C6 at 25°C in sds medium. Arrows indicate the direction of spectroscopic change.

micelles due to the electrostatic interaction of negatively charged porphyrins with cationic $NMe_3(C_{16}H_{33})Br$ while strong hydrophobic interactions could be responsible in neutral TX-100. These results parallel the findings of Kadish et.al.¹⁴⁹ on H_2tpps^{4-} and its metal derivatives in micellar media.

A comparison of the dimerization induced shifts in aqueous media with that of 0.1 mol dm^{-3} sds solution indicate that the magnitude of shifts for $\text{H}_2\text{tcp}^{4-}$ and its Cu^{2+} and Ni^{2+} derivatives are similar. However, for Zn^{2+} derivatives, the magnitude of shifts are larger in 0.1 mol dm^{-3} sds solution relative to that found in aqueous solutions (Fig. 7.7). This suggests an enhanced dimerization of Zn^{2+} derivatives in 0.1 mol dm^{-3} sds. Recently, a similar effect of enhanced aggregation was observed for $[\text{Zn}(\text{tpps})]^{4-}$ in 0.1 mol dm^{-3} sds.¹⁷

7.4.3 EFFECT OF CATIONS AND CROWN ETHERS

In order to see whether different cations had different effects on dimer formation, optical spectra of solutions containing the same amount of $\text{H}_2\text{tcp}^{4-}$ [$5 \times 10^{-5} \text{ mol dm}^{-3}$] and 0.1 mol dm^{-3} LiCl , NaCl , KCl and NH_4Cl were recorded. It was found that in the absence of crown ether only a relatively small variation in the amount of dimer formed was observed on changing the cation. However, in the presence of added crown-ether, substantial differences can be seen in the spectra with respect to the magnitude of red shifts and intensity decrease depending on which cation is added. For example, when 18-crown-6 was present, the magnitude of red shifts decreased in the order $\text{K}^+ \approx \text{NH}_4^+ > \text{Na}^+ > \text{Li}^+$; for 15-crown-5, the order is $\text{K}^+ \approx \text{NH}_4^+ \approx \text{Na}^+ > \text{Li}^+$ while for 12-crown-4, Li^+ gives rise to shifts comparable to those observed for Na^+ in presence of 15-crown-5 (table 7.1). Similar effects were observed for several crown-ether linked porphyrins and phthalocyanines upon complexation with alkali metal cations^{142b,144,145}. Selectivity towards the different cations

varies with crown ether ring size and maximum effects were observed when the size of the crown ether cavity and the ionic radii of the metal ions match. Apparently, in the absence of crown ether, the role of cations is to shield the negative charges in the periphery of the porphyrins that oppose dimerization. However, in the presence of crown ethers, one has to relate the observed effects to the stability and structure of the cation-crown ether complexes formed since the crown ethers have different affinity for different cations depending on their cavity size¹⁵⁰. A literature study reveals that the stability constants (log K) for K^+ and NH_4^+ binding with 18-crown-6 are 2.06 and 1.1, respectively while it is < 0.3 for Na^+ and no detectable complex formation is found for Li^+ with 18-crown-6¹⁵¹. On the other hand, 15-crown-5 has much larger affinity for Na^+ compared to 18-crown-6 while 12-crown-4 and 14-crown-4 have larger affinity for Li^+ ions¹⁵⁰. This is thought to be due to the different ionic sizes of cations and the differing sizes of the holes in the crown ether. Thus, the magnitude of dimerization induced shifts follows the same order of formation constants for the cation-crown complexes¹⁵¹ and that the amount of dimer formed depends on the stability of the cation-crown ether complexes. Also, it is seen from table 7.1 that the dimerization induced shift for the Li^+ -12-crown-4 complex is smaller than those observed for K^+ -18-crown-6 complex indicating that the shielding power of the Li^+ complex is not as effective as that of the K^+ complex. This could be due to the small size of the Li^+ complex relative to K^+ complex as well as the large solvation energy of Li^+ compared to K^+ . It is also observed that the magnitude of red shifts observed

when only cations are present is much less than when both cations and crown ether are present; in the presence of 0.1 mol dm^{-3} KCl, the Q-bands of $\text{H}_2\text{tcpp}^{4-}$ experience a shift of 10, 4 and 2 nm, respectively while in the presence of the K^+ -18-crown-6 complex the same bands experience a shift of 20, 16 and 13 nm, respectively. This observation indicates that the involvement of crown-ether forces the dimer into a conformation which allows for increased π - π interaction between the two porphyrin rings¹⁴².

7.4.4 'K' VALUES

The following explanation is offered for the higher values of K of dimers of present study compared to dimers reported in literature formed by concentration effects in the presence of electrolytes : (a) since crown ethers have very large affinity for cations and since the amount of dimer formed depends on the stability of the cation-crown ether complex, we tend to believe that the formation constants (K) reported here represent a composite of the dimer formation constant and the cation-crown ether complex stability although it is difficult to estimate the individual contribution of these two effects to the overall formation constant. However, the results indicate the high selectivity of cation-crown ether complexes to shift the equilibrium to formation of the dimer. (b) The dimers formed here are discrete and the dimerization process differs from aggregation promoted by concentration effects in the presence of electrolyte^{135,136}. Despite the difference in magnitude between dimer formation studied here and in the absence of crown ethers, the general trend of stabilities follows the same order in both instances.

7.4.5 EMISSION SPECTRA

The red shifts with quenching of fluorescence bands are the effects of dimer formation. Similar spectral changes were observed upon dimer formation of H_2TMPyP^{4+} in the presence of electrolytes¹³⁵. The studies in micellar media suggest that dimerization is possible only in anionic micellar medium and porphyrin remain monomeric both in cationic and neutral micellar media and reason for this behaviour is already provided in earlier section 7.4.2. Furthermore, it is well known fact that the consequence of dimerization results in the quenching of fluorescence, since internal conversion is more efficient in the dimer than in the monomer¹⁵². However, the extent of fluorescence quenching depends upon the amount of exciton coupling in the dimer and upon the structure of the dimer.

7.4.6 ORIGIN OF ABSORPTION AND EMISSION BAND SHIFTS

A knowledge of the dimer structure is essential to account for the spectral shifts. Our previous ESR and ENDOR (electron nuclear double resonance) studies on the cation-induced dimerization of crown-ether linked porphyrins and of cation-crown ether induced dimers of water-soluble porphyrins have established the face-to-face orientation of the two porphyrin rings with cation-crown ether complex sandwiched between the negatively charged groups¹⁴³. Additional support for this conclusion comes from the observation that many covalently linked diporphyrins¹³⁹⁻¹⁴¹ and porphyrin crown dimers of well defined geometry exhibit spectral shifts of similar magnitude to those in the present study.

The dimerization-induced blue shift observed for Soret bands of $[\text{Cu}(\text{tcpp})]^{4-}$, $[\text{Cu}(\text{tpps})]^{4-}$, $[\text{Ni}(\text{tcpp})]^{4-}$ and $\text{Cu}(\text{tpps})]^{4-}$ and the fluorescence quenching are in accordance with the predictions of exciton theory¹³⁶ (Fig. 7.8). This considers the dipole-dipole interaction between the transition moment integrals associated with optical transitions in the dimer constituents. Thus, the exciton coupling of two S_1 states leads to two new levels corresponding to an inphase and out of phase couplings. The transition to higher energy inphase component is allowed and the transition to lower energy out of phase component is forbidden. The result is that the dimerization gives rise to a blue shift of the Soret absorption band. Indeed, in the present study Cutcpp^{4-} , Cutpps^{4-} , Nltcpp^{4-} and the Nltpps^{4-} show the expected blue shift (Fig. 7.6a). The exciton coupling parameter between two parallel transition dipoles is given by

$$V = \frac{e^2 u^2}{R^3} \cdot G \quad (i)$$

where u and R are the dipole moment and the perpendicular distance between the two porphyrin planes, respectively. G is a geometric factor which should be close to unity. The dipole moment can be estimated by the relation

$$u^2 = \frac{\lambda_{\text{max}}}{2500 M} \cdot \frac{\Delta\lambda}{\epsilon_{\text{max}}} \quad (ii)$$

where M is the degeneracy = 2 here and $\Delta\lambda$ is the bandwidth at half maximum. The exciton coupling parameters calculated from available spectral data (table 7.2) are of comparable magnitude to those observed for several diporphyrins¹⁴¹ and dimers of metal crowned phthalocyanins¹⁴¹.

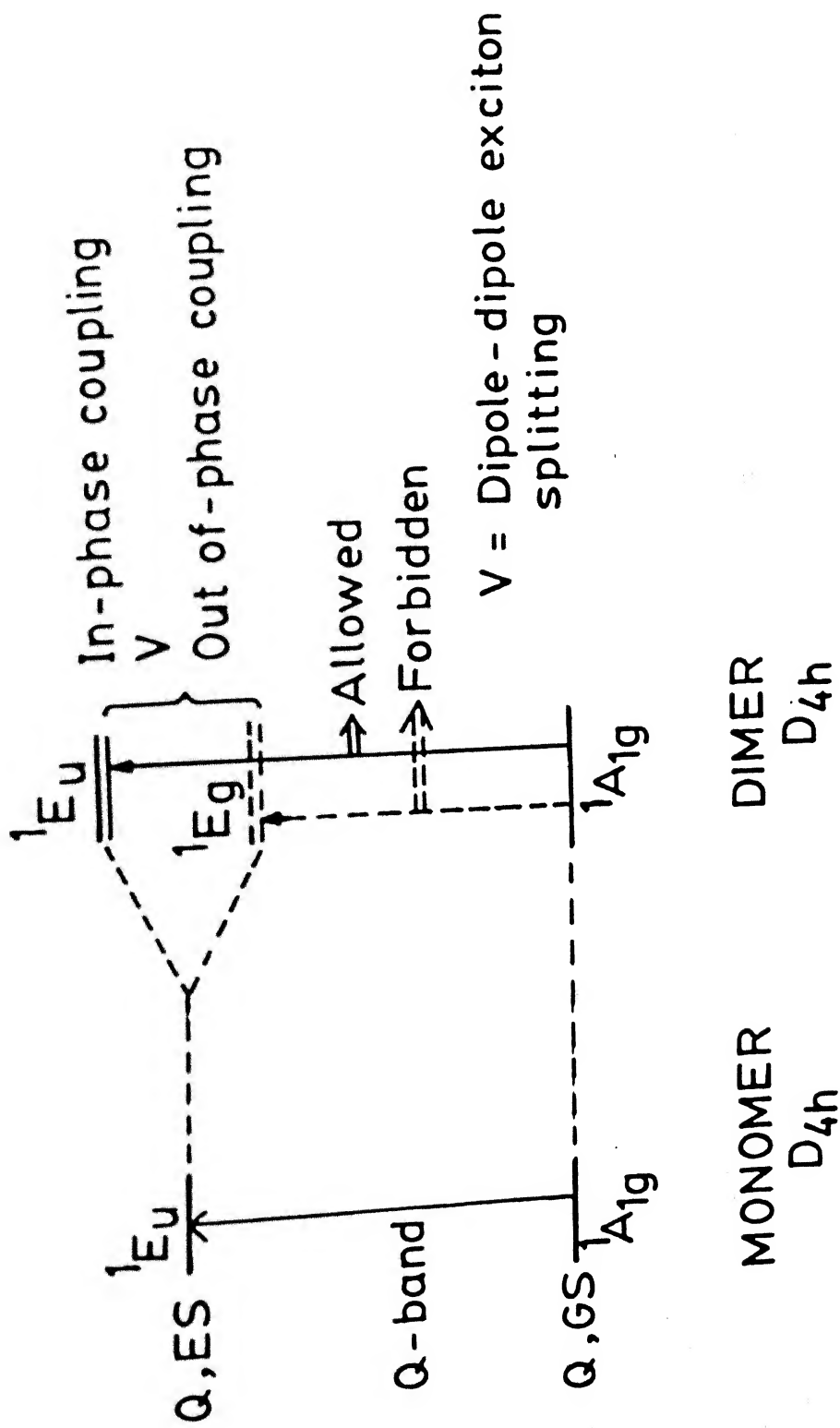


Fig. 7.8 : Energy level diagram for Soret absorption.

Experimentally, it is found that both H_2tcpp^{4-} and H_2tpps^{4-} do not give rise to Soret band shifts. There are, of course, a range of configurations for which the exciton theory predicts only a small or zero Soret band shift. So this experimental finding can be accounted for within the framework of exciton formalism. This finding is also experimentally supported by the fact that many diporphyrins which have well defined structure such as the dimer of 5,10,15,20-tetraphenylporphyrin [H_2tpp]₂ synthesized by Kagan et.al.¹⁴⁰ do not show a Soret band shift relative to the monomer. However, the Q-bands and emission bands do show a large red shift on dimerization as observed in the present study. Interestingly, a recent report by Firman et.al.¹⁵³ on the induced dimerization of H_2tpps^{4-} by a polyammonium macrocycle indicates a blue shift of the Soret band of H_2tpps^{4-} upon dimerization. Evidently, relatively minor changes in dimer geometry can have a profound effect on spectral characteristics.

However, the exciton formalism does not explain the large red shifts of Q-bands observed both in optical and fluorescence spectra upon dimerization. In these systems, the bonding between the dimer constituents is due, at least in part, to attraction between the porphyrin rings. The absence of any covalent links allows the rings to assemble in such a way so as to promote the interaction between π -molecular orbitals of chromophores resulting in strong π - π interactions. The strength of this interaction may be reflected in the magnitude of red shifts of the Q-bands. This kind of interaction has been suggested as a substantial source of red shifts found between absorption bands for *in vitro* and *in vivo* chlorophyll a. A theoretical account of the nature of such π - π

interactions has appeared recently¹⁵⁴.

The Zn^{2+} derivatives of both the porphyrins H_2tcpp^{4-} and H_2tpps^{4-} surprisingly show a red shift of the Soret band upon dimerization (Fig. 7.6a). A purely excitonic interaction cannot account for this observation¹⁵². In the absence of excitonic interaction, one has to invoke a charge-transfer mechanism to explain the observed shifts. A complete charge transfer is ruled out based on our earlier studies on photoexcited triplets of the $Zn(tpps)$ dimer^{148b}. This study indicated that the observed changes in the zero-field splitting parameter D and the associated changes in the kinetic decay parameters would fit a model of a delocalized triplet state with some charge transfer contribution. We believe that an excitonic interaction with some charge transfer contribution could explain the observed red shift in the Soret region. However, the question as to why zinc porphyrins behave differently from those of Ni^{2+} and Cu^{2+} derivatives is not clearly understood at this time. It is possible that the nonplanar structure of zinc porphyrin causes rearrangement of energy levels leading to availability of low-lying charge-transfer states. However, further studies are required to explore this possibility.

7.7 CONCLUSIONS

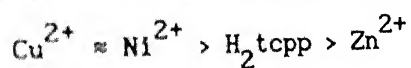
The following conclusions can be drawn from the above study :

- * Dimerization is observed only in aqueous and anionic micellar media in the presence of crown-ether-cation complex. The driving force for the formation of dimer, the

crown-ether-cation complex has high tendency to form sandwich type of complexes and brings two porphyrin units in close proximity there by promoting interaction between the two π -systems.

- Magnitude of dimer formation depends on the metal ion in the porphyrin cavity and nature of cation-crown-ether complex.
- Dimerisation is observed for Zn^{2+} derivatives for the first time and the abnormal behaviour relative to other metallo-derivatives may be due to presence of low lying charge-transfer states.

- The formation constants follow the order



- Exciton coupling, π - π interaction and charge-transfer contribution has been taken into account to explain the observed optical and emission spectral changes.

CHAPTER 8

SUMMARY

The investigations carried out in this thesis are based on three aspects of porphyrin chemistry involved in many biological processes in which the porphyrin ligand takes part in diverse functions. They are; (1) The presence and role of nonplanar porphyrin cores, (2) Magnetic interactions in paramagnetic metalloporphyrin π -cation radicals and (3) Chlorophyll dimers in photosynthesis.

The first part of the work describes the methodology adopted to introduce deformation into the porphyrin skeleton and its effect on various spectroscopic and electrochemical properties. The deformation is induced in phases. In the first step, it is induced by bridging at the ortho position of mesophenyl groups present at the periphery of the porphyrin ring with various short alkyl and aryl groups. The degree of deformation in the porphyrin skeleton is controlled with changing the chain length and nature of the bridging group. When we used different alkyl chain as bridging group, because of the flexible nature, it imposes less

tension on the porphyrin ring. Hence, in the next step, an aromatic ring is introduced into the bridging alkyl chain to make it rigid so that it causes more deformation into the porphyrin skeleton. In the further step, an electron withdrawing groups (Cl^- , Br^-) are introduced on the phenyl group of the bridging chain. These groups create more deformation in the porphyrin skeleton and also acts as electron acceptor since porphyrin ring is a good donor. In the final step, in addition to distortion due to steric effect as stated above, a bulky electron withdrawing bromine groups are introduced stepwise at the β -pyrrole carbons which directly affect the π -electron cloud of the porphyrin ring.

The ring deformation results in the following effects on ground state properties compared to planar porphyrin :

- * In ^1H NMR, 6H and NH protons are shifted downfield and the maximum shifts are observed for cross-trans-linked isomer with short bridging groups relative to adjacent-trans and adjacent-cis isomers. The magnitude of shifts can be related to the degree of distortion. A plot of (Fig. 8.1) the magnitude of deshielding of 6H and NH protons of various cross-trans-linked isomers versus the number of carbons in the bridging chain suggests that deformation depends on the chain length and it increases with decrease in the chain length.
- * Optical absorption bands are shifted towards lower energy and the magnitude of shift is directly related to the degree of distortion in the porphyrin skeleton. A linear plot (Fig. 8.2) of magnitude of shifts for the Soret and Q-bands versus the number of atoms of the bridging chain, further supports

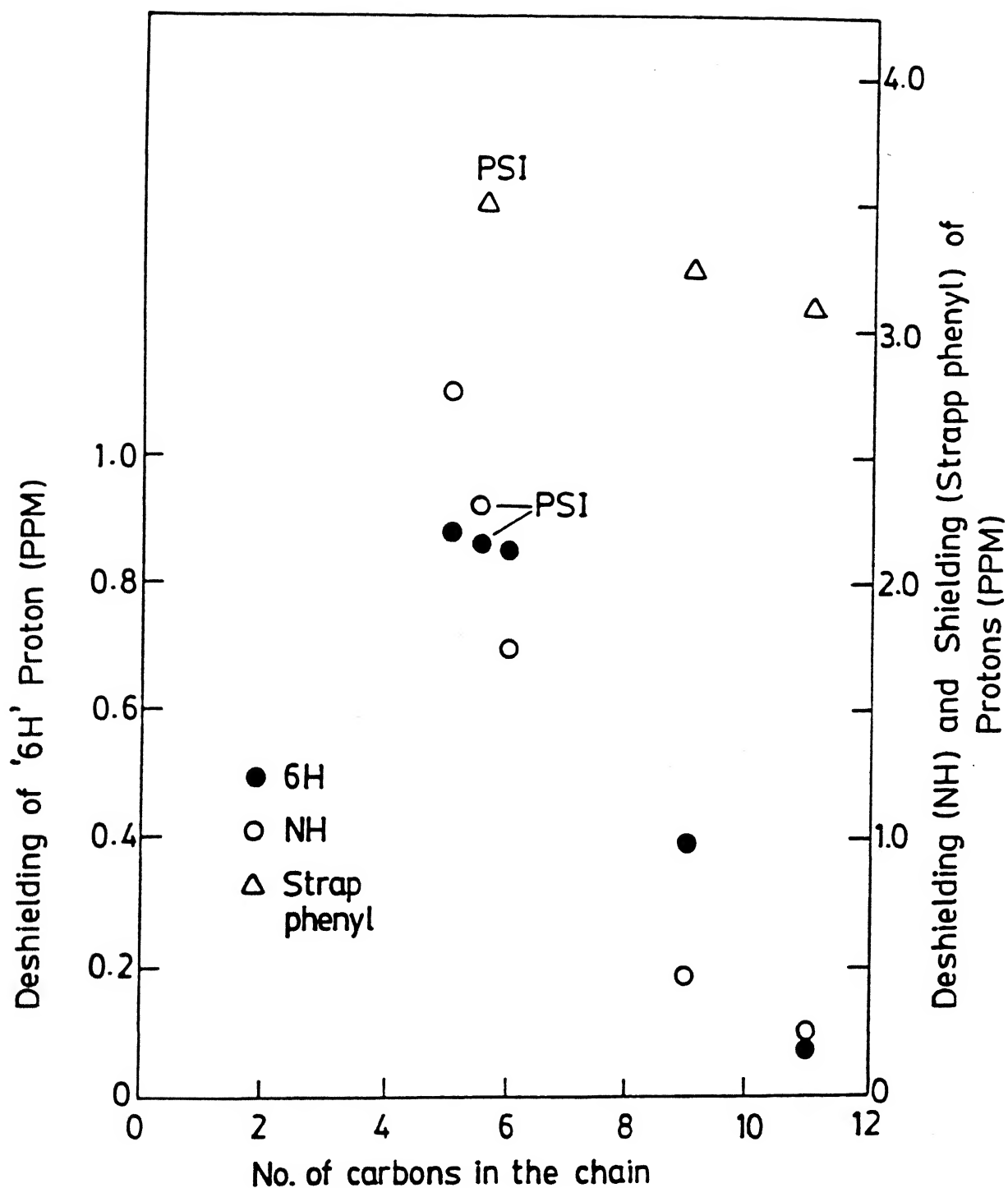


Fig. 8.1 : Plot of deshielding of 6H and NH protons and shielding of strap phenyl protons versus chain length of various cross-trans-linked basket handle porphyrins.

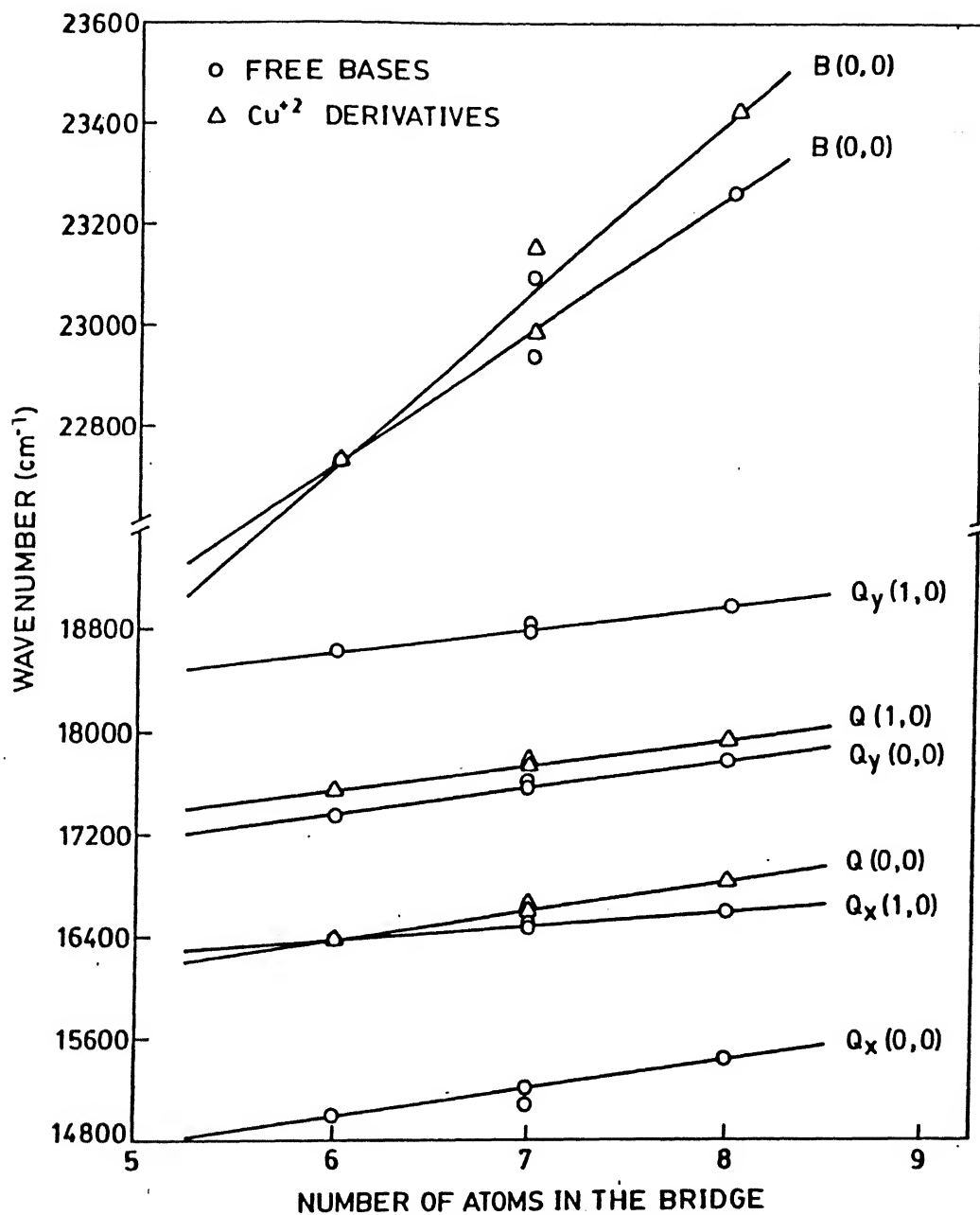


Fig. 8.2 : Plot of absorption band shifts in Soret and Q-band region for various free base and Cu(II) derivatives versus the number of atoms (6 for MSiCl₈ and CuMSiCl₈; 7 for PSI, PSIBr₈, CuPSI and CuPSIBr₈; 8 for Hexyl I and CuHexyl I) in the bridging chain.

the linear relation of degree of distortion to that of chain length of the bridging group.

- * Electrochemical studies reveal that oxidations become easier and reductions harder and maximum effects are seen for cross-trans-linked isomer.

However, introduction of bromines at the β -pyrrole carbons of deformed porphyrins results in further increase of deformation in the porphyrin skeleton and also affects the π -electron cloud of the porphyrin ring since they are in direct conjugation. This results in the reversal of electrochemical potential shifts, since these electron withdrawing groups make the porphyrin ring difficult to oxidise and easier to reduce by removing electron density from the porphyrin ring. However, a nonlinear nature of the plot (Fig. 8.3) suggests that the specific potential shift induced per bromine decreases with increase in the number of bromines on the porphyrin ring. This type of nonadditive nature is also observed for optical absorption band shifts.

It has been shown by absorption and electrochemical potential shifts that the introduction of metal ion into the porphyrin core hardly affect the degree of distortion. Moreover, the electronic structure of the metal ion as reflected from the ESR studies on copper(II) basket handle porphyrins remain unaltered.*

Theoretical, (IEH and INDO calculations) and experimental findings on a variety of Ni^{2+} and Zn^{2+} distorted porphyrins indicate that the nonplanarity in the porphyrin ring affects the frontier orbitals involved in transition. It has been shown in this thesis that the energy gap between HOMO and LUMO decreases as

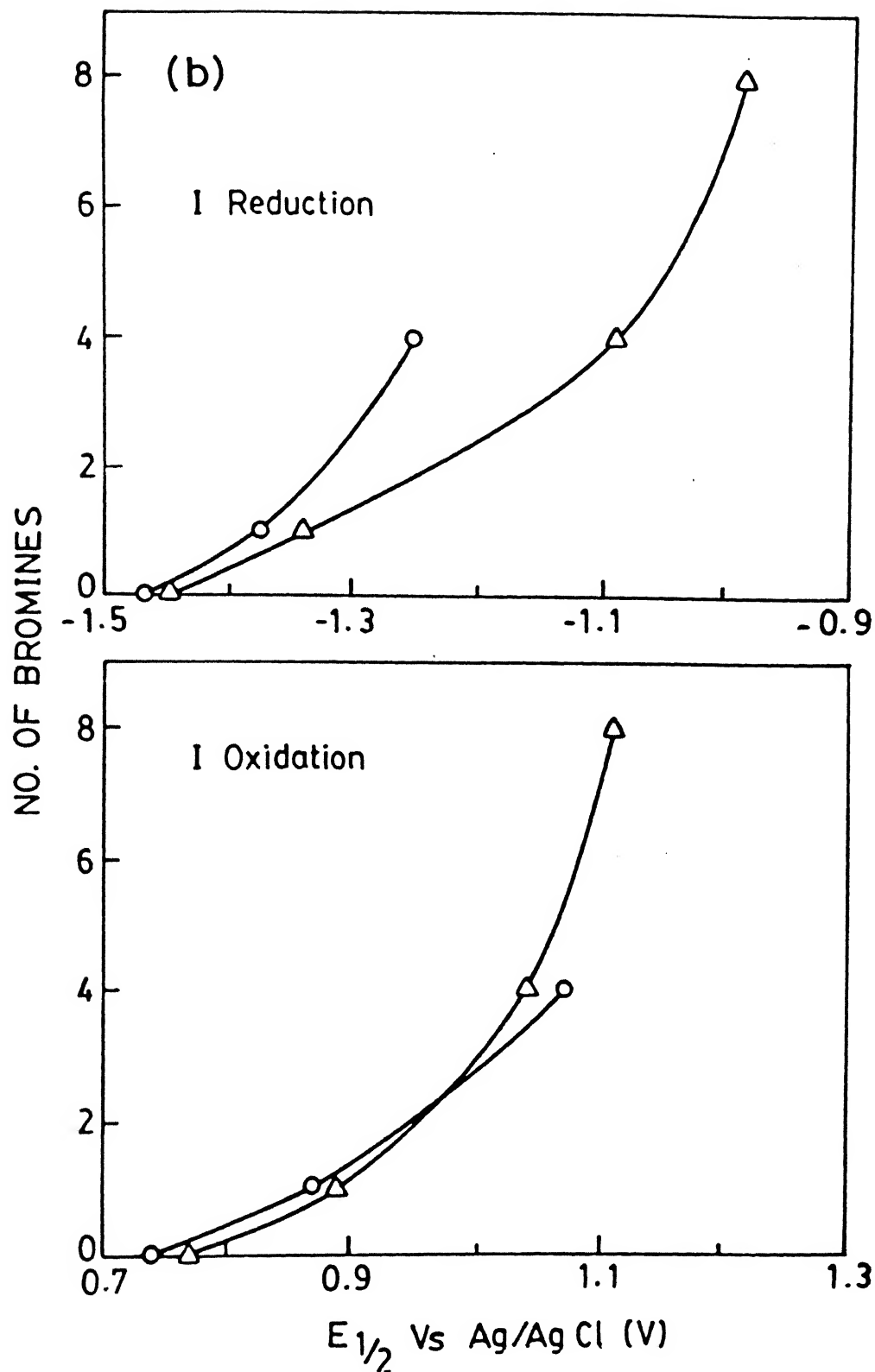
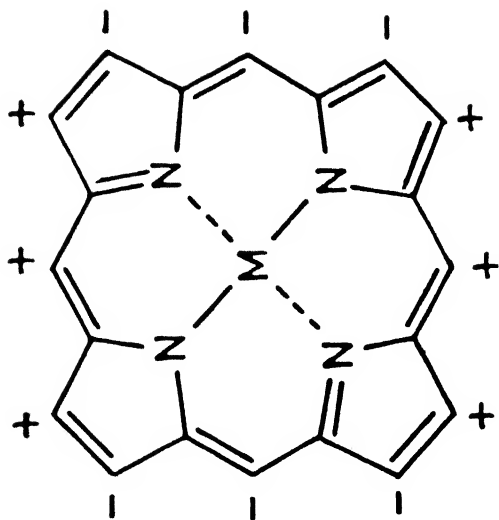


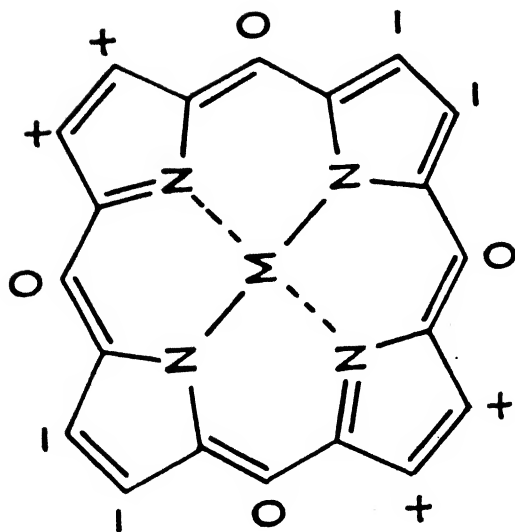
Fig. 8.3 : Plot of $E_{1/2}$ versus number of bromines of pyrrole brominated short chain basket handle porphyrins : (Δ) corresponds to free base porphyrins and (o) corresponds to Cu(II) derivatives.

a result of nonplanarity and the magnitude of this decrease is directly related to the degree of distortion.¹ However, the mechanism of decrease of energy gap between HOMO and LUMO upon β -substitution and upon distortion are different. β -Substitution results in stabilisation of HOMO and LUMO whereas distortion results in destabilisation of HOMO and LUMO and the net effect is the reduction of energy gap between HOMO and LUMO as reflected in the red shift of the optical bands. It is also noted² that distortion as well as β -substitution leads to increase of energy separation between A_{1u} and A_{2u} and the relative increase in energy separation is smaller upon distortion compared to β -substitution.³ This is because distortion is a simple steric effect whereas β -substitution directly affects the π -conjugation of porphyrin skeleton.

To estimate qualitatively the magnitude of distortion present in various basket handle porphyrins, an attempt has been made to generate the energy optimised structures of these porphyrins by molecular mechanics calculations.⁴ The result clearly reveals the expected deformation in the porphyrin skeleton by covalent attachment of the short bridging chain and β -substitution. The calculated structure of adjacent-cis-isomer can be compared to saddle conformation and adjacent-trans-isomer to that of ruffled conformation according to the definition of Scheidt and Lee (Fig. 8.4). Another interesting feature in these calculations is the orientation of the phenyl group of the bridging chain with respect to the mean plane which is nearly parallel in para xylyl bridged porphyrins and almost perpendicular in meta xylyl bridged porphyrins. Thus, the unusual spectral and electrochemical



RUFFLED



SADDLE

Fig. 8.4 : Idealised saddle and ruffled distortion modes for the porphyrin macrocycle using the nomenclature of Scheidt and Lee. Displacement of the atoms with respect to the porphyrin least-squares plane are shown as + = above the plane, - = below the plane and o = in the plane.

behaviour observed for short chain basket handle porphyrins can be ascribed to the distorted structures.

Porphyrins studied in present thesis retain deformation in the porphyrin skeleton in singlet and triplet excited states as well. Fluorescence and photoexcited triplet ESR studies provide justification for this. The effect of nonplanarity results in increase in the energy of the emission bands. A linear plot (Fig. 8.5) of the energy $Q(0,0)$ and $B(0,0)$ emission bands versus number of carbon atoms in the bridging chain suggests that HOMO and LUMO energy gap decreases with increase in the degree of distortion. The reduction in quantum yields in distorted porphyrins compared to planar derivative is attributed to decay of S_1 state through the combined effect of rate of internal conversion and intersystem crossing.

Another unusual feature observed is that the protonation of basket handle porphyrins result in blue shift of emission bands in contrast to red shift seen for protonation of H_2TPP . This is due to lack of interaction between phenyl groups and the porphyrin plane because of the substitution of bridging chain at the ortho position which hinders the free rotation around the porphyrin-phenyl bond and prevents the extension of conjugation between phenyl groups and porphyrin plane.

All Zn^{2+} derivatives of basket handle porphyrins show S_2 emission in addition to S_1 emission. Emission from S_2 state is a rare phenomenon and observed in only few metalloporphyrins. It mainly depends on energy gap between S_2 and S_1 state. If the energy gap is small, S_2 emission can not be observed due to rapid

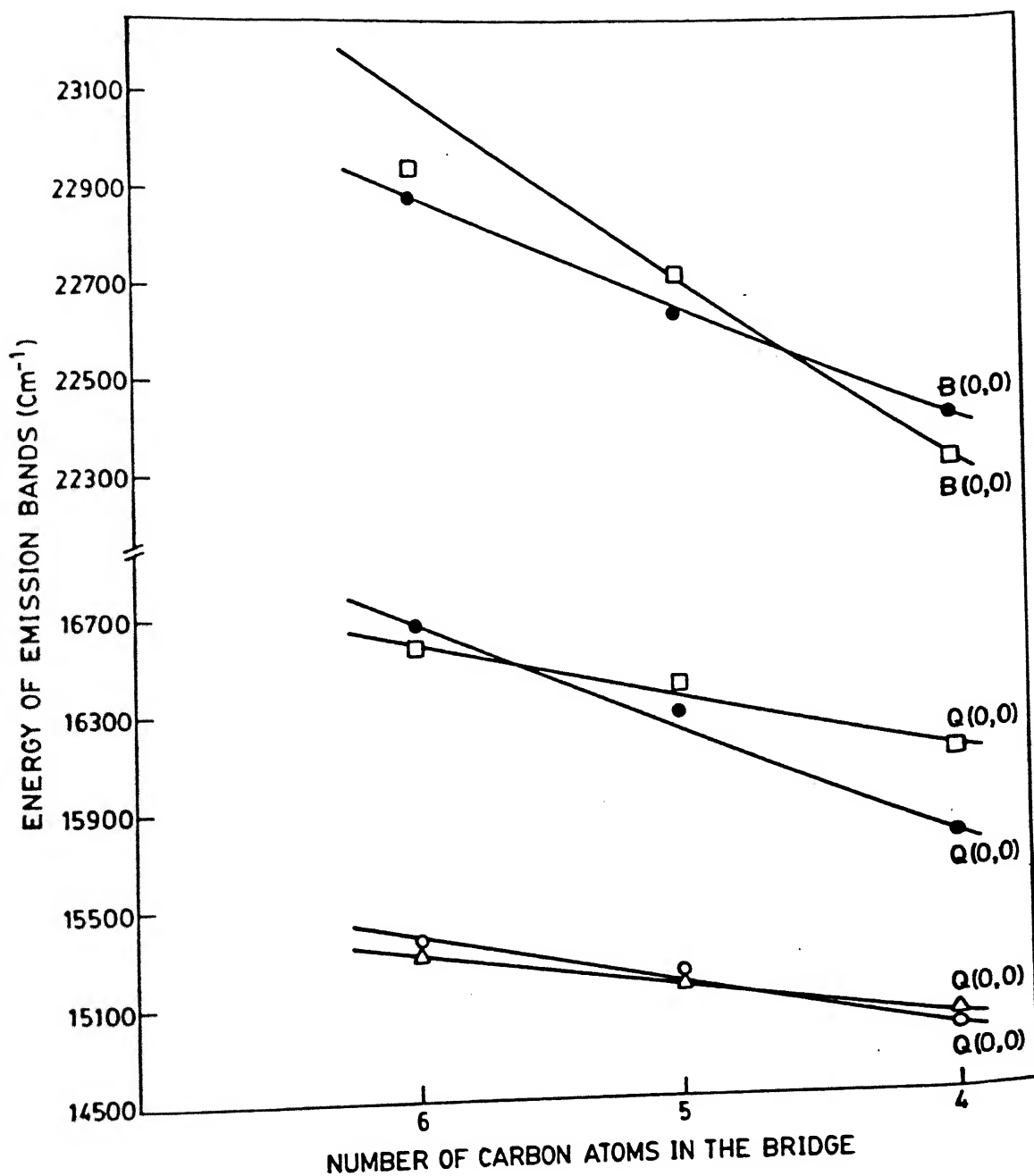


Fig. 8.5 : Plot of the energy of Q(0,0) and B(0,0) emission bands versus number of carbon atoms in the bridging chain of alkyl bridged basket handle porphyrins : (o) Free base Isomer II, (Δ) Free base Isomer III, (*) Zn^{2+} Isomer II and (\square) Zn^{2+} Isomer III.

radiationless decay to S_1 state. The observation of S_2 emission in all Zn^{2+} derivatives reported in this thesis suggest that the energy gap is sufficiently large. The distortion in the porphyrin skeleton of Zn^{2+} derivatives results in red shift of both S_1 and S_2 emission maxima with reduction of energy gap between S_1 and S_2 state as reflected in decreased S_2 quantum yields relative to ZnTPP.

The photoexcited triplet state studies has clearly suggested the retainment of distortion in the triplet excited state. The decrease in zero field splitting parameter, D can be linearly related to the degree of distortion. It is worth mentioning that the Electron Spin Polarization (ESP) pattern is sensitive to the structural variation especially for most distorted $MSiCl_8$ and $PSiBr_8$. In these two compounds, the observed redirection of the triplet state population and decay process relative to planar H_2TPP justifies the above conclusion. Another noteworthy result is the temperature and solvent dependence of ESP pattern for $PSiBr_8$. In this compound the bridging phenyl group carrying the electron withdrawing functionality can act as a electron acceptor and is oriented in a favourable geometry with respect to porphyrin plane so that one can expect a charge-transfer from porphyrin ring to the bridging phenyl group upon irradiation with light. The electrochemical result indicates that first electron reduction is bridged phenyl group centred (Chapter 3 and 4) prior to the porphyrin ring reduction which strongly support the idea of charge-transfer upon irradiation.

The nonvanishing E values observed for the Zn^{2+} derivatives

demonstrates the existence of rhombic distortion in these derivatives. Again here, the change in the ESP pattern for Zn Butyl II and ZnMSIICl_8 relative to ZnTPP highlights the sensitivity of triplet population decay kinetics to the structural variation.

These interesting deformed porphyrin systems containing paramagnetic metal in the porphyrin cavity offer an opportunity to study the magnetic interactions between the oxidised porphyrin ring and the paramagnetic metal. Some interesting observations from these studies are;

- The diamagnetic nature of Cu^{2+} porphyrin radical cations in solution. It should be mentioned here that to the best of our knowledge this is the first report which describes the diamagnetic Copper(II) porphyrin radical cations in solution.
- This study substantiates the emerging trend that the planar porphyrin core leads to ferromagnetic coupling while the ruffled porphyrin core leads to antiferromagnetic coupling as suggested by Reed and coworkers.
- However, this study does not support the suggestion of Reed and coworkers that the ruffling of porphyrin core is a prerequisite for dimer formation observed for many metalloporphyrin π -cation radicals. It has been shown here that metalloporphyrin radical cations studied are monomeric in nature but yet they have ruffled cores needed for antiferromagnetic exchange.

The last part of the work describes the induced dimerisation effect on optical and fluorescence spectra of anionic

water-soluble porphyrins. It has been shown that the role of cation-crown ether complex is to reduce the electrostatic repulsion by shielding the negative charge thus facilitating the close approach of the two porphyrin rings in a cofacial geometry. It is interesting to note that the magnitude of the red shifts on going from monomer to dimer (~ 25 nm) is comparable to that of chlorophyll monomeric and dimeric species, probably, suggesting comparable structural features in dimer.

Thus, the present results unambiguously demonstrate that skeleton of porphyrins are highly flexible and can adopt a variety of conformations *in vitro* and *in vivo*. The consequences of this conformational flexibility is to modulate the optical, redox and excited state properties as shown in the present thesis. This reinforces the promise that such variations offer an attractively simple mechanism for modulating the physical and chemical properties of porphyrin chromophores and prosthetic groups *in vitro* and *in vivo*. The electrochemical studies clearly show that nonplanarity in the porphyrin ring makes it a good donor in the ground and singlet excited state. Thus, it is tempting to speculate that this could be the one of the reasons for preference of nonplanar conformations at the active sites of many biomolecules which take part in electron transport reactions. Lastly, it would be interesting to study how the deformed porphyrins especially the iron derivatives react with small molecules such as O_2 , CO, NO, CN^- etc. It is hoped that such studies will be taken up soon in this laboratory.

APPENDIX

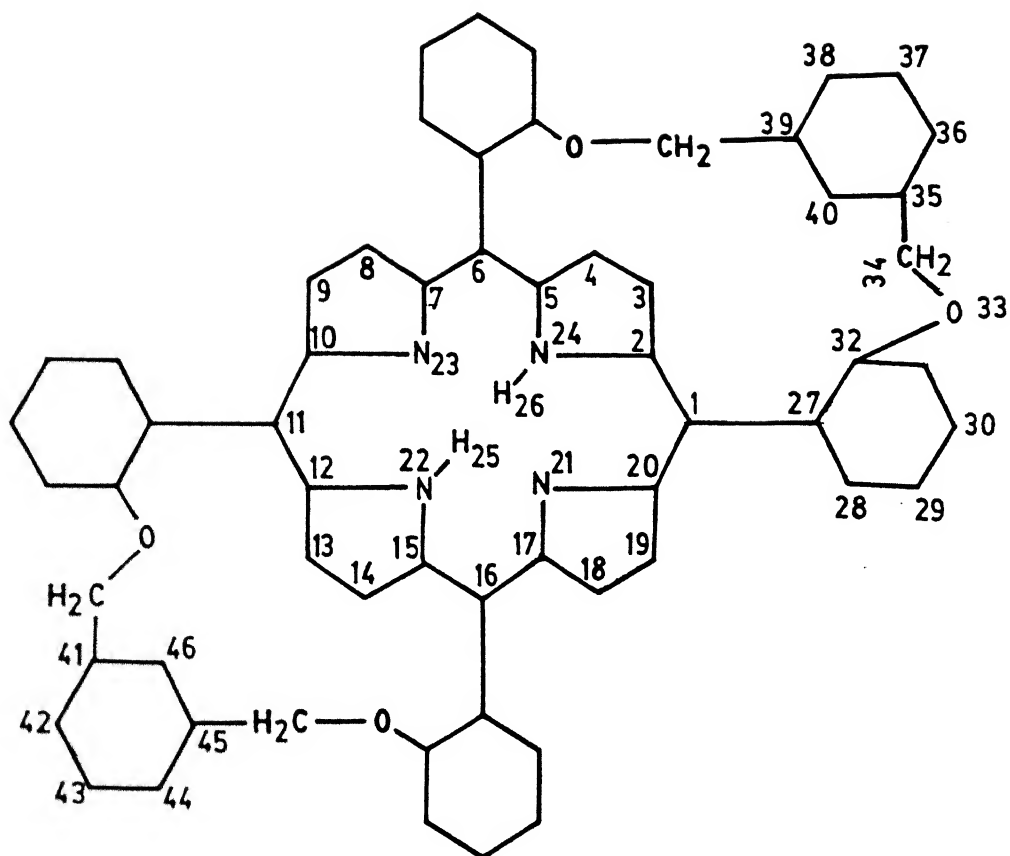


Fig. A1 : Skeletal structure of meta xylyl linked basket handle porphyrins showing numbering system. The numbering system used for para xylyl linked (in which the link is at carbon- 36) basket handle porphyrins is same.

TABLE A-1: CENTRE TYPES USED IN THE GEOMETRY OPTIMIZATIONS FOR PORPHYRINS.

CORE	HYBRIDISATION	ATOMIC NUMBER	DESCRIPTION
C2	sp^3	6	with 2 implicit H atoms
CH	sp^3	6	with 1 implicit H atom
CD	sp^2	6	aromatic, in a 6-ring with an implicit H atom
CA	sp^2	6	aromatic, in a 6-ring with one substituent
CF	sp^2	6	aromatic, in a 5-ring neighbouring N, without an H atom
CG	sp^2	6	aromatic, in a 5-ring neighbouring N-H
CJ	sp^2	6	in pyrimidines at position 5 and 6 with one implicit H atom
NA	sp^2	7	aromatic, in a 5-ring with an explicit H atom
NB	sp^2	7	aromatic, in a 5-ring with an electron pair
O3	sp^3	8	in ether and esters
HC	-	1	explicit on C
2C	sp^2	6	generalized centre type
3C	sp^3	8	generalized centre type
DY	-	-	dummy centre without attributes

Table A2: Atomic coordinates for the final structure obtained for isomer MSII

Center	At.No.	X-Coord.	Y-Coord.	Z-Coord
1	6	-0.1685184E+01	-0.1746275E+00	-0.2825844E+01
2	6	-0.3086208E+00	-0.1943702E+00	-0.2968611E+01
3	6	0.3817438E+00	-0.6679542E-01	-0.4208572E+01
4	6	0.1694803E+01	0.8864860E-01	-0.3939600E+01
5	6	0.1862272E+01	0.5156927E-01	-0.2524665E+01
6	6	0.3072249E+01	0.2024728E+00	-0.1867349E+01
7	6	0.3244601E+01	0.5818933E-01	-0.4945030E+00
8	6	0.4535184E+01	-0.1630040E-01	0.1990337E+00
9	6	0.4271026E+01	-0.1894838E+00	0.1513534E+01
10	6	0.2811708E+01	-0.2027182E+00	0.1663002E+01
11	6	0.2124167E+01	-0.3312780E+00	0.2865344E+01
12	6	0.7634073E+00	-0.1192946E+00	0.3014363E+01
13	6	0.6530046E-01	-0.1413696E+00	0.4256944E+01
14	6	-0.1241362E+01	0.8310868E-01	0.4005175E+01
15	6	-0.1397229E+01	0.2408215E+00	0.2597549E+01
16	6	-0.2613788E+01	0.2969431E+00	0.1939212E+01
17	6	-0.2766064E+01	0.1639162E+00	0.5615418E+00
18	6	-0.4056711E+01	0.1666893E+00	-0.1346698E+00
19	6	-0.3799006E+01	0.6032019E-01	-0.1455563E+01
20	6	-0.2342867E+01	-0.1820672E-01	-0.1608806E+01
21	7	0.6245673E+00	-0.1563618E+00	-0.1952623E+01
22	7	-0.1495605E+00	0.1478717E+00	-0.2015649E+01
23	7	0.2203455E+01	-0.5271221E-01	0.4213544E+00
24	7	-0.1726118E+01	0.4863736E-01	-0.3600157E+00
25	1	0.4284166E+00	-0.2035861E+00	-0.9630218E+00
26	1	0.5049616E-01	0.2008849E+00	0.1027070E+01
27	6	-0.2686976E+01	0.2092149E-01	-0.4314812E+01
28	6	-0.3327282E+01	0.1243474E+01	-0.4524133E+01
29	6	-0.4090214E+01	0.1447192E+01	-0.5679355E+01
30	6	-0.4194541E+01	0.4257856E+00	-0.6632459E+01
31	6	-0.3505536E+01	-0.7803960E+00	-0.6446435E+01
32	6	-0.2730410E+01	-0.9748197E+00	-0.5296480E+01
33	6	0.3023229E+01	-0.9945297E+00	0.4281445E+01
34	6	0.4393601E+01	-0.7607826E+00	0.4438508E+01

35	6	0.5077180E+01	-0.1338264E+01	0.5515443E+01
36	6	0.4392888E+01	-0.2159402E+01	0.6421483E+01
37	6	0.3024070E+01	-0.2404884E+01	0.6252052E+01
38	6	0.2338969E+01	-0.1818452E+01	0.5181509E+01
39	6	0.4468070E+01	0.8093968E+00	-0.2835287E+01
40	6	0.4207975E+01	0.1661999E+01	-0.3912943E+01
41	6	0.5267788E+01	0.2202497E+01	-0.4650151E+01
42	6	0.6587735E+01	0.1882233E+01	-0.4307888E+01
43	6	0.6846803E+01	0.1034152E+01	-0.3222607E+01
44	6	0.5785640E+01	0.5031246E+00	-0.2478478E+01
45	6	-0.4118195E+01	0.1762667E+00	0.2929218E+01
46	6	-0.4491547E+01	0.1197286E+01	0.3809507E+01
47	6	-0.5663532E+01	0.1066422E+01	0.4564841E+01
48	6	-0.6429279E+01	-0.1037997E+00	0.4473326E+01
49	6	-0.6011201E+01	-0.1153358E+01	0.3645134E+01
50	6	-0.4848072E+01	-0.1012559E+01	0.2880069E+01
51	8	0.3230375E+01	0.1906232E+01	-0.4137143E+01
52	1	0.5077936E+01	0.2832748E+01	-0.5442472E+01
53	1	0.7369459E+01	0.2275851E+01	-0.4850992E+01
54	1	0.7818412E+01	0.8052421E+00	-0.2968449E+01
55	1	0.5974234E+01	-0.1137865E+00	-0.1675413E+01
56	1	0.4897056E+01	-0.1647938E+00	0.3765783E+01
57	1	0.6084919E+01	-0.1163804E+01	0.5638271E+01
58	1	0.4898566E+01	-0.2587873E+01	0.7210101E+01
59	1	0.2523373E+01	-0.3015390E+01	0.6913523E+01
60	8	0.1334226E+01	-0.2006381E+01	0.5032534E+01
61	8	-0.4389202E+01	-0.1836851E+01	0.2469497E+01
62	1	-0.6538032E+01	-0.2038454E+01	0.3626806E+01
63	1	-0.7281750E+01	-0.2060943E+00	0.5042239E+01
64	1	-0.5957378E+01	0.1826428E+01	0.5195046E+01
65	1	-0.3925572E+01	0.2055091E+01	0.3876567E+01
66	1	-0.2219869E+01	-0.1858949E+01	-0.5159834E+01
67	1	-0.3561227E+01	-0.1520523E+01	-0.7160662E+01
68	1	-0.4750176E+01	0.5743269E+00	-0.7487102E+01
69	1	-0.4543746E+01	0.2357085E+01	-0.5845473E+01
70	8	-0.3033464E+01	0.2040405E+01	-0.3943383E+01
71	1	-0.4353615E-01	-0.7642309E-01	-0.5135405E+01
72	1	0.2437310E+01	0.2123187E+00	-0.4627857E+01

73	1	0.5461596E+01	0.3948758E-01	-0.2242702E+00
74	1	0.4962866E+01	-0.2816041E+00	0.2257079E+01
75	1	0.4802024E+00	-0.2998049E+00	0.5174986E+01
76	1	-0.1988081E+01	0.1192218E+00	0.4699047E+01
77	1	-0.4980672E+01	0.2392372E+00	0.2911375E+00
78	1	-0.4494179E+01	0.3615804E-01	-0.2201510E+01
79	6	0.2962913E+01	0.3001455E+01	-0.3259491E+01
80	6	-0.1837270E+01	0.2411574E+01	-0.4630174E+01
81	6	0.1521581E+01	0.3463584E+01	-0.3205480E+01
82	6	0.1156688E+01	0.4524845E+01	-0.2367173E+01
83	6	-0.1855925E+00	0.4913685E+01	-0.2268762E+01
84	6	-0.1166961E+01	0.4239340E+01	-0.3005894E+01
85	6	-0.8018343E+00	0.3177402E+01	-0.3840899E+01
86	6	0.5413304E+00	0.2787992E+01	-0.3942525E+01
87	1	0.3163511E+01	0.3596936E+01	-0.3661391E+01
88	1	0.2899713E+01	0.2672055E+01	-0.2593412E+01
89	1	0.8046696E+00	0.1996539E+01	-0.4546910E+01
90	1	-0.2154965E+01	0.4520219E+01	-0.2928769E+01
91	1	-0.4517469E+00	0.5691585E+01	-0.1648443E+01
92	1	0.1875628E+01	0.5014837E+01	-0.1815635E+01
93	1	-0.1420886E+01	0.1794302E+01	-0.4586336E+01
94	1	-0.2034550E+01	0.3025644E+01	-0.5004496E+01
95	6	-0.3582683E+01	-0.2240561E+01	0.3577568E+01
96	6	0.1342248E+01	-0.3110630E+01	0.4125812E+01
97	6	-0.2378060E+01	-0.3101398E+01	0.3277689E+01
98	6	-0.1140419E+01	-0.2741027E+01	0.3830295E+01
99	6	-0.7470177E-02	-0.3523793E+01	0.3575442E+01
100	6	-0.1140271E+00	-0.4661479E+01	0.2765599E+01
101	6	-0.1350977E+01	-0.5019268E+01	0.2213883E+01
102	6	-0.2484995E+01	-0.4238770E+01	0.2469830E+01
103	1	-0.3141176E+01	-0.1649538E+01	0.3686927E+01
104	1	-0.3954149E+01	-0.2822581E+01	0.3859398E+01
105	1	-0.3394538E+01	-0.4499568E+01	0.2062992E+01
106	1	-0.1425790E+01	-0.5855438E+01	0.1617226E+01
107	1	0.7200371E+00	-0.5233334E+01	0.2570733E+01
108	1	-0.1063645E+01	-0.1898282E+01	0.4417401E+01
109	1	0.1365626E+01	-0.3703365E+01	0.4577937E+01
110	1	0.1530089E+01	-0.2794527E+01	0.3476981E+01

TABLE A3 : Some selected bond distances (in Å) of adjacent trans linked isomer (MSII).

ATOM PAIR	DISTANCE	ATOM PAIR	DISTANCE
1-2	1.38	17-18	1.46
2-3	1.42	18-19	1.35
3-4	1.34	19-20	1.46
4-5	1.42	20-1	1.39
5-6	1.38	22-25	1.01
6-7	1.39	24-26	1.01
7-8	1.46	22-12	1.37
8-9	1.35	22-15	1.38
9-10	1.46	24-2	1.37
10-11	1.39	24-5	1.37
11-12	1.38	21-17	1.39
12-13	1.42	21-20	1.39
13-14	1.34	23-7	1.39
14-15	1.42	23-10	1.39
15-16	1.38	21-23	4.00
16-17	1.39	22-24	4.05

Table A4 : Selected bond angles (°) of adjacent trans isomer
(MSII)

BOND	ANGLE	BOND	ANGLE
2-1-20	124.1	9-8-7	107.1
20-19-18	107.2	8-7-23	110.0
19-18-17	107.2	7-6-5	124.4
17-21-20	105.4	5-24-2	107.8
17-16-15	124.2	31-32-33	120.6
15-14-13	107.9	32-33-34	103.1
15-22-12	107.7	33-34-35	115.8
12-11-10	124.3	35-36-37	119.9
10-23-7	105.6	1-27-32	118.5
10-9-8	107.1		

Table A5: Atomic coordinates for the final structure obtained for isomer MSIII.

Center	At.No.	X-Coord.	Y-Coord.	Z-Coord.
1	6	-0.2922405E+01	-0.1523113E+01	-0.1627634E+01
2	6	-0.1722573E+01	-0.1678866E+01	-0.2290457E+01
3	6	-0.1597611E+01	-0.1712679E+01	-0.3709202E+01
4	6	-0.2903567E+00	-0.1582073E+01	-0.4011021E+01
5	6	0.4330442E+00	-0.1489618E+01	-0.2786849E+01
6	6	0.1786578E+01	-0.1232405E+01	-0.2709053E+01
7	6	0.2522704E+01	-0.1238460E+01	-0.1527884E+01
8	6	0.3971907E+01	-0.1031351E+01	-0.1414353E+01
9	6	0.4285848E+01	-0.1107947E+01	-0.1018697E+00
10	6	0.3038043E+01	-0.1360507E+01	0.6296037E+00
11	6	0.2914001E+01	-0.1515586E+01	0.2007273E+01
12	6	0.1709121E+01	-0.1500910E+01	0.2676815E+01
13	6	0.1587729E+01	-0.1357482E+01	0.4089014E+01
14	6	0.2963812E+00	-0.1088550E+01	0.4365612E+01
15	6	-0.4213389E+00	-0.1085131E+01	0.3134675E+01
16	6	-0.1748363E+01	-0.7290889E+00	0.3017886E+01
17	6	-0.2488728E+01	-0.8276953E+00	0.1843942E+01
18	6	-0.3913716E+01	-0.5080751E+00	0.1694260E+01
19	6	-0.4241271E+01	-0.7360595E+00	0.4031953E+00
20	6	-0.3026947E+01	-0.1202575E+01	-0.2777046E+00
21	7	-0.4589025E+00	-0.1605532E+01	-0.1740989E+01
22	7	0.4544209E+00	-0.1390911E+01	0.2114692E+01
23	7	0.1972941E+01	-0.1440743E+01	-0.2645313E+00
24	7	-0.1967492E+01	-0.1254044E+01	0.6246047E+00
25	1	-0.2378547E+00	-0.1534658E+01	-0.7579639E+00
26	1	0.2363216E+00	-0.1415974E+01	0.1128942E+01
27	6	-0.4378408E+01	-0.1376310E+01	-0.2678816E+01
28	6	-0.5181148E+01	-0.2436967E+00	-0.2545565E+01
29	6	-0.6190501E+01	0.1352850E-01	-0.3480510E+01
30	6	-0.6431812E+01	-0.9003912E+00	-0.4513988E+01
31	6	-0.5643570E+01	-0.2052640E+01	-0.4629566E+01
32	6	-0.4606556E+01	-0.2285843E+01	-0.3717934E+01
33	6	0.4384956E+01	-0.1469108E+01	0.3046922E+01
34	6	0.5267859E+01	-0.3953147E+00	0.2923300E+01

35	6	0.6365159E+01	-0.2888340E+00	0.3786193E+01
36	6	0.6582071E+01	-0.1268206E+01	0.4763602E+01
37	6	0.5689947E+01	-0.2340071E+01	0.4892174E+01
38	6	0.4582640E+01	-0.2434406E+01	0.4040755E+01
39	6	0.2526736E+01	-0.5871333E+00	-0.4219574E+01
40	6	0.1722504E+01	0.1506764E+00	-0.5093174E+01
41	6	0.2286960E+01	0.7438395E+00	-0.6228447E+01
42	6	0.3647296E+01	0.5591313E+00	-0.6507424E+01
43	6	0.4442185E+01	-0.2140780E+00	-0.5650783E+01
44	6	0.3881228E+01	-0.7909110E+00	-0.4504546E+01
45	6	-0.2430116E+01	0.1366005E+00	0.4442852E+01
46	6	-0.1558563E+01	0.8560749E+00	0.5266681E+01
47	6	-0.2063924E+01	0.1572329E+01	0.6357889E+01
48	6	-0.3436301E+01	0.1541796E+01	0.6637312E+01
49	6	-0.4302207E+01	0.7936659E+00	0.5828838E+01
50	6	-0.3798285E+01	0.8467675E-01	0.4731391E+01
51	8	0.7079235E+00	0.2211218E+00	-0.4910032E+01
52	1	0.1699616E+01	0.1297594E+01	-0.6869051E+01
53	1	0.4062331E+01	0.9860943E+00	-0.7348565E+01
54	1	0.5441491E+01	-0.3527559E+00	-0.5860938E+01
55	1	0.4467814E+01	-0.1347287E+01	-0.3865881E+01
56	8	0.5043529E+01	0.3651569E+00	0.2265519E+01
57	1	0.7007280E+01	0.5133818E+00	0.3709270E+01
58	1	0.7389675E+01	-0.1191756E+01	0.5398901E+01
59	1	0.5842047E+01	-0.3052950E+01	0.5620503E+01
60	1	0.3917116E+01	-0.3214097E+01	0.4144291E+01
61	1	-0.4434529E+01	-0.4601922E+00	0.4131546E+01
62	1	-0.5310136E+01	0.7664093E+00	0.6041041E+01
63	1	-0.3808022E+01	0.2061706E+01	0.7445474E+01
64	1	-0.1425839E+01	0.2105089E+01	0.6966737E+01
65	8	-0.5395206E+00	0.8035544E+00	0.5099024E+01
66	1	-0.4003584E+01	-0.3114694E+01	-0.3822634E+01
67	1	-0.5813155E+01	-0.2717870E+01	-0.5397970E+01
68	1	-0.7182123E+01	-0.7193318E+00	-0.5196766E+01
69	1	-0.6761230E+01	0.8679817E+00	-0.3403915E+01
70	8	-0.4953012E+01	0.4432043E+00	-0.1812736E+01
71	1	-0.2363858E+01	-0.1798052E+01	-0.4377379E+01
72	1	0.1099079E+00	-0.1548982E+01	-0.4948890E+01

73	1	0.4626335E+01	-0.8617888E+00	-0.2178422E+01
74	1	0.5218951E+01	-0.1007306E+01	0.2983337E+00
75	1	0.2347400E+01	-0.1423643E+01	0.4766687E+01
76	1	-0.9668854E-01	-0.9122613E+00	0.5290408E+01
77	1	-0.4545326E+01	-0.1768900E+00	0.2423827E+01
78	1	-0.5163602E+01	-0.6063634E+00	-0.1321720E-01
79	6	0.5538977E+00	0.1544263E+01	-0.4398704E+01
80	6	-0.3535398E+01	0.3025174E+00	-0.1689227E+01
81	6	-0.9153233E+00	0.1732097E+01	-0.4078800E+01
82	6	-0.1657714E+01	0.2717872E+01	-0.4741001E+01
83	6	-0.3008220E+01	0.2916257E+01	-0.4418859E+01
84	6	-0.3624334E+01	0.2132918E+01	-0.3432934E+01
85	6	-0.2889421E+01	0.1146789E+01	-0.2765062E+01
86	6	-0.1541023E+01	0.9566280E+00	-0.3095170E+01
87	1	0.5087678E+00	0.1348892E+01	-0.3815288E+01
88	1	0.3176895E+00	0.1756120E+01	-0.4927831E+01
89	1	-0.1210774E+01	0.3301985E+01	-0.5462606E+01
90	1	-0.3549989E+01	0.3644156E+01	-0.4907235E+01
91	1	-0.4615925E+01	0.2285953E+01	-0.3198242E+01
92	1	-0.9967185E+00	0.2361143E+00	-0.2598827E+01
93	1	-0.3471570E+01	0.8503846E+00	-0.1412848E+01
94	1	-0.3501449E+01	-0.7177171E-01	-0.2178528E+01
95	6	-0.2019167E+00	0.2123011E+01	0.4670895E+01
96	6	0.4574707E+01	0.1391505E+01	0.3142948E+01
97	6	0.8146743E+00	0.1996018E+01	0.3554232E+01
98	6	0.4383030E+00	0.2264184E+01	0.2232473E+01
99	6	0.1394340E+01	0.2224194E+01	0.1207578E+01
100	6	0.2731605E+01	0.1918489E+01	0.1496887E+01
101	6	0.3118563E+01	0.1649124E+01	0.2814905E+01
102	6	0.2154673E+01	0.1693829E+01	0.3831899E+01
103	1	0.3434606E+00	0.2105088E+01	0.4958202E+01
104	1	-0.5529663E+00	0.2082466E+01	0.4165609E+01
105	1	0.2441422E+01	0.1521269E+01	0.4806281E+01
106	1	0.3431282E+01	0.1905211E+01	0.7404389E+00
107	1	0.1114415E+01	0.2430865E+01	0.2374528E+00
108	1	-0.5394593E+00	0.2504468E+01	0.2013499E+01
109	1	0.4267175E+01	0.9888152E+00	0.3494048E+01
110	1	0.4596817E+01	0.1819878E+01	0.2700066E+01

Table A6: Selected bond distances (in Å) of adjacent cis isomer
(MSIII)

ATOM PAIR	DISTANCE	ATOM PAIR	DISTANCE
1-2	1.37	17-18	1.46
2-3	1.42	18-19	1.35
3-4	1.34	19-20	1.46
4-5	1.42	20-1	1.39
5-6	1.38	22-25	1.01
6-7	1.39	24-26	1.00
7-8	1.46	22-12	1.37
8-9	1.35	22-15	1.37
9-10	1.46	24-2	1.37
10-11	1.39	24-5	1.37
11-12	1.37	21-17	1.39
12-13	1.42	21-20	1.39
13-14	1.34	23-7	1.39
14-15	1.42	23-10	1.39
15-16	1.37	21-23	4.04
16-17	1.39	22-24	3.96

Table A7: The distances (in Å) of the strap phenyl carbons from the nitrogens on the porphyrin plane and the hydrogens which are attached to the nitrogens for adjacent cis isomer (MSIII). See figure for details on the numbering of carbons on the strap phenyls.

Strap Phenyl	N(23)	N(22)	N(21)	N(24)	H(25)	H(26)
Carbon 35	5.89	7.87	8.85	7.05	7.66	7.23
Carbon 36	5.88	7.42	8.64	7.24	7.38	7.29
Carbon 37	5.83	7.16	8.79	7.66	7.25	7.53
Carbon 38	5.78	7.36	9.14	7.88	7.41	7.70
Carbon 39	5.78	7.81	9.33	7.70	7.69	7.64
Carbon 40	5.83	8.05	9.19	7.28	7.81	7.41
Carbon 41	9.48	8.10	5.74	7.57	7.84	7.53
Carbon 42	9.68	8.12	5.89	7.97	7.89	7.79
Carbon 43	9.65	7.74	5.89	8.30	7.68	7.96
Carbon 44	9.41	7.32	5.74	8.26	7.40	7.88
Carbon 45	9.21	7.31	5.59	7.89	7.34	7.63
Carbon 46	9.25	7.71	5.59	7.54	7.57	7.45

Table A8: The distances (in Å) between the carbons of the two phenyl rings of the strap in adjacent cis isomer (MSIII). Carbons numbered 35 to 40 belong to phenyl ring of one strap and the carbons numbered 41 to 46 belong to the phenyl ring of the second strap.

Strap Phenyl	Carbon 41	Carbon 42	Carbon 43	Carbon 44	Carbon 45	Carbon 46
Carbon 35	13.68	14.32	14.42	13.89	13.23	13.12
Carbon 36	13.41	13.04	14.04	13.39	12.73	12.73
Carbon 37	13.80	14.33	14.20	13.53	12.97	13.12
Carbon 38	14.43	14.87	14.73	14.15	13.70	13.85
Carbon 39	14.68	15.12	15.09	14.62	14.16	14.20
Carbon 40	14.31	14.86	14.94	14.50	13.94	13.85

TABLE A9: Selected bond angles (°) of adjacent cis isomer (MSIII)

BOND	ANGLE	BOND	ANGLE
2-1-20	124.4	9-8-7	107.2
20-19-18	107.2	8-7-23	109.9
19-18-17	107.2	7-6-5	123.8
17-21-20	105.7	31-32-33	120.7
17-16-15	123.8	32-33-34	103.4
15-14-13	107.7	33-34-35	115.1
12-11-10	124.4	34-35-36	120.0
10-23-7	105.7	1-27-32	118.4
10-9-8	107.2		

TABLE A-10: SOME SELECTED BOND DISTANCES (in Å) OF MSiCl_8

ATOM PAIR	DISTANCE	ATOM PAIR	DISTANCE
1 - 2	1.38	18 - 19	1.35
2 - 3	1.42	19 - 20	1.46
3 - 4	1.35	20 - 1	1.38
4 - 5	1.42	22 - 25	1.01
5 - 6	1.38	24 - 26	1.01
6 - 7	1.38	22 - 12	1.37
7 - 8	1.46	22 - 15	1.37
8 - 9	1.35	24 - 2	1.37
9 - 10	1.46	24 - 5	1.37
10 - 11	1.38	21 - 17	1.38
11 - 12	1.38	21 - 20	1.38
12 - 13	1.42	23 - 7	1.38
13 - 14	1.35	23 - 10	1.38
14 - 15	1.42	21 - 22	2.72
15 - 16	1.38	22 - 23	2.73
16 - 17	1.38	23 - 24	2.72
17 - 18	1.46	24 - 21	2.73

TABLE A-11: SELECTED BOND ANGLES (°) OF MSiCl_8

BOND	ANGLE	BOND	ANGLE
2 - 1 - 20	122.0	33 - 34 - 35	148.4
17 - 16 - 15	138.4	36 - 35 - 40	117.5
12 - 11 - 10	122.0	35 - 40 - 39	123.7
10 - 23 - 7	100.7	38 - 39 - 40	117.4
10 - 9 - 8	106.8	5 - 24 - 26	125.8
9 - 8 - 7	106.8	5 - 4 - 3	107.9
8 - 7 - 23	110.2	4 - 3 - 2	107.9
7 - 6 - 5	121.9	3 - 2 - 24	107.8
5 - 24 - 2	108.2	24 - 5 - 4	107.9
31 - 32 - 33	120.0	2 - 1 - 20	122.0
32 - 33 - 34	111.3		

TABLE A-12: SOME SELECTED BOND DISTANCES (in Å) OF PSI

ATOM PAIR	DISTANCE	ATOM PAIR	DISTANCE
1 - 2	1.39	11 - 12	1.39
2 - 3	1.46	12 - 13	1.46
3 - 4	1.35	13 - 14	1.35
4 - 5	1.46	14 - 15	1.46
5 - 6	1.39	15 - 16	1.39
6 - 7	1.38	16 - 17	1.38
7 - 8	1.42	17 - 18	1.42
8 - 9	1.35	18 - 19	1.35
9 - 10	1.42	19 - 20	1.42
10 - 11	1.38	20 - 1	1.38

TABLE A-13: SELECTED BOND ANGLES (°) OF PSI

BOND	ANGLE	BOND	ANGLE
2 - 1 - 20	123.0	7 - 6 - 5	122.9
20 - 19 - 18	107.7	5 - 24 - 2	125.8
19 - 18 - 17	107.7	27 - 28 - 29	119.5
17 - 21 - 20	108.2	28 - 29 - 30	120.1
17 - 16 - 15	122.9	5 - 24 - 26	125.9
15 - 14 - 13	107.1	5 - 4 - 3	107.1
15 - 22 - 12	105.8	4 - 3 - 2	107.1
12 - 11 - 10	123.0	3 - 2 - 24	109.9
10 - 23 - 7	108.2	2 - 1 - 20	123.0
10 - 9 - 8	107.7	2 - 24 - 5	105.8
9 - 8 - 7	107.7		

TABLE A-14: SOME SELECTED BOND LENGTHS (in Å) OF PSiBr_8

ATOM PAIR	DISTANCE	ATOM PAIR	DISTANCE
1 - 2	1.37	19 - 20	1.46
2 - 3	1.42	20 - 1	1.38
3 - 4	1.35	22 - 25	1.01
4 - 5	1.42	24 - 26	1.01
5 - 6	1.37	22 - 12	1.37
6 - 7	1.38	22 - 15	1.37
7 - 8	1.46	24 - 2	1.37
8 - 9	1.35	24 - 5	1.37
9 - 10	1.46	21 - 17	1.39
10 - 11	1.38	21 - 20	1.39
11 - 12	1.37	23 - 7	1.39
12 - 13	1.42	23 - 10	1.39
13 - 14	1.35	21 - 22	2.72
14 - 15	1.42	22 - 23	2.72
15 - 16	1.37	23 - 24	2.72
16 - 17	1.38	24 - 21	2.72
17 - 18	1.46	25 - 26	1.89
18 - 19	1.35		

TABLE A-15: SELECTED BOND ANGLES (°) OF PSIBr_8

BOND	ANGLE	BOND	ANGLE
2 - 1 - 20	121.8	9 - 8 - 7	107.1
29 - 30 - 31	120.0	8 - 7 - 23	110.0
35 - 40 - 39	120.3	7 - 6 - 5	121.8
37 - 38 - 39	119.5	5 - 24 - 2	107.9
17 - 16 - 15	121.8	31 - 32 - 33	120.7
15 - 14 - 13	107.8	32 - 33 - 34	117.8
15 - 22 - 12	107.9	33 - 34 - 35	149.4
12 - 11 - 10	121.8	34 - 35 - 36	121.6
10 - 23 - 7	105.5	32 - 27 - 28	120.3
10 - 9 - 8	107.1		

TABLE A-16: SOME SELECTED BOND DISTANCES (in Å) OF PSIBr_{12}

ATOM PAIR	DISTANCE	ATOM PAIR	DISTANCE
1 - 2	1.38	16 - 17	1.38
2 - 3	1.42	17 - 18	1.46
3 - 4	1.34	18 - 19	1.34
4 - 5	1.42	19 - 20	1.46
5 - 6	1.38	20 - 1	1.38
6 - 7	1.38	22 - 25	1.01
7 - 8	1.46	24 - 26	1.00
8 - 9	1.34	22 - 12	1.37
9 - 10	1.46	22 - 15	1.37
10 - 11	1.38	24 - 2	1.37
11 - 12	1.38	24 - 5	1.37
12 - 13	1.42	21 - 17	1.38
13 - 14	1.34	21 - 20	1.38
14 - 15	1.42	23 - 7	1.38
15 - 16	1.38	23 - 10	1.38

TABLE A-17: SELECTED BOND ANGLES (°) OF PSIBr₁₂

BOND	ANGLE	BOND	ANGLE
5 - 6 - 7	117.4	21 - 17 - 16	123.9
7 - 23 - 10	105.5	16 - 15 - 22	125.0
5 - 24 - 2	108.0	11 - 12 - 22	124.9
20 - 21 - 17	105.5	11 - 10 - 23	123.9
15 - 22 - 12	108.0	1 - 27 - 32	118.1
12 - 22 - 25	125.9	27 - 28 - 29	119.7
15 - 22 - 25	125.9	30 - 31 - 32	119.8
5 - 24 - 26	125.9	32 - 33 - 34	118.8
2 - 24 - 26	125.9	33 - 34 - 35	146.1
23 - 7 - 6	123.9	34 - 35 - 36	122.0
6 - 5 - 24	125.0	35 - 36 - 37	122.2
24 - 2 - 1	124.9	37 - 38 - 39	115.5
1 - 20 - 21	123.9		

REFERENCES

1. a. T. Takano, *J. Mol. Biol.*, **1977**, 110, 537.
b. J.F. Deatherage, R.S. Loe, C.M. Anderson and K. Moffat, *J. Mol. Biol.*, **1976**, 104, 687.
2. a. J. Deisenhofer, O. Epp, K. Miki, R. Huber and H. Michel, *Nature*, **1985**, 318, 618.
b. J. Deisenhofer, O. Epp, K. Miki, R. Huber and H. Michel, *J. Mol. Biol.*, **1984**, 180, 385.
c. W. Zinth, E.W. Knapp, S.F. Fischer, W. Kaiser, J. Deisehofer and W. Michel, *Chem. Phys. Lett.*, **1985**, 119, 1.
d. J. Barber, *Nature*, **1985**, 305, 278.
3. M.K. Geno and J. Halpern, *J. Am. Chem. Soc.*, **1987**, 109, 1238.
4. J.A. Ibers, L.J. Pace, J. Martinsen and B.M. Hoffman, *Struc. Bond*, **1982**, 50, 1.
5. a. L.R. Furenlid, M.W. Renner, K.M. Smith and J. Fajer, *J. Am. Chem. Soc.*, **1990**, 112, 1634.
b. L.R. Furenlid, M.W. Renner and J. Fajer, *J. Am. Chem. Soc.*, **1990**, 112, 8987.
6. a. C.E. Schulz, P.W. Devaney, H. Winkler, P.G. Debrunner, N. Doan, R. Chiang, R. Rutter and L.P. Hager, *FEBS Lett.*, **1979**, 103, 102.
b. J.E. Roberts, B.M. Hoffman, R. Rutter and L.P. Hager, *J. Biol. Chem.*, **1981**, 256, 2118.
c. R. Rutter, L.P. Hager, H. Dhonau, M. Hendrich, M. Valentine and P.G. Debrunner, *Biochemistry*, **1984**, 23, 6809.
d. C.E. Schulz, R. Rutter, J.T. Sage, P.G. Debrunner and L.P. Hager, *Biochemistry*, **1984**, 23, 4743.

- e. D. Mandon, R. Weiss, K. Jayaraz, A. Gold, J. Turner, E. Bill and A.K. Trautwein, *Inorg. Chem.*, **1992**, 31, 4404.
7. J. H. Dawson and M. Sono, *Chem. Rev.*, **1987**, 87, 1255.
8. R.C. Ladner, E.J. Heidner and M.F. Perutz, *J. Mol. Biol.*, **1977**, 114, 385.
9. a. J. P. Collman, R.R. Gagne, C.A. Reed, W.T. Robinson and G.A. Rodley, *Proc. Natl. Acad. Sci. USA*, **1974**, 71, 1326.
- b. J.F. Kirner and R. Scheidt, *Inorg. Chem.*, **1975**, 14, 2081.
- c. R.G. Little, K.R. Dymock and J.A. Ibers, *J. Am. Chem. Soc.*, **1975**, 97, 4532.
10. a. V.W. Day, B.R. Stults, E.L. Tasset, R.O. Day and R.S. Marianelli, *J. Am. Chem. Soc.*, **1974**, 96, 2650.
- b. V.W. Day, B.R. Stults, E.L. Tasset, R.S. Marianelli, and L.J. Boucher, *Inorg. Nucl. Chem. Lett.*, **1975**, 11, 505.
- c. B.M.Chen, Ph.D. Thesis, Michigan State University, **1970**.
11. B.R. Gelin and M. Karplus, *Proc. Natl. Acad. Sci. USA*, **1977**, 74, 801.
12. M.E. Michel-Beyerle, M. Plato, J. Deisenhofer, H. Michel, M. Bixon and J. Jortner, *Biochim. Biophys. Acta.*, **1988**, 932, 52.
13. J. Deisenhofer and H. Michel, *Science*, **1989**, 245, 1463.
14. a. J. Glusker, In B_{12} ; D. Dolphin, Ed. Wiley, New York, **1982**, Vol. 1, P.23 and references therein.
- b. J. Halpern, *Science.*, **1985**, 227, 869 and references therein.
15. a. A. Ulman, J. Manassen, F. Frolow and D. Rabinovich, *Tetrahedron Lett.*, **1978**, 167.
- b. A. Ulman and J. Manassen, *J. Am. Chem. Soc.*, **1975**, 97, 6540.
- c. A. Ulman, J. Manassen, F. Frolow and D. Rabinovich, *Tetrahedron Lett.*, **1978**, 1885.

- d. A. Ulman and J. Manassen, *J. Chem. Soc., Perkin Trans. I.*, **1979**, 1066.
- e. O.P. Anderson, A.B. Kopelove and D.K. Levallee, *Inorg. Chem.*, **1980**, 19, 2101.
- f. L.L. Grazynski, J. Lisowski, M.M. Olmstead and A.L. Balch, *J. Am. Chem. Soc.*, **1987**, 109, 4428.
- g. W. Haas, B. Knipp, M. Sicken, J. Lex and E. Vogel, *Angew. Chem. Int. Ed. Engl.*, **1988**, 27, 309.
- h. E. Vogel, W. Haas, B. Knipp, J. Lex and H. Schmickler, *Angew. Chem. Int. Ed. Engl.* **1988**, 27, 406.
- i. L.L. Grazynski, J. Lisowski, M.M. Olmstead and A.L. Balch, *Inorg. Chem.*, **1989**, 4065.
- 16. a. D.K. Levallee and O.P. Anderson, *J. Am. Chem. Soc.*, **1982**, 104, 4707.
- b. D.E. Goldberg and K.M. Thomas, *J. Am. Chem. Soc.*, **1976**, 98, 913.
- 17. a. D. Kulia, D.K. Levallee, C.K. Schauer and O.P. Anderson, *J. Am. Chem. Soc.*, **1984**, 106, 448.
- 18. D.K. Levallee, A.B. Kopelove and O.P. Anderson, *J. Am. Chem. Soc.*, **1978**, 100, 3025.
- 19. C.K. Schauer, O.P. Anderson, D.K. Levallee, J.P. Battioni and D. Mansuy, *J. Am. Chem. Soc.*, **1987**, 109, 3922.
- 20. S.C. Aizawa, Y. Tsuda, Y. Ito, K. Hatano and S. Funahashi, *Inorg. Chem.*, **1993**, 32, 1119.
- 21. P. Bhyrappa and V. Krishnan, *Inorg. Chem.*, **1991**, 30, 239.
- 22. M.B. Hursthouse and S. Neidle, *J. Chem. Soc., Chem. Commun.*, **1972**, 449.
- 23. Guo-Zhang wu, Wei-Xing Gan and Hiu-Kwong Leung, *J. Chem. Soc.*,

Faraday Trans. 1991, 87, 2933.

24. a. A. Ulman, J. Gallucci, D. Fisher and J.A. Ibers, *J. Am. Chem. Soc.*, 1980, 102, 6852.
b. L.D. Spaulding, L.C. Andrews and G.J.B. Williams, *J. Am. Chem. Soc.*, 1977, 99, 6918.
c. R. Serlin, H.C. Chow and C.E. Strouse, *J. Am. Chem. Soc.*, 1975, 97, 7237.
25. K.M. Barkigia, J. Fajer, K.M. Smith and G.J.B. Williams, *J. Am. Chem. Soc.*, 1981, 103, 5890.
26. a. K.M. Barkigia, J. Fajer, L.D. Spaulding and G.J.B. Williams, *J. Am. Chem. Soc.*, 1981, 103, 176.
b. C. Kratky, C. Angst and J. Eigill, *Angew. Chem. Int. Ed. Engl.* 1981, 20, 211.
c. M.O. Senge, N.W. Smith and K.M. Smith, *Inorg. Chem.*, 1993, 32, 1259.
27. S.H. Strauss, M.E. Silver, K.M. Long, R.G. Thompson, R.A. Hudgens, K. Spartalian and J.A. Ibers, *J. Am. Chem. Soc.*, 1985, 107, 4207.
28. M.P. Suh, P.N. Swebston and J.A. Ibers, *J. Am. Chem. Soc.*, 1984, 106, 5164.
29. a. A.M. Stolzenberg and M.T. Stershic, *Inorg. Chem.*, 1988, 27, 1614.
b. A.M. Stolzenberg and L.J. Schussel, *Inorg. Chem.*, 1991, 30, 3205.
c. A.M. Stolzenberg and M.T. Stershic, *J. Am. Chem. Soc.*, 1988, 110, 6391.
d. A.M. Stolzenberg and M.T. Stershic, *Inorg. Chem.*, 1987, 26, 3082.

- e. A.M. Stolzenberg and M.T. Stershic, *J. Am. Chem. Soc.*, **1988**, 110, 5397.
- f. A.M. Stolzenberg, P.A. Glazer and B.M. Foxman, *Inorg. Chem.*, **1986**, 25, 983.
- ✓ 30. K.M. Barkigia, L. Chantranupong, K.M. Smith and J. Fajer, *J. Am. Chem. Soc.*, **1988**, 110, 7566.
- ✓ 31. E. Gudowska-Nowak, M.D. Newton and J. Fajer, *J. Phys. Chem.*, **1990**, 94, 5795.
- ✓ 32. K.M. Barkigia, M.D. Berber, J. Fajer, C.J. Medforth, M.W. Renner and K.M. Smith, *J. Am. Chem. Soc.*, **1990**, 112, 8851.
- ✓ 33. a. J.A. Shellnut, C.J. Medforth, M.D. Berber, K.M. Barkigia and K.M. Smith, *J. Am. Chem. Soc.*, **1991**, 113, 4077.
- b. C.J. Medforth, M.O. Senge, K.M. Smith, L.D. Sparks and J.A. Shelnut, *J. Am. Chem. Soc.*, **1992**, 114, 9859.
- c. K.M. Barkigia, M.W. Renner, L.R. Furenlid, C.J. Medforth, K.M. Smith and J. Fajer, *J. Am. Chem. Soc.*, **1993**, 115, 3627.
- ✓ 34. L.D. Sparks, C.J. Medforth, M.S. Park, J.R. Chamberlain, M.R. Ondrias, M.O. Senge, K.M. Smith and J.A. Shelnut, *J. Am. Chem. Soc.*, **1993**, 115, 581.
35. M.O. Senge, C.J. Medforth, L.D. Sparks, J.A. Shelnut and K.M. Smith, *Inorg. Chem.*, **1993**, 32, 1716.
36. a. D. Dolphin, Z. Muljiani, K. Rousseau, D.C. Borg, J. Fajer and R.H. Felton, *Ann. N.Y. Acad. Sci.*, **1973**, 206, 177.
- b. A. Stanienda and G. Biebl, *Z. Physik. Chem. (Frankfurt)*, **1967**, 52, 254.
- c. A. Wolberg and J. Manassen, *J. Am. Chem. Soc.*, **1970**, 92, 2982.
- d. J.H. Fuhrhop and D. Mauzerall, *J. Am. Chem. Soc.*, **1969**, 91,

- e. D. Dolphin, A. Forman, D.C. Borg, J. Fajer and R.H. Felton, *Proc. Natl. Acad. Sci. USA*, **1971**, 68, 614.
37. T.G. Spiro, R.S. Czernuszewicz and X.Y. Li, *Coord. Chem. Rev.*, **1990**, 100, 541 and references therein.
38. a. H. Yamaguchi, M. Nakano and K. Itoh, *Chem. Lett.*, **1982**, 1397.
b. D. Kim, L.A. Miller, G. Rakhit and T.A. Spiro, *J. Phys. Chem.*, **1986**, 90, 3320.
c. A. Salehi, W.A. Oertling, G.T. Babcock and C.K. Chang, *J. Am. Chem. Soc.*, **1986**, 108, 5630.
d. W.A. Oertling, A. Salehi, Y.C. Chung, G.E. Leroi, C.K. Chang and G.T. Babcock, *J. Phys. Chem.*, **1987**, 91, 5887.
e. R.S. Czernuszewicz, K.A. Macor, X.Y. Li, J.R. Kincaid and T.G. Spiro, *J. Am. Chem. Soc.*, **1989**, 111, 3860.
39. a. R.H. Felton, G.S. Owen, D. Dolphin and J. Fajer, *J. Am. Chem. Soc.*, **1971**, 93, 6332.
b. R.H. Felton, G.S. Owen, D. Dolphin, A. Forman, D.C. Borg and J. Fajer, *Ann. N.Y. Acad. Sci.*, **1973**, 206, 504.
40. a. M.A. Phillippi and H.M. Goff, *J. Am. Chem. Soc.*, **1979**, 101, 7641.
b. M.A. Phillippi, E.T. Shimomura and H.M. Goff, *Inorg. Chem.*, **1981**, 20, 1322.
c. M.A. Phillippi and H.M. Goff, *J. Am. Chem. Soc.*, **1982**, 104, 6026.
d. A.D. Boersma and H.M. Goff, *Inorg. Chem.*, **1984**, 23, 1671.
41. C.A. Reed, "Electrochemical and Spectrochemical Studies of Biological Redox Components", K.M. Kadish, Ed. *Advances in Chemistry 201*, American Chemical Society : Washington, DC,

- 1982, pp 333-356.
42. P. Gans, J.C. Marchon, C.A. Reed and J.R. Regnard, *New. J. Chem.* 1981, 5, 203.
 43. E.T. Shimomura, M.A. Phillippi, H.M. Goff, W.F. Scholz and C.A. Reed, *J. Am. Chem. Soc.*, 1981, 103, 6778.
 44. W.F. Scholz, C.A. Reed, Y.J. Lee, W.R. Scheidt and G. Lang, *J. Am. Chem. Soc.*, 1982, 104, 6791.
 45. G. Buisson, A. Deronzier, E. Duee, P. Gans, J.C. Marchon and J.R. Regnard, *J. Am. Chem. Soc.*, 1982, 104, 6793.
 46. a. K.M. Barkigia, L.D. Spaulding and J. Fajer, *Inorg. Chem.*, 1983, 22, 349.
b. L.D. Spaulding, P.G. Eller, J.A. Bertrand and R.H. Felton, *J. Am. Chem. Soc.*, 1974, 96, 982.
 47. P. Gans, G. Buisson, E. Duee, J.C. Marchon, B.S. Erler, W.F. Scholz and C.A. Reed, *J. Am. Chem. Soc.*, 1986, 108, 1223.
 48. a. L.D. Spreer, A.C. Maliyakel, S. Holbrook, J.W. Otvos and M. Calvin, *J. Am. Chem. Soc.*, 1986, 108, 1949.
b. W.R. Scheidt, H. Song and C.A. Reed, Abstracts of Papers, 196th National Meeting of the American Chemical Society, American Chemical Society, Washington, DC, 1988, Abstract 144.
 49. H. Song, C.A. Reed and W.R. Scheidt, *J. Am. Chem. Soc.*, 1989, 111, 6865.
 50. G.M. Godziela and H.M. Goff, *J. Am. Chem. Soc.*, 1986, 108, 2237.
 51. B.S. Erler, W.F. Scholz, Y.J. Lee, W.R. Scheidt and C.A. Reed, *J. Am. Chem. Soc.*, 1987, 109, 2644.
 52. H.M. Goff and M.A. Phillippi, *J. Am. Chem. Soc.*, 1983, 105, 7567.

53. M. Lee, O.K. Song, J.C. Seo and D. Kim, *J. Phys. Chem.*, **1992**, 96, 8374.
54. W.R. Scheidt, B. Cheng, K.J. Haller, A. Mislanker, A.D. Rae, K.V. Reddy, H. Song, R.D. Orosz, C.A. Reed, F. Cukiermik and J.C. Marchon, *J. Am. Chem. Soc.*, **1993**, 115, 1181.
55. a. Vogel's Text Book of Practical Organic Chemistry; ELBS and Longman, Fourth Edition, **1978**, Chapter 2.
- b. A. Weissberger, E.S. Proskaner, J.A. Riddick, E.F. Toppos Jr., "Organic Solvents in Techniques of Organic Chemistry", Third Edition, Inc. N.Y. Vol. 7, **1970**.
56. *Organic Synthesis*, Vol. 34, p. 100.
57. R.L. Hill, M. Gouterman and A. Ulman, *Inorg. Chem.*, **1982**, 21, 1450.
58. P.G. Seybold and M. Gouterman, *J. Mol. Spectrosc.*, **1982**, 31, 1.
59. H. Kobayashi and Y. Kaizu, *ACS Symp. Ser.*, **1986**, 321, 105.
60. V. Balzani, F. Bolletta, M.T. Ganadolfi and M. Maestri, *Topics in Current Chemistry*, **1978**, 75, 1.
61. D.F. Evans, *J. Chem. Soc.*, **1959**, 2003.
62. C.K. Chang, *J. Am. Chem. Soc.*, **1977**, 99, 2819.
63. J.P. Collman, *Acc. Chem. Res.*, **1977**, 10, 265.
64. A.R. Batterby and A.D. Hamilton, *J. Chem. Soc., Chem. Commun.*, **1990**, 117.
65. J.E. Baldwin, M.J. Crossley, T. Klose, E.A. O'Rear and M.K. Peters, *Tetrahedron*, **1982**, 38, 27.
66. M. Momenteau, J. Mispelter, B. Looock and E. Bisagni, *J. Chem. Soc., Perkin Trans I*, **1983**, 189.

67. U. Simonis, F.A. Walker, P.L. Lee, B. Hanquet, D. J. Meyerhoff and W.R. Scheidt, *J. Am. Chem. Soc.*, **1987**, 109, 2659.
68. A.D. Adler, F.R. Longo, J.D. Finarelli, J. Goldmacher, J. Assour and L. Korsakoff, *J. Org. Chem.*, **1967**, 32, 476.
69. J. Almog, J.E. Baldwin, M.J. Crossley, J.F. Debernardis, R.L. Dyer, J.R. Huff and K.K. Peters, *Tetrahedron*, **1981**, 37, 3589.
70. a.H.J. Callot, *Bull. Chem. Soc. Fr.*, **1974**, 8, 1492.
b.H.J. Callot, *Tetrahedron Lett.*, **1973**, 1487.
71. D. Reddy and T.K. Chandrashekar, *J. Chem. Soc., Dalton Trans.*, **1992**, 619.
72. a. R.J. Abraham, S.C.R. Fell and K.M. Smith, *Org. Magn. Resn.*, **1977**, 9, 367.
b. R.J. Abraham, G.R. Bedford, R.F. McNeillia and B. Wright, *Org. Magn. Resn.*, **1980**, 14, 418.
c. R.J. Abraham, *J. Magn. Resn.*, **1981**, 43, 491.
73. P.J. Spellane, M. Gouterman, A. Antipas, S. Kim and Y.C. Liu, *Inorg. Chem.*, **1980**, 19, 386.
74. a. H.J. Callot, A. Giraudeau and M. Gross, *J. Chem. Soc., Perkin Tans II.*, **1975**, 12, 1321.
b. J.E. Falk, *The Porphyrins and Metalloporphyrins*, Elsevier, Amsterdam, **1964**.
75. A. Giraudeau, A. Louati, M. Gross, H.J. Callot, L.K. Hanson, R.K. Rhodes and K.M. Kadish, *Inorg. Chem.*, **1992**, 21, 1581.
76. a. J. Ridley and M. Zerner, *Theor. Chim. Acta. (Berlin)*, **1973**, 32, 111.
b. J. Ridley and M. Zerner, *Theor. Chim. Acta. (Berlin)*, **1976**, 42, 223.

77. A. Giraudeau, H.J. Callot, J. Jordan, I. Ezhar and M. Gross, *J. Am. Chem. Soc.*, **1979**, 101, 3857.
78. J.Y. Becker, D. Dolphin, J.B. Paine and T. Wijesekera, *J. Electroanal. Chem.*, **1984**, 164, 335.
79. K.M. Kadish, *Prog. Inorg. Chem.*, **1986**, 34, 437.
80. A. Giraudeau, H.J. Callot and M. Gross, *Inorg. Chem.*, **1979**, 18, 201.
81. a. H.H. Inhoffen and P. Jager, *Tetrahedron Lett.*, **1964**, 1317.
b. M. Zerner and M. Gouterman, *Theor. Chim. Acta.*, **1966**, 4, 44.
82. a. W.H. Fuchsman, Q.R. Smith and H.M. Stein, *J. Am. Chem. Soc.*, **1977**, 99, 4190.
b. E.W. Baker, C.B. Storm, G. McGrew and A.H. Corwin, *Bioinorg. Chem.*, **1973**, 3, 49.
83. A.J. Gordon and R.A. Ford, *The Chemist's Companion*, Wiley, New York, **1972**.
84. a. A. Stanienda and G. Biebl, *Z. Phys. Chem. (Frankfurtam Main)*, **1967**, 52, 254.
b. A. Stanienda, *Z. Naturforsch B*, **1968**, 23, 147.
85. W.R. Scheidt and Y.J. Lee, *Struct. Bond.*, **1987**, 64, 1.
86. a. T.G. Traylor, *Acc. Chem. Res.*, **1981**, 14, 102.
b. W.R. Scheidt and C.A. Reed, *Chem. Rev.*, **1981**, 81, 543.
c. K.M. Kadish, in *Iron Porphyrins*, Part one, Ed. A.B.P. Lever and H.B. Gray, Addison-Wisley Publishing Company, Massachusetts, USA.
87. R.D. Jones, D.A. Summerville and F. Basolo, *Chem. Rev.*, **1979**, 79, 139 and references therein.

88. B. Morgan and D. Dolphin, *Struct. Bond.*, 1987, 64, 148 and references therein.
89. M. Momenteau, B. Looock and B.E. Bisagni, *Can. J. Chem.*, 1979, 57, 1804.
90. R.A. Binstsad, M.C. Crossley and N.S. Hush, *Inorg. Chem.*, 1991, 30, 1259.
91. A. Wolberg, *Isr. J. Chem.*, 1974, 12, 1031.
92. a. J.M. Assour, *J. Chem. Phys.*, 1965, 43, 2477.
b. P.T. Manoharan and M.T. Rogers in *Electron Spin Resonance of Metal Complexes*, Ed. by Teh Fu Yen, Plenum Press, New York, 1969, 143.
93. H. Yokoi and A.W. Addison, *Inorg. Chem.*, 1977, 66, 1341.
94. U. Sakaguchi and A.W. Addison, *J. Chem. Soc., Dalton Trans.*, 1979, 600.
95. A.H. Maki and B.R. McGarvey, *J. Chem. Phys.*, 1958, 29, 31.
96. C.C.J. Roothaan, *Rev. Mod. Phys.*, 1951, 23, 69.
- ✓ 97. J.A. Shelnutt and V. Oritz, *J. Phys. Chem.*, 1985, 89, 4733.
98. A. Giraudeau, I. Ezhar, M. Gross, H.J. Callot and J. Jordan, *Bioelectrochem. Bioenerg.*, 1976, 3, 519.
99. P.W. Lau and W.C. Lin, *J. Inorg. Nucl. Chem.*, 1975, 37, 2389.
100. E.B. Fleisher, *Acc. Chem. Res.*, 1970, 3, 105.
101. G.N. La Mar and F.A. Walker; in *the Porphyrins*, Vol. IV, D. Dolphin (Ed.), Academic, New York, 1979, pp. 61-157.
102. F.A Walker; M.W. Lo; M.T. Ree; *J. Am. Chem. Soc.*, 1976, 98, 5552.
103. a. L. Latos-Grazynski; R.J. Cheng, G.N. La Mar and A. Balch; *J. Am. Chem. Soc.*, 1982, 104, 5993.
b. J.P. Collman; J.I. Brauman; K.M. Doxsee; J.L. Sessler;

- R.M. Morris and Q.H. Gibson, *Inorg. Chem.*, **1983**, *22*, 1427 and references therein.
- c. K.S. Suslick; M.M. Fox and T.J. Reinert, *J. Am. Chem. Soc.*, **1984**, *106*, 4522 and references therein.
104. K.M. Kadish, in *Iron Porphyrins*, Part two, A.B.P. Lever and H.B. Gray (Ed.,) Addison-Wesley Publishing Company, Massachusetts, USA, 161-241.
105. J. Deisenhofer, H. Michel, *Angew. Chem. Int. Ed. Engl.* **1989**, *28*, 829.
- 106 a. J.R. Bolton, T.F. Ho, S. Liaw, A. Siemiarczuk, C.S.K. Wan and A.C. Waedon, *J. Chem. Soc. Chem. Commun.*, **1985**, 559.
- b. J.S. Lindsey, and D.C. Mauzerall, *J. Am. Chem. Soc.*, **1982**, *104*, 4498.
- c. D. Gust, T.A. Moore, D. Barrett, L.O. Harding, L.R. Makings, P.A. Liddell, F.C. De Schryver, M. van der Auweraer, R.V. Benasasson and M. Raugee, *J. Am. Chem. Soc.*, **1988**, *110*, 321 and references therein.
107. S. Tsuchiya, *Chem. Phys. Lett.*, **1990**, *169*, 608.
108. J. Takeda, T. Ohya and M. Sato, *Chem. Phys. Lett.*, **1991**, *183*, 384.
109. D. Reddy, T.K. Chandrashekar and H. van Willigen, *Chem. Phys. Lett.*, **1993**, *202*, 120.
110. a. M. Meot-Ner, A.D. Adler, *J. Am. Chem. Soc.*, **1975**, *97*, 5107.
- b. D.J. Quimby and F.R. Longo, *J. Am. Chem. Soc.*, **1975**, *97*, 5111.

111. D. Gust and T.A. Moore, (eds.), *Tetrahedron Symposia*, 1989, 45, 4669, Pergamon Press, Oxford, New York.
112. K. Kalyanasundaram and M.N. Spellart, *J. Phys. Chem.*, 1982, 86, 5163.
113. a. K. Sauer, *Acc. Chem. Res.*, 1980, 13, 249.
b. M. Calvin, *Acc. Chem. Res.*, 1978, 11, 869.
114. A. Stone and E.B. Feischer, *J. Am. Chem. Soc.*, 1968, 90, 2735.
115. M. Gouterman, in "The Porphyrins", D. Dolphin, (ed.), Vol. III, Academic Press, New York, 1978, Ch. 1.
116. L.A. Martarano; C. Wong, W.D. Morrocos Jr. and A.M.P. Gonclaves, *J. Phys. Chem.*, 1976, 80, 2389.
117. a. M.P. Tsuiruo, G.F. Stelmakh, V.E. Pyatosin, K.N. Solvayov and T.F. Kachura, *Chem. Phys. Lett.*, 1980, 73, 86.
b. Y. Kurabayashi, K. Kikuchi, H. Kokubun, Y. Kaizu and H. Kobayashi, *J. Phys. Chem.*, 1984, 88, 1308.
118. H. Kobayashi and Y. Kaizu, *ACS Symp. Ser.* 1986, 321, 105.
119. a. G.F. Stelmakh and M.P. Tsvirko, *Opt. Spectrosc.*, 1980, 48, 105.
b. G.F. Stelmakh and M.P. Tsvirko, *Opt. Spectrosc.*, 1980, 49, 278.
c. G.F. Stelmakh and M.P. Tsvirko, *Opt. Spectrosc.*, 1981, 50, 547.
120. H. Levanon and J.R. Norris, *Chem. Rev.*, 1978, 78, 185.
121. Z.P. Gribova and L.P. Kayushin, *Russ. Chem. Rev.*, 1972, 41, 154.
122. G.B. Jamesson and J.A. Ibers, *J. Am. Chem. Soc.*, 1980, 102, 2823.

123. J.H. vander Walls, W.A. van Dorp and T.J. Schaafsma, in "*The Porphyrins*", D. Dolphin Ed., Academic Press, New York, 1979, Vol. IV, p. 257.
124. E. Antonini and M. Brunori, "*Hemoglobin and Myoglobin in Reaction with Ligands*", North Holland Publishers, Amsterdam, 1971.
125. S.L. Kelly and K.M. Kadish, *Inorg. Chem.*, 1982, 21, 3631.
126. M.A. Stifkin, *Charge transfer complexes in Biomolecules*, Academic Press, London, 1971.
127. M.C. Thurnauer, J.J. Katz and J.R. Norris, *Proc. Natl. Acad. Sci., U.S.A.* 1975, 72, 3270.
128. R.H. Clarke, R.E. Connors, T.J. Schaafsma, J.F. Kleibeuker and R.J. Platenkamp, *J. Am. Chem. Soc.*, 1976, 98, 3674.
129. W.G. van Dorp, *Ph.D Thesis*, Leideu, 1975.
130. E. Nissani, A. Scherz and H. Levanon, *Photochem. Photobiol.*, 1977, 25, 93.
131. H. van Willigen and T.K. Chandrashekar, *J. Chem. Phys.*, 1983, 78, 7093.
132. J. Fajer and S. Davis in *The Porphyrins*, Ed. D. Dolphin, Acad. Press, New York, 1979, Vol. 4, 198.
133. W.D. Edwards and M.C. Zerner, *Can. J. Chem.*, 1985, 63, 1763.
134. X.Y. Li, R.S. Czernuszewicz, J.R. Kincaid, O. Su and T.G. Spiro, *J. Phys. Chem.*, 1990, 94, 31.
135. R.F. Pasternack, L. Francesconi, D. Raff and E. Spiro, *Inorg. Chem.* 1973, 12, 2606.
136. a. M. Krishnamurthy, J.R. Sutter and P. Hambright, *J. Chem. Soc., Chem. Commun.* 1975, 13.
b. A. Corsini and O. Hermann, *Talanta.*, 1986, 33, 335.

137. W.I. White, in *The Porphyrins*, Ed. D. Dolphin, Academic Press, New York, 1978, Vol. 5, Ch. 7.
138. a. R.L. Brookfield, H. Ellul and A. Harriman, *J. Photochem.*, 1985, 31, 97.
- b. G.S. Nahor, J. Rabani and F. Grieser, *J. Phys. Chem.*, 1981, . 85, 697.
139. J.P. Collman, C.M. Elliot, T.R. Halbert and B.S. Tourog, *Proc. Natl. Acad. Sci., USA*, 1977, 74, 18.
140. N.E. Kagan, D. Mauzerall and R.B. Merrifield, *J. Am. Chem. Soc.*, 1977, 99, 5484.
141. a.C.K. Chang, M.S. Kuo and C.B. Wang, *J. Heterocycl. Chem.*, 1977, 14, 943.
- b. C.K. Chang, *J. Heterocycl. Chem.*, 1977, 14, 1285.
- c. C.K. Chang, *Adv. Chem. Ser.*, 1979, 173, 162.
- d. S.S. Eaton, G.R. Eaton and C.K. Chang, *J. Am. Chem. Soc.*, 1985, 107, 3177.
142. a.V. Thanabal and V. Krishnan, *J. Am. Chem. Soc.*, 1982, 102, 3463.
- b. V. Thanabal and V. Krishnan, *Inorg. Chem.*, 1982, 21, 3606.
143. a. N. Kobayashi and Y. Nishiyama, *J. Chem. Soc., Chem. Commun.*, 1986, 1462.
- b. A.R. Koray, V. Ahsen and O. Bakaroglu, *J. Chem. Soc., Chem. Commun.*, 1986, 932.
- c. R. Hendriks, D.E. Sielcken, W. Drenth and R.J.M. Nolte, *J. Chem. Soc., Chem. Commun.*, 1986, 1464.
144. N. Kobayashi and A.B.P. Lever, *J. Am. Chem. Soc.*, 1967, 109, 7433.

145. D.E. Sielcken, M.M. van Tilborg, M.F.M. Roks, R. Hendriks, W. Drenth and R.J.M. Nolte, *J. Am. Chem. Soc.*, **1987**, 109, 4261.
146. V. Ahsen, E. Yilmazer, M. Ertas and D. Bekaroglu, *J. Chem. Soc., Dalton Trans.*, **1988**, 401.
147. G.B. Maiya and V. Krishnan, *J. Phys. Chem.* **1985**, 89, 5225.
148. a. T.K. Chandrashekar and H. van Willigen, *J. Am. Chem. Soc.*, **1983**, 105, 6323.
- b. T.K. Chandrashekar and H. van Willigen, *Chem. Phys. Lett.*, **1984**, 106, 237.
- c. T.K. Chandrashekar, H. van Willigen and M.H. Ebersole, *J. Phys. Chem.*, **1985**, 89, 3453.
- d. H. van Willigen, and T.K. Chandrashekar, *J. Am. Chem. Soc.*, **1986**, 108, 709.
- e. T.K. Chandrashekar, H.V. Willigen and M.H. Ebersole, *J. Phys. Chem.*, **1984**, 88, 4326.
- f. H. van Willigen, T.K. Chandrashekar, V. Das and M.H. Ebersole, *ACS Symp. Ser.*, **1986**, 321, 140.
149. K.M. Kadish, G.B. Maiya, C. Araullo and R. Guillard, *Inorg. Chem.*, **1989**, 28, 2725.
150. C.J. Pedersen, *J. Am. Chem. Soc.*, **1967**, 89, 7017.
151. H.K. Frensdorff, *J. Am. Chem. Soc.*, **1971**, 93, 600.
152. a. M. Kasha, H.R. Rawls and M. El-Bayoumi, *Pure Appl. Chem.*, **1965**, 11, 371.
- b. M. Gouterman, D. Holten and E. Lieberman, *Chem. Phys.*, **1977**, 25, 139.
- c. C.A. Hunter, J.K.M. Sanders and A.J. Stone, *Chem. Phys.*, **1989**, 133, 395.

153. P. Firman, R.G. Wilkins and S.P. Kasprzyk, *J. Am. Chem. Soc.*,
1989, 111, 4990.
154. a. A. Warshel, *J. Am. Chem. Soc.*, 1979, 101, 744.
b. C.A Hunter and J.K.M. Sanders, *J. Am. Chem. Soc.*, 1990, 112
5525.

LIST OF PUBLICATIONS

Most of the work reported in this thesis has been published in the following Journals:

1. Effect of Porphyrin Ring Deformation on the Spectral and Electrochemical Properties of Short Chain Basket Handle Porphyrins.

J. Chem. Soc. Dalton Trans. **1993**, 1137.

2. Brominated Short Chain Basket Handle Porphyrins and their Copper (II) Derivatives: Spectral and Electrochemical Studies on Effect of β -Substitution Versus Distortion.

J. Chem. Soc., Dalton Trans., (In Press) **1993**.

3. Fluorescence Properties of Distorted Short Chain Basket Handle Porphyrins.

J. Photochem. Photobiol. A: Chem., **1993**, 72, 61.

4. Effect of Porphyrin Ring Deformation on the Singlet Excited State Properties of Alkyl Bridged Basket Handle Porphyrins.

J. Photochem. Photobiol. A: Chem., (In Press) **1993**.

5. Π -cation Radicals of Copper (II) Derivatives of Short Chain Basket Handle Porphyrins.

Inorg. Chem. (In press), **1993**.

6. Π -cation Radicals of Iron (III) Derivatives of Short Chain Basket Handle Porphyrins.

J. Chem. Soc. Dalton Trans., (In Press), **1993**.

7. Dimerization Effects on Spectroscopic Properties of Water-Soluble Porphyrins in Aqueous and Micellar Media.

J. Chem. Soc. Dalton Trans., **1991**, 2103.

MANUSCRIPTS IN PREPARATION:

1. Porphyrin Ring Deformation Effect on Triplet State Properties of Basket Handle Porphyrins.
2. Reactions of Small Molecules with Iron (II) Derivatives of Short Chain Basket Handle Porphyrins.